

Physico-chemical characterization of a novel class of bolaamphiphilic hydrogelators

D i s s e r t a t i o n

zur Erlangung des akademischen Grades

doctor rerum naturalium (Dr. rer. nat.)

vorgelegt der

Naturwissenschaftlichen Fakultät I

Biowissenschaften

der Martin-Luther-Universität Halle-Wittenberg

von

Martin Bastrop

geboren am 02. Februar 1980 in Parchim

Gutachter /in:

1. Prof. Dr. Karsten Mäder
2. Prof. Dr. Alfred Blume
3. Prof. Dr. Heike Bunjes

Halle (Saale), 09/2010

Verteidigungstermin: 28.01.2011

Contents

1 Introduction	1
1.1 Bolaamphiphiles	1
1.1.1 General remarks	1
1.1.2 Single-chain bolaphospholipids	2
1.2 Hydrogels	9
1.3 Aim of this thesis	11
2 Materials and methods	13
2.1 Materials	13
2.1.1 Bolaamphiphiles used in the present thesis	13
2.1.2 Other materials	13
2.2 Methods	14
2.2.1 Oscillatory rheometry	14
2.2.1.1 General remarks	14
2.2.1.2 Flow of viscous fluids	14
2.2.1.3 Deformation of elastic materials	15
2.2.1.4 Oscillatory rheometry	16
2.2.1.5 Experimental part	19
2.2.2 Nuclear magnetic resonance (NMR) spectroscopy	23
2.2.2.1 General remarks	23
2.2.2.2 Spin	23
2.2.2.3 Magnetism	24
2.2.2.4 Spin precession and Larmor frequency	25
2.2.2.5 Longitudinal magnetization and longitudinal relaxation	26
2.2.2.6 Transverse magnetization and transverse relaxation	27
2.2.2.7 NMR signal and NMR spectroscopy	28
2.2.2.8 Relaxation	29
2.2.2.9 Experimental part	31

2.2.3	Electron spin resonance (ESR) spectroscopy	37
2.2.3.1	General remarks	37
2.2.3.2	Definitions	37
2.2.3.3	The ESR experiment	38
2.2.3.4	Motion dependence of ESR spectra	39
2.2.3.5	Experimental part	41
2.2.4	Bolaamphiphiles with a diacetylene group	43
2.2.4.1	Diacetylenes – general remarks	43
2.2.4.2	Experimental part	43
2.2.5	Biological tests	45
2.2.5.1	MTT-assay	45
2.2.5.2	Testing the antifungal activity	46
3	Results and discussion	48
3.1	Oscillatory rheometry	48
3.1.1	Influence of silicone oil	48
3.1.2	Concentration dependence at 25 °C	49
3.1.3	Temperature dependence	54
3.1.3.1	PC-C32-PC	54
3.1.3.2	Me ₂ PE-C32-Me ₂ PE at pH 5	56
3.1.4	Time tests	58
3.1.4.1	Cooling from 75 °C to 25 °C	58
3.1.4.2	Mechanical stress	61
3.2	Nuclear magnetic resonance (NMR) spectroscopy	62
3.2.1	Relaxation behavior of the water protons	62
3.2.1.1	PC-C32-PC in deionized water	62
3.2.1.2	Me ₂ PE-C32-Me ₂ PE in acetate buffer pH 5	69
3.2.2	Mean diffusion coefficients of the water molecules	83
3.2.3	Relaxation behavior of the bolaamphiphile protons	86
3.2.3.1	PC-C32-PC in D ₂ O	86
3.2.3.2	Me ₂ PE-C32-Me ₂ PE in acetate buffer pD 5	90

3.3	Electron spin resonance (ESR) spectroscopy	93
3.3.1	ESR measurements with tempolbenzoate	93
3.3.2	ESR measurements with n-doxyl stearic acid	95
3.3.2.1	General remarks	95
3.3.2.2	n-DSA in PC-C32-PC	97
3.3.2.3	n-DSA in Me ₂ PE-C32-Me ₂ PE	113
3.4	Bolaamphiphiles with a diacetylene group	128
3.4.1	General remarks	128
3.4.2	PC-C32diAc-PC	129
3.4.2.1	Properties	129
3.4.2.2	UV-polymerization	130
3.4.2.3	Characterization of the polymerized PC-C32diAc-PC	133
3.4.3	Me ₂ PE-C32diAc-Me ₂ PE	138
3.4.3.1	Properties	138
3.4.3.2	UV-polymerization	139
3.5	Biological tests	141
3.5.1	MTT-assay	141
3.5.1.1	General remarks	141
3.5.1.2	Obtained results	142
3.5.2	Testing the antifungal activity	144
3.5.2.1	General remarks	144
3.5.2.2	Obtained results	144
4	Summary and perspectives	146
5	References	152

Supplement

List of publications

Acknowledgements

Curriculum vitae

Abbreviations

12-DSA	12- doxyl stearic acid
16-DSA	16- doxyl stearic acid
$2A_{\max}$	maximum hyperfine splitting
5-DSA	5- doxyl stearic acid
A/V-ratio	glass surface-to-volume ratio
CPMG method	Carr-Purcell-Meiboom-Gill method
CSD	controlled shear deformation
cw	continuous wave
D_m	mean diffusion coefficient
d_m	mean diffusion distance
DSC	differential scanning calorimetry
ESR	electron spin resonance
FID	free-induction decay
FT-IR	Fourier transform infrared spectroscopy
G'	storage modulus
G''	loss modulus
H_2O_b	unperturbed water
H_2O_p	perturbed water
IC50	half-maximal inhibitory concentration
LMW	low molecular weight
LVE-region	linear visco-elastic region
MTT	3-(4,5-dimethylthiazol-2-yl)-2,5-diphenyl-tetrazoliumbromid
$M_{Z(eq)}$	longitudinal magnetization at thermal equilibrium
n-DSA	n-doxyl stearic acid
NMR	nuclear magnetic resonance
PDA	polydiacetylene
PGSE method	pulsed-gradient spin-echo method
PGSTE method	pulsed-gradient stimulated-echo method
pHEMA	poly(hydroxyethyl methacrylate)
REF	relaxation rate enhancement factor
rf	radiofrequency
R_{HS}	head/spacer diameter ratio

SANS	small angle neutron scattering
T_1	longitudinal relaxation time
T_2	transverse relaxation time
T_{2m}	mean value of T_2
TB	tempolbenzoate
TEM	transmission electron microscopy
UV	ultraviolett
WinDXP	Windows Distributed EXPOnential analysis software
λ_{\max}	absorption maximum
τ_R	rotational correlation time

1 Introduction

1.1 Bolaamphiphiles

1.1.1 General remarks

Boleadoras or bolas (from Spanish: ball) are South American missile weapons. In their simplest form, they consist of two stone or leather balls attached to the ends of a cord. Therefore, molecules with two charged groups connected by a chain were called bolaform electrolytes by Fuoss and co-workers.^[1] In analogy, amphiphiles with a hydrophobic core attached to a hydrophilic group on both ends were named bolaamphiphiles.^[2]

Such bipolar molecules are naturally found in the membranes of the Archaea (formerly called archaebacteria), which are, besides the Eukaryotes and Procaryotes, the third domain of life on this planet. Many of the bipolar molecules found in the membranes of the Archaea are derived from caldarchaeol. Caldarchaeol is the dimer of the diphytanylglycerol diether archaeol and exhibits a tetraether structure with a hydrophobic core and hydrophilic domains on both ends.^[3] Among the Archaea, there are many species living under extreme conditions, such as low pH values, very high salt concentrations or temperatures. One prerequisite to survive at such conditions is a robust membrane. Therefore, the unique lipid composition of the Archaea membranes may have its origin in an adaptation to such extreme environments.

Bipolar lipids are also found in some plants. In search for new antifungal substances, Bierer et al. isolated the bipolar plant metabolite 1,22-bis[[[2-(trimethylammonium)ethoxy]phosphinyloxy]docosane (irlbacholine, PC-C22-PC).^[4] The chemical structure is shown in Figure 1.1. This substance was found in two different plants, namely Irlbachia alata and Anthocleista djalonensis. An in-vitro susceptibility test was described by Bierer et al. that revealed antifungal activity of irlbacholine against *Candida albicans*, *Cryptococcus neoformans*, *Aspergillus fumigatus* and *Trichophyton rubrum*.^[4]

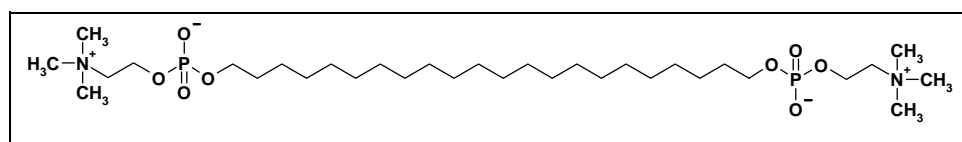


Figure 1.1 Chemical structure of irlbacholine (PC-C22-PC).

The synthesis of bolaamphiphiles as model substances of the complex archaelipids started in the early 1980s with the main target of producing monolayered asymmetric membranes for light-induced charge separation.^[5] Meanwhile, a wide variety of bolaamphiphiles was

synthesized.^[5,6] Depending on their hydrophobic and hydrophilic groups, these synthetic bolaamphiphiles can self-assemble, for example, into monolayers, fibers, ribbons, tubules or micelles. Monolayered liposomes, formed by bipolar lipids, can be an alternative to conventional liposomes due to their higher stability for example to the low pH value present in the stomach.^[7] Bolaamphiphiles can also be used as specific surface coatings, since they form fluid or rigid layers on smooth surfaces.^[5] Moreover, some bolaamphiphiles were reported to form aqueous gels. Among these hydrogelators are bolaamphiphiles with headgroups containing nucleotides, sugars or amino acids.^[8]

1.1.2 Single-chain bolaphospholipids

Dotriacontane-1,32-diyl-bis[2-(trimethylammonio)ethylphosphate] (PC-C32-PC, Figure 1.2) is a long chain derivative of the above mentioned 1,3-bis(sn-3-phosphatidyl)-sn-glycero-3-phosphocholine (PC-C22-PC). PC-C32-PC was first synthesized by Heiser et al.^[9-11] together with other bolaamphiphiles as a model substance for archaeal lipids.

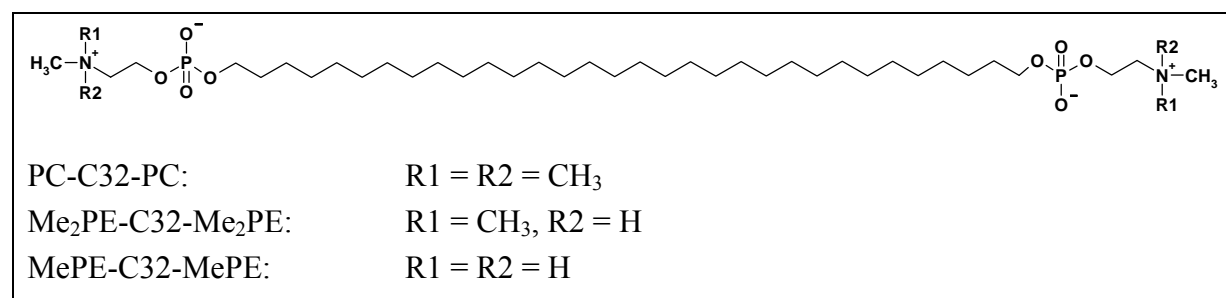


Figure 1.2 Chemical structures of PC-C32-PC, Me₂PE-C32-Me₂PE and MePE-C32-MePE.

In the course of the physico-chemical characterization, PC-C32-PC was found to exhibit unique aggregation behavior and excellent hydrogelator properties.^[12,13] After dispersing PC-C32-PC in water at temperatures above 80 °C and cooling down to room temperature, PC-C32-PC molecules are self-assembling into a dense network of nanofibers (Figure 1.3A). Macroscopically, the formation of a transparent hydrogel is observed, and when the sample tube is turned upside down, the fiber network prevents the water from flowing freely (Figure 1.3B). This finding is impressive, since in a sample containing 1 mg/ml of PC-C32-PC, the PC-C32-PC/water molar ratio is about 1/45000.

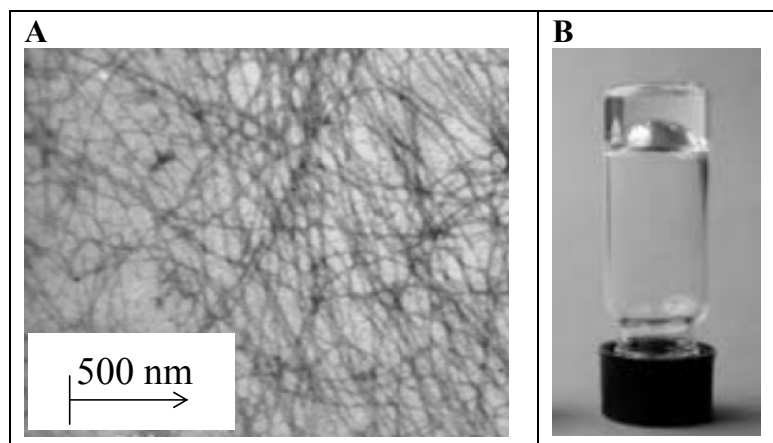


Figure 1.3

PC-C32-PC in deionized water at room temperature:

(A) TEM image of 0.3 mg/ml PC-C32-PC stained with uranylacetate (taken from ^[13]).

(B) Photograph of a hydrogel formed by 1 mg/ml PC-C32-PC (taken from ^[12]).

The nanofibers, formed by PC-C32-PC, are several micrometers long. The fiber thickness of about 5-6 nm roughly corresponds to the length of the PC-C32-PC molecule in its extended conformation. Moreover, a helical structure of these fibers seemed to be discernable from cryo-TEM micrographs. Recently, atomic force microscopy experiments gave evidence for this helical structure and also for the concomitant existence of right and left handed helices^[14]. Unlike other bolaamphiphilic hydrogelators, PC-C32-PC molecules do not possess any hydrogen-bond donor atoms. Therefore, the self-assembly into an interconnected three-dimensional fiber network is solely driven by hydrophobic interactions between the long alkyl chains of the molecules. Packing restrictions play an important role in the PC-C32-PC/water system owing to the larger space requirement of the phosphocholine headgroups compared to the small cross-sectional area of the alkyl chains. The influence of the space requirement of headgroups and chains on the structure, the size and the shape of the resulting aggregates was also demonstrated by Monte Carlo simulations.^[14] These simulations of the self-assembly were performed using a coarse-grain model. When the head/spacer diameter ratio (R_{HS}) was adjusted in the range $1.25 \leq R_{HS} \leq 2.1$, spontaneous self-assembly into fibers with helical structure could be observed. At larger ratios ($R_{HS} > 2.1$), only micellar aggregates were observed. A self-assembled nanofiber obtained with a head/spacer diameter of 1.4 is shown in Figure 1.4. It contains around 400 bolaamphiphile molecules and the headgroups (blue) of the bolaamphiphiles are forming a helical superstructure resulting from the molecular arrangement in an inclined orientation with regard to the length axis of the helical aggregate. Obviously, there are still hydrophobic parts that are exposed to the aqueous phase. Therefore, one can expect that the fibers in the three-dimensional network are cross-linked by van der Waals interactions between their hydrophobic parts.

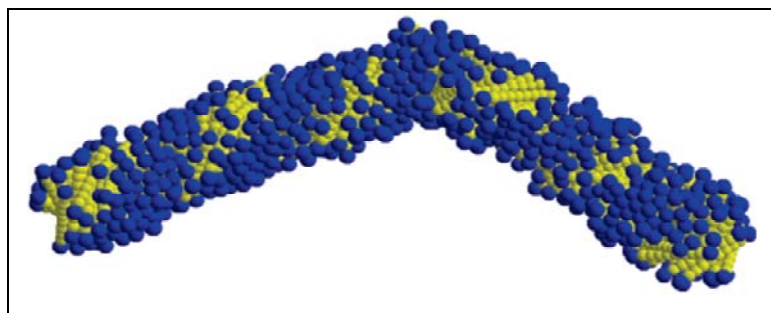


Figure 1.4
Self-assembled helical fiber obtained from Monto Carlo simulations with 397 bolalipid molecules and a head/spacer diameter ratio of 1.4 (taken from ^[14]).

Hydrogels of PC-C32-PC can be regarded as thermoreversible gels. The gel character can be completely destroyed by increasing the temperature above 50 °C, but it is reestablished, when the sample is cooled down again. The temperature dependent behavior of PC-C32-PC was intensively studied. Differential scanning calorimetry (DSC) was used to check, whether the breakdown of the gel is connected to enthalpic effects.^[13] Representative DSC thermograms of PC-C32-PC at different concentrations are displayed in Figure 1.5. Three endothermic peaks are detected by DSC. The main transition is observed at 49 °C, which is exactly the temperature at which the breakdown of the macroscopic hydrogel state is observed. This is due to a disintegration of the fiber network into smaller micellar aggregates as was shown by electron microscopy.^[13] FT-IR measurements revealed that the alkyl chains predominantly adopt an all-trans-conformation at low temperatures.^[13] The main transition is related to a distinct decrease in the trans-gauche ratio and therefore to a fluidization of the alkyl chains. A pre-transition is detected at 42 °C with only a small transition enthalpy. A third broad peak is detected at 73 °C in the temperature range, in which only micellar aggregates exist. The results obtained by FT-IR revealed that this transition is accompanied by a further increase in the number of gauche conformers.

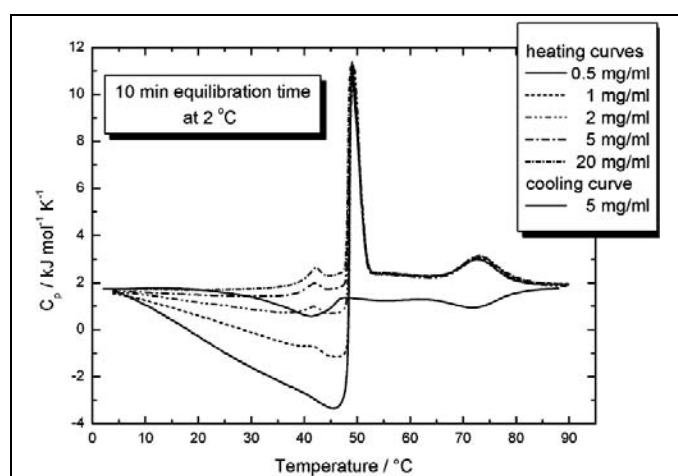


Figure 1.5
DSC thermograms obtained at a scan rate of 60 °C/h for PC-C32-PC at different concentrations in deionized water (taken from ^[13]).

The hydrogel state was found to be reflected in the data obtained by oscillatory rheometry, since the values of the storage moduli exceeded that of the loss moduli.^[12] Moreover, the values for the dynamic viscosity η were determined by means of rotational rheometry (Figure 1.6).^[13] A dramatic decrease of the dynamic viscosity was observed at about 40 °C, which corresponds to the temperature of the pre-transition. Above the pre-transition temperature, the fibers are still intact. Therefore, it was concluded that the decrease in the dynamic viscosity might be caused by a significant decrease in the number of cross-links between the fibers. The breakdown of the fibers at about 50 °C was also detected by a smaller drop in η .

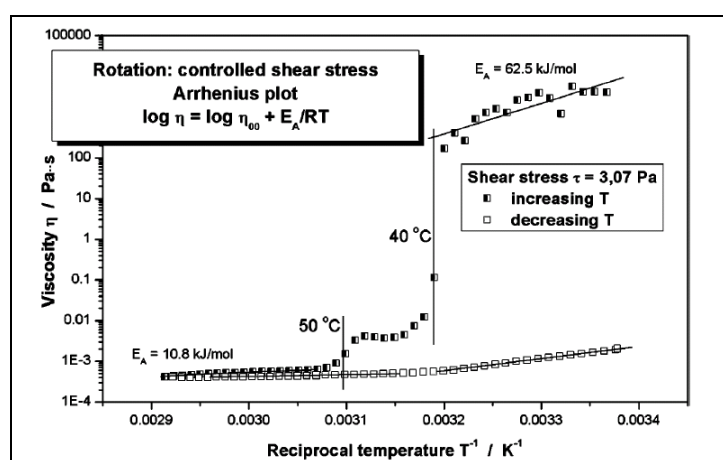


Figure 1.6
8 mg/ml PC-C32-PC in deionized water: Temperature dependent values for the dynamic viscosity η obtained by rotational rheometry (taken from^[13]).

In order to study the influence of the headgroups on the self-assembly, the bolaamphiphile dotriacontane-1,32-diyl-bis[2-(dimethylammonio)ethylphosphate] ($\text{Me}_2\text{PE-C32-Me}_2\text{PE}$, Figure 1.2) was first synthesized by Ziethe.^[15,16] In $\text{Me}_2\text{PE-C32-Me}_2\text{PE}$, one methyl group per headgroup was replaced by a hydrogen atom. This substitution decreases the volume of the headgroups and enables them to form hydrogen bonds, namely between the $\text{NH}(\text{CH}_3)_2^+$ and the PO_2^- groups. Additionally, the aggregation behavior of $\text{Me}_2\text{PE-C32-Me}_2\text{PE}$ is pH dependent. The pK_a values were determined to be 3.3 and 6.5 for the phosphate groups and for the dimethylammonium groups, respectively.^[15] In order to ensure that all headgroups are in their zwitterionic form analogous to PC-C32-PC, acetate buffer at pH 5 was chosen as the aqueous medium instead of deionized water. The aggregation behavior of $\text{Me}_2\text{PE-C32-Me}_2\text{PE}$ at pH 5 was found to show many similarities to that of PC-C32-PC in deionized water: At room temperature, a hydrogel is obtained for $\text{Me}_2\text{PE-C32-Me}_2\text{PE}$ at pH 5, which results from the formation of a dense network of helical fibers (Figure 1.7).^[15] Besides the fibers, however, there are also darker, almost rectangular areas to be found in the electron micrographs.^[15] It was suggested that these areas might be caused by sheet-like aggregates, but the exact arrangement was unclear at that time.

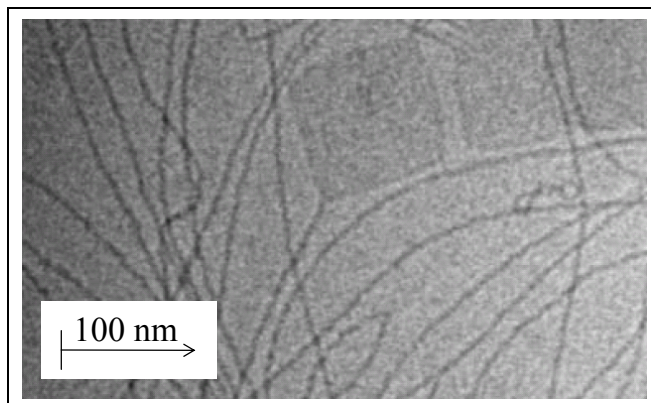


Figure 1.7
Cryo-TEM image obtained for a dispersion of 0.3 mg/ml Me₂PE-C32-Me₂PE in acetate buffer pH 5 at room temperature (taken from ^[15]).

The DSC thermograms again show three endothermic peaks (Figure 1.8A), but the transition temperatures are shifted upwards with respect to PC-C32-PC (Table 1.1). The same effect is observed for the gel to liquid crystalline phase transitions of phosphatidylethanolamine bilayers^[17] and can be explained with the stabilizing effect of hydrogen bonding.

For Me₂PE-C32-Me₂PE at pH 5, the first transition at 45.5 °C is related to a partial fluidization of the alkyl chains^[15] and to an increased motion of the headgroups.^[18] Oscillatory rheometry revealed a significant decrease of the storage and loss moduli above this temperature, but the hydrogel state was found to still persist (Figure 1.8B).^[18] Considerably lower values for G' and G'' above 50 °C indicate a significant decrease in the number of cross-links between the fibers in the three-dimensional network. This could be explained by a loss of hydrophobic interactions between the fibers and by the simultaneous breaking up of hydrogen bonds between molecules of different fibers.^[18] The second peak, detected in the DSC thermograms at 69.5 °C, marks the complete disintegration of the fiber network into micellar aggregates. Therefore, the hydrogel is breaking down at this temperature. In analogy to PC-C32-PC, a third transition is detected above this fiber-to-micelle transition at approximately 85 °C and is presumably caused by a further disordering of the alkyl chains.

Table 1.1 Transition temperatures of the different bolaamphiphiles obtained from the DSC thermograms.

bolaamphiphile	medium	concentration	transition temperatures		
PC-C32-PC	deionized water	1 mg/ml	43.8 °C	48.7 °C	73.0 °C
Me ₂ PE-C32-Me ₂ PE	acetate buffer pH 5	1 mg/ml	45.5 °C	69.5 °C	85.0 °C
Me ₂ PE-C32-Me ₂ PE	carbonate buffer pH 10	1 mg/ml	43.5 °C	52.0 °C	70.0 °C
MePE-C32-MePE	acetate buffer pH 5	1 mg/ml	80 °C		

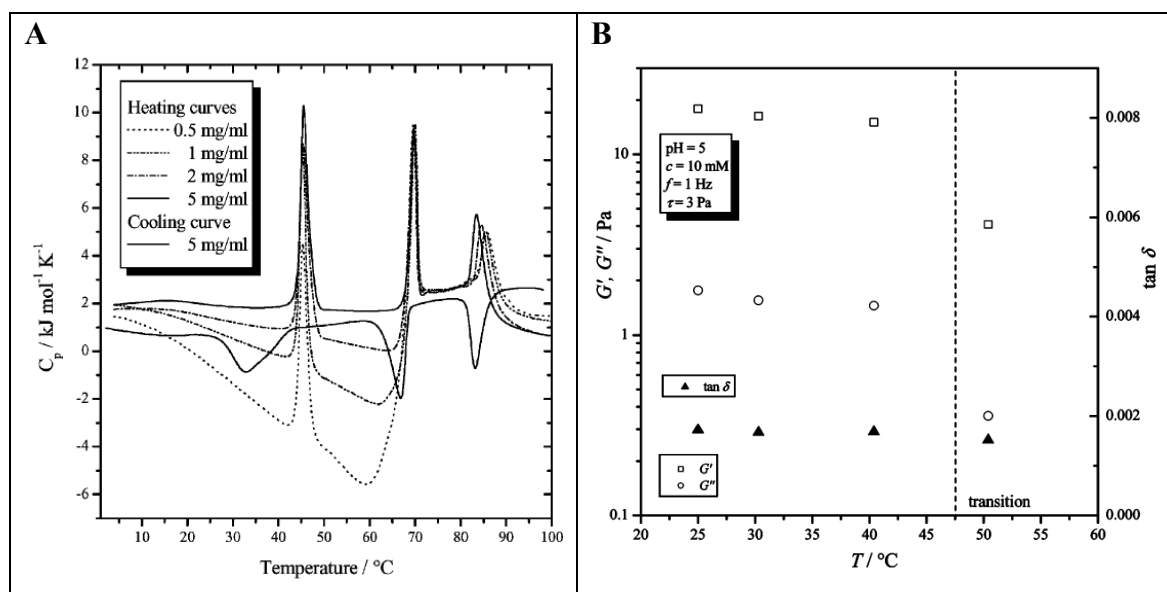


Figure 1.8 (A) DSC thermograms obtained for $\text{Me}_2\text{PE-C32-Me}_2\text{PE}$ in acetate buffer pH 5 at different concentrations (taken from [15]). (B) Temperature dependence of the G' , G'' and $\tan \delta$ values obtained by oscillatory rheometry for a hydrogel formed by 8 mg/ml $\text{Me}_2\text{PE-C32-Me}_2\text{PE}$ in acetate buffer pH 5 (taken from [18]).

Increasing the pH value from 5 to 10 results in a negative charge of the $\text{Me}_2\text{PE-C32-Me}_2\text{PE}$ headgroups due to deprotonation of the dimethylammonium groups. At pH 10, the aggregation behavior of $\text{Me}_2\text{PE-C32-Me}_2\text{PE}$ was found to be changed considerably and hydrogel formation was not observed.^[15] This can be explained by electrostatic repulsion between the now negatively charged bolaamphiphiles, which prevents a dense packing of the alkyl chains. This is supported by the $^{31}\text{P-NMR}$ data, which indicate a significantly higher rotational mobility of the headgroups at pH 10 compared to pH 5.^[18] Both TEM and cryo-TEM show smaller micellar aggregates, but also many fibers at a concentration of 0.3 mg/ml $\text{Me}_2\text{PE-C32-Me}_2\text{PE}$ at pH 10.^[15] However, it could be shown by SANS that these fibers have to be regarded as artifacts resulting from the preparation procedure of the samples prior to the electron microscopy.^[18] According to these results, there are only small micellar aggregates present at low concentrations (1 to 2 mg/ml) of $\text{Me}_2\text{PE-C32-Me}_2\text{PE}$ at pH 10. A considerable number of fibers could be found only for the sample containing 10 mg/ml $\text{Me}_2\text{PE-C32-Me}_2\text{PE}$. DSC measurements were carried out for $\text{Me}_2\text{PE-C32-Me}_2\text{PE}$ at pH 10 as well. For 1 mg/ml $\text{Me}_2\text{PE-C32-Me}_2\text{PE}$ at pH 10, three peaks are again observed, but the transition temperatures were found to be decreased with respect to pH 5 (Table 1.1).

Further derivatization of the bolaamphiphile headgroup was realized by substituting a second methyl group by a hydrogen atom and dotriacontane-1,32-diyl-bis[2-(methylammonio)ethyl-phosphate] (MePE-C32-MePE) was obtained (Figure 1.2).^[19]

The aggregation behavior of MePE-C32-MePE was found to completely differ from that of PC-C32-PC and Me₂PE-C32-Me₂PE. The smaller space requirement of the monomethylammonium group enables the bolaamphiphile molecules to adopt a more parallel ordering and only lamellar aggregates are observed in the obtained electron micrographs (Figure 1.9). For MePE-C32-MePE, only a single transition at 80 °C was observed in the DSC thermograms (Table 1.1).^[19]

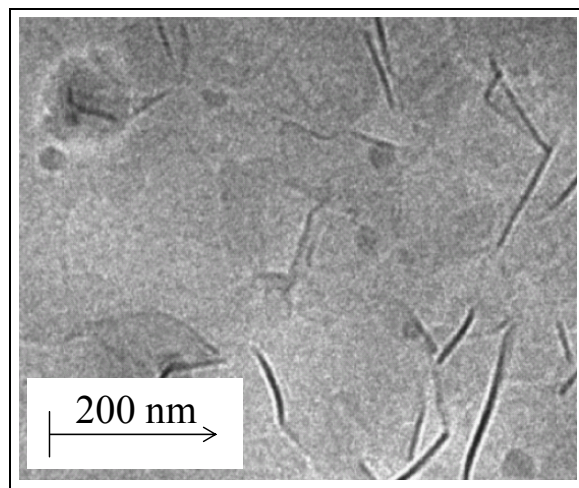


Figure 1.9
Cryo-TEM image obtained for 1 mg/ml MePE-C32-MePE in acetate buffer pH 5 (taken from ^[19])

Several bolaamphiphiles were shown to stabilize liposomes due to their membrane spanning properties.^[7] To find substances with stabilizing effects on conventional bilayers was one of the motivations for the synthetic work that lead to the single-chain bolaphospholipids, which are described here. Therefore, the mixing behavior of PC-C32-PC with conventional phospholipids was studied. However, PC-C32-PC molecules showed no tendency to be incorporated into lipid bilayers formed by DPPC, DMPC or POPC in a membrane spanning conformation.^[20] Instead, these phospholipids were found to be incorporated into the bolaamphiphilic fiber structures to a measurable extent.

Systematic synthetic work was also done to study the effect of the chain length on the aggregation behavior. Bolaamphiphiles with chain lengths between 22 and 36 CH₂ groups, both even and odd numbers, were synthesized for PC-C_n-PC and Me₂PE-C_n-Me₂PE.^[19,21,22] Their aggregation behavior was studied by DSC and electron microscopy. In the case of the PC-C_n-PC family, the temperature of the main transition was found to be shifted upwards by about 5 K per additional CH₂ group.^[21] No even-odd effect was observed.^[19] For the bolaamphiphiles with longer chain lengths ($n \geq 34$), the main transition in the DSC thermograms was found to be splitted into two peaks. Fibers were observed for all samples below the main transition temperature, whereas only micellar aggregates are present above this temperature as could be shown by electron microscopy and SANS.^[19] The transition temperatures obtained for the Me₂PE-C_n-Me₂PE family were found to be upshifted by about 15 K with respect to their PC-C_n-PC analogues.^[19] This supports the conclusion that hydrogen bonding substantially stabilizes the bolaamphiphilic aggregates. A subsequent

increase of the transition temperatures with increasing chain lengths is again observed and also the splitting of the main transition peak, which is visible for Me₂PE-C_n-Me₂PE with $n \geq 28$.^[19] For Me₂PE-C34-Me₂PE and Me₂PE-C36-Me₂PE at pH 5, the phenomenon of syneresis was observed upon storage and could be attributed to the transformation of nanofibers into lamellar aggregates.^[23] A model for the arrangement of the bolaamphiphile molecules inside these lamellar aggregates was proposed. According to this model, the lamellae are formed by tilted bolalipids interdigitated in a crossed fashion.^[23] Compared to the nanofibers, the formation of such lamellae leads to a significant reduction of the surface that is exposed to the aqueous medium. The first transition, detected for Me₂PE-C34-Me₂PE and Me₂PE-C36-Me₂PE at approximately 50 and 60 °C, respectively, is obviously related to a disintegration of the lamellae, since only fibers seem to exist above this transition temperature.^[23] As described above, lamellar aggregates were also found in small numbers in the cryo-TEM image of a sample with 0.3 mg/ml Me₂PE-C32-Me₂PE at pH 5 (Figure 1.7). Further modifications of the bolaamphiphile molecules were realized. For example, bolaamphiphiles with partially deuterated alkyl chains were synthesized in order to selectively study the central part of the alkyl chains by ²D-NMR and FT-IR.^[23] Another modification attempt was the functionalization of the bolaamphiphiles by the introducing sulfur groups as binding sites for gold nanoparticles.^[14,24]

1.2 Hydrogels

Gels combine the properties of fluids and solids. Despite being mostly liquid by weight and volume, a gel has the mechanical properties of a solid, since it can maintain its form under the stress of its own weight.^[25] Gels are used in exceeding quantities in food products, cosmetics and also in agriculture and oil industries. Gels containing water as the dispersive phase are called hydrogels. Due to their high water content and their soft consistency, hydrogels possess a good biocompatibility and resemble natural living tissue more than any other class of synthetic biomaterials.^[26] Therefore, they have found numerous applications in the biomedical field, for example as contact lenses,^[27] as drug delivery systems,^[28] and in regenerative medicine.^[29] There are many different hydrogel systems available today, which are all composed of an aqueous phase and one or more hydrophilic or amphiphilic components that are cross-linking into a three-dimensional network by either covalent bonds or noncovalent interactions.^[30] Most of these hydrogelators are natural or synthetic polymers, but the ability to gel water was reported for several low molecular weight (LMW) molecules as well.^[8,31]

The common feature of these LMW hydrogelators is their amphiphilic character that determines their specific self-assembly into a three-dimensional network of fibers, which is usually required for hydrogelation.

It is useful to break down the self-assembled network into a primary, secondary and tertiary structure in order to understand the underlying principles of the hydrogelation phenomenon. According to Estroff et al.,^[8] the primary structure (angstrom to nanometer scale) is determined by the molecular level recognition events that promote anisotropic aggregation of the gelator molecules in one or two dimensions. In aqueous environments, hydrophobic forces play a major role in this aggregation process. Depending on the molecular structure of the gelator molecules, different aggregate morphologies like micelles, vesicles, fibers, ribbons or sheets will result from the self-assembly. This is the secondary structure (nano- to micrometer scale) of the gel, whereas the tertiary structure involves the interaction of these individual aggregates.

The bolaamphiphiles PC-C32-PC and Me₂PE-C32-Me₂PE belong to the class of LMW hydrogelators. For PC-C32-PC, the primary structure is solely determined by hydrophobic interactions between the long alkyl chains, which align not perfectly parallel to each other, but are slightly twisted relative to each other because of the bulky headgroups. For Me₂PE-C32-Me₂PE at pH 5, the self-assembly is similar, but hydrogen bonding is also involved in this process. Both bolaamphiphiles self-assemble into fibers with a thickness that roughly corresponds to the length of the bolaamphiphile molecules in their extended conformation. For Me₂PE-C32-Me₂PE at pH 5, however, this secondary structure additionally involves a small number of lamellar aggregates as is outlined in Section 1.1. At 20 °C and a bolaamphiphile concentration ≥ 1 mg/ml, the tertiary structure of the obtained hydrogels is mainly determined by the presence of the fibers, which are several micrometers long. Noncovalent cross-linking of these fibers is due to hydrophobic interactions between the parts of the alkyl chain region that are not shielded from the water by the hydrophilic headgroups (see fiber model in Figure 1.4). The resulting three-dimensional fiber network is capable of preventing macroscopic flow and a hydrogel is obtained.

1.3 Aim of this thesis

As described in Section 1.1, the compilation of the collected experimental data leads to a good understanding of the underlying principles of the aggregation behavior of PC-C32-PC and Me₂PE-C32-Me₂PE in dependence of various factors. However, the knowledge about these systems is far from being complete up to now and there are still important questions to be answered. Therefore, the aim of this thesis is the further physico-chemical characterization of the aggregation behavior of PC-C32-PC and Me₂PE-C32-Me₂PE in aqueous media in order to contribute to a better understanding of these interesting systems.

Until now, rheological measurements of hydrogels formed by PC-C32-PC and Me₂PE-C32-Me₂PE were performed only for a single bolaamphiphile concentration, namely 8 mg/ml. For PC-C32-PC and Me₂PE-C32-Me₂PE, the temperature dependence of the rheological behavior was investigated by applying different methods, namely rotational and oscillatory rheometry, respectively.^[13,18] In this thesis, oscillatory rheometry was used to systematically study the concentration and the temperature dependence of the rheological properties of aqueous samples of PC-C32-PC and Me₂PE-C32-Me₂PE (Section 3.1). The obtained rheological data enable, for the first time, a direct comparison of the rheological properties of these bolaamphiphilic hydrogels. In addition to the mechanical properties of the hydrogels, oscillatory rheometry was also used to study the recovery kinetics of the fiber networks that were destroyed before either by heat or by extreme mechanical stress.

To gain information about the dynamics, that are present inside the bolaamphiphilic hydrogel systems, is essential for a deeper understanding of the aggregation process itself and also for potential applications. When dealing with dynamics, one has to differentiate between the different motional modes inside the particular sample. Sophisticated methods have to be applied for studying these individual motions, since the characteristic time constants for these motions cover a wide range.^[32] The dynamics of the water molecules inside the aqueous samples of PC-C32-PC and Me₂PE-C32-Me₂PE were studied intensively by performing ¹H-NMR relaxation and diffusion experiments (Section 3.2). NMR relaxation times of the water protons and mean diffusion coefficients of the water molecules depend strongly on their rotational and translational mobilities. Therefore, they are a sensitive measure for the water dynamics that are present in the particular sample. By substituting H₂O by D₂O, the NMR relaxation behavior of the bolaamphiphile protons could also be addressed.

For PC-C32-PC and Me₂PE-C32-Me₂PE as well as for their partially deuterated derivatives, FT-IR and ²H nuclear magnetic resonance (NMR) spectroscopy were used to study the

dynamics that are present in the alkyl chain region of the self-assemblies.^[13,15,23] In order to obtain further information about the alkyl chain region, electron spin resonance (ESR) spectroscopy was used. By applying different spin probe molecules, information about the motional dynamics present in different parts of this alkyl chain region could be achieved. The results are presented and discussed in Section 3.3. Moreover, sampling the bolaamphiphile system with a water soluble spin probe was used to obtain a further insight into the dynamics of the water molecules.

An attempt to chemically cross-link the three-dimensional fiber network is described in Section 3.4 of this thesis. The idea behind this approach is the combination of the advantages of the well-defined and controllable self-assembly into a nanofiber network with that of a permanent polymeric network. For this purpose, two adjacent triple bonds were introduced into the center of the alkyl chain of the bolaamphiphiles as polymerizable groups. In theory, UV-irradiation is supposed to chemically cross-link the alkyl chains of adjacent bolaamphiphile molecules after completion of the self-assembly. This would transform the dynamic physical network into a permanent chemical network. The diacetylene bolaamphiphiles dotriaconta-15,17-diyn-1,32-diylbis[2-(trimethylammonio)ethylphosphate] (PC-C32diAc-PC) and dotriaconta-15,17-diyn-1,32-diylbis[2-(dimethylammonio)ethylphosphate] (Me₂PE-C32diAc-Me₂PE) were synthesized^[22,33,34] and their aggregation and UV-polymerization behavior was studied.

The last part of this thesis concerns with some biological aspects of the single-chain bolaphospholipids. Potential biomedical applications of the bolaamphiphilic hydrogels presuppose their biological compatibility. In order to attain first data about the cytotoxicity of PC-C32-PC and Me₂PE-C32-Me₂PE, a MTT-assay was carried out with these substances.

As described above, interesting results about the antifungal activity of irlbacholine (PC-C22-PC) were reported.^[4] Antifungal activity in combination with the hydrogelation properties would open a very interesting prospective for a practical application of the bolaamphiphiles. Therefore, an in-vitro test was performed in order to assess a potential antifungal activity for a number of different single-chain bolaamphiphiles.

2 Materials and methods

2.1 Materials

2.1.1. Bolaamphiphiles used in the present thesis

All bolaamphiphiles used in this thesis were synthesized in the group of Prof. B. Dobner (Department of Pharmacy, Martin-Luther-University Halle-Wittenberg). The investigations presented in this thesis were mainly focussed on dotriacontane-1,32-diyl-bis[2-(trimethylammonio)ethylphosphate] (PC-C32-PC) and dotriacontane-1,32-diyl-bis[2-(dimethylammonio)ethylphosphate] (Me₂PE-C32-Me₂PE, which are the most intensively characterized substances of the single-chain bolaamphiphiles.

Substitution of four CH₂ groups by a diacetylene group in the center of the alkyl chain lead to dotriacontane-15,17-diyn-1,32-diylbis[2-(trimethylammonio)ethylphosphate] (PC-C32diAc-PC, Figure 3.4.1) and dotriacontane-15,17-diyn-1,32-diylbis[2-(dimethylammonio)ethylphosphate] (Me₂PE-C32diAc-Me₂PE, Figure 3.4.1). These substances were used for the UV-polymerization attempts.

Me₂PE-C28-Me₂PE, Me₂PE-C34-Me₂PE and Me₂PE-C36-Me₂PE were used for reference measurements in the course of the NMR relaxation experiments.

Besides PC-C32-PC and Me₂PE-C32-Me₂PE, the antifungal activity was also tested for PC-C22-PC, Me₂PE-C22-Me₂PE, PC-C24-PC, Me₂PE-C24-Me₂PE, PC-C26-PC, Me₂PE-C26-Me₂PE, Me₂PE-C28-Me₂PE, PC-C30-PC, Me₂PE-C30-Me₂PE and PC-C11-S-C8-S-C11-PC.

2.1.2 Other materials

Buffer substances Sodium acetate, acetic acid, sodium carbonate and sodium hydrogencarbonate were purchased from Merck (Darmstadt, Germany), Riedel-de Haën (Seelze, Germany), Acros (New Jersey, U.S.A.), and Solvay Alkali GmbH (Rheinsberg, Germany), respectively.

Rheometry Silicon oil Nr. 1 (kinematic viscosity $\nu = 100 \text{ cSt} = 0.01 \text{ m}^2/\text{s}$) was from Roth (Karlsruhe, Germany).

NMR Sephadex G10, Sephadex G25, Sephadex G50, Sephadex G75, Sephadex G100 and 2-hydroxyethyl cellulose were purchased from Sigma Aldrich (Taufkirchen, Germany). D₂O was from Isotec Inc. (Miamisburg, USA).

ESR Tempolbenzoate, 5-DSA, 16-DSA and ascorbic acid were purchased from Sigma Aldrich (Taufkirchen, Germany). 12-DSA was from Chemos GmbH (Regenstauf, Germany).

MTT-assay A549 cells were from DSZM GmbH (Braunschweig, Germany). Cell culture media, fetal serum albumin, and phosphate buffered saline were supplied by PAA Laboratories GmbH (Cölbe, Germany). All other substances including 3-(4,5-dimethylthiazol-2-yl)-2,5-diphenyl-tetrazoliumbromid (MTT) were purchased from Sigma Aldrich (Taufkirchen, Germany).

Antifungal activity test *Candida albicans* and *Trichophyton rubrum*, inoculated on agar plates, were provided from internal test series by PD Dr. med. J. Wohlrab (Experimental Dermatology, Universitätsklinik, Martin-Luther-Universität Halle-Wittenberg).

2.2 Methods

2.2.1 Oscillatory rheometry

2.2.1.1 General remarks

Rheology is the science of flow and deformation of materials. Rheometry is the measuring technique, which is used to collect the rheological data. Viscosity measurements are mostly performed by means of rotational rheometry, whereas the (visco-)elastic behavior is investigated by performing creep tests, relaxation tests or oscillatory rheometry.

Since gels clearly belong to the visco-elastic materials, oscillatory rheometry was employed to collect rheological data for hydrogels formed by PC-C32-PC and Me₂PE-C32-Me₂PE.

Here, only a brief description of the measuring principle and the important definitions is given.

All figures and formula presented below were taken from Mezger.^[35]

2.2.1.2 Flow of viscous fluids

For ideally viscous fluids, the shear viscosity is independent of the applied shear stress.

The rheological parameters shear stress, shear rate and shear viscosity can be defined by using the two-plate model shown in Figure 2.2.1.

The upper plate with shear area A is moved by the shear force F . The resulting velocity v is measured. The bottom plate does not move ($v = 0$). Therefore, the sample is sheared by the shear stress between both plates. As a result, a shear gradient is observed. For ideally viscous fluids (Newtonian fluids), the shear viscosity is independent of the amplitude and time of the applied shear stress ($\tau \sim \dot{\gamma}$ with constant η).

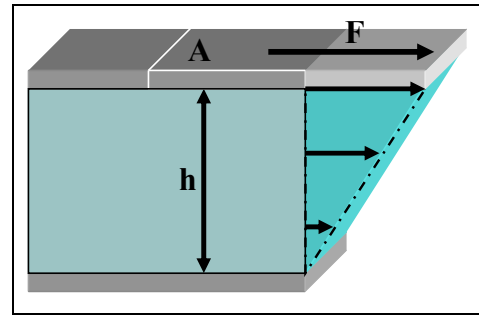


Figure 2.2.1 Two-plate model for the flow of fluids.

Definitions:

- shear stress τ :
$$\tau = \frac{F}{A} \text{ [Pa]} \quad (2.1)$$

- shear rate (shear gradient) $\dot{\gamma}$:
$$\dot{\gamma} = \frac{v}{h} \text{ [s}^{-1}\text{]} \quad (2.2)$$

- shear (dynamic) viscosity η :
$$\eta = \frac{\tau}{\dot{\gamma}} \text{ [Pas]} \quad (2.3)$$

2.2.1.3 Deformation of elastic materials

To define the parameters describing the deformation characteristics of elastic materials, it is again useful to use the two-plate model (Figure 2.2.2).

The upper plate with shear area A is moved by the shear force F . The resulting displacement s is measured. The bottom plate does not move ($s = 0$). Therefore, the sample is sheared by the shear stress between both plates.

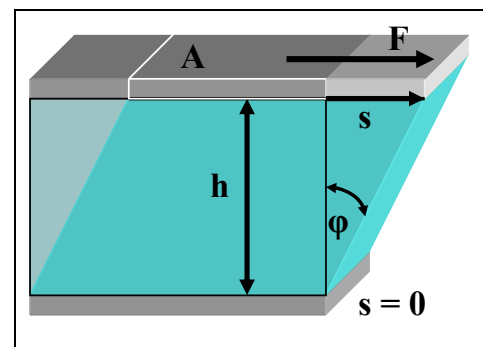


Figure 2.2.2 Two-plate model for the deformation of elastic materials.

- deformation (strain) γ :
$$\gamma = \frac{s}{h} = \tan \varphi \text{ [1; \%]} \quad (100\% : s = h \text{ or } \varphi = 45^\circ) \quad (2.4)$$

- shear modulus G :
$$G = \frac{\tau}{\gamma} \text{ [Pa]} \quad (2.5)$$

- shear rate $\dot{\gamma}$:
$$\dot{\gamma} = \frac{\Delta\gamma}{\Delta t} = \frac{\gamma_1 - \gamma_0}{t_1 - t_0} = \frac{d\gamma}{dt} \text{ [s}^{-1}\text{]} \quad (2.6)$$

In the reversible region (linear-elastic region), G represents a material constant and gives information about the rigidity of the material. Higher intermolecular attraction increases the rigidity of the material and the resulting G value is increased.

2.2.1.4 Oscillatory rheometry

Oscillatory rheometry can be used to investigate all visco-elastic materials ranging from low-viscous fluids, pastes, gels or polymer melts to elastomers or rigid solids.

Although a cone/plate measuring system was used for the rheological investigations described below, it is again helpful to use the two-plate model in order to describe the oscillation experiment and to define the parameters (Figure 2.2.3).

In the two-plate model for the oscillation experiment, a rotating wheel (left) is connected to the upper plate by a push rod. Therefore, the upper plate with area A is moved back and forth by the shear force $\pm F$. The bottom plate does not move and the sample is sheared between both plates. The applied shear stress is $\pm\tau = \pm F/A$ (Equation 2.1) and the

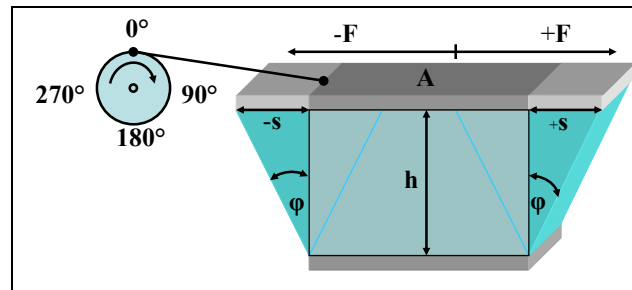


Figure 2.2.3 Two-plate model for the oscillation experiment.

resulting deformation is $\pm\gamma = \pm s/h$ (Equation 2.4). If a controlled deformation is applied to the sample by moving the upper plate, the resulting shear stress is measured at the bottom plate.

Ideally elastic materials

- complex shear modulus G^* :
$$G^* = \frac{\tau(t)}{\gamma(t)} [\text{Pa}] \quad (2.7)$$

In oscillatory rheometry, the complex shear modulus G^* represents information about the rigidity of the sample, *i.e.* about the resistance of the sample to deformation.

In the case of a full rotation of the wheel, the rotation angle is 360° and determines the length of one oscillation period of the functions $\tau(t)$, $\gamma(t)$ and $\dot{\gamma}(t)$. At angles of 0° and 180° , the plate is in its zero-position and $\tau = 0$, $\gamma = 0$ and $\dot{\gamma} = \dot{\gamma}_{\text{max}}$. At angles of 90° and 270° , the plate displacement is at its maximum ($\tau = \tau_{\text{max}} = \tau_A$, $\gamma = \gamma_{\text{max}} = \gamma_A$, $\dot{\gamma} = 0$).

The sinusoidal deformation function $\gamma(t)$ can be written as

$$\sin \gamma = \gamma_A \sin \omega t \quad (2.8)$$

where γ_A [%] and ω [s^{-1}] are the deformation amplitude and the angular frequency, respectively.

In the linear-elastic region, G^* is constant. Therefore, the shear stress function $\tau(t)$ is always in-phase with the sinusoidal deformation function $\gamma(t)$, whereas the shear rate function $\dot{\gamma}(t)$ is shifted with respect to $\gamma(t)$ by 90° (Figure 2.2.4A). For ideally elastic materials, no phase shift is observed between the sinusoidal functions $\tau(t)$ and $\gamma(t)$ and, as a consequence, the angle for the phase shift δ is 0° .

Ideally viscous materials

- complex viscosity η^* :
$$\eta^* = \frac{\tau(t)}{\dot{\gamma}(t)} [\text{Pa s}] \quad (2.9)$$

In oscillatory rheometry, the complex viscosity η^* represents information about the resistance of the sample to flow.

In the linear visco-elastic region (LVE-region), the complex viscosity is constant.

Therefore, $\tau(t)$ is in-phase with $\dot{\gamma}(t)$ and both are synchronous cosines if $\gamma(t)$ is displayed as a sinusoidal function (Figure 2.2.4B). Consequently, the delay of $\tau(t)$ with respect to $\gamma(t)$ is described by a phase shift angle δ of 90° .

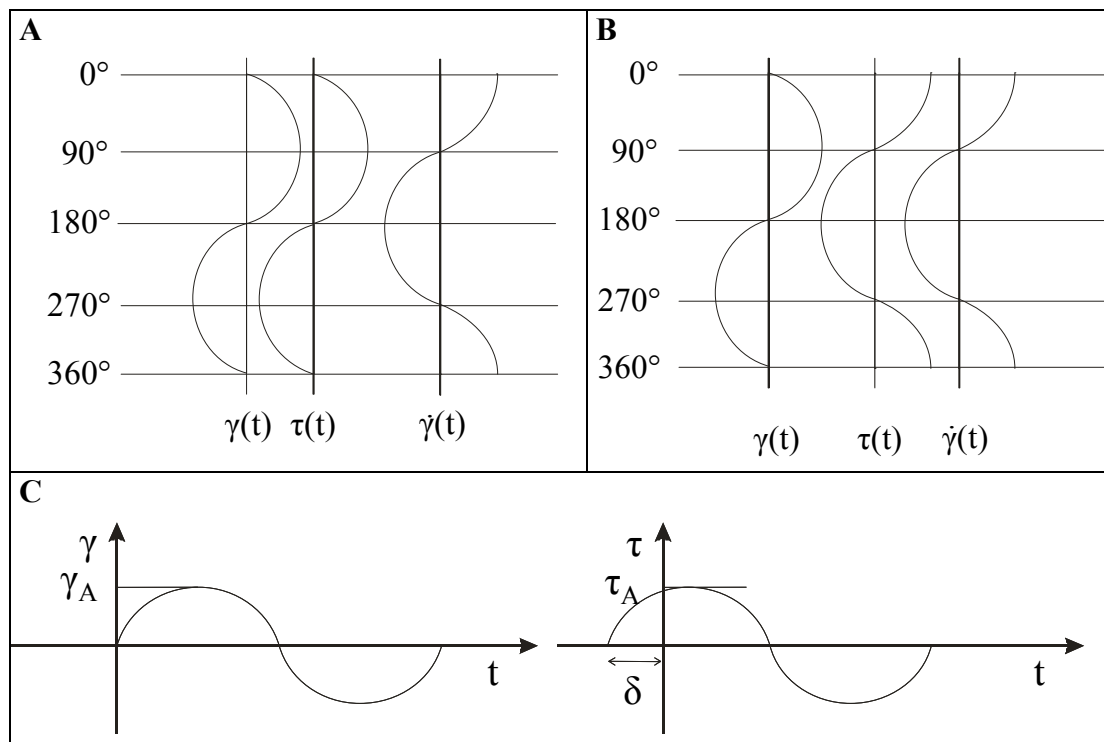


Figure 2.2.4 The functions $\tau(t)$, $\gamma(t)$ and $\dot{\gamma}(t)$ for (A) ideally elastic and (B) ideally viscous materials. (C) Determination of the phase shift angle δ .

Visco-elastic behavior

In the case of a rheometer that works in the controlled shear deformation (CSD) mode, a well defined deformation γ is applied to the sample as the sinusoidal function $\gamma(t) = \gamma_A \sin \omega t$. The resulting phase shifted sinusoidal function $\tau(t) = \tau_A \sin (\omega t + \delta)$ is measured, in which δ is the phase shift angle between the $\gamma(t)$ and the $\tau(t)$ functions (Figure 2.2.4C). This phase shift angle is lying in the range from 0° (ideally elastic materials) to 90° (ideally viscous fluids).

Definitions:

- storage modulus G' :
$$G' = \frac{\tau_A}{\gamma_A} \cos \delta \quad [\text{Pa}] \quad (2.10)$$

The storage modulus G' represents the elastic behavior of the sample and gives information about the stored part of the deformation energy. After the relief of the strain, this part will cause a partial re-deformation to the original state. For ideally elastic materials, G' has its maximum value G'_{\max} ($\cos 0^\circ = 1$), whereas for ideally viscous fluids, it is 0 ($\cos 90^\circ = 0$). The storage modulus G' is often used as a parameter describing the “structure strength” or “consistency” of the samples. In the case of gels, a larger G' value is indicating a more cross-linked network, *i.e.* a stronger gel.

- loss modulus G'' :
$$G'' = \frac{\tau_A}{\gamma_A} \sin \delta \quad [\text{Pa}] \quad (2.11)$$

The loss modulus G'' represents the viscous behavior of the sample and gives information about the lost part of the deformation energy. After the relief of the strain, this part will not contribute to the partial re-deformation back to the original state. For ideally elastic materials G'' is 0 ($\sin 0^\circ = 0$), whereas for ideally viscous fluids, it reaches its maximum G''_{\max} ($\sin 90^\circ = 1$).

- loss factor $\tan \delta$:
$$\tan \delta = \frac{G''}{G'} \quad [1] \quad (2.12)$$

The loss factor $\tan \delta$ represents the ratio between the viscous and the elastic behavior of a sample. The value for $\tan \delta$ will be 0 for ideally elastic behavior ($\tan 0^\circ = 0$), 1 for $G'' = G'$ ($\tan 45^\circ = 1$) and ∞ for ideally viscous behavior ($\tan 90^\circ = \infty$).

The visco-elastic behavior of all real materials will contain a viscous and an elastic part. The vectorial sum G^* of G' and G'' is called the complex shear modulus. G^* can be calculated with the Pythagorean theorem (Figure 2.2.5).

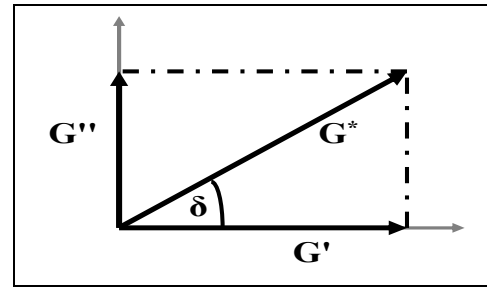


Figure 2.2.5 Vector diagram relating G' and G'' to G^* .

- complex shear modulus G^* :
$$|G^*| = \sqrt{(G')^2 + (G'')^2} \quad [\text{Pa}] \quad (2.13)$$

Instead of G^* , one can also use the complex viscosity η^* .

- complex viscosity η^* :
$$|\eta^*| = \frac{\tau_A}{\dot{\gamma}_A} = \frac{|G^*|}{\omega} \quad [\text{Pa s}] \quad (2.14)$$

2.2.1.5 Experimental part

Instrumentation

All rheological investigations were carried out with a Physica MCR 301 rheometer (Anton Paar Germany, Ostfildern) using a cone/plate measuring system. This rheometer works in the controlled shear deformation (CSD) mode and is equipped with a Peltier element for temperature control including an actively heated Peltier hood to prevent temperature gradients in the samples.

A schematic representation of the cone/plate measuring system is given in Figure 2.2.6. It consists of a measuring device with a cone shaped surface and the stationary plate. A 50 μm part of the top of the cone is removed in order to prevent friction. Therefore, the distance between cone and plate has to be carefully adjusted to 50 μm , which is automatically done by the Physica MCR 301 rheometer. The geometry of the cone can be described by its diameter $d = 2r = 49.935 \text{ mm}$ and by the angle α of 1.983° .

The advantage of the cone/plate measuring system is that the shear rate $\dot{\gamma}$ is constant throughout the sample, which is not the case for other measuring geometries. A defined deformation γ is applied to the sample by oscillation of the cone and the resulting torque M is measured at the bottom plate. The shear stress τ can be calculated from this torque M and

radius r :
$$\tau = \frac{3M}{2\pi r^3} \quad [\text{Pa}] \quad (2.15)$$

The rheometer calculates the $\tau(t)$ function and its phase shift angle δ with respect to the applied $\gamma(t)$ function, which enables the calculation of the rheological parameters G' , G'' , G^* , η^* and $\tan \delta$.

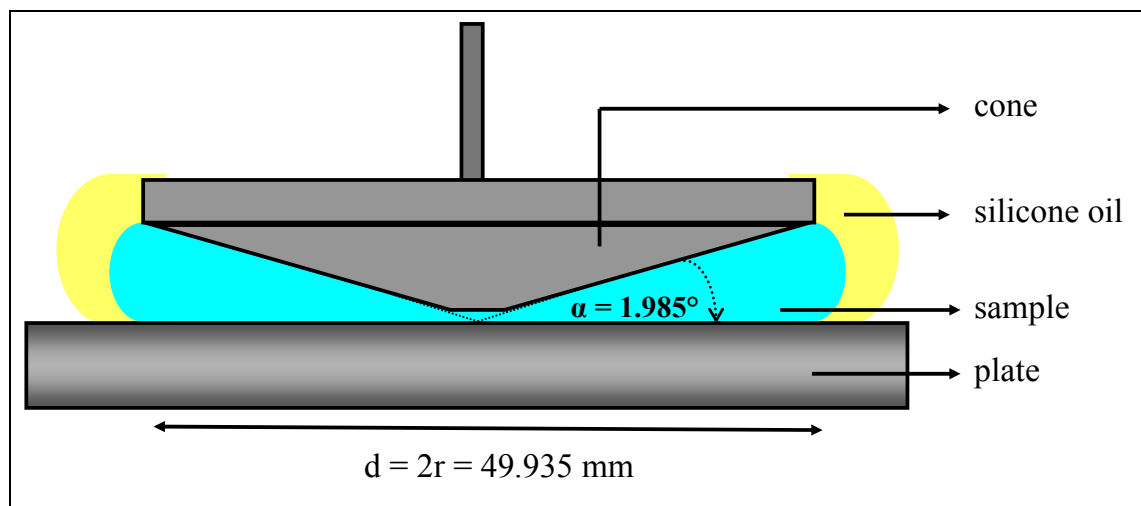


Figure 2.2.6 Schematic representation of the cone/plate measuring system including the sample and silicone oil.

Sample preparation

Hydrogels with 1, 2, 4 or 8 mg/ml PC-C32-PC were prepared by weighing the appropriate amount of the bolaamphiphile into a small glass vessel. After addition of deionized water, the sample was heated in a water bath at a temperature above 80 °C for at least one minute followed by thorough vortexing. This procedure was repeated until a homogeneous dispersion was achieved. Upon cooling, a hydrogel was obtained and stored between 2 and 8 °C for 24 hours. For Me₂PE-C32-Me₂PE, the preparation was the same, but acetate buffer pH 5 was used instead of deionized water .

Sample loading

The samples were gently loaded onto the plate of the rheometer with a spatula in order not to destroy too many cross-links. However, this process and the dipping in of the cone are imposing significant mechanical stress on the sample. Therefore, a waiting period is required prior to the measurements after filling the sample into the gap. During this waiting time, it is useful to determine the G' value until it remains constant instead of increasing with time. The sample volume required for evenly filling the gap between cone and plate is approximately 1.5 ml. In order to prevent water evaporation during the measurements, a thin layer of low viscous silicon oil Nr. 1 (Roth, Karlsruhe; kinematic viscosity $\nu = 100 \text{ cSt} = 0.01 \text{ m}^2/\text{s}$) was placed around the sample as indicated in Figure 2.2.6.

Amplitude sweep test

Amplitude sweep tests are performed in order to determine the LVE-region. In the LVE-region, the G' and G'' values are nearly constant, which is indicating that the internal structures are not destroyed by the measurements. Therefore, all rheometric investigations should be performed inside the LVE-region.

In the amplitude sweep experiment, the measuring frequency is held constant and the amplitude of the applied deformation is varied over a wide range. The LVE-region ends, when the G' and G'' values start to deviate from their plateau values due to distinct structural changes inside the sample as a result of the applied mechanical stress. For the amplitude sweep tests, the angular frequency ω was either 1 or 10 rad/s. The deformation was varied over three decades from 0.3% to 300%, where 100% deformation corresponds to a deflection angle ϕ of 45° (Equation 2.4). The G' and G'' values were calculated automatically by the rheometer software Rheoplus (Anton Paar Germany, Ostfildern) using the equations 2.10 and 2.11.

Qualitatively, the obtained results of the amplitude sweep tests were found to be very similar for PC-C32-PC and Me₂PE-C32-Me₂PE and also for all investigated concentrations. Only the obtained values for G' and G'' vary between the different samples. The result of a representative amplitude test, carried out with a hydrogel with 2 mg/ml PC-C32-PC, is displayed in Figure 2.2.7. The storage and loss moduli have a plateau value up to about 10% deformation. A further increase of the deformation causes significant changes in the internal structure and finally results in a breakdown of the macroscopic hydrogel state at a deformation of about 75%. Therefore, the deformation of 10% can be regarded as the boundary of the LVE-region. In order to perform the frequency sweep tests well inside the LVE-region, a value of 1% for the deformation was chosen for all experiments discussed below.

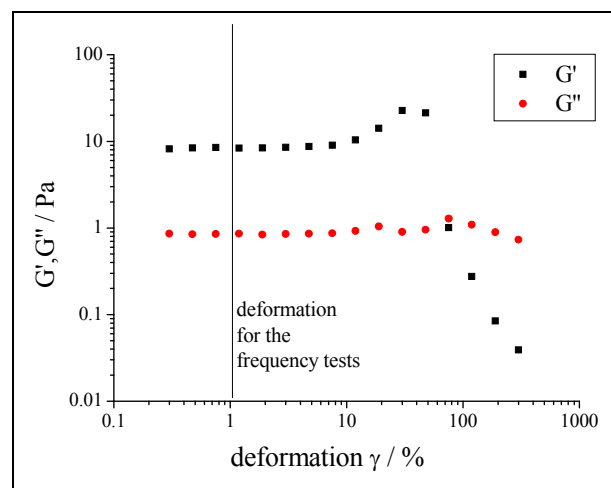


Figure 2.2.7 2 mg/ml PC-C32-PC in deionized water: Results of the amplitude sweep test at 10 rad/s. As is indicated, a deformation of 1% was chosen for all frequency sweep tests.

Frequency sweep test

In the frequency sweep experiment, the deformation is held constant and the frequency is varied. In this work, frequency tests were used to study the concentration and temperature dependence of the aqueous samples of PC-C32-PC and Me₂PE-C32-Me₂PE. A deformation of 1% was used for all frequency tests. The angular frequency ω was varied only from 1 to 10 rad/s in order to minimize the time required for one experiment. All G' and G'' values presented below are average values of three measurements.

Time dependent rheometry upon cooling from 75 °C

The time dependent experiments after a heating-cooling-cycle were carried out as follows: The hydrogel sample was placed between cone and plate and covered by silicone oil as described above. The fiber network was completely destroyed by heating the samples to 75 °C for at least 15 minutes. Afterwards, the samples were cooled down to 25 °C. The rheometer is equipped with a Peltier element, which allows rapid cooling of the sample. The cooling rate was about 15 K/min. For the time dependent measurement of G', a constant deformation of 1% and a constant angular frequency of 1 rad/s were used. The time tests were always started, when the decreasing temperature reached 50 °C (t = 0 min) and after one minute, the first G' value was measured at about 35 °C (G'_{1min}). When the second G' value was measured after two minutes (G'_{2min}), the temperature display already showed 25 °C. The G' values for the first 60 minutes were determined for PC-C32-PC and Me₂PE-C32-Me₂PE at different concentrations.

Time dependent rheometry after mechanical stress

A simple test was carried out for studying the self-healing properties of the self-assembled bolaamphiphile network at 25 °C. For this purpose, considerable mechanical stress was applied on samples with 2 mg/ml of the particular bolaamphiphile at a temperature of 25 °C. This was realized by performing an amplitude test with deformations up to 300%, which cause a complete breakdown of the elastic moduli to values that correspond to that of pure water. The time test was started immediately after the amplitude test, and the first G' value was measured after 1 minute. Again, the G' values were determined over a time period of 60 minutes.

2.2.2 Nuclear magnetic resonance (NMR) spectroscopy

2.2.2.1 General remarks

NMR spectroscopy is a very powerful tool for a wide variety of scientific investigations. It can be used, for example, to determine the exact chemical structure of a substance, to study reaction kinetics, to investigate the dynamics of molecules in solution or to perform three-dimensional imaging of organs.

The nucleus of an atom must possess a non-zero ground state nuclear spin to be detectable by NMR. Fortunately, there are many of these atoms such as ^1H , ^2H , ^{13}C , ^{15}N , ^{17}O and ^{31}P .

Here, only a brief description of the basic principles of NMR and the performed experiments is given. Most of the definitions, formula and diagrams used here were taken from Levitt^[36] and Winter/Noll.^[37] For further reading see, for example, the books of Kimmich^[38] or Abragam.^[39]

2.2.2.2 Spin

A rotating object possesses a quantity called angular momentum. In quantum mechanics, angular momentum is quantized. Spin is also a form of angular momentum. However, it is not produced by a rotation of the particle, but is an intrinsic property of the particle itself. Most of the nuclear isotopes possess spin. The nuclear spin quantum number is denoted as I . ^1H , the main isotope of hydrogen, contains only a single proton with $I = 1/2$ and therefore its value for I is $1/2$, too. The spins of other nuclei are formed by combining the spins of the protons and neutrons. The value of I in the lowest energy state is called the ground state nuclear spin, which may be one of a large number of possible spin configurations. The ground state nuclear spin is an empirical property of each isotope.

A second spin quantum number, m_S , is specified. It characterizes the $(2I+1)$ possible orientations of the nuclear spin in the magnetic field. Therefore, only two orientations are possible in the case of $I = 1/2$.

In the absence of an external magnetic field, the $2I+1$ states with the same value of I , but different values of $m_S = -I, -I+1, \dots, +I$ have the same energy, the states are degenerate.

The application of a magnetic field breaks the degeneracy, causing each of the $2I+1$ states to have a slightly different energy. This is called the Zeeman effect. The energy separation between the m_I sublevels in a magnetic field is called the Zeeman splitting. This is shown in Figure 2.2.8 for a single spin with $I = 1/2$ and a positive magnetogyric ratio (e.g. ^1H), which can adopt two states, the α - ($+1/2$) and the β -state ($-1/2$). A spin, which is in the α -state, is said to be polarized along the Z -axis, whereas a spin in the β -state is polarized along the $-Z$ -axis.

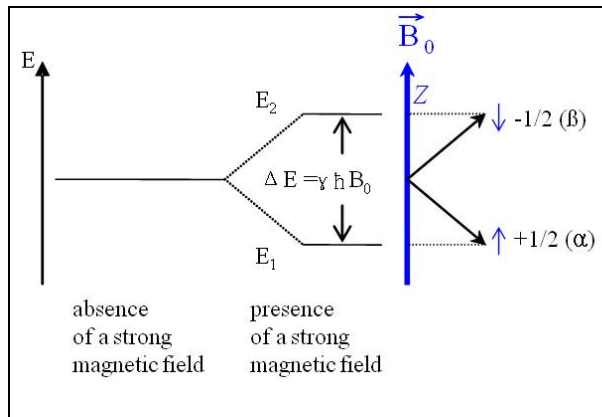


Figure 2.2.8 Zeeman splitting caused by the presence of a strong magnetic field with \vec{B}_0 , shown for a single spin with $I = 1/2$ and a positive magnetogyric ratio.

2.2.2.3 Magnetism

In the classical description, every point of space in the electromagnetic field is associated with two vectors, \vec{E} and \vec{B} . The electric field \vec{E} interacts with electric charges and the magnetic field \vec{B} interacts with magnetic moments. The magnetic moments are the result of the movement of electric charges. The magnitude of the magnetic field is specified in units of T (tesla) or G (gauss). The conversion is as follows: $1 \text{ G} = 10^{-4} \text{ T}$

Magnetism simply is the capability to interact with magnetic fields. This interaction is usually expressed in terms of a magnetic moment μ . The magnetic energy of a small object depends on the interaction of its magnetic moment with the \vec{B} field: $E_{\text{mag}} = -\mu \vec{B}$. Therefore, the magnetic energy has its lowest value if the magnetic moment μ is parallel to the \vec{B} field. The magnetic moment can be permanent (for example a compass needle) or only present, when it is induced by an external magnetic field.

There are three sources of magnetism: (I) The circulation of electric currents, (II) the magnetic moments of electrons and (III) the magnetic moments of nucleons. The electronic contributions (I) and (II) are many orders of magnitude larger than the nuclear contribution (III). In diamagnetic substances, contribution (I) is larger than contribution (II) and (III), because the pairing of the electrons cancels out the magnetic moments of the electrons. On the other hand, the strong magnetism of paramagnetic and ferromagnetic materials is due to unpaired electrons.

Electrons and nuclei both possess intrinsic magnetism, which is not due to a circulating current. This means that they simply ‘have’ a magnetic moment, just like they simply ‘have’ spin angular momentum. Spin and magnetism are very closely linked:

$$\mu = \gamma S \quad (2.16)$$

The proportionality constant γ is called the magnetogyric ratio and specified in units of rad/sT. The magnetogyric ratio may have either sign. For particles with positive values (most atomic nuclei), the magnetic moment μ is parallel to the total spin angular momentum S . For particles with negative γ (electrons and some atomic nuclei), μ is opposite in direction to S .

2.2.2.4 Spin precession and Larmor frequency

The spin angular momentum of a particle is a vector. Here, the direction of the spin angular momentum is called the spin polarization axis. In general, particles with spin have spin polarization axes pointing in all possible directions (Figure 2.2.9A). If no external magnetic field is present and the sample is in equilibrium, the distribution of the magnetic moments is completely isotropic, which means that all possible directions are equally represented.

What happens to the spin magnetic moments if an external magnetic field is suddenly applied? A compass needle will rotate, so as to bring the magnetic moment parallel to the field in order to minimize the magnetic energy. However, a nuclear spin is not a compass needle and possesses an angular momentum besides the magnetic moment. As a result, the response of the spin polarization is to move around the field, which causes the magnetic moment to move on a cone, keeping a constant angle with respect to the magnetic field. This motion is called spin precession. The angle of the cone only depends on the initial spin polarization as is outlined in Figure 2.2.9B. If the spin is initially polarized exactly along or against the magnetic field, it will simply stay there. If the spin is initially polarized exactly perpendicular to the field, the spin polarization will move on a flat disk. For the majority of spins, the angle is intermediate between these extremes.

The frequency of precession is the Larmor frequency ω_0 . It is proportional to the applied magnetic field:

$$\omega_0 = -\gamma \vec{B}_0 \text{ [rad/s]} \quad (2.17)$$

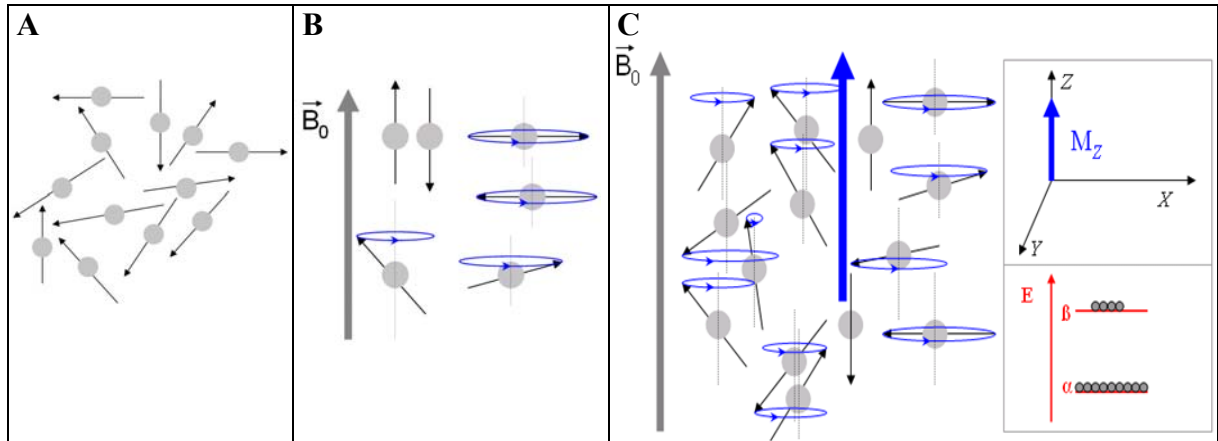


Figure 2.2.9 Development of a longitudinal magnetization by applying a magnetic field \vec{B}_0 :
(A) Isotropic distribution of the nuclear spin polarization axes in the absence of an external magnetic field.
(B) Schematic representation of the spin precession in the presence of a strong magnetic field.
(C) Longitudinal magnetization $M_{Z(\text{eq})}$ at thermal equilibrium due to anisotropic distribution of the polarization axes ($N_\alpha > N_\beta$).

2.2.2.5 Longitudinal magnetization and longitudinal relaxation

In the absence of a magnetic field, a sample of water contains many proton nuclei with uniformly distributed spin polarizations. As a result, the total magnetic moment of the sample is very close to zero. If a magnetic field is suddenly applied, all proton spins begin executing Larmor precession around the field. This precessional motion is essentially invisible and does not change the total magnetic moment, since the spin polarizations are still isotropically distributed. In addition to the precessional motion, the water molecules undergo vigorous motion that constantly changes the positions and orientations of all molecules. These motions slightly influence the nuclear magnets, because their environment is full of nuclei and electrons, which are all sources of magnetic fields. These fields are small and fluctuate rapidly. Therefore, a nuclear spin at any given time t precesses about a magnetic field $\vec{B}_{\text{tot}}(t)$, which is a sum of the static external field \vec{B}_0 and a very small fluctuating microscopic field $\vec{B}_m(t)$:

$$\vec{B}_{\text{tot}}(t) = \vec{B}_0 + \vec{B}_m(t) \quad (2.18)$$

As a consequence, the total magnetic field experienced by each spin has a slightly fluctuating magnitude and also a slightly fluctuating direction. This is very important, since it allows the isotropy to be broken and a macroscopic nuclear magnetic moment to develop. The spin polarization of a single spin is fluctuating over time. This wandering motion is not completely isotropic, but it is slightly more probable that the spin is driven towards an orientation with lower magnetic energy than to an orientation with higher magnetic energy. This leads to a

stable anisotropic distribution of the spin polarizations with slightly more magnetic moments along the direction of the external magnetic field than opposed to it. As a result, a net magnetic moment has developed in the direction of the field \vec{B}_0 (Z-direction by convention, see Section 2.2.3), denoted as longitudinal magnetization M_Z (Figure 2.2.9C). No net magnetization is found in X- or Y-direction ($M_X = M_Y = 0$), since no differences in the magnetic energies are present in these directions. The anisotropy of the polarization distribution is directly proportional to the ratio of the magnetic and thermal energies and is given by the Boltzmann distribution:

$$\frac{N_\beta}{N_\alpha} = e^{-\Delta E/k_B T} \quad (2.19)$$

where N_α and N_β are the numbers of spins in the low- (α) and the high-energy state (β), $k_B = 1,38066 \cdot 10^{-23}$ J/K is the Boltzmann constant and T is the temperature. ΔE is the energy difference between the α - and β -state (Figure 2.2.8). A spin in the α -state is said to be polarized along the Z-axis, whereas a spin in the β -state is polarized along the $-Z$ -axis. For the majority of spins, the polarization angle is intermediate between these extremes, but there will be slightly more spins pointing in Z-direction compared to the $-Z$ -direction. The population difference is exceedingly small at ordinary temperatures and fields, namely about 1 part in 10^5 . This means that at thermal equilibrium, there is only a very slight polarization of the spin angular momentum vectors along the direction of the external magnetic field.

If the external magnetic field is suddenly turned on, the longitudinal magnetization is initially zero, but gradually grows exponentially towards $M_{Z(\text{eq})}$, its value at thermal equilibrium:

$$M_Z(t) = M_{Z(\text{eq})} (1 - e^{-t/T_1}) \quad (2.20)$$

The exponential time constant T_1 is called longitudinal relaxation time constant or spin-lattice relaxation time constant. The term ‘longitudinal’ simply indicates that the magnetization builds up in the same direction as the applied magnetic field. The relaxation time constant T_1 takes into account the drift of the populations towards their thermal equilibrium values. T_1 depends on the nucleus and on various parameters such as the temperature and the viscosity of the sample.

2.2.2.6 Transverse magnetization and transverse relaxation

The longitudinal nuclear spin magnetization parallel to the Z-axis is almost undetectable, since it is too small compared to \vec{B}_0 . In NMR, the magnetization perpendicular to the applied field is therefore measured. As noted above, there is no net nuclear magnetization present

perpendicular to the applied field. By applying a small radiofrequency (rf) pulse, the polarization of every single spin can be rotated by the same angle of $\pi/2$ radians around the X -axis. Therefore, the pulse also rotates the entire nuclear magnetization distribution of the sample and a net magnetization M_Z is transferred into a net magnetization along the $-Y$ -axis (Figure 2.2.12). This net magnetic moment perpendicular to the applied magnetic field is called transverse magnetization (M_{XY}). Since every single spin precesses, the bulk magnetic moment precesses, too and the nuclear magnetization rotates in the XY -plane, perpendicular to the applied magnetic field. The transverse magnetic moment precesses at the nuclear Larmor frequency ω_0 and decays slowly at the same time:

$$M_Y(t) = -M_{Z(\text{eq})} \cos(\omega_0 t) e^{-t/T_2} \quad (2.21)$$

$$M_X(t) = -M_{Z(\text{eq})} \sin(\omega_0 t) e^{-t/T_2} \quad (2.22)$$

The exponential time constant T_2 takes into account the homogeneous decay of the precessing macroscopic nuclear magnetization. It is called transverse relaxation time constant or spin-spin relaxation time constant. The transverse magnetization decays, because it is impossible to maintain exact synchrony between the precessing nuclear magnets. As described above, the microscopic magnetic fields fluctuate slightly. Therefore, different spins will precess with slightly different frequencies after the rf pulse. As a result, the precessing nuclear magnets get out of phase with each other. In order to visualize this, one can assume a large number of clocks that show exactly the same time at the beginning. This means that they are in phase with each other. Small fluctuations in the timing of the different clocks will lead to a loss of synchrony with time. After a very long period, the times shown by the clocks may be completely random. This means that the clocks will have completely lost coherence with each other.

2.2.2.7 NMR signal and NMR spectroscopy

The precessing transverse magnetization after a rf pulse is very small, but detectable, because it oscillates at a very well-defined frequency. In practice, a wire coil is placed near the sample with the winding axis perpendicular to the external magnetic field. The rotating magnetic field is inducing a small oscillating current in this coil, which can be detected by a sensitive radiofrequency detector. The resulting NMR signal is called free-induction decay (FID).

A NMR spectrometer is basically a device capable of (1) magnetizing the nuclear spins with a large applied magnetic field, (2) rotating the spin polarizations by rf pulses to produce transverse magnetizations, and (3) detecting the small oscillating currents induced by the

precessing transverse spin magnetization. After detecting the FID, Fourier transformation is performed and generates a function of the following mathematical form:

$$S(\omega) = \frac{\lambda}{\lambda^2 + (\omega - \omega_0)^2} \quad (2.23)$$

The value of $S(\omega)$ is at a maximum, when the frequency coordinate ω is equal to the Larmor frequency ω_0 . The parameter λ is called the coherence decay rate constant and is equal to the

inverse of T_2 :
$$\lambda = \frac{1}{T_2} \quad (2.24)$$

The function of Equation 2.23 is called an absorption Lorentzian. The Lorentzian peakshape has a finite width. As outlined in Figure 2.2.10, the peakwidth at half-height, measured in rad/s, is equal to $2/T_2 = 2\lambda$.

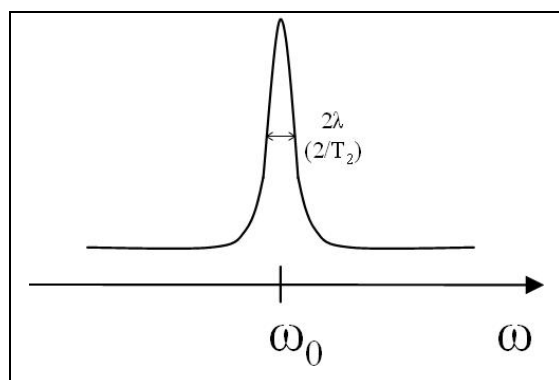


Figure 2.2.10
Schematic representation of a NMR spectrum.

2.2.2.8 Relaxation

Relaxation is the process, by which an equilibrium state is regained, for example, after disturbing it by a rf pulse. The underlying mechanisms of NMR relaxation are very complex. Therefore, only some basic principles of the relaxation processes are outlined below.

To describe an ensemble of isolated spins with $I = 1/2$, only two time constants for the relaxation processes are needed, namely T_1 for the equilibration of populations ($M_Z \rightarrow M_{Z(\text{eq})}$) and T_2 for the decay of single-quantum coherences ($M_{XY} \rightarrow 0$). Both relaxation processes require fluctuating magnetic fields of proper frequency to be effective. There are different sources of local magnetic fields that are capable of causing relaxation:

- direct dipole-dipole coupling between two nuclear spins
- quadrupole couplings for nuclei with $I \geq 1$
- chemical shift anisotropy
- spin rotation
- J coupling

For spins with $I = 1/2$ like ^1H , the dipole-dipole relaxation mechanism usually dominates the relaxation. Dipole-dipole relaxation is due to the fact that each nucleus is magnetic and generates a small magnetic field. A second nucleus interacts with this magnetic field. The coupling can be intra- or intermolecular and will depend on the distance between the two nuclei. In a liquid, the magnetic fields, exerted by the nuclei on each other, are modulated by the random molecular tumbling. The correlation time τ_c of these random fields corresponds to the rotational correlation time τ_R of the molecules. τ_R is the average time taken for the molecules to rotate by one radian. Depending on the molecule size, the viscosity and the temperature, the mean correlation time of the fluctuating magnetic fields will change and thus the relaxation rate.

Quadrupole couplings are only found in nuclei with $I \geq 1$ that exhibit an electric quadrupole moment. An electric quadrupole moment interacts strongly with the surrounding electric field gradients, generated by the electron clouds. For these nuclei, the quadrupolar mechanism is therefore often dominating the relaxation. The chemical shift anisotropy becomes increasingly important at high magnetic fields. The applied magnetic field induces currents in the electron clouds in the molecule and these currents, in turn, generate fluctuating magnetic fields. These induced fields are small, but large enough to cause measurable shifts in the spin precession frequencies. The spin rotation mechanism is of minor importance for the relaxation in liquids, but often dominates the relaxation in gases. Rotation of the molecules causes a circulation of the charged nuclei and electrons, which corresponds to a small electric current that is associated with a fluctuating local magnetic field. The J coupling is an indirect dipole-dipole coupling between nuclear spins with the participation of the bonding electrons. It is exclusively intramolecular.

As written above, the relaxation time constants T_1 and T_2 are sensitive to the mobility of the particular nuclei. The effect of molecular mobility on the relaxation processes was first quantitatively described by Bloembergen, Purcell and Pound.^[40] An excellent description of the derivation was given by Abragam.^[39]

The mobility of the molecules can be taken into account by the autocorrelation function $G(\tau)$. It describes, how long the motional state of a nucleus is correlated with its previous state. The autocorrelation function is often assumed to have the form of a decaying exponential:

$$G(\tau) = e^{-\tau/\tau_R} \quad (2.25)$$

The Fourier transform of $G(\tau)$ is the spectral density function $J(\omega)$:

$$J(\omega) = \frac{2\tau_R}{1 + \omega^2\tau_R^2} \quad (2.26)$$

If the spectral density function has a large value at the frequency required for relaxation, the relaxation will be very rapid and the relaxation time will be short.^[41] If the mobility is high, the correlation time τ_R is short and the spectral density function has a uniformly low value over a wide range of frequencies. This means that relaxation is not very efficient and T_1 and T_2 have similarly large values (Figure 2.2.11). As the correlation time increases, the spectral density function increases in intensity, but the range of frequencies decreases. Since longitudinal and transverse relaxation require fluctuating magnetic fields of different frequencies, the behavior of T_1 and T_2 as a function of τ_R is qualitatively different. Longitudinal relaxation requires the transition of nuclear spins from their β - to their α -state in order to reestablish the magnetization $M_{Z(\text{eq})}$ at thermal equilibrium. This transition requires fluctuating magnetic fields at the Larmor frequency and will be most efficient if $J(\omega)$ has a relatively large value at the Larmor frequency. Therefore, with decreased mobility, T_1 first decreases up to a minimum corresponding to $1/\omega_0$ and then increases monotonically again. Transverse relaxation is the loss of coherences and leads to the decay of the precessing transverse magnetization. This can occur by low-energy transitions, for example, when two spins exchange positions in their α - and β -states, respectively. The transverse relaxation is most efficient if the spectral density function has a relatively large value at low frequencies. Therefore, with decreased mobility, T_2 decreases continuously (Figure 2.2.11).

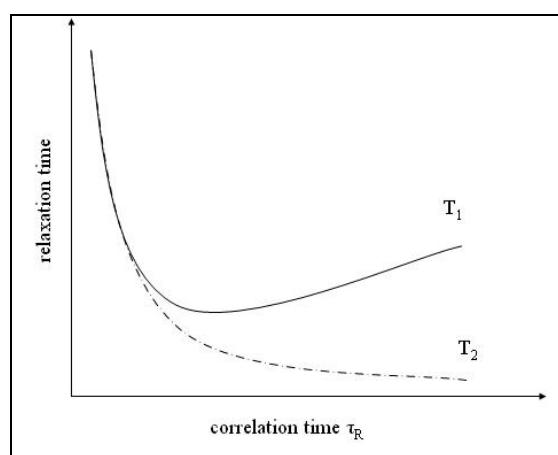


Figure 2.2.11
Effect of the molecular mobility, characterized by the correlation time τ_R , on the relaxation times T_1 and T_2 .

2.2.2.9 Experimental part

Instrumentation

All ^1H -NMR measurements were carried out with a low field benchtop Maran Ultra ^1H -NMR spectrometer (Oxford Instruments, Abingdon, UK). The spectrometer is equipped with an air flow temperature regulation and a 3D imaging unit.

¹H-NMR relaxometry – measurement of transverse relaxation times

¹H-NMR relaxometry is not dealing with detecting NMR spectra, but only with the measurement of relaxation time constants. These experiments are performed by applying simple pulse sequences and often do not require superconducting magnets. The determination of the relaxation behavior of protons in H₂O can provide unique information about the motion and dynamics of the water molecules inside the investigated sample.

As indicated in Figure 2.2.10, the transverse relaxation time constant T_2 could be measured by determining the width of the spectral peak. However, the peak width is not only determined by T_2 , but there is also an appreciable contribution caused by magnetic field inhomogeneities. Therefore, Hahn^[42] introduced the spin echo method, which applies a series of 90° and 180° pulses. In order to circumvent the effect of diffusion, Carr and Purcell^[43] used a single 90° pulse followed by a series of 180° pulses. This method was modified by Meiboom and Gill^[44] so as to eliminate the necessity of the accurate adjustment of the 180° pulses and to improve the reproducibility. Therefore, the method of detecting spin echos for the determination of T_2 is known as the Carr-Purcell-Meiboom-Gill (CPMG) method. The CPMG pulse sequence and the resulting NMR signal is shown in Figure 2.2.12.

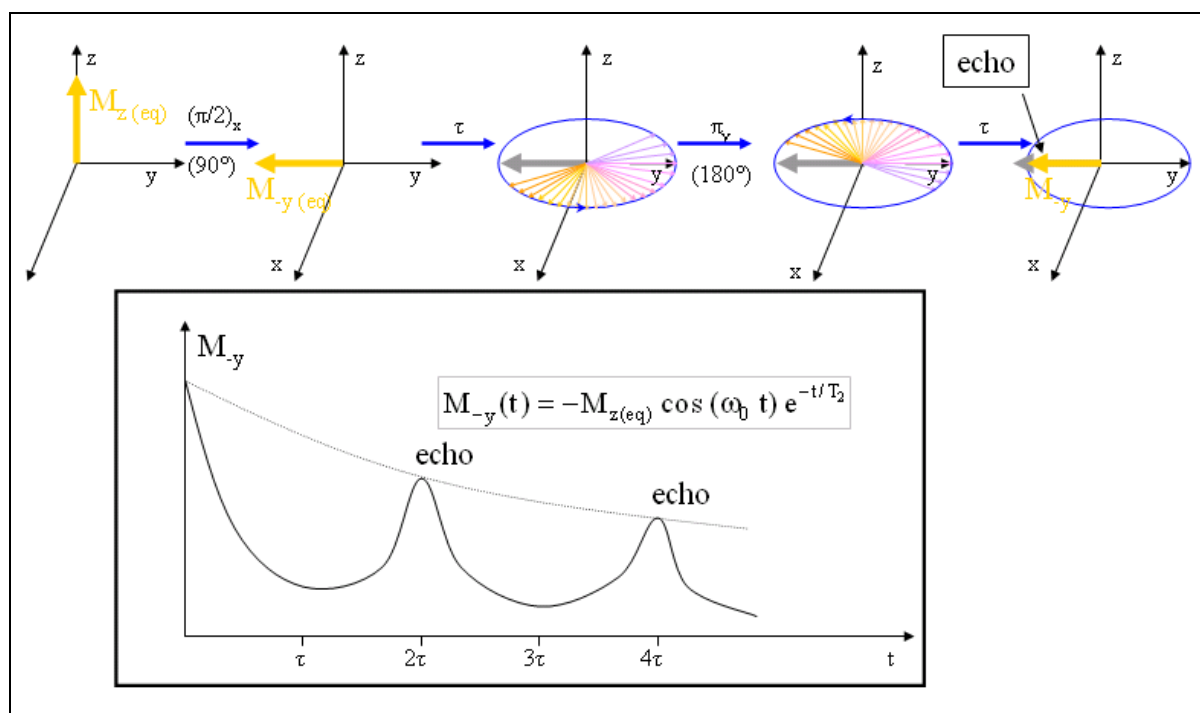


Figure 2.2.12 Schematic representation of the Carr-Purcell-Meiboom-Gill (CPMG) method, which is used to determine the transverse relaxation time constant T_2 in the with ω_0 around Z rotating frame.

The CPMG technique involves the following steps: An external magnetic field is applied and the sample is allowed to reach thermal equilibrium with a net magnetic moment in Z-direction ($M_{Z(\text{eq})}$). A ($\pi/2$) pulse (90° pulse) is applied from X-direction, which rotates the entire nuclear magnetization distribution of the sample. As a result, the net magnetization $M_{Z(\text{eq})}$ is transferred into a net magnetization along the $-Y$ -axis (M_{-y}). Following the removal of this pulse, the total net magnetic moment precesses in the XY -plane and induces a rf signal in the coil. Viewed from the rotating frame of reference, the incremental moment vectors appear to fan out during the first waiting time τ .^[44] The magnitude of the total magnetic moment vector, and hence the induced signal, is thereby decreased. After time τ , a π pulse (180° pulse) is applied from Y -direction. Following the removal of this pulse, all incremental vectors are again in the XY -plane, but rotated about 180° and each will continue to precess in the same sense and with exactly the same angular frequency as it did before the 180° pulse. Therefore, the incremental moment vectors will all recluster together exactly after another waiting time τ , this means, at a time of 2τ after the 90° pulse. At this time, there will be a maximum total magnetic moment vector in $-Y$ -direction and the detected signal will reach a maximum. This is called a spin echo. Following this echo, the incremental moment vectors will again start to fan out. After another time τ , a 180° pulse is again applied and the next echo is detected at a time equal to 4τ after the 90° pulse. This process is continued throughout the natural lifetime of the nuclear signal and additional echos of decreasing amplitude are detected. The envelope of these echos indicates the decay of the polarization in the XY -plane and is used to determine T_2 . By applying the CPMG method, several thousand data points (spin echos) are obtained within a single relaxation process of about 20 s.

Transverse magnetization decays were obtained for samples of PC-C32-PC and Me₂PE-C32-Me₂PE at temperatures between 5 °C and 80 °C by applying the CPMG pulse sequence.

For the samples with H₂O, each pulse sequence was detecting 36864 echoes with the time $2\tau = 0.27$ ms between two echoes and a relaxation delay time of 20 s. Every recorded transverse magnetization decay is the average of 32 of these pulse sequences.

For the samples with D₂O, 256 pulse sequences were averaged, each with 512 echos and a relaxation delay time of 0.8 s.

The obtained transverse magnetization decays were fitted with the program Windows Distributed EXponential analysis software (WinDXP, Oxford Instruments, Abingdon, UK)^[45] and T_2 -distributions with 256 points are calculated in the relaxation time range from 10 μ s to 20 s.

¹H-NMR diffusometry

Due to their thermal energy, molecules in a low viscous liquid undergo Brownian motion. This process of undirected diffusion is called self-diffusion. It can be characterized by a diffusion coefficient D , which is a measure for the mean displacement of the molecules during a time t .

A standard method for the determination of diffusion coefficients is the pulsed-gradient spin-echo (PGSE) method developed by Stejskal and Tanner.^[46] As the name implies, the spin echo method is used and in addition to the rf pulses, time dependent magnetic field gradients are applied (Figure 2.2.13A).

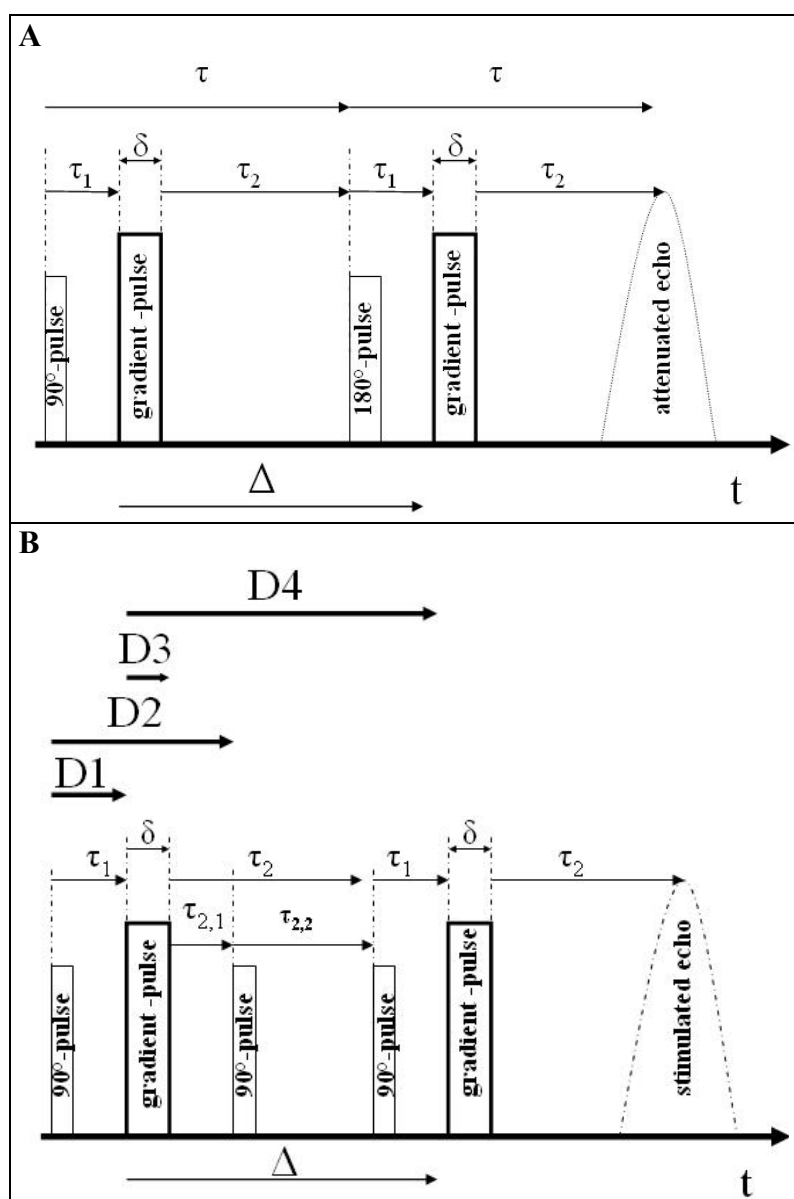


Figure 2.2.13

NMR diffusometry for the determination of diffusion coefficients:

(A) Schematic representation of the pulsed-gradient spin-echo (PGSE) method.

(B) Schematic representation of the pulsed-gradient stimulated-echo (PGSTE) method.

The PGSE method involves the following steps: A 90° pulse is applied, which rotates the magnetization $M_{Z(\text{eq})}$ into a net magnetization in the XY -plane. This transverse magnetization

precesses and is slowly decreased due to a loss of coherence. After a time τ_1 , a magnetic field gradient pulse is applied. The amplitude of this pulse is denoted as g and the duration of the pulse as δ . Due to the inhomogeneous magnetic field, the Larmor frequency of the particular nuclei becomes position dependent and a fast dephasing of the spins is caused. This fast dephasing stops after the removal of the gradient pulse. After a waiting time τ_2 , a 180° rf pulse is applied. Following the removal of this pulse, all incremental vectors are again in the XY -plane, but rotated about 180° . A second field gradient pulse with the same amplitude and duration as the first one is applied at time τ_1 after the 180° rf pulse. This field gradient allows for a fast rephasing of the spins for the case that they did not diffuse substantially during the time Δ between the two gradient pulses. After another waiting time τ_2 , a spin echo will be detected in analogy to the CPMG method. Due to diffusion of the molecules, the application of the magnetic field gradient pulses results in an attenuation of the echo amplitude according to^[46]

$$\ln\left(\frac{A_{2\tau}}{A_0}\right) = -\gamma^2 g^2 D \delta^2 \left(\Delta - \frac{1}{3}\delta\right) \quad (2.27)$$

where $A_{2\tau}$ is the obtained attenuated echo amplitude, A_0 corresponds to the echo amplitude obtained without applying the gradient pulses and γ is the magnetogyric ratio.

The field-gradient stimulated-echo (PGSTE) method is a modification of the field-gradient spin-echo method.^[47] Instead of a $90^\circ/180^\circ$ rf pulse sequence, a $90^\circ/90^\circ/90^\circ$ rf pulse sequence is used (Figure 2.2.13B). Therefore, the relaxation attenuation of the obtained echo has a T_1 dependence during the interval between the second and the third rf pulse.^[47] Since longitudinal relaxation is usually slower than transversal relaxation, this modification extends the accessible range of diffusion coefficients.

For aqueous samples of PC-C32-PC and Me₂PE-C32-Me₂PE, mean diffusion coefficients of water were determined by means of the pulsed-gradient stimulated-echo (PGSTE) method using the Program RiDiff (Oxford Instruments, Abingdon, UK).^[48] These measurements were performed in the temperature range from 30 to 52 °C with the following parameters: The time D1 (also denoted as τ_1 in Figure 2.2.13B) between the first 90° -pulse and the first field gradient pulse was always 0.1 ms. The time D2 ($\tau_1 + \delta + \tau_{2,1}$) was 7 ms. D3 (δ), the duration of the field gradient pulse, was varied in the range from 0.28 to 1.5 ms. The theoretical amplitude g of the field gradient pulse was 0.922 T/m. Calibration of the measurement with pure deionized water leads to a correction factor of 0.784. Therefore, the value of g was calculated to be 0.723 T/m. The time D4 (Δ), which is the time between the two gradient pulses, was adjusted to 20 ms.

Stimulated echoes were recorded for different values of the duration (D3) of the field-gradient pulses. With increasing D3, the echo amplitudes ($A_{2\tau}$) decrease substantially compared to the echo amplitude obtained without the application of the gradient pulses (A_0).

The decreasing echo amplitudes are related to the mean diffusion coefficient of water (D_m) by^[46,48]

$$\ln\left(\frac{A_{2\tau}}{A_0}\right) = -\gamma^2 g^2 D_m \delta^2 \left(\Delta - \frac{1}{3}\delta\right) = -\gamma^2 g^2 D_m D3^2 \left(D4 - \frac{1}{3}D3\right) \quad (2.28)$$

The obtained values of $\ln\left(\frac{A_{2\tau}}{A_0}\right)$ were plotted against the term $D3^2 \left(D4 - \frac{1}{3}D3\right)$.

By linear fitting, the values for the slope were obtained. According to Equation 2.28, the slope is corresponding to $-\gamma^2 g^2 D_m$. With $\gamma = 267,538,030 \text{ s}^{-1}\text{T}^{-1}$ and $g = 0.723 \text{ T/m}$, the values for the mean diffusion coefficient D_m of the water molecules in the hydrogels could be calculated.

Sample preparations

1 mg or 30 mg PC-C32-PC were weighed into a small glass vessel and 1 ml deionized water were added to obtain a PC-C32-PC concentration of 1 mg/ml or 30 mg/ml, respectively. The glass vessels were carefully closed. These samples were alternately heated in a water bath above 80 °C and vortexed until all PC-C32-PC was homogeneously dispersed. Prior to the NMR measurements, the samples were stored between 2 and 8 °C for 2 hours. For Me₂PE-C32-Me₂PE, Me₂PE-C28-Me₂PE, Me₂PE-C34-Me₂PE and Me₂PE-C36-Me₂PE, the preparation was the same, but 100 mM acetate buffer at pH 5 were used for the samples instead of deionized water.

In order to assess the transverse relaxation times of the bolaamphiphile protons, D₂O or acetate buffer pH 5 were used to prepare the hydrogels with 30 mg/ml PC-C32-PC or Me₂PE-C32-Me₂PE, respectively.

The reference samples with 30 mg/ml of Sephadex G10-G100 and 30 mg/ml 2-hydroxyethyl cellulose were prepared by weighing 30 mg of the particular substance into a small glass vessel. After addition of 1 ml of deionized water and subsequent vortexing, the samples were stored for 48 hours at a temperature between 2 and 8 °C prior to the measurements.

The glass vessel containing the particular NMR sample was carefully checked to be closed. A piece of string, tightly attached to the vessel, was used to bring the vessel down into the resonator hole, where it became fixed to prevent it from tumbling in the air stream. Each sample was prepared and measured two times.

2.2.3 Electron spin resonance (ESR) spectroscopy

2.2.3.1 General remarks

ESR does not deal with nuclear spins, but with the spins of unpaired electrons contained in paramagnetic substances. Such substances are rather rare among the commonly used organic molecules. However, there is a wide variety of stable radicals available that can be used as reporter molecules (spin probes) and therefore allow to study diamagnetic systems by ESR.

ESR and NMR are analogous in many aspects. Both methods use strong magnetic fields to produce net magnetizations at thermal equilibrium. By electromagnetic radiation, this equilibrium is disturbed, but will be restored after some time due to longitudinal and transversal relaxation.

However, the theoretical framework, which is used to describe the spectroscopic data, is different for both methods due to experimental and historical reasons.

2.2.3.2 Definitions

Here, only a brief description of the ESR technique is given. Most of the definitions were taken from the books of Berliner^[49] and Winter/Noll.^[37]

The unpaired electrons of an atom have an orbital angular momentum \vec{L} and spin \vec{S} . The total angular momentum is

$$\vec{J} = \vec{L} + \vec{S} \quad (2.29)$$

and the magnetic moment of these electrons is

$$\vec{\mu}_J = \vec{\mu}_L + \vec{\mu}_S = -g \frac{e}{2m_e} \vec{J} \quad (2.30)$$

where e is the charge, m_e the mass and g is the spectroscopic splitting factor of the electrons

$$g = 1 + \frac{J(J+1) + S(S+1) - L(L+1)}{2J(J+1)} \quad (g = 2.00232 \text{ for a free electron}) \quad (2.31)$$

The magnetic moment is often given in form of the Bohr magneton

$$\mu_B = \frac{|e|\hbar}{2m_e} = 9,27410^{-24} \text{ J T}^{-1} \quad (2.32)$$

For free electrons, $\vec{\mu}_L$ can often be neglected:

$$|\vec{\mu}_J| = |\vec{\mu}_S| = g \mu_B \sqrt{S(S+1)} \quad (2.33)$$

If an external magnetic field is applied with \vec{B}_0 , the magnetic moment of an unpaired electron is interacting with this field. The magnetic energy is

$$E_{\text{mag}} = -\vec{\mu}_s \cdot \vec{B}_0 = g \mu_B m_s B_0 \quad (2.34)$$

Analogous to NMR, m_s characterizes the $2S+1$ possible orientations of the electron spin in the magnetic field. Therefore, only two orientations are possible in the case of $S = 1/2$, namely $+1/2$ and $-1/2$. The difference in energy between these two levels is $\Delta E = g \mu_B B_0$ (Figure 2.2.14A). At a given temperature, a net magnetization will develop in the direction of the magnetic field at thermal equilibrium according to the Boltzmann distribution.

2.2.3.3 The ESR experiment

ESR experiments are usually performed at a fixed microwave frequency and the magnetic field is varied. When the resonance condition is satisfied ($h\nu = \Delta E = g \mu_B B_0$), an excitation from the lower to the higher energy level is induced and a net energy absorption can be detected. In ESR, field modulation is commonly used to obtain more efficient signal amplification. This causes the displayed curve to be the derivative of the absorption curve (Figure 2.2.14B). The peak-to-peak distance of this derivative curve (δ) corresponds to the width of the absorption curve at the points of maximum slope.

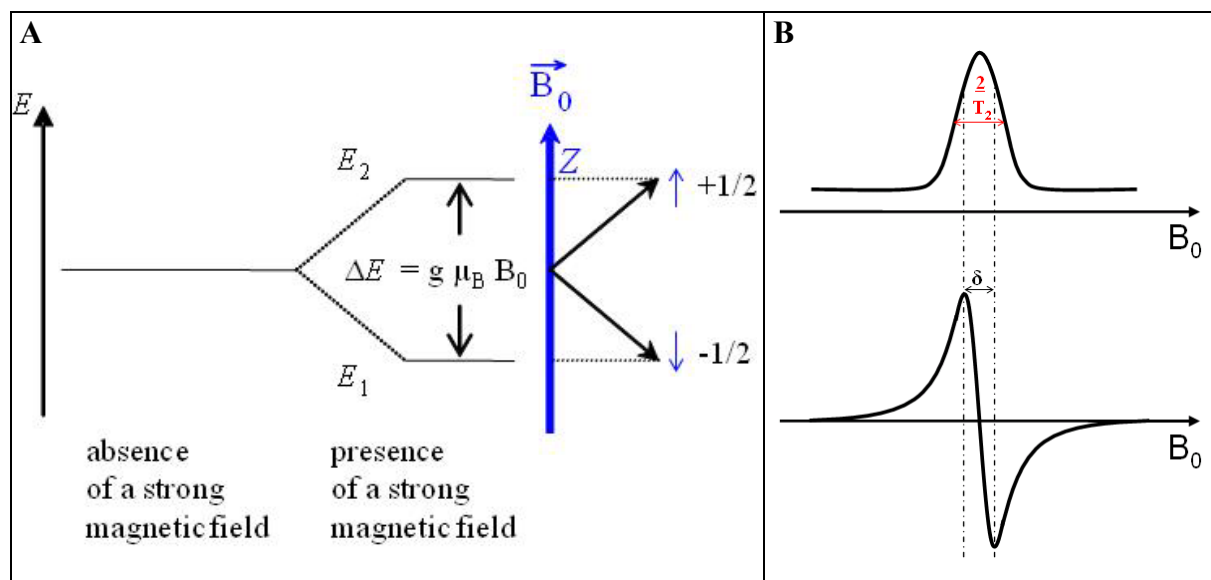


Figure 2.2.14 Origin of the ESR signal: (A) Zeeman splitting caused by the presence of a strong magnetic field shown for a single electron spin with $S = 1/2$. (B) The absorption curve (top) and its first derivative (bottom), which is the commonly obtained ESR signal.

Usually, ESR spectra show multiplet structures, called hyperfine structures. This is due to an interaction of the magnetic moment of the unpaired electron spins with nuclear magnetic moments, such as that from ^1H , ^{14}N and ^{13}C . As described in Section 2.2.2, the nuclear spins can assume $2I+1$ orientations. The electron spin magnetic moment experiences a different total magnetic field for any of these orientations. In the present work, ESR measurements were performed by using nitroxide spin probes. In such nitroxides, hyperfine splitting of the ESR signal is mainly due to the interaction of the unpaired electron with the nuclear magnetic moment of ^{14}N with $I=1$. Therefore, the obtained ESR spectrum consists of $2I+1=3$ hyperfine components as is shown in Figure 2.2.15. The resonance condition is satisfied for each component at a field

$$\vec{B}_{\text{res}} = \vec{B}_0 - A m_I \quad (2.35)$$

Factor A is called hyperfine splitting constant and is defined by the distance between the lines as outlined in Figure 2.2.15.

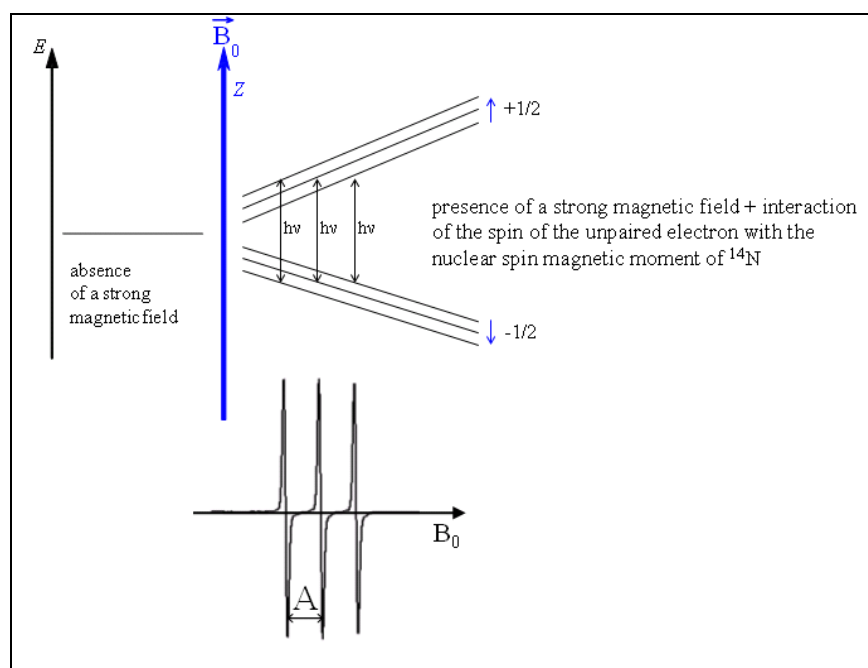


Figure 2.2.15
Hyperfine splitting of the ESR signal by interaction of the electron spin magnetic moment of the unpaired electron with the nuclear spin magnetic moment of ^{14}N .

2.2.3.4 Motion dependence of ESR spectra

The hyperfine splitting constants and the g factors are depending on the orientation of the spin probe with respect to \vec{B}_0 , which determines the spectral anisotropy $\Delta\omega$ in ESR spectroscopy. Therefore, different axis systems are defined to describe this spectral anisotropy, namely the laboratory, the magnetic and the molecular axes system.

(1) The laboratory axes system (X, Y, Z) is set by the spectrometer. By convention, the direction of the applied magnetic field \vec{B}_0 is denoted as the Z -direction.

(2) In the case of the nitroxide spin probes, the magnetic axis system (x, y, z) is defined as follows:^[50] The x -axis is along the N-O bond, the z -axis is parallel to the nitrogen and oxygen $2p\pi$ -orbitals, containing the unpaired electron, and the y -axis is perpendicular to the xz -plane.

(3) The molecular axis system for a spin probe is defined by three main axes in x -, y - and z -direction, denoted here as the x_m -, y_m - and z_m -axis, respectively. The anisotropy of the hyperfine splitting factor A is then characterized by the three tensors A_{xx} , A_{yy} and A_{zz} . For the case of an axial symmetric molecular system, which can be assumed for most nitroxide spin probes, the value of A_{xx} is almost equal to A_{yy} , but different from A_{zz} ($A_{xx} \approx A_{yy} \neq A_{zz}$). By convention, A_{zz} is the hyperfine splitting, which is obtained in the ESR spectrum if the symmetry axis of the molecule is parallel to the direction of the applied magnetic field ($A_{||}$). Therefore, the obtained A value corresponds to A_{xx} and A_{yy} , if the symmetry axis is oriented perpendicular to \vec{B}_0 (A_{\perp}). The principal values of the g and A tensors can be determined by single crystal experiments (see for example Appendix II in the book of Berliner^[49]).

The spectral anisotropy $\Delta\omega$ is determining the ESR timescale. In spin probe ESR, the most important dynamic process is the rotational reorientation of the spin probe molecules in the external magnetic field, which is characterized by the rotational correlation time τ_R . Four dynamic regimes with distinct types of ESR spectra can be distinguished by comparing τ_R and $1/\Delta\omega$.^[51] The isotropic limit is reached for $\tau_R \ll 1/\Delta\omega$. Isotropic spectra (an example is displayed in Figure 2.2.15) are observed when rotational reorientation is fast enough (τ_R about 1 - 0.01 ns for cw-ESR at X-band) to completely average out the spectral anisotropies. The obtained isotropic hyperfine constant is $A_N = 1/3 (A_{zz} + A_{yy} + A_{xx})$. For $\tau_R \gg 1/\Delta\omega$, the continuous wave spectrum becomes motion independent and full spectral anisotropy is obtained. Such a rigid limit spectrum is observed in powder samples or frozen solutions with $\tau_R > 500$ ns. In between these two limits, the ESR line shape is highly sensitive to changes of the rate of rotational reorientation of the nitroxyl group in the magnetic field. Here, one can differentiate between the regimes of fast ($5 - 10$ ns $> \tau_R > 1 - 0.01$ ns) and slow motion (500 ns $> \tau_R > 5 - 10$ ns). Even small changes in the molecular mobility of the spin probes will result in distinct changes of the ESR line shape. This sensitivity to molecular motion makes ESR a powerful tool for studying the dynamics present in the system under investigation.

2.2.3.5 Experimental part

Instrumental settings and spectral analysis

All ESR measurements were carried out with a Miniscope MS 200 X-Band spectrometer (Magnettech Berlin, Germany) equipped with a nitrogen gas flow temperature regulation. The ESR measurements were performed using the following parameters: Microwave frequency power 10 mW, B_0 field 334.9 mT, field sweep 98 mT, sweep time 40 s, accumulative scans 12-18, modulation amplitude 0.125 mT.

A series of spectra was generally recorded by gradually increasing the temperature from 0 to 60 °C with at least 10 minutes waiting time at each temperature in order to allow the system to reach thermal equilibrium prior to each measurement.

The obtained ESR spectra were analyzed regarding their line shapes. Maximum hyperfine splittings $2A_{\max}$ were obtained and used for determination of the transition temperatures. Rotational correlation times and orientational order parameters were obtained from full line shape simulations with the programs EasySpin^[51,52] version 2.6.1 and EPRSIM.^[53]

Sample preparation

100 μ l of a stock solution containing 10 mg/ml of the particular bolaamphiphile in a mixture of chloroform and methanol were pipetted into a small Eppendorf vial. The appropriate amount of stock solution of the selected spin probe was added. After thorough mixing, the solvent was removed under a gentle stream of argon. The lipid residue was subsequently maintained under vacuum, which was applied for at least four hours.

For PC-C32-PC, 100 μ l deionized water were then added in order to obtain a bolalipid concentration of 10 mg/ml (12.3 mM). The resulting concentrations of the spin probes were approximately 0.025 mM and 0.13 mM for tempolbenzoate (TB) and n-doxyl stearic acid (n-DSA), respectively. Therefore, spin probe and bolaamphiphile were adjusted to a molar ratio of approximately 1 : 500 for TB and 1 : 100 for n-DSA. After addition of the aqueous phase, the sample was heated in a water bath at a temperature above 80 °C for at least 1 minute followed by thorough vortexing. This procedure was repeated until a homogeneous sample was achieved. This aqueous sample was heated again in order to fill about 50 μ l into a small glass capillary, which was sealed immediately with inert wax. Prior to the ESR measurements, this capillary was stored for 2 hours at a temperature between 2 and 8 °C.

For preparing the ESR samples containing 10 mg/ml (12.7 mM) Me₂PE-C32-Me₂PE at pH values of 5 and 10, 100 μ l of 100 mM acetate buffer at pH 5 and 100 mM carbonate buffer at pH 10 were used, respectively. Each of the samples was prepared and measured two times.

Reduction assay

For the reduction assay, the particular ESR sample was prepared as described above, but stored between 2 and 8 °C for 2 h in the Eppendorf vial. Prior to the measurements, 10 µl of a freshly prepared ascorbic acid solution was added into the Eppendorf vial in order to adjust the concentration of ascorbic acid to 1 mM. As a consequence, the obtained molar ratio between ascorbic acid and n-DSA was about 8. After thorough mixing, the sample was immediately filled into a ESR capillary, which was sealed with inert wax and immediately inserted into the sample holder.

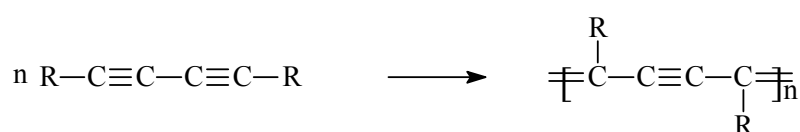
All spectra were recorded at 25 °C as the average of 2 runs, each with a sweep time of 12 s. The first ESR measurement was started about 1min 45 s after addition of the ascorbic acid to the sample. The resulting spectrum was assumed to represent the spin probe concentration after 2 minutes. The height of the central line in this spectrum was measured and taken as the starting value for the signal intensity ($I_{2\text{min}}$). In order to obtain time dependent signal intensities (I_t), ESR spectra were recorded every minute for each sample during a period of 15 minutes after addition of ascorbic acid. A last spectrum was obtained after 20 minutes.

2.2.4 Bolaamphiphiles with a diacetylene group

2.2.4.1 Diacetylenes – general remarks

Diacetylene derivatives are known to polymerize in lattice controlled reactions. Therefore, organized monomer media are required for the polymerization reaction. Polymerized diacetylenes were obtained in the bulk crystalline state as well as in low-dimensional systems like multichannel inclusion compounds, lipid layer structures and monolayers absorbed on solid substrates.^[54]

When diacetylenes are exposed to UV-, X- or γ -radiation, the topochemical reaction from the diacetylene monomers to polydiacetylenes (PDAs) is proceeding according to



The polymerization behavior was studied for a wide variety of amphiphilic diacetylene compounds including a small number of bolaamphiphiles.^[55-59] The photoreactivity of the amphiphilic monomers depends strongly on the packing geometry, which is mainly determined by the side groups. The crucial geometrical condition is the mean distance between two diacetylene units, which has to be close to the polymer equilibrium repeat distance of 4.9 Å.^[60]

The resulting polydiacetylenes exhibit strong optical absorption, which occurs via a π -to- π^* absorption within the linear π -conjugated polymer backbone. The polymerization of diacetylenes is therefore accompanied by a rapid color change of the sample. These colors can range from yellow, greenish-blue, red, purple, deep blue to black.

One of the most striking features that was observed for a wide range of PDAs is the occurrence of chromatic transitions. These transitions usually involve a color change from blue ($\lambda_{\text{max}} \sim 640 \text{ nm}$) to red ($\lambda_{\text{max}} \sim 540 \text{ nm}$), manifested by a significant shift in absorption. PDAs were found to show such a chromatic response to various stimuli, namely optical exposure (photochromism),^[61,62] heat (thermochromism),^[63,64] applied stress (mechanochromism)^[65,66] or changes in the chemical environment.^[57,67,68] Therefore, PDAs have attracted attention for application in sensor devices.^[69,70]

2.2.4.2 Experimental part

Sample preparations

The appropriate amount of PC-C32diAc-PC or Me₂PE-C32diAc-Me₂PE were weighed into a glass vessel. After addition of the particular aqueous phase, the sample was heated in a water bath at a temperature above 80 °C for at least 1 minute followed by thorough vortexing. This

procedure was repeated until a homogeneous sample was achieved. Prior to the experiments, these samples were stored between 2 and 8 °C for two hours.

Transmission electron microscopy (TEM)

TEM images obtained by negative staining with uranyl acetate were obtained in cooperation with Dr. G. Hause (Biozentrum, Martin-Luther-Universität Halle-Wittenberg). The negatively stained samples were prepared by spreading 5 μ l of the particular dispersion onto a Cu grid coated with a formvar-film. After 1 min of adsorption, excess liquid was blotted off with filter paper and 5 μ l of 1% aqueous uranyl acetate were placed on the grid and drained off after 1 min. The dried specimens were examined with a Zeiss EM 900 transmission electron microscope.

Cryo-TEM images were obtained in cooperation with G. Karlsson and Prof. M. Almgren (Department of Physical and Analytical Chemistry, Uppsala University, Sweden) with a Zeiss 902A instrument, operating at 80 kV. Specimens were prepared by a blotting procedure, performed in a chamber with controlled temperature and humidity. A drop of the sample solution was placed onto an EM grid coated with a perforated polymer film. Excess solution was then removed with a filter paper, leaving a thin film of the solution spanning the holes of the polymer film on the EM grid. Vitrification of the thin film was achieved by rapid plunging of the grid into liquid ethane held just above its freezing point. The vitrified specimen was kept below 108 K during both transfers to the microscope and investigation.

Differential scanning calorimetry (DSC)

DSC measurements were performed in the temperature range from 2 to 95 °C by using a MicroCal VP-DSC (Microcal, Northampton, USA). Sample dispersions and reference solutions were degassed under vacuum prior to the measurements. A heating rate of 60 K/h was used. To check the reproducibility, three consecutive scans of each sample were recorded. The DSC scans were evaluated using the MicroCal ORIGIN 5.0 software and the reference thermogram (water–water baseline) was subtracted from the thermograms of the samples.

UV-VIS spectroscopy

The UV-VIS spectra, used to follow the progress of the UV-polymerization and to investigate the temperature dependence, were recorded at a HP 84524 spectrometer and a HP 8453 spectrometer, respectively. For every spectrum, the reference spectrum of water was subtracted.

2.2.5 Biological tests

2.2.5.1 MTT-assay

General remarks

The MTT-assay is a colorimetric standard assay to assess the cytotoxicity of a given substance or formulation. The assay is based on the pale yellow tetrazolium salt MTT (3-(4,5-dimethylthiazol-2-yl)-2,5-diphenyl-tetrazoliumbromid), which is enzymatically reduced to a dark blue formazan by mitochondrial dehydrogenases (Figure 2.2.16).^[71]

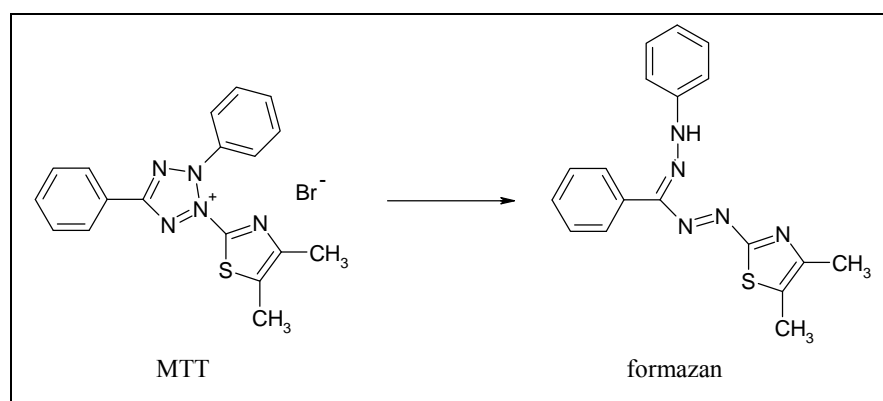


Figure 2.2.16
Reduction of MTT to a formazan by mitochondrial dehydrogenases.

MTT is transformed to the formazan only in living and metabolically active cells. The formazan absorption is therefore a quantitative measure for the viability of the cells after incubation with the substance or formulation under investigation. Since multi-well plates are used and no washing steps are needed, the MTT-assay enables rapid analysis of large numbers of samples with a high precision.

Experimental procedures

All experiments were performed in cooperation with Martin Heinze (Group of Prof. Langner, Department of Pharmaceutical Chemistry, Martin-Luther-University Halle-Wittenberg).

A549 cells (human lung carcinoma cells) were cultured in 75 cm² tissue culture flasks in Dulbecos's modified eagle medium (DMEM) adjusted to contain 4.5 g/l glucose, 10% FBS, and 0.05 mg/ml gentamycin at 37 °C and 5% CO₂. The cells were grown confluent and were splitted twice a week. The cells were seeded 24 hours prior to the MTT-assay with approximately 2.5*10⁴ cells per well.

The MTT-assay was performed in 96-well microtiter plates with PC-C32-PC or Me₂PE-C32-Me₂PE at concentrations ranging from 0.01 mmol/l to 1 mmol/l. Fetal bovine serum was

added four hours after starting the assay. The incubation of the A549 cells was continued for further 20 hours, before the medium was refreshed and MTT solution was added. After incubation of the treated cells with MTT for four hours at 37 °C, the cells were lysed with a mixture of 10% sodium dodecyl sulfate in acetic acid/dimethyl sulfoxide. The absorbance was determined for each well at 570 nm ($A_{570 \text{ nm}}$) as a measure for the viability of the treated cells. The results were expressed as percent viability according to:

$$\text{viability (\%)} = [A_{570 \text{ nm}} (\text{treated cells}) - \text{background}] / [A_{570 \text{ nm}} (\text{untreated cells}) - \text{background}] \times 100$$

The number of independent experiments was four, each involving a six-fold determination of the cell viability for the particular bolaamphiphile concentration.

2.2.5.2 Testing the antifungal activity

In cooperation with PD Dr. med. J. Wohlrab (Experimental Dermatology, Universitätsklinik, Martin-Luther-Universität Halle-Wittenberg), the antifungal activity was tested for 12 different bolaamphiphiles (Figure 2.2.17). For this in-vitro test, *Candida albicans* and *Trichophyton rubrum* inoculated on agar plates were selected.

The test samples were prepared by dispersing 1 mg of the particular bolaamphiphile in 1 ml deionized water at a temperature above 80 °C and subsequent vortexing. After storage between 2 and 8 °C for 24 hours, these dispersions were used to impregnate filter discs, which were placed on the agar plates according to the sampling scheme shown in Table 2.2.1. After incubation for 1, 2 and 7 days, the plates were examined for zones of inhibited fungal growth.

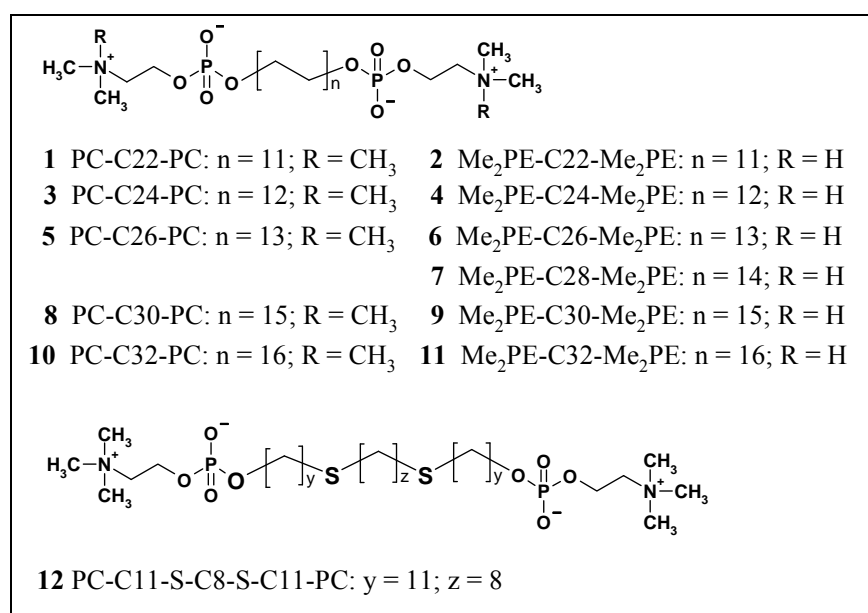


Figure 2.2.17
Chemical structures of the 12 bolaamphiphiles tested for a potential antifungal activity.

Table 2.2.1 Sampling scheme for testing the antifungal activity: Plates I – V = *Candida albicans* and plates VI – IX = *Trichophyton rubrum*.

bolaamphiphile	concentration of the test samples	number of the plate / position
PC-C22-PC	1 mg/ml	I/1; III/2; VI/1; VIII/1
Me ₂ PE-C22-Me ₂ PE		I/2; V/2; VI/2; VIII/2
PC-C24-PC		I/3; IV/2; VI/3; VIII/3
Me ₂ PE-C24-Me ₂ PE		I/4; IV/3; VI/4; VIII/4
PC-C26-PC		I/5; IV/4; VI/5; VIII/5
Me ₂ PE-C26-Me ₂ PE		II/1; V/1; VI/6; VIII/6
Me ₂ PE-C28-Me ₂ PE		II/2; V/2; VII/1; IX/1
PC-C30-PC		II/3; V/3; VII/2; IX/2
Me ₂ PE-C30-Me ₂ PE		II/4; V/4; VII/3; IX/3
PC-C32-PC		II/5; V/5; VII/4; IX/4
Me ₂ PE-C32-Me ₂ PE		II/6; V/6; VII/5; IX/5
PC-C11-S-C8-S-C11-PC		III/1; V/7; VII/6; IX/6

3 Results and discussion

3.1 Oscillatory rheometry

As described in Section 1.1, the previous rheological characterization of aqueous samples of PC-C32-PC and Me₂PE-C32-Me₂PE was done with different methods. For a hydrogel with 8 mg/ml PC-C32-PC, the temperature dependence of the dynamic viscosity was investigated by performing rotational rheometry.^[13] For 8 mg/ml Me₂PE-C32-Me₂PE at pH 5, the G', G'' and tan δ values were determined by means of oscillatory rheometry using a cone/plate measuring system at only four temperatures, namely at 25, 30, 40 and 50 °C.^[18] On the basis of these results it is not appropriate to compare the rheological behavior of hydrogels formed by PC-C32-PC and Me₂PE-C32-Me₂PE. Therefore, a detailed rheological characterization of PC-C32-PC and Me₂PE-C32-Me₂PE was carried out by performing a series of oscillatory rheometry experiments using a cone/plate measuring geometry.

3.1.1 Influence of silicone oil

One serious problem, arising in rheological measurements with aqueous samples, is the evaporation of water at the air-water surface. In order to overcome this problem and to obtain reproducible results especially at higher temperatures or longer measuring times, low viscous silicone oil was used to minimize evaporation by covering the air-water surface as is shown in Figure 2.2.6.^[72] Silicone oil is chemically inert and does not mix with water.

As is shown for 2 mg/ml PC-C32-PC in Figure 3.1.1, the addition of silicone oil is found to have only a small influence on the obtained G' and G'' values. For all investigated samples, the range of the observed differences was -10 to -15% for the G' values and +2 to +6% for the G'' values. This finding could be explained as follows: The silicon oil is sheared to some extent, although it was not placed directly inside the gap between cone and plate, and therefore leads to a measurable influence of the calculated $\tau(t)$ function and its phase shift

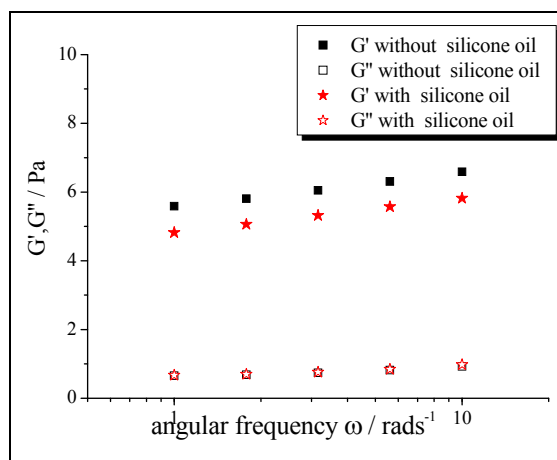


Figure 3.1.1 2 mg/ml PC-C32-PC in deionized water: Frequency sweep with and without addition of silicone oil.

angle δ . Silicon oil does not exhibit significant elastic behavior, but only contributes to the viscous part. As a result, the obtained storage moduli are found to be decreased, whereas the loss moduli are increased with respect to measurements without silicone oil.

The use of silicone oil allows to measure a single aqueous sample over a period of several hours and enables detailed investigation of the temperature dependence up to 75 °C without any sign of evaporation. The observed effect of silicone oil on the absolute values of all determined G' and G'' values seems to be acceptable, since all presented investigations were rather concerned with relative differences than with the absolute values of G' and G'' . Therefore, all results discussed below were obtained by covering the air-water surface of the aqueous samples with a thin layer of silicone oil.

3.1.2 Concentration dependence at 25 °C

For PC-C32-PC, the self-assembly into the three-dimensional network of fibers is solely driven by hydrophobic interactions.^[13] For Me₂PE-C32-Me₂PE at pH 5, a similar fiber network is obtained, which is additionally stabilized by the formation of hydrogen bonds between the bolaamphiphilic headgroups. Due to this stabilizing effect, the fiber-to-micelle transition was found to be up-shifted for Me₂PE-C32-Me₂PE at pH 5 (69.5 °C) with respect to PC-C32-PC (49 °C). The question arises, whether there are also differences observable between the obtained hydrogels of PC-C32-PC and Me₂PE-C32-Me₂PE regarding their “structure strength”. All rheological data collected for PC-C32-PC and Me₂PE-C32-Me₂PE until now, were obtained by using a bolaamphiphile concentration of 8 mg/ml (Section 1.1). For this concentration, no clear differences in the G' and G'' values were observed between PC-C32-PC^[12] and Me₂PE-C32-Me₂PE.^[18] However, this finding needs to be clarified since different rheometers were used and no data exist about the concentration dependence of the rheological parameters.

Rheograms that are showing the concentration dependence of the G' and G'' values obtained for PC-C32-PC or Me₂PE-C32-Me₂PE at 25 °C, are displayed in Figure 3.1.2A and 3.1.2B, respectively.

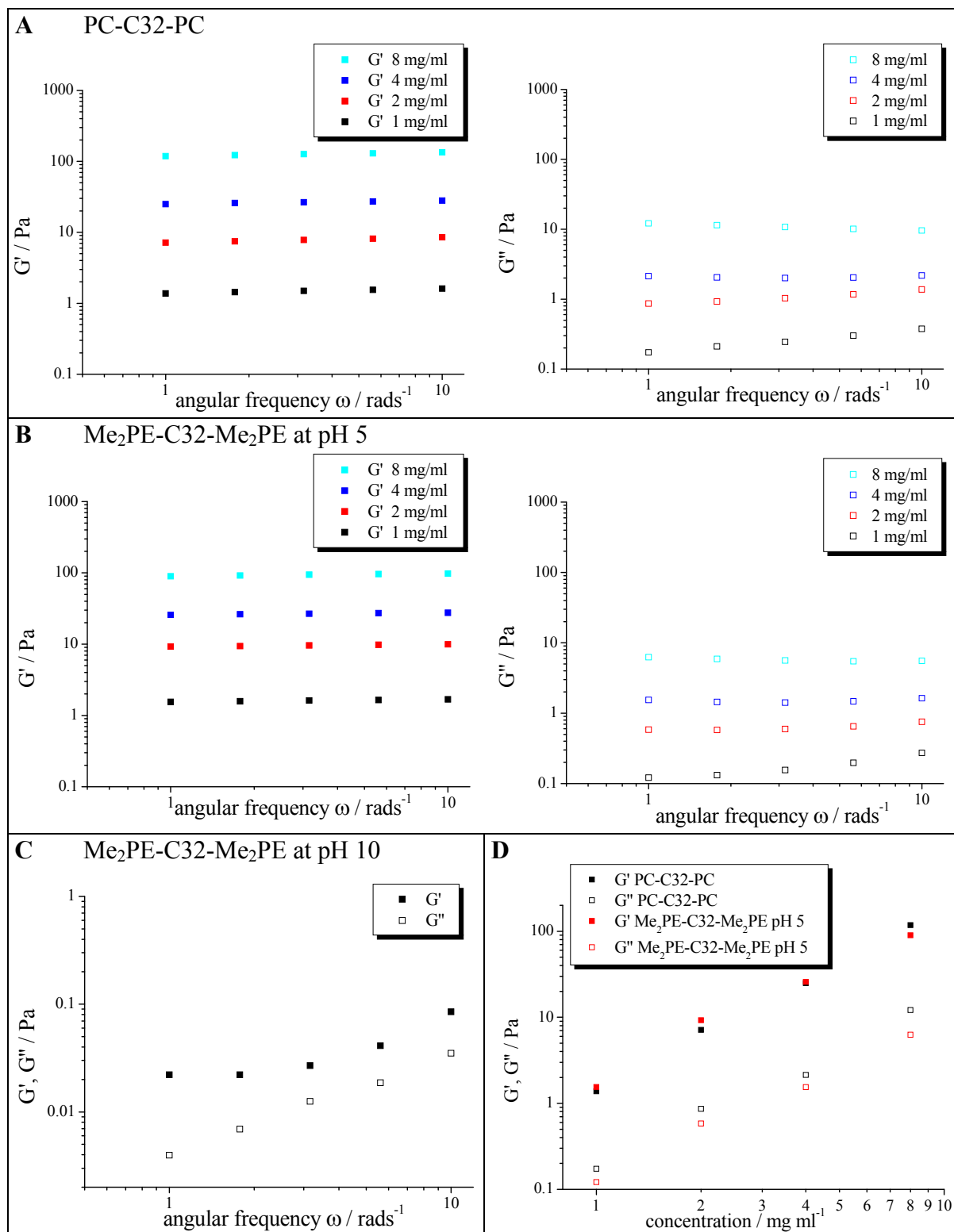


Figure 3.1.2 Concentration dependence of the G' and G'' values of PC-C32-PC and Me₂PE-C32-Me₂PE at 25 °C and 1% deformation:

(A) 1, 2, 4 and 8 mg/ml PC-C32-PC in deionized water - (**left**) G' and (**right**) G'' values.

(B) 1, 2, 4 and 8 mg/ml Me₂PE-C32-Me₂PE in acetate buffer pH 5 - (**left**) G' and (**right**) G'' .

(C) 1 mg/ml Me₂PE-C32-Me₂PE in carbonate buffer pH 10 - G' and G'' .

(D) Comparison of PC-C32-PC and Me₂PE-C32-Me₂PE at pH 5 - G' and G'' values at 1 rad/s.

When Me₂PE-C32-Me₂PE is dispersed in carbonate buffer pH 10, no hydrogel is obtained, but a micellar fluid with the rheological behavior that corresponds to pure water. Therefore, at a concentration of 1 mg/ml Me₂PE-C32-Me₂PE at pH 10 and an angular frequency of 1 rad/s, the obtained G' and G'' values are only approximately 0.02 Pa and 0.004 Pa, respectively (Figure 3.1.2C). The corresponding G' and G'' values for Me₂PE-C32-Me₂PE at pH 5 and PC-C32-PC in water are about two orders of magnitude larger at the same concentration. This is a clear indication that in these samples hydrogel networks are present.

As shown in Figure 3.1.2A and B, the G' and G'' values for all concentrations are almost parallel to each other with only slightly larger values at increasing angular frequencies. At 25 °C, the G'' values are always about one order of magnitude lower than the corresponding G' values. Therefore, the resulting values for the loss factor tan δ (G''/G') are always in the order of 0.1 with slightly larger values for PC-C32-PC compared to Me₂PE-C32-Me₂PE. These values are 0.12 and 0.08, respectively.

Oscillatory rheometry only detects the macroscopic properties of the whole fiber network. The determined value of the storage modulus G' is a measure for the structure strength of this network, since it characterizes the ability of the network to resist the applied deformational stress (Section 2.2.1). For the self-assembled fiber networks present in the hydrogels of PC-C32-PC and Me₂PE-C32-Me₂PE, this ability will be mainly determined by the total number of fiber-fiber cross-links and by their individual stability. If the storage moduli are obtained for the aqueous samples of PC-C32-PC and Me₂PE-C32-Me₂PE inside the LVE-region, larger G' values are indicating more stable fiber networks. As expected, hydrogels with increasing bolaamphiphile concentration are characterized by increasing G' values (Figure 3.1.2D, Table S.1 in the Supplement) and may therefore be regarded as stronger hydrogels.

Comparing the concentration dependence of the G' values obtained for hydrogels of PC-C32-PC and Me₂PE-C32-Me₂PE at an angular frequency of 1 rad/s, reveals interesting differences between both bolaamphiphiles. In theory, the stabilizing effect of hydrogen bonding between the headgroups of Me₂PE-C32-Me₂PE should lead to an increased strength of the hydrogels at all concentrations, that is, in larger G' values compared to PC-C32-PC. However, this is only observed at concentrations of 1 and 2 mg/ml. At these concentrations, the G' values of Me₂PE-C32-Me₂PE exceed that of PC-C32-PC by 12.5 and 29%, respectively. At 4 mg/ml, on the other hand, there are no clear differences observable between both bolaamphiphiles and at 8 mg/ml, the G' value obtained for PC-C32-PC is larger by 24% than that of Me₂PE-C32-Me₂PE. A possible explanation for this finding may be found in some small differences in the aggregation behavior of both bolaamphiphiles. Figure 3.1.3 shows photographs

obtained for aqueous samples of Me₂PE-C32-Me₂PE at pH 5. These samples were prepared according to the procedure described in Section 2.2.1 at concentrations of 1, 2, 4 and 8 mg/ml Me₂PE-C32-Me₂PE in acetate buffer pH 5. The photographs show that all samples are gels, because their fiber networks are preventing any flow when they are turned upside down. The stress, exposed on the hydrogel network by its own weight, is reflected in a clearly visible curvature. This curvature is clearly decreased when the bolaamphiphile concentration is increased from 1 to 8 mg/ml due to the increased cross-link density. This is in agreement with the increasing G' values. Whereas hydrogels of PC-C32-PC remain completely transparent even at higher concentrations (Figure 3.1.3B), a certain degree of turbidity is observed for Me₂PE-C32-Me₂PE at pH 5 starting at a concentration of 2 mg/ml. With increasing concentration of Me₂PE-C32-Me₂PE from 2 to 8 mg/ml, this turbidity becomes more obvious and this trend is continued for the hydrogel with 30 mg/ml Me₂PE-C32-Me₂PE, which was used for NMR measurements (Figure 3.2.10A). As described above, cryo-TEM images of PC-C32-PC show a dense network of stiff fibers.^[13] The fibers observed for Me₂PE-C32-Me₂PE at pH 5 seem to be more flexible and additionally, lamellar structures were also found in small quantities for the sample with 0.3 mg/ml Me₂PE-C32-Me₂PE (Figure 1.7).^[15] The occurrence of turbidity for hydrogels with higher concentrations of Me₂PE-C32-Me₂PE can be ascribed to the existence of these lamellar aggregates in considerably larger quantities. This is supported by the results obtained from the NMR relaxation measurements, which can only be interpreted in terms of a certain degree of heterogeneity caused by the presence of domains of stacked lamellae in a hydrogel with 30 mg/ml Me₂PE-C32-Me₂PE at pH 5 (Section 3.2). It was tried to obtain transmission electron images for the turbid hydrogels by means of a negative staining technique. This approach to give direct evidence for the existence of the lamellar aggregates in large numbers was not successful due to the high bolaamphiphile concentration. However, this could be done for 0.3 mg/ml Me₂PE-C34-Me₂PE and Me₂PE-C36-Me₂PE at pH 5, which were found to show a more pronounced tendency to form such lamellar aggregates due to their longer alkyl chains compared to Me₂PE-C32-Me₂PE.^[23] The aqueous samples of Me₂PE-C34-Me₂PE and Me₂PE-C36-Me₂PE at pH 5 also appear to be turbid, which allows to conclude that there is a clear indication for the existence of a considerable number of lamellar aggregates inside the hydrogels with ≥ 2 mg/ml Me₂PE-C32-Me₂PE at pH 5. The occurrence of these lamellar aggregates can be expected to disturb the three-dimensional fiber network and to prevent efficient cross-linking to some extent. On the other hand, the formation of hydrogen bonds between the headgroups of Me₂PE-C32-Me₂PE can be expected to increase the number and the stability of the fiber-fiber cross-links

compared to hydrogels of PC-C32-PC. Hence, the observed concentration dependent differences between PC-C32-PC and Me₂PE-C32-Me₂PE may be interpreted as follows: At concentrations of 1 and 2 mg/ml, the number of lamellar aggregates is small for the samples with Me₂PE-C32-Me₂PE. The positive effect of hydrogen bonding on the fiber-fiber cross-linking is therefore exceeding the disturbing effect of the lamellae. As a result, the G' values observed for Me₂PE-C32-Me₂PE are larger than that for PC-C32-PC at a bolaamphiphile concentration of ≤ 2 mg/ml. At a concentration of 4 mg/ml Me₂PE-C32-Me₂PE, both effects seem to balance each other and nearly identical G' values are observed for PC-C32-PC and Me₂PE-C32-Me₂PE. Increasing the bolaamphiphile concentration to 8 mg/ml, obviously results in a significant increase of the number of lamellar aggregates inside the hydrogel of Me₂PE-C32-Me₂PE. Therefore, the disturbing effect of these lamellar aggregates seems to dominate over the effect of the formed hydrogen bonds. As a result, the G' value obtained for PC-C32-PC exceeds that obtained for Me₂PE-C32-Me₂PE at pH 5. In order to support this interpretation of the presented data, further measurements have to be performed with higher concentrations of PC-C32-PC and Me₂PE-C32-Me₂PE up to 30 mg/ml.

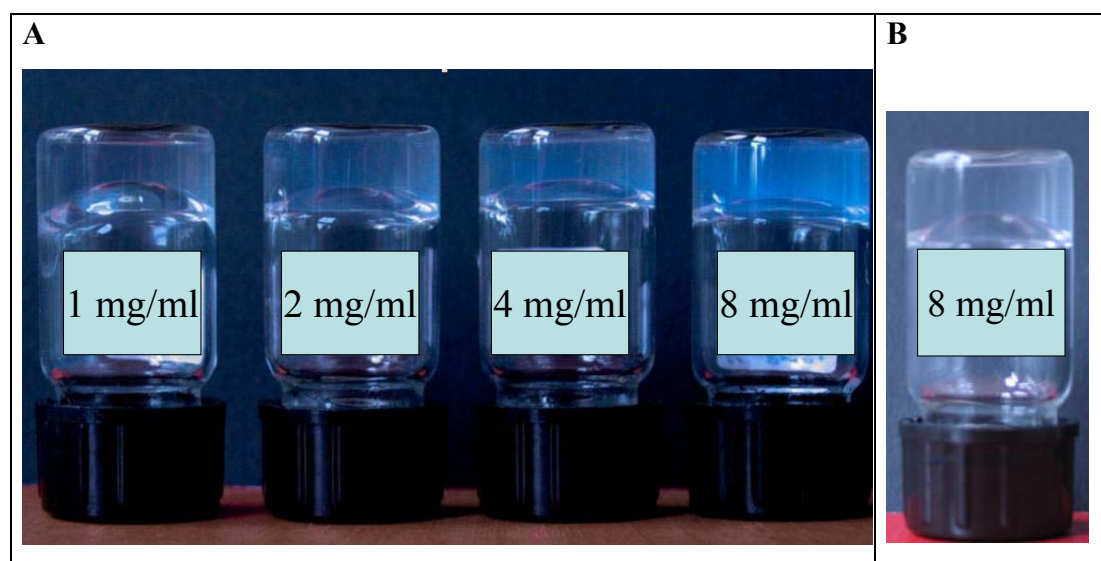


Figure 3.1.3 Photographs of hydrogels formed by (A) 1, 2, 4 and 8 mg/ml Me₂PE-C32-Me₂PE in acetate buffer pH 5 and (B) 8 mg/ml PC-C32-PC in deionized water.

One can conclude that increasing the concentration of PC-C32-PC and Me₂PE-C32-Me₂PE leads to increasing G' values. This indicates a considerable increase in the number of fiber-fiber cross-links with increasing concentration. A possible explanation for the observed differences between the G' values of PC-C32-PC and Me₂PE-C32-Me₂PE was suggested, but further investigations are required to support this interpretation.

3.1.3 Temperature dependence

The hydrogels formed by PC-C32-PC and Me₂PE-C32-Me₂PE are thermoreversible hydrogels. The gel character can be completely destroyed by increasing the temperature above a certain point and is reestablished, when the sample is cooled down again. As described above, first attempts were made to relate the transitions, observed by DSC, to the rheological behavior of gels with 8 mg/ml PC-C32-PC or Me₂PE-C32-Me₂PE. For PC-C32-PC, the temperature dependence of the dynamic viscosity was measured by applying a temperature ramp from 20 to 80 °C.^[13] For Me₂PE-C32-Me₂PE at pH 5, the G', G'' and tan δ were determined at only four temperatures.^[18]

Further rheological characterization was done in order to obtain more detailed information about the temperature dependence of the rheological parameters G' and G'' for hydrogels of PC-C32-PC and Me₂PE-C32-Me₂PE at concentrations of 1, 2, 4 and 8 mg/ml.

3.1.3.1 PC-C32-PC

Figure 3.1.4 shows the temperature dependence of the G' and G'' values that were obtained for different concentrations of PC-C32-PC ($\gamma = 1\%$, $\omega = 1$ rad/s).

The general temperature dependence of the G' and G'' values is very similar for all concentrations of PC-C32-PC. Starting from 25 °C, the G' and G'' values are slightly decreasing with increasing temperature due to disturbances introduced by faster thermal motions. The main transition is found between 48 and 49 °C in the DSC thermograms. This main transition of PC-C32-PC is clearly detected at approximately 48 °C for all concentrations, namely by a decrease of the G' and G'' values by two to three orders of magnitude. The very low G' and G'' values obtained above the transition temperature correspond to that of the free flowing sample of 1 mg/ml Me₂PE-C32-Me₂PE at pH 10 (Figure 3.1.2C). This indicates that the network is completely disintegrated and the gel character is lost. This finding exactly confirms the results obtained from a simple “table-top” rheological test.^[25] For this test, a sample was placed in a thermostated water bath. After equilibration at the particular temperature, the sample tube was carefully turned upside down. Up to about 48 °C, the hydrogels of PC-C32-PC were found to be stable and showed no sign of flow. When the samples were heated above 48 °C, the aqueous phase was found to flow freely, which indicated the breakdown of the fiber network and the loss of the gel character.

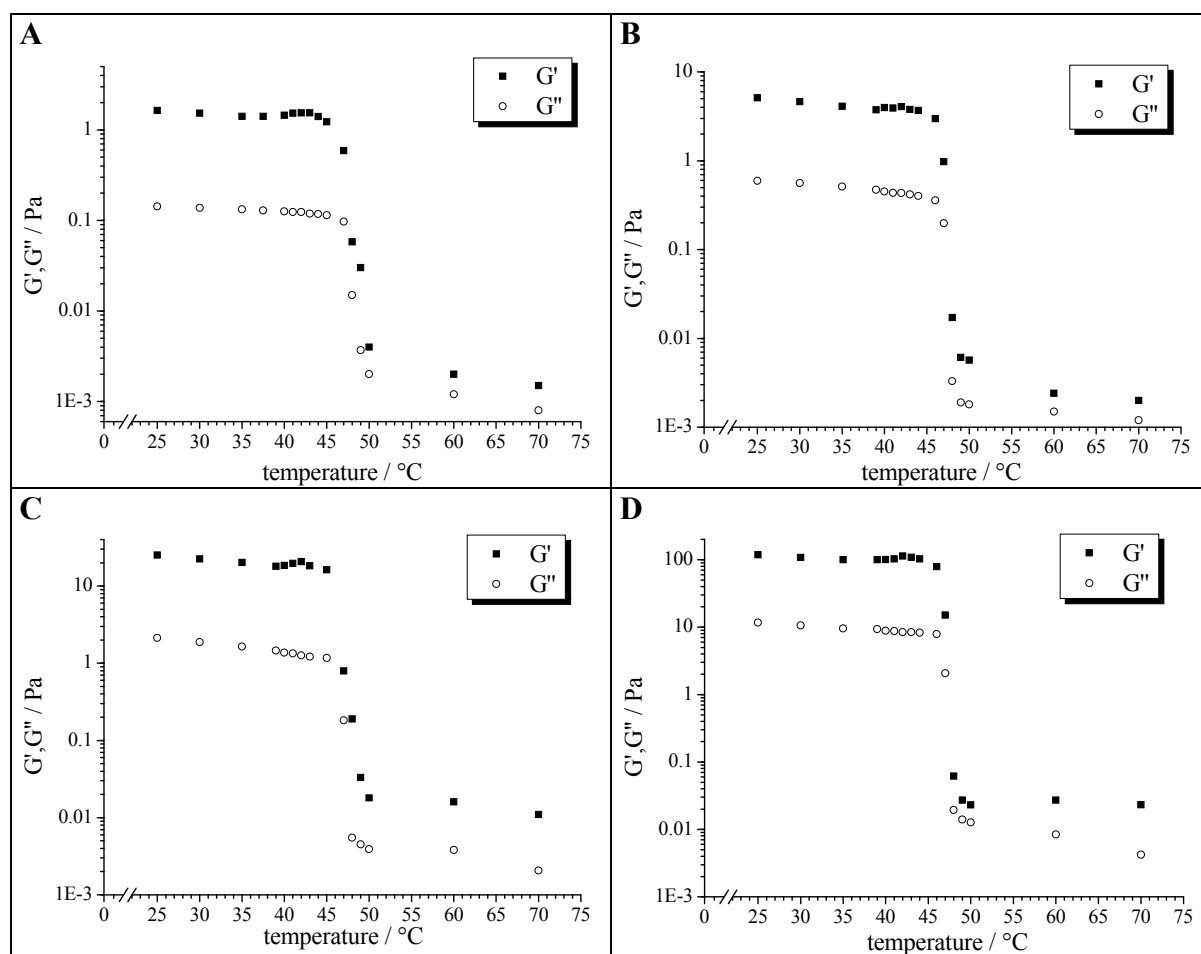


Figure 3.1.4 Temperature dependence of the G' and G'' values obtained for hydrogels formed by PC-C32-PC at different concentrations: (A) 1 mg/ml (B) 2 mg/ml (C) 4 mg/ml (D) 8 mg/ml

As described above, the temperature dependence of the dynamic viscosity η was determined before for a hydrogel with 8 mg/ml PC-C32-PC (Figure 1.6). In these investigations, the dynamic viscosity was found to be dramatically decreased at the temperature of the pre-transition (40 °C). This was indicating that most of the fiber-fiber cross-links were already broken down above this temperature. On the other hand, the main transition at about 48 °C was only related to a small additional decrease in η . The data, presented here, show some disagreement with these earlier investigations, since only the main transition is found to be related to a significant decrease in the G' and G'' values. The pre-transition is also detected, but not by a decrease in the storage modulus, but as a slight increase in G' . This phenomenon is observed for all concentrations and for several repetitions. ^{31}P -NMR revealed that the pre-transition is related to a significant increase in the headgroup mobility.^[18] A slight increase of the storage modulus can only be interpreted in terms of an increase of the number and/or of the stability of the fiber-fiber cross-links. One could speculate that the increased flexibility of the headgroups allow for a more efficient hydrophobic interaction between the fibers. This

finding seems to be in contradiction to the earlier investigations. However, the dynamic viscosity η and the storage modulus G' are determined in a quite different way. The dynamic viscosity is determined by means of rotational rheometry, which is based on the application of a constant shear stress. The G' values are determined by performing oscillatory rheometry, which allows the system to release the applied deformational stress in order to maintain the internal structure and is therefore the preferred method to investigate the rheological behavior of gels. Additionally to the differences between the measuring techniques, there are also differences in the heating procedures. The G' values were obtained after a sufficient waiting time at each temperature in order to allow the system to reach thermal equilibrium, whereas a temperature ramp from 20 to 80 °C was applied to determine η . This shows that the results of both methods cannot easily be compared with each other.

One can conclude that the main transition is clearly detected by a decrease in the G' and G'' values indicating the breakdown of the gel network. The pre-transition is detected by a slight increase in the G' values. This points to a slightly more efficient fiber-fiber cross-linking above the pre-transition temperature.

3.1.3.2 *Me₂PE-C32-Me₂PE at pH 5*

Figure 3.1.5 shows the temperature dependence of the G' and G'' values obtained for different concentrations of *Me₂PE-C32-Me₂PE* at pH 5 ($\gamma = 1\%$, $\omega = 1$ rad/s).

The obtained G' and G'' values are again very similar for all concentrations, since they are slightly decreased between 25 and 40 °C and show two distinct discontinuities between 40 and 70 °C. These discontinuities indicate significant changes in the self-assembled bolaamphiphile network and the temperatures of these transitions are in agreement with the DSC data (Table 1.1). The first transition is detected at about 45 °C by a decrease in G' and G'' . Above this transition temperature, the G' and G'' values are found to be decreased by about one order of magnitude for all concentrations. However, these G' and G'' values remain relatively large, which is due to the still persisting gel character above this transition temperature. ³¹P-NMR measurements revealed increased motional freedom of the headgroups above this temperature, but headgroup rotations were found to be still restricted. It is also known from FT-IR spectroscopy that this transition is related to a partial fluidization of the alkyl chains due to increased trans-gauche isomerization. The reduced values for G' and G'' above the first transition temperature clearly indicate that the increase of the mobility of the headgroups and alkyl chains leads to a distinct decrease in the number of cross-links between the fibers inside the three-dimensional network. It was argued before that this decrease in G' and G'' could be due to a decreased interaction between the hydrophobic fiber regions and

also by the simultaneous breaking-up of some hydrogen bonds.^[18] As described above, lamellar aggregates seem to be present in the hydrogels with increasing numbers, when the concentration of Me₂PE-C32-Me₂PE is increased. Results obtained for Me₂PE-C34-Me₂PE and Me₂PE-C36-Me₂PE indicate that these lamellar aggregates are transformed into fibers above the first transition temperature.^[23] This can be assumed for Me₂PE-C32-Me₂PE at pH 5 as well. This is supported by the results obtained by performing the “table-top” rheological test, because above the first transition temperature, all gels were found to be transparent without showing any sign of turbidity. As discussed for the concentration dependence of G' and G'', the presence of the lamellar aggregates can be assumed to affect the rheological behavior of the hydrogels of Me₂PE-C32-Me₂PE to some extent. Therefore, their transformation can be expected to also contribute to the changes observed for G' and G'' at the first transition temperature.

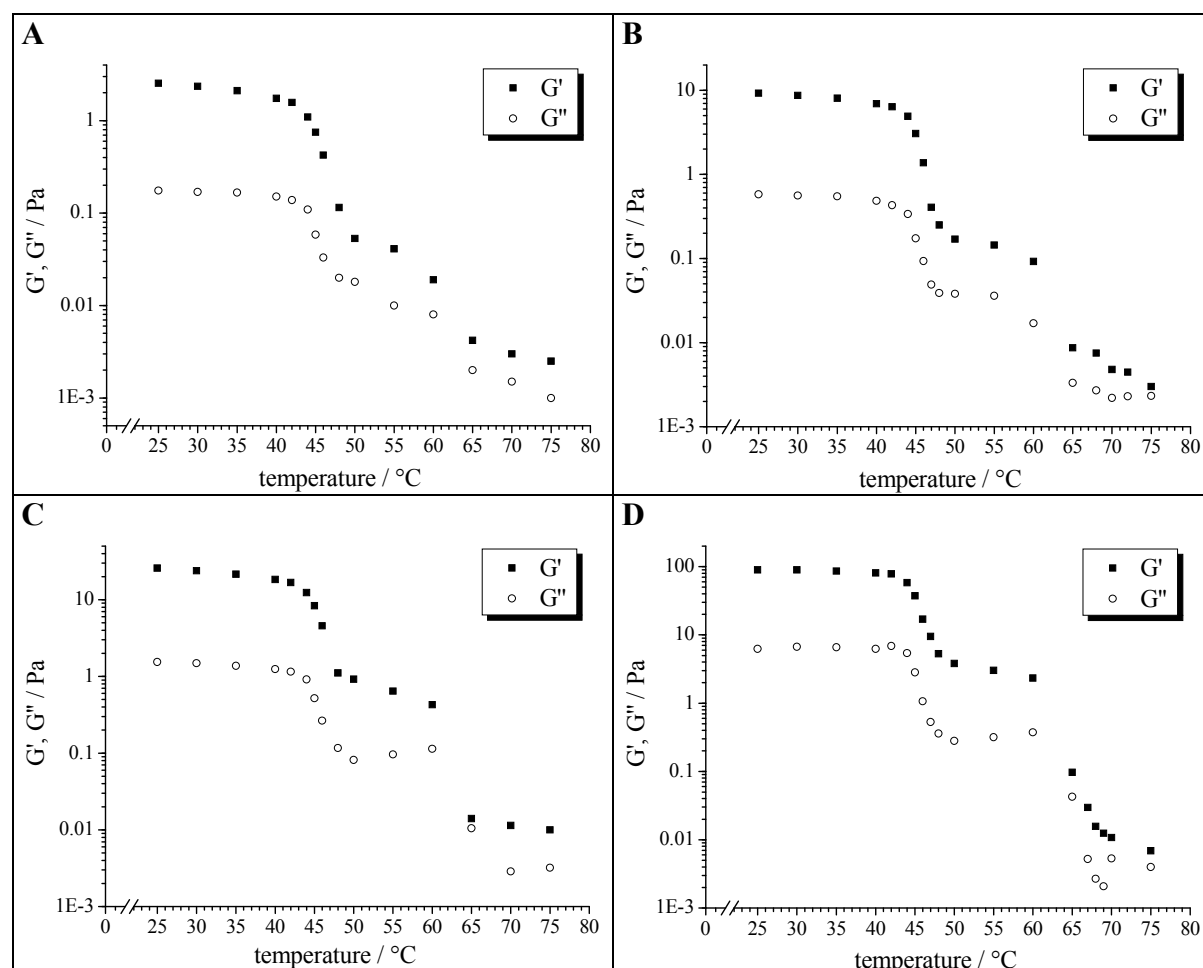


Figure 3.1.5 Temperature dependence of the G' and G'' values obtained for hydrogels formed by Me₂PE-C32-Me₂PE at different concentrations in acetate buffer pH 5: (A) 1 mg/ml (B) 2 mg/ml (C) 4 mg/ml (D) 8 mg/ml

The transition temperature of the second transition was determined by DSC to be 69.5 °C. Figure 3.1.5 shows that this transition is also clearly reflected in the G' and G'' values, but is already completed at approximately 65 °C, which might be due to imperfect temperature control by the rheometer at these high temperatures. The “table-top” rheological test revealed free flowing of the sample, when the temperature is increased above 67 °C.

Above the second transition temperature, the fiber network becomes completely disintegrated and a micellar solution is obtained. Therefore, the G' and G'' are found to be decreased to values that correspond to that of pure water. As a result of the fact that the G' and G'' values at 50 °C were dependent of the Me₂PE-C32-Me₂PE concentration, this decrease is more pronounced for the samples with a higher content of the bolaamphiphile.

One can conclude that both transitions of Me₂PE-C32-Me₂PE could be detected independently of the concentration. Above the first transition temperature, the strength of the fiber network is reduced leading to a “weaker” hydrogel. The hydrogel character is completely destroyed above the second transition temperature due to the breakdown of the bolaamphiphilic nanofibers into micellar aggregates.

3.1.4 Time tests

3.1.4.1 Cooling from 75 °C to 25 °C

When aqueous samples of PC-C32-PC and Me₂PE-C32-Me₂PE are cooled from temperatures above 70 °C to room temperature, Me₂PE-C32-Me₂PE was found to form a hydrogel faster than PC-C32-PC. In order to directly detect the differences between both bolaamphiphiles regarding the kinetics of network formation, time dependent rheometry was performed. However, the data presented here have to be regarded as a preliminary result, since no study with long waiting times could be carried out due to time restrictions.

The time dependent experiments were carried out according to the procedure described in Section 2.2.1. The obtained G' values for the first 60 minutes are shown in Figure 3.1.6 for PC-C32-PC and Me₂PE-C32-Me₂PE at different concentrations.

It has to be mentioned that there is some uncertainty about the true temperature inside the samples during the first period of the experiment. The sample volume of about 1.5 ml was relatively small and spread over about 20 cm². As a result, one can expect that the sample should be cooled immediately by the plate. The uncertainty results from the fact that the warm cone might be cooled down more slowly than the plate, since its temperature is only regulated by air flow that is controlled by the Peltier element. This could lead to a temperature gradient inside the samples for the first minutes, which would have an unpredictable influence on the

measured G' values. However, the conditions should be nearly identical for all samples and the important information lies rather in the observed relative differences between the samples than in the quantitative kinetics.

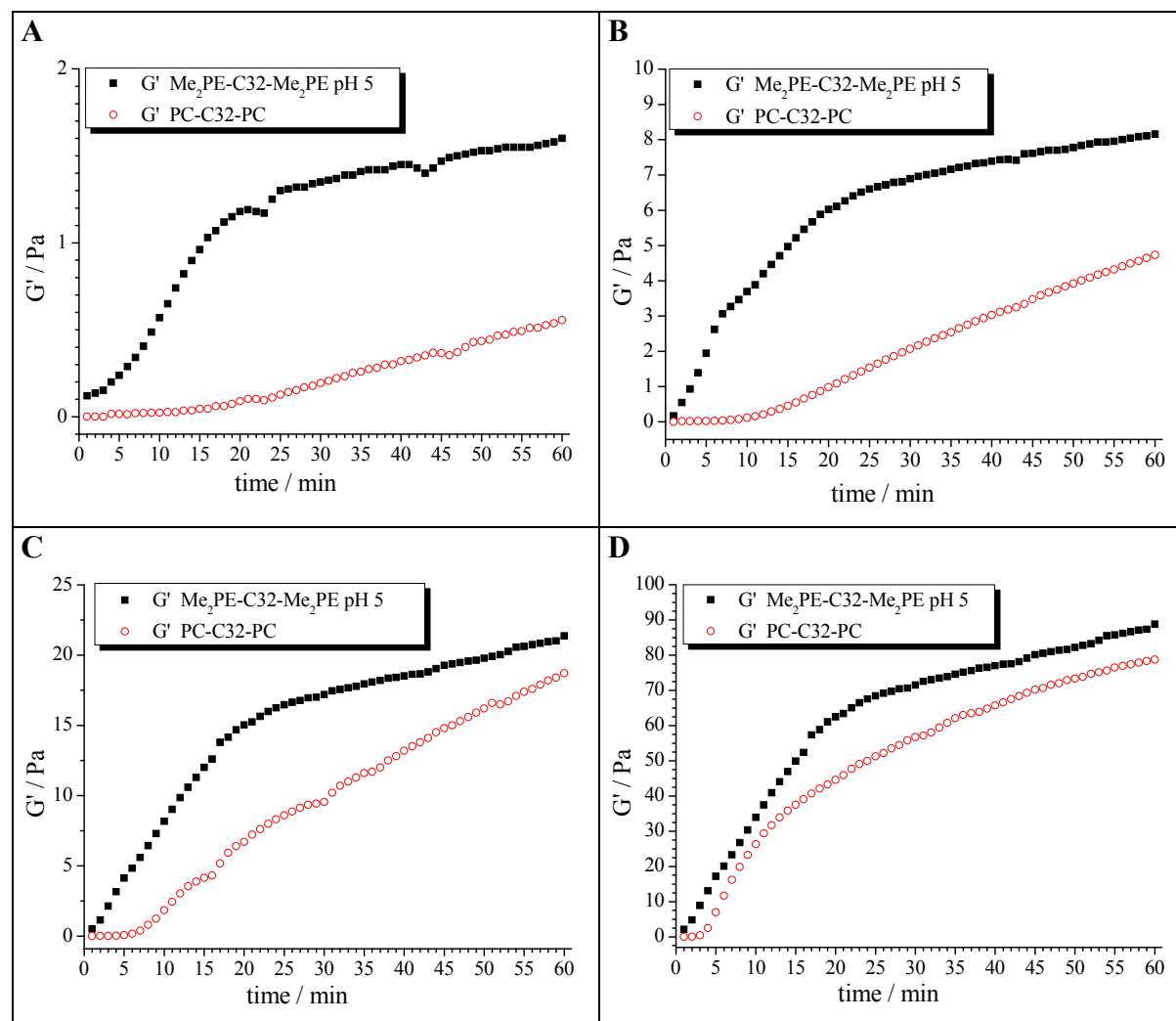


Figure 3.1.6 Time-dependent recovery of the G' values obtained for PC-C32-PC and Me₂PE-C32-Me₂PE at different concentrations after cooling down from 75 to 25 °C: (A) 1 mg/ml (B) 2 mg/ml (C) 4 mg/ml and (D) 8 mg/ml

For concentrations up to 4 mg/ml, the time-dependent recovery of the G' values is completely different for PC-C32-PC and Me₂PE-C32-Me₂PE (Figures 3.1.6A-C). For PC-C32-PC, there is always a lag time observable before the G' values start to increase linearly. This lag time extends to about 15 minutes for 1 mg/ml PC-C32-PC and becomes considerably shorter for 2 mg/ml (about 10 min) and 4 mg/ml (5 min) PC-C32-PC. During this lag time, no fiber network seems to be present inside the samples, but the transformation of the micellar aggregates into short rod-like aggregates can be expected to have already started. When the number and the lengths of these rod-like aggregates reach a certain limit, a three-dimensional network of fibers will be formed and the G' values will start to increase. Further elongation

and cross-linking of the fibers will increase the strength of the fiber network with time. Obviously, this is a very slow process for PC-C32-PC at concentrations ≤ 4 mg/ml as is indicated by the only slightly increasing G' values. As a consequence, the G' values, that are reached within the 60 minutes of the experiment, are considerably lower than the equilibrium values presented in Figure 3.1.4. However, these processes become significantly faster with increasing concentration. The $G'_{60\text{min}}$ value for 1 mg/ml PC-C32-PC reaches only about 40% of the equilibrium value, whereas for 4 mg/ml PC-C32-PC it corresponds to about 75%. At a concentration of 8 mg/ml PC-C32-PC, the reconstitution kinetics of the G' values are differing to some extent from that observed for the lower concentrations. Only a very short lag time of two to three minutes is observed, which is followed by an increase in the G' values that can be divided into two different phases. The first phase from 4 to about 12 minutes, is characterized by a relatively large increase of G' with time. This is indicating that during this time the formation of new cross-links between the bolaamphiphilic fibers is considerably fast. Obviously, these processes are proceeding noticeably slower in the second phase, because the increase in G' with time is not as large as in the first phase.

A two-phase behavior is also observed for all concentrations of $\text{Me}_2\text{PE-C32-Me}_2\text{PE}$ at pH 5. For these samples, the lag time is significantly decreased with respect to PC-C32-PC and is only visible for the sample with 1 mg/ml $\text{Me}_2\text{PE-C32-Me}_2\text{PE}$. This indicates that the processes involved in the transformation from small micelles to very long fibers are considerably faster for $\text{Me}_2\text{PE-C32-Me}_2\text{PE}$ due to the effect of hydrogen bonding. The two-phase behavior is particularly obvious for the samples with 4 and 8 mg/ml $\text{Me}_2\text{PE-C32-Me}_2\text{PE}$. The first phase is determined by a rapid linear increase of the G' values, which is indicating a fast increase in the number of cross-links during this phase. For all concentrations, the first phase ends after 20 minutes and the G' values reach about 60 to 70% of the equilibrium values within this time. During the second phase, the G' values are found to increase only slowly. Therefore, it seems likely that the formation of additional cross-links needs considerably more time. This is indicating that extensive reformations of the fibers inside the network might be necessary to achieve a more efficient cross-linking. At the end of the measuring period of 60 minutes, the G' values obtained for all samples with $\text{Me}_2\text{PE-C32-Me}_2\text{PE}$ correspond to more than 90% of their particular equilibrium values at 25 °C. Inside these hydrogels, formed by $\text{Me}_2\text{PE-C32-Me}_2\text{PE}$ within 60 minutes, the expected number of lamellar aggregates is smaller compared to the samples that were stored for 24 hours prior to the measurements. By performing the time test not for 60 minutes, but for 24 hours or longer, the influence of the increasing number of lamellae on the determined G' values should be clearly observable.

3.1.4.2 Mechanical stress

Another time test was carried out in order to study the self-healing properties of the bolaamphiphilic fiber networks. For this purpose, considerable mechanical stress was applied to samples with 2 mg/ml of the bolaamphiphiles at a temperature of 25 °C (Section 2.2.1).

Figure 3.1.9 clearly shows that after the application of mechanical stress, the recovery of the G' values is considerably faster compared to the temperature treatment described above. No lag time is observed even for PC-C32-PC, and the storage moduli measured after 1 minute have already reached about 65% of their equilibrium values. This can be explained by the fact that the applied mechanical stress only causes a breaking-up of as many cross-links as needed to allow for the drastic deformation of 300%. This can be expected to result in the breakdown of some fibers as well, but the main structure of the fibers will remain intact. The introduced defects inside the network seem to be repaired almost immediately to a large extent for both bolaamphiphiles. As a consequence, the equilibrium values are reached within the 60 minutes of the experiment. The G' values obtained in this test for 2 mg/ml PC-C32-PC and 2 mg/ml Me₂PE-C32-Me₂PE at pH 5 are almost parallel to each other. Therefore, these repair processes seem to be very similar for both bolaamphiphiles.

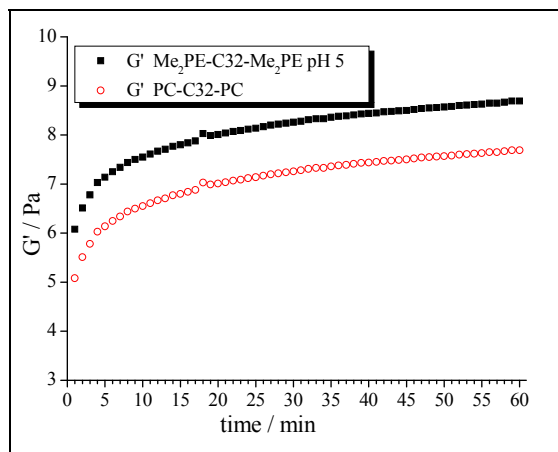


Figure 3.1.7

Recovery of the G' values of 2 mg/ml PC-C32-PC in deionized water and 2 mg/ml Me₂PE-C32-Me₂PE at pH 5 following to the amplitude test with a deformation of 300%.

One can conclude that there are significant differences observable in the formation kinetics of fiber networks of Me₂PE-C32-Me₂PE and PC-C32-PC upon cooling from 75 °C to 25 °C. Fibers and fiber-fiber cross-links are formed considerably faster for Me₂PE-C32-Me₂PE at pH 5, which can be explained by its ability to form hydrogen bonds between the bolaamphiphilic headgroups. On the other hand, breaking down the hydrogels by applying a deformation of 300% was found to be followed by fast self-healing processes, which seem to be very similar for both bolaamphiphiles.

3.2 Nuclear magnetic resonance (NMR) spectroscopy

3.2.1 Relaxation behavior of the water protons

For all potential biomedical applications of hydrogels, the physico-chemical properties of water in these systems are of crucial importance, since they mainly determine the transport processes through the gel, such as the release of drugs or the nutrient supply for cells and tissues. The properties of water in a hydrogel are affected by its interaction with the gel network, by the pore sizes and by the pore interconnections.^[73] At a given time, one can generally distinguish two classes of water in a hydrogel, which are in exchange with each other: One class of water molecules that is remote from the network and is not influenced by its presence (unperturbed water) and one that is interacting with the network and therefore changed in its properties compared to pure water (perturbed water).^[74] The physico-chemical properties of water in various hydrogel systems were studied by a number of techniques, such as calorimetry, dilatometry, differential thermal analysis, specific conductivity and nuclear magnetic resonance spectroscopy.

For the characterization of water in hydrogels of PC-C32-PC and Me₂PE-C32-Me₂PE, the proton nuclear magnetic resonance (¹H-NMR) technique was chosen in order to gain information about the dynamics of the water molecules. As described in Section 2.2.2, ¹H-NMR relaxometry allows the measurement of the transverse relaxation times (T₂) of the protons by applying the CPMG pulse sequence. Relaxation processes in ¹H-NMR are dominated by dipole-dipole interactions between neighboring protons and depend on fluctuating magnetic fields of proper frequencies that result from rotations and Brownian motion of the molecules. Therefore, NMR relaxation is highly sensitive to the dynamics of the water molecules. The transverse relaxation behavior of the water protons was studied for hydrogels formed by PC-C32-PC and Me₂PE-C32-Me₂PE at concentrations of 1 or 30 mg/ml.

3.2.1.1 PC-C32-PC in deionized water

Initially, the T₂-relaxation behavior of protons in pure deionized water was determined at temperatures between 25 and 80 °C. The measured decays of the transverse magnetization are shown in Figure 3.2.1.

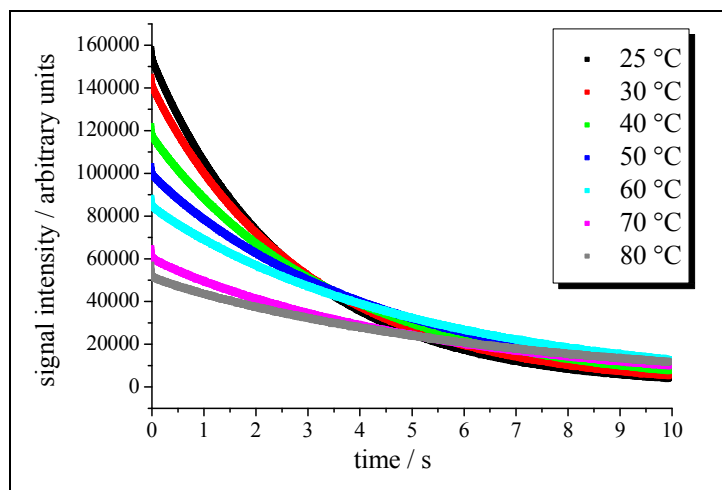


Figure 3.2.1

Transverse magnetization decays obtained for H₂O at different temperatures. Each data point corresponds to one of the 36864 detected echos.

Figure 3.2.1 shows that the signal intensities detected during the first second are found to be significantly decreased with increasing temperature. This can be explained by a smaller difference between the populations of spins in the α - and β -state (Boltzmann distribution, Equation 2.19), when the temperature is increased. As a consequence, the net magnetization at thermal equilibrium $M_{Z(\text{eq})}$ is decreased. This lower $M_{Z(\text{eq})}$ is then transferred into the transverse magnetization M_{-Y} and detected as the first data points of the decaying echo intensities. Furthermore, the decays of the transverse magnetization become significantly flattened with increasing temperature. This indicates prolonged relaxation processes due to a distinct increase in the relaxation time constant T_2 .

There are different ways to determine the mean T_2 -values from the magnetization decays. In the present relaxation study, the program WinDXP^[45] was used to obtain continuous T_2 -distributions from each CPMG echo envelope. Analogous to the well known program CONTIN,^[75-78] WinDXP uses Laplace inversion to calculate the T_2 -distributions. WinDXP was used before to investigate the relaxation behavior of water in a variety of samples, such as starch,^[79,80] silica gels,^[81] soil^[82] and chicken breast.^[83]

The results obtained by fitting the NMR data with WinDXP were found to be highly reproducible. Figure 3.2.2A shows a typical full-range T_2 -distribution obtained by fitting the echo envelope obtained for H₂O at 25 °C with WinDXP. The major peak of this T_2 -distribution is found at approximately 2.8 s. This major T_2 -peak is representing the majority of the water protons of the particular sample. T_{2m} , the mean T_2 -value, is therefore determined from the center of this major T_2 -peak as outlined in Figure 3.2.2A. For comparison, a fit for a first order exponential decay is also shown for the same echo envelope. The T_2 -value obtained from this fit was 2.77 s, which is in good agreement with the determined T_{2m} -value of 2.83 s. Therefore, the determination of T_{2m} from the major peak of the T_2 -distributions yields values that can be assumed to be a reliable measure for the transverse relaxation

behavior of the water molecules. Moreover, the particular shape and amplitude of the major peak of the T_2 -distributions contain important additional information about the relaxation behavior of the sample as will be shown below.

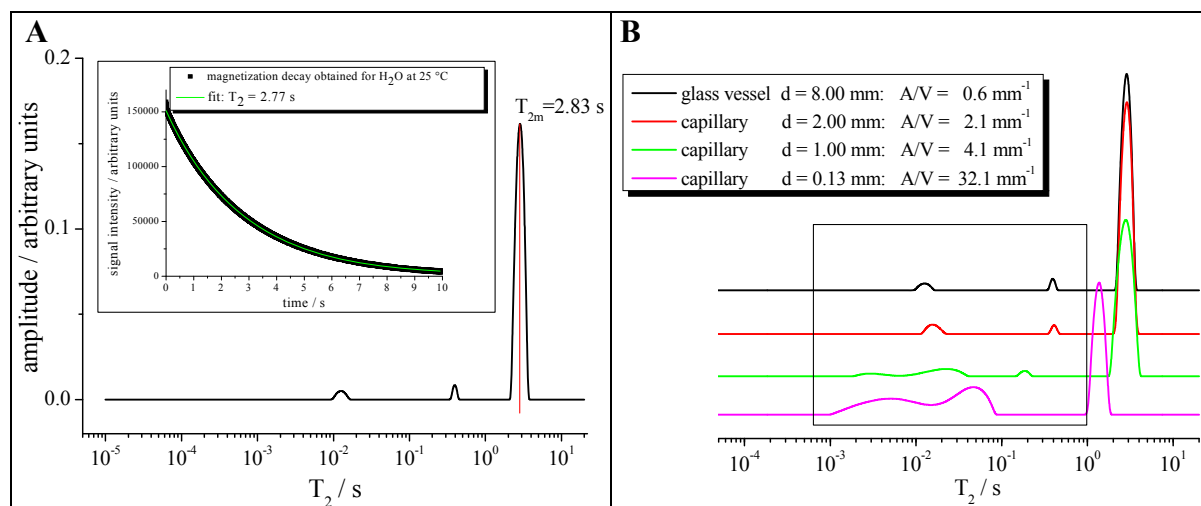


Figure 3.2.2 (A) Typical T_2 -distribution calculated by WinDXP for H_2O at $25\text{ }^\circ\text{C}$. The determination of the T_{2m} -value is indicated. For comparison, a fit for a first order exponential decay is also shown. (B) Presentation of T_2 -distributions obtained for H_2O samples with increasing glass surface-to-volume (A/V) ratios in order to demonstrate the increasing influence of surface relaxation on the obtained T_2 -distributions.

Besides the major T_2 -peak, two small peaks are visible in the T_2 -distribution displayed in Figure 3.2.2A. These peaks are centered at approximately 10 ms and 400 ms, respectively. In order to reveal the origin of these additional peaks, measurements were performed using water samples with increasing glass surface-to-volume (A/V -ratios). Additional to the standard glass vessel for the NMR measurements ($d = 8\text{ mm}$), three capillaries with decreasing diameters were filled with deionized water up to 10 mm in height. Therefore, the A/V -ratio is subsequently increased from 0.6 to 32.1 mm^{-1} . The obtained T_2 -distributions (Figure 3.2.2B) clearly indicate that the small peaks are related to the relaxation of water protons at the glass surface, which can be expected to act as a relaxation sink.^[76] When the A/V -ratio is increased from 0.6 to 2.1 mm^{-1} , the peak areas of the small peaks take up only about 5% of the total peak area, whereas for a A/V -ratio of 4.1 mm^{-1} , this is approximately 12%. The effect of surface relaxation becomes striking for the A/V -ratio of 32.1 mm^{-1} . Here, these peaks take up about 55% of the total peak area and the major peak is significantly shifted in position with respect to the T_2 -distribution obtained for the glass vessel. This position shift is not observed for the other capillaries. This indicates that the position of the major T_2 -peak is almost independent of surface relaxation in the glass vessel. This is an

important finding, since it shows that the determined T_{2m} -values can be attributed to the properties of the water molecules in the particular sample and not to surface phenomena. As outlined in Section 2.2.2, transverse relaxation of the protons is dominated by the dipole-dipole relaxation mechanism, which is highly sensitive to molecular motion. Therefore, significant changes in mobility of the water molecules will be reflected in the determined T_{2m} -values. This becomes evident in Figure 3.2.3A, which shows the normalized major peaks of the T_2 -distributions obtained from the echo envelopes displayed in Figure 3.2.1.

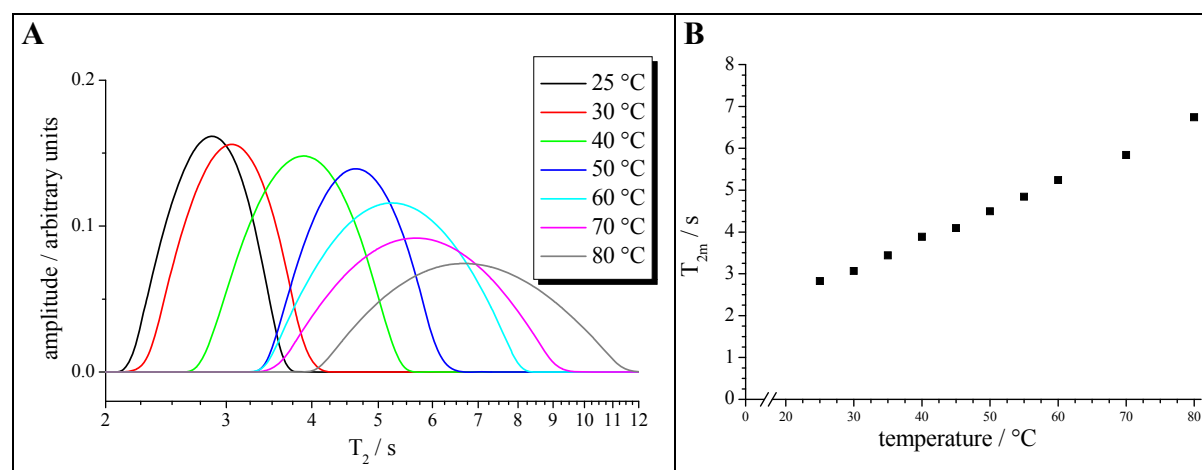


Figure 3.2.3 Transverse relaxation behavior determined for H₂O at temperatures from 25 to 80 °C: (A) Major T_2 -peaks of the calculated T_2 -distributions, which are normalized to the same peak area. (B) Corresponding T_{2m} -values plotted against temperature.

With increasing temperature, the major T_2 -peaks are found to be considerably broadened. This is due to the wider distribution of the rotational correlation times of the water molecules. Simultaneously, the peaks are gradually shifted to larger T_2 -values. The resulting T_{2m} -values, determined from each peak, are plotted against temperature in Figure 3.2.3B. They were found to increase linearly with increasing temperature by approximately 70 ms/K. This linear increase is due to the fact that dipole-dipole relaxation requires fluctuating magnetic fields of low frequency and short distances between the interacting species. With increasing temperature, the frequency of the fluctuating magnetic fields increases due to increased thermal motion of the water molecules. Therefore, transverse relaxation becomes less efficient and the relaxation rate $R_2 = 1/T_2$ decreases.

As described above, PC-C32-PC is a very efficient LMW hydrogelator. After dispersion at temperatures above 80 °C, where micelle-like aggregates are formed, the PC-C32-PC molecules self-assemble into helically structured nanofibers when the sample is cooled down to room temperature. Unlike other LMW hydrogelators, PC-C32-PC cannot form hydrogen

bonds between the headgroups. Therefore, its self-assembly into fibers and the cross-linking between these fibers is solely driven by hydrophobic interactions between the long hydrocarbon chains. The role of water in these processes is not fully understood up to now. Therefore, the question arises, whether the presence of the three-dimensional network of bolaamphiphilic nanofibers influences the relaxation behavior of the water molecules.

T_2 -distributions obtained at 25 °C for hydrogels with 1 and 30 mg/ml PC-C32-PC in deionized water are presented in Figure 3.2.4.

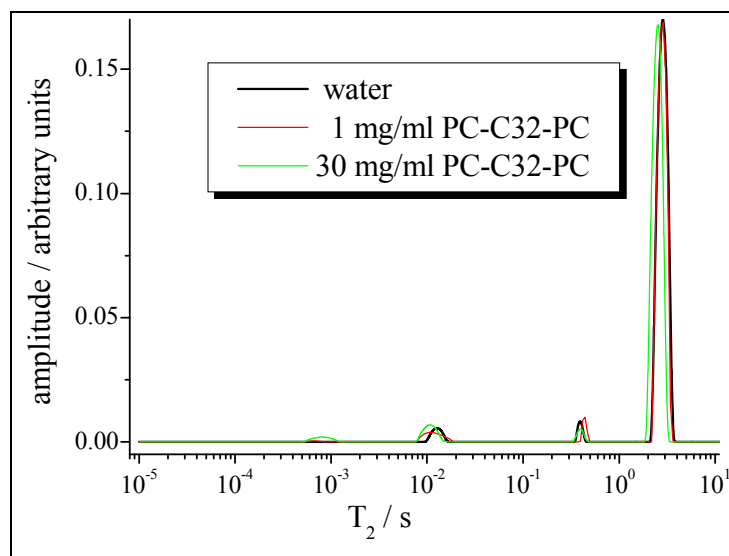
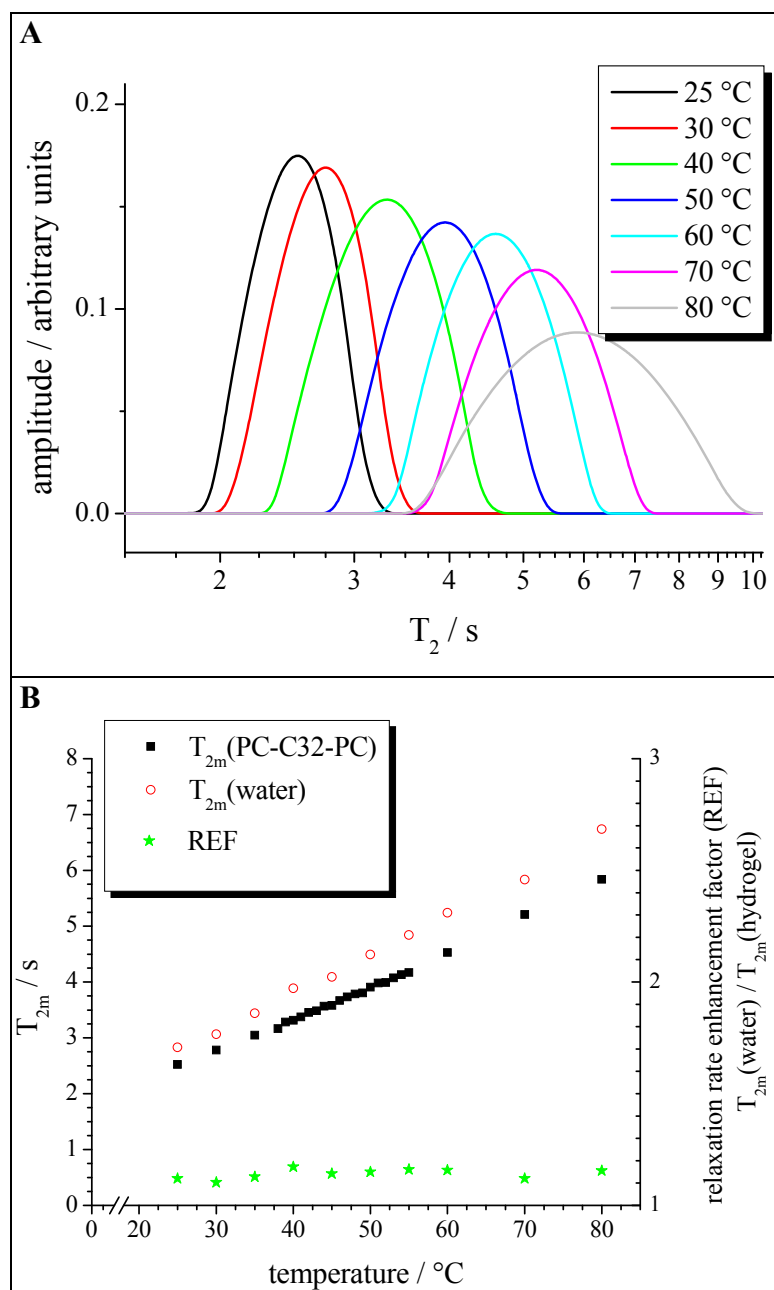


Figure 3.2.4

1 mg/ml and 30 mg/ml PC-C32-PC in deionized water: Normalized T_2 -distributions obtained at 25 °C compared to that of pure deionized water.

There is no significant difference observable between the T_2 -distributions of pure deionized water and the sample containing only 1 mg/ml PC-C32-PC. For the hydrogel with 30 mg/ml PC-C32-PC, the major T_2 -peak is found to be slightly broadened and shifted to lower T_2 -values. This peak again represents the majority of the protons of the water molecules and the determined T_{2m} -value is decreased by about 0.3 s with respect to that of pure water. Besides the peaks that correspond to proton relaxation at the glass surface, an additional T_2 -peak is detected at about 1 ms. This peak represents the relaxation of the protons of the bolaamphiphile molecules. More detailed information about the transverse relaxation of the bolaamphiphile protons can be achieved by performing relaxation experiments with PC-C32-PC dispersed in D_2O instead of H_2O . Such experiments were performed and confirmed that the T_2 -peak at approximately 1 ms can be ascribed to the bolalipid protons (Section 3.2.4).

The temperature dependence of the relaxation behavior was only investigated for the hydrogel containing the higher concentration, namely 30 mg/ml PC-C32-PC. In analogy to pure H₂O, the major T₂-peaks become significantly broadened and gradually shifted to larger T₂-values when the temperature is increased from 25 to 80 °C (Figure 3.2.5A).



For the sample with 30 mg/ml PC-C32-PC, the T_{2m}-values are found to be increased linearly by about 60 ms/K with increasing temperature (Figure 3.2.5B). Above 50 °C, the fibers are replaced by micelle-like aggregates and the hydrogel character is lost. However, this change in the aggregate morphology is not reflected in the T₂-distributions or in the determined T_{2m}-values. Therefore, there is obviously no relationship between the formed aggregates and the

relaxation behavior of the water protons for hydrogels formed by 30 mg/ml PC-C32-PC. This situation is not unexpected, since relaxation is not directly related to the macroscopic properties of the sample, but is essentially a local phenomenon.^[84]

The conclusion is that the relaxation behavior of the water protons was found to be almost unaffected by the presence of the dense network of nanofibers even when the PC-C32-PC concentration was increased to 30 mg/ml. Compared to pure water, there is only a slight decrease in the T_{2m} -values observable for the sample with 30 mg/ml PC-C32-PC. This decrease was found to be independent of the type of aggregates and is therefore not correlated to the hydrogel status. As shown by Roorda et al. for poly(hydroxyethyl methacrylate) (pHEMA) hydrogels,^[74] the small effect on the relaxation of the water protons can be fully explained as a concentration dependent effect. These authors determined the relaxation rate enhancement factors (REFs)

$$\text{REF} = \frac{R_{1,2}(\text{hydrogel})}{R_{1,2}(\text{water})} = \frac{T_{1,2}(\text{water})}{T_{1,2}(\text{hydrogel})} \quad (3.1)$$

for a large number of pHEMA hydrogels with varying polymer contents, cross-linking densities and number of hydrophilic binding sites. Roorda and co-workers found the REF to be dependent only of the polymer content, but independent of the number of binding sites or of the degree of cross-linking. The authors therefore concluded that the decrease of the average mobility of the water molecules in pHEMA hydrogels is mainly determined by the concentration of the polymer and not by the cross-linker content. Another important conclusion was drawn by Roorda et al. from their ¹⁷O relaxation study: They could confirm earlier results, obtained by thermal analysis of pHEMA hydrogels,^[85,86] that ruled out one of the commonly referred models for water in hydrogels. This model distinguishes between at least three different classes of water, namely bound water, intermediate water and free water.^[87-89] However, Roorda et al. could show that all the water in pHEMA hydrogels at 25 °C was found to be in exchange on a timescale of a millisecond or less. This means, if different states of water are present at this temperature, the exchange between these states is so fast that it results in the detection of only one averaged relaxation rate.

The relaxation rate enhancement factors were also determined for PC-C32-PC. The results are shown in Figure 3.2.5B and confirm that the relaxation behavior of the water protons is independent of the type of the PC-C32-PC aggregates, since no discontinuity could be observed for the REFs. The uniformly low REFs as well as the relatively narrow major T_2 -peaks obtained for the sample with 30 mg/ml PC-C32-PC can be explained as follows: Because of the small volume fraction of PC-C32-PC, the particular bolaamphiphilic

aggregates can be expected to be uniformly distributed throughout the water volume. Moreover, it can be assumed that only the first layers of water around the aggregates are dynamically perturbed.^[90] These perturbed water molecules are in a diffusional exchange with the surrounding unperturbed water on a submillisecond level. Extremely rapid exchange can be assumed, since the diffusion distance from the surface layers to the surrounding water volume is very short. As a consequence, the water molecules will experience only a small perturbation by the aggregate surface. The resulting influence on the proton relaxation behavior is therefore very small, which is reflected in a major T_2 -peak that is only slightly broadened and shifted with respect to that of pure water.

For aqueous samples of PC-C32-PC at concentrations up to 30 mg/ml, one can therefore conclude that the relaxation behavior of the water protons is essentially the same as that of pure water. No relationship could be found between the presence of the nanofibers and the obtained REFs. As discussed above, the observed relaxation rate enhancement compared to pure water is simply determined by the bolaamphiphile concentration and not by the formation of nanofibers or by the number of cross-links between these fibers. This means that even in the presence of a dense network of PC-C32-PC nanofibers, the particular water molecules are not seriously restricted in their mobility. Only a very small decrease in the T_{2m} -values is observed, which can be explained by interactions between the water and the PC-C32-PC molecules independent of the formed PC-C32-PC self-assemblies.

3.2.1.2 Me₂PE-C32-Me₂PE in acetate buffer pH 5

The transverse relaxation behavior was also determined for water protons in hydrogels formed by Me₂PE-C32-Me₂PE at pH 5. Prior to these measurements, the influence of the change of the aqueous medium on the relaxation behavior was investigated. Figure 3.2.6 shows that the temperature dependent relaxation behavior observed for 100 mM acetate buffer at pH 5 is essentially the same as that for pure water.

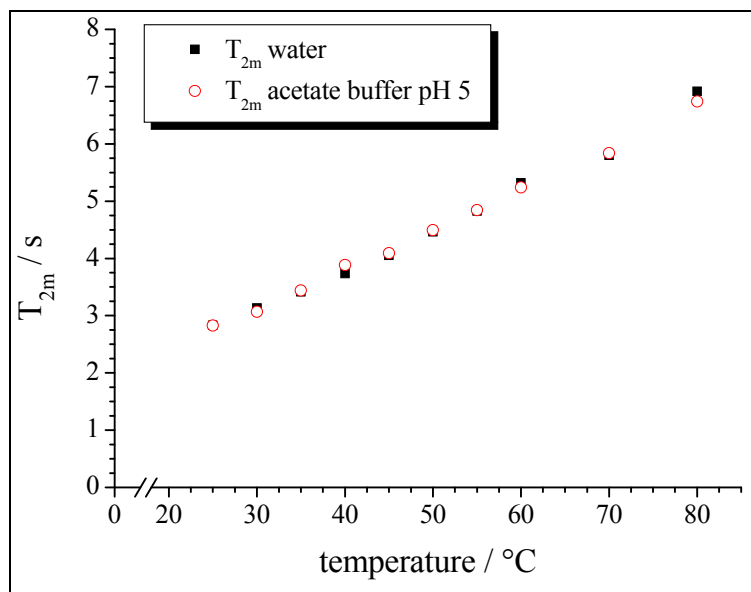


Figure 3.2.6
Comparison of the T_{2m} -values of pure deionized water and pure acetate buffer pH 5.

As described above, $\text{Me}_2\text{PE-C32-Me}_2\text{PE}$ forms a hydrogel after dispersion in acetate buffer at pH 5. Because of the similarities in the aggregation behavior of $\text{Me}_2\text{PE-C32-Me}_2\text{PE}$ at pH 5 compared to PC-C32-PC , one could also expect similarities in the relaxation behavior of the water protons in their hydrogels. Figure 3.2.7 shows that this is the case only for the two samples containing 1 mg/ml of the particular bolaamphiphile. At a higher concentration of 30 mg/ml $\text{Me}_2\text{PE-C32-Me}_2\text{PE}$, however, the relaxation behavior of the water protons was found to differ distinctly from that of a sample with 30 mg/ml PC-C32-PC . The major peak of the obtained T_2 -distributions is considerably broadened and shifted to significantly lower T_2 -values. Therefore, one can assume significant differences to be present between the two bolaamphiphiles regarding their interaction with the water molecules.

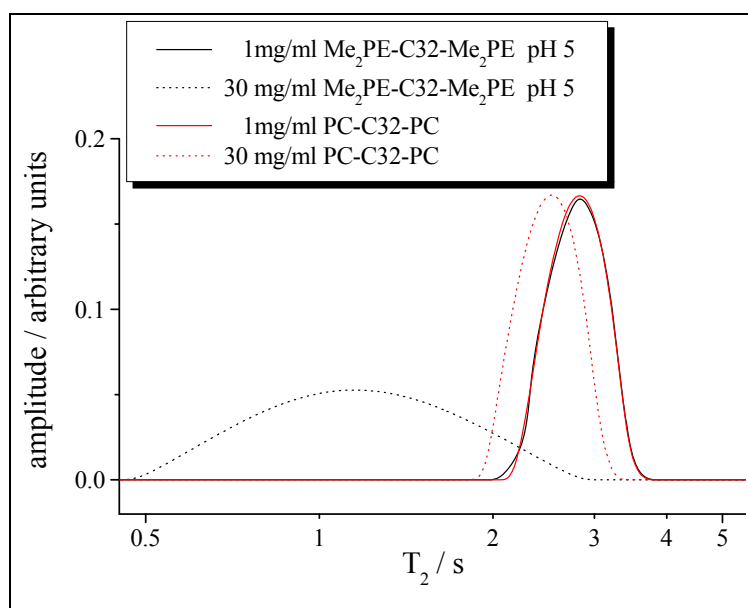


Figure 3.2.7
Normalized major T_2 -peaks obtained at 25 °C for hydrogels containing 1 mg/ml or 30 mg/ml $\text{Me}_2\text{PE-C32-Me}_2\text{PE}$ compared to that of PC-C32-PC .

The changed relaxation behavior of the water protons in hydrogels containing 30 mg/ml Me₂PE-C32-Me₂PE at pH 5 is also reflected in the temperature dependence of the major T₂-peak (Figure 3.2.8A). In accordance to the results discussed above, this major T₂-peak is found to be shifted to larger values with increasing temperatures from 25 to 80 °C. This indicates an increasing mobility of the water molecules in the hydrogel sample. In contrast to the results obtained for the hydrogel of PC-C32-PC, the major T₂-peak is found not be gradually broadened with increasing temperature, but to show a two phase behavior. Between 25 and 50 °C, the peak becomes substantially narrower and its height is increased. Between 50 to 80 °C, the width of the distribution peak increases again accompanied by a decrease in the peak height. Finally, the major T₂-peak almost resembles that of 30 mg/ml PC-C32-PC at 80 °C (Figure S.1 in the Supplement).

The two phase behavior of the relaxation becomes also evident, when the T_{2m}-values and the REFs are plotted against temperature (Figure 3.2.8B). For 30 mg/ml PC-C32-PC, the T_{2m}-values increase linearly by about 60 ms/K with increasing temperature. For Me₂PE-C32-Me₂PE at pH 5, the T_{2m}-values also initially increase linearly (72 ms/K), but between 42 and 48 °C a clearly visible discontinuity indicates distinct changes of the relaxation behavior. In this region, T_{2m} increases by approximately 150 ms/K and, simultaneously, a significant decrease of the REFs is detected between 40 and 50 °C. This points to drastic changes in the organization of the bolaamphiphile molecules. In fact, DSC thermograms show an endothermic peak at 45.5 °C, which is macroscopically related to a decrease of the number of cross-links inside the three-dimensional network of nanofibers.^[18] Microscopically, an increase of the motional freedom of the alkyl chains and of the headgroups were observed.^[15,18,91] However, the hydrogel state still persists above 45.5 °C. The transition temperature of 45 °C, determined from the T_{2m}-values, agrees well with that obtained by DSC. This allows to conclude that the determination of the relaxation behavior of the water protons by ¹H-NMR is capable of detecting the temperature induced transition in the investigated Me₂PE-C32-Me₂PE hydrogel. Similar results were reported, for example, for hydrogels formed by carrageenan^[92] and various polyacrylamides.^[93,94]

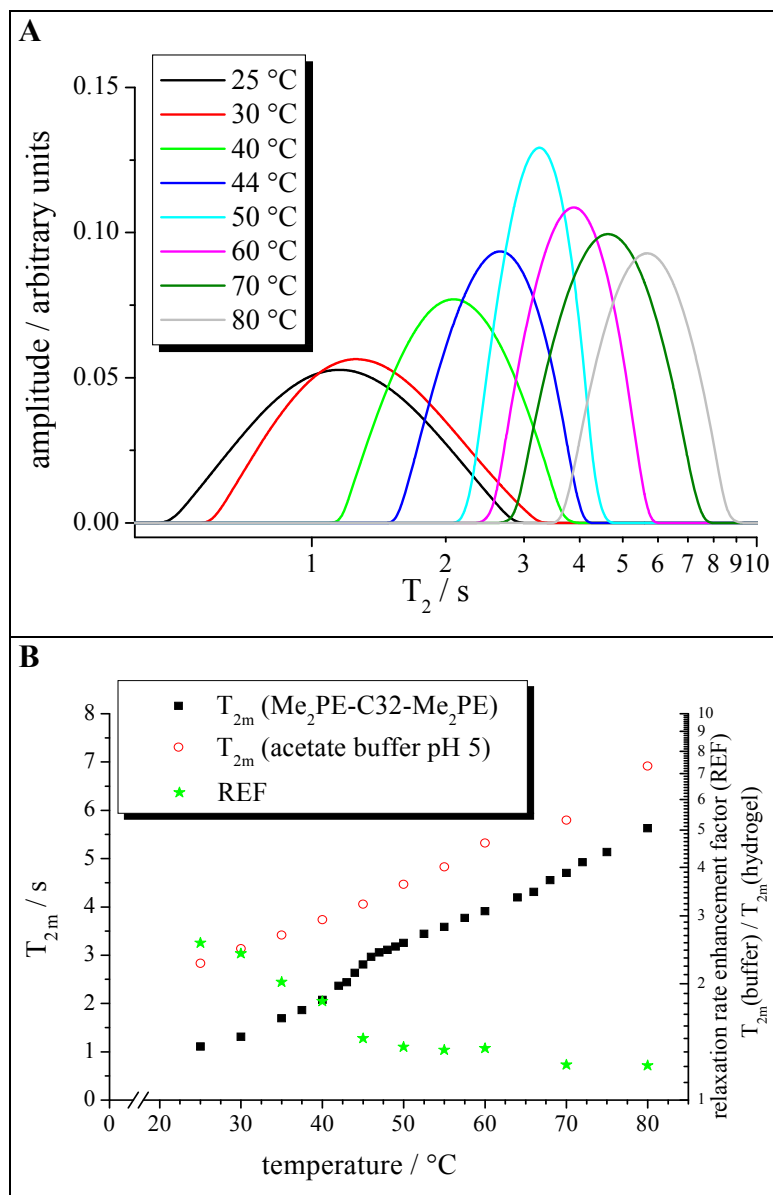


Figure 3.2.8

30 mg/ml $\text{Me}_2\text{PE-C32-Me}_2\text{PE}$ in acetate buffer pH 5 at temperatures from 25 to 80 °C:

(A) Major peaks of the calculated T_2 -distributions, which are normalized to the same peak area.

(B) T_{2m} -values plotted against temperature. For comparison, the T_{2m} -values for pure buffer and the resulting REFs are also shown.

The second endothermic transition of $\text{Me}_2\text{PE-C32-Me}_2\text{PE}$ at 69.5 °C is related to a complete breakdown of the three-dimensional network, but is not detected by the plotted T_{2m} - and REF-values. One can therefore conclude that there is no correlation between the hydrogel state and the observed relaxation behavior analogous to the PC-C32-PC sample. On the other hand, there is an obvious correlation between the relaxation behavior of the water protons and the self-assembled $\text{Me}_2\text{PE-C32-Me}_2\text{PE}$ at temperatures up to the first transition temperature, which was not observed for PC-C32-PC. The explanation for this correlation is given below.

Another remarkable result was obtained for the hydrogel with 30 mg/ml $\text{Me}_2\text{PE-C32-Me}_2\text{PE}$ at pH 5 by decreasing the sample temperature from 25 to 5 °C. The resulting major T_2 -peak was found to be changed from a monomodal to a bimodal peak (Figure 3.2.9). The two separated peaks are centered at approximately 0.43 and 1.75 s. For PC-C32-PC, however, only a narrow monomodal major T_2 -peak was obtained for 30 mg/ml PC-C32-PC at 5 °C.

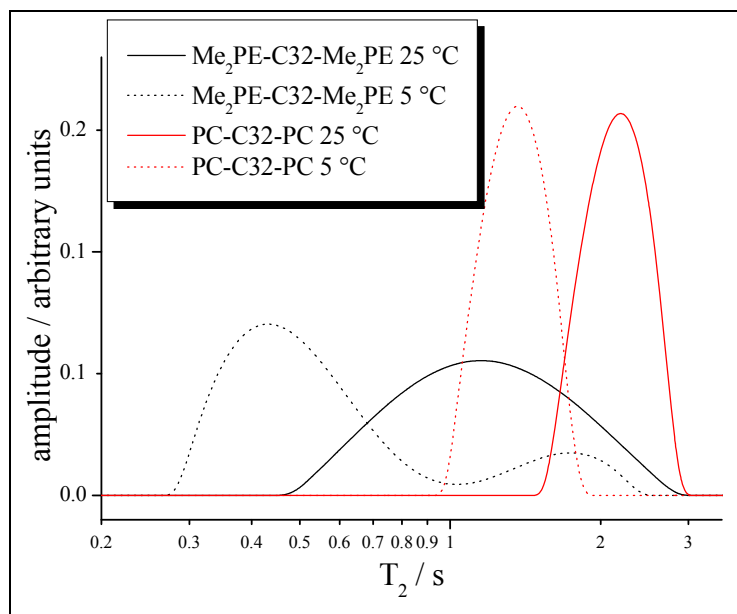


Figure 3.2.9
30 mg/ml Me₂PE-C32-Me₂PE at pH 5: Observation of a bimodal major T₂-peak by decreasing the temperature from 25 to 5 °C. For 30 mg/ml PC-C32-PC in deionized water, a bimodal major T₂-peak is not obtained at 5 °C.

The hydrogel sample with 30 mg/ml Me₂PE-C32-Me₂PE at pH 5 also revealed interesting behavior upon storage. Samples for NMR measurements were completely transparent for PC-C32-PC and did not show any changes in their properties upon storage. The NMR sample with 30 mg/ml Me₂PE-C32-Me₂PE at pH 5 was only transparent directly after the preparation, but became highly turbid during the next two hours of storage time prior to the NMR measurements (Figure 3.2.10A). Upon storage at room temperature for only 48 hours, this sample was found to show shrinkage of the hydrogel volume, which was accompanied by an expulsion of part of the water. This well known phenomenon of syneresis was not observed before for Me₂PE-C32-Me₂PE at pH 5 due to the low concentrations (≤ 10 mg/ml) or the small sample volumes (≤ 100 μ l) that were used for other investigations. A picture of the hydrogel after syneresis is presented in Figure 3.2.10B and shows that the cylindrical shape is preserved upon shrinkage and that about one third of the total buffer content is expelled. The T₂-distribution, obtained for this sample at 25 °C, shows a splitting of the major peak into two separated peaks (Figure 3.2.10C) analogous to the situation at 5 °C (Figure 3.2.9). These separated peaks at T₂-values of 0.95 and 2.75 s obviously correspond to one fraction of water molecules that are highly perturbed by the presence of the bolaamphiphiles and a second fraction that is almost unperturbed. At 40 °C, however, only a broad monomodal major T₂-peak is obtained for the same sample (Figure 3.2.10C), although these two different fractions of water can be expected to be still present at this temperature.

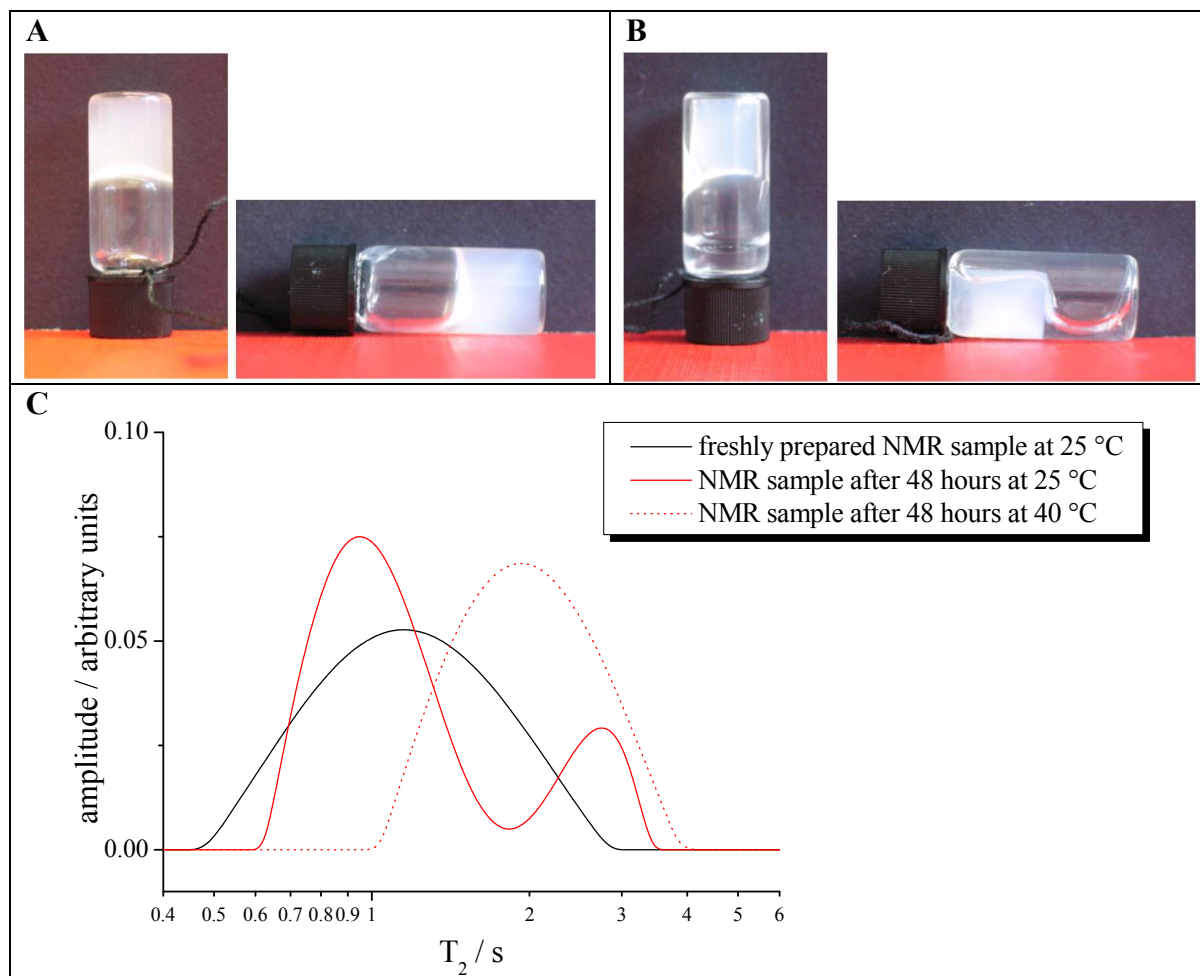


Figure 3.2.10 Syneresis upon storage observed for the hydrogel containing 30 mg/ml Me₂PE-C32-Me₂PE at pH 5: (A) Freshly prepared NMR sample. (B) NMR sample after storage at room temperature for 48 hours. (C) After syneresis, two separated populations of water protons become visible in the T₂-distribution at 25 °C, but at 40 °C a broad monomodal major T₂-peak is again obtained.

The results of the relaxation measurements, performed for 30 mg/ml Me₂PE-C32-Me₂PE at pH 5, can be summarized as follows: (I) The major T₂-peak, which is resulting from the relaxation of the majority of the water protons, is considerably broadened and shifted with respect to that of PC-C32-PC at the same concentration. (II) In contrast to PC-C32-PC, the relaxation behavior could be related to one of the endothermic transitions obtained by DSC. (III) The macroscopic hydrogel state was found not to be correlated to the relaxation behavior for both bolaamphiphiles. (IV) By decreasing the temperature from 25 to 5 °C, the major T₂-peak was found to become bimodal. (V) Upon storage, the hydrogel with 30 mg/ml Me₂PE-C32-Me₂PE at pH 5 showed syneresis. As a result, the major T₂-peak was found to be bimodal at 25 °C. At 40 °C, however, a broad monomodal major T₂-peak was again obtained.

One can conclude from these results that between the aqueous samples of PC-C32-PC and Me₂PE-C32-Me₂PE at a concentration of 30 mg/ml, there must be distinct differences present

regarding the structural organization of the bolaamphiphiles. The observation of morphological differences between PC-C32-PC and Me₂PE-C32-Me₂PE is a remarkable finding, since previous experimental data obtained for these bolaamphiphiles were rather interpreted in terms of the similarities of the formed aggregates and of differences mainly occurring in the temperature dependent properties of these aggregates. However, the concentrations used for these investigations were only about 1-2 mg/ml, whereas a distinctly higher concentration of 30 mg/ml was used for the NMR measurements.

Before providing a detailed discussion of the NMR results in terms of the special aggregate morphology inside the hydrogel with 30 mg/ml Me₂PE-C32-Me₂PE at pH 5, further relaxation data are presented that help for the interpretation of these results.

In order to find a hydrogel system that can be used to confirm the relaxation behavior of 30 mg/ml Me₂PE-C32-Me₂PE at pH 5, a number of polymeric hydrogel systems with a gelator concentration of 30 mg/ml was prepared. Among these systems, only the aqueous sample of Sephadex G75 showed clear similarities with that of Me₂PE-C32-Me₂PE regarding the relaxation behavior (Figure 3.2.11). The T₂-distributions of all other tested hydrogels resembled that of PC-C32-PC. As an example, the major T₂-peak obtained for 30 mg/ml 2-hydroxyethyl cellulose in water is also shown in Figure 3.2.11.

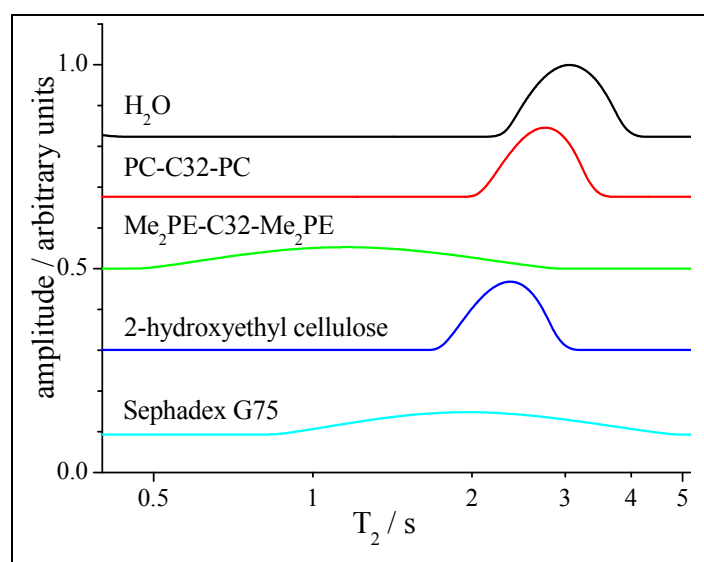


Figure 3.2.11

Pure deionized water and different hydrogels at a gelator concentration of 30 mg/ml: Comparison of the major T₂-peaks obtained at 30 °C.

The transparent hydrogels with 30 mg/ml PC-C32-PC or 2-hydroxyethyl cellulose represent a two phase system that consists of the gelator network and surrounding water. On a distance scale of about 1 μm, these systems can be regarded as homogeneous systems.

On the other hand, the aqueous sample of Sephadex G75 has to be regarded as a heterogeneous system. Sephadex G75 is chemically cross-linked dextran that swells up to

spherical hydrogel particles when water is added. Due to the well defined range of pore sizes in these Sephadex beads, they are used in size exclusion chromatography for substances with a molecular weight between 3000 and 80000. In the NMR sample with 30 mg/ml Sephadex G75, the volume of the swollen particles is only about 0.4 ml. Therefore, the aqueous sample of 30 mg/ml Sephadex G75 is not a homogeneous gel, but consists of swollen hydrogel beads, sedimented on the bottom of the glass vessel, and a large amount of excess water. The relaxation behavior of the water protons in the excess water is essentially that of pure water. As described above, this fraction of water can be called unperturbed or “bulk-like” water (H_2O_b).^[74] The dynamical properties of the water molecules that are near the surface of the particles, especially these inside the pores, will be changed by the interaction with the surface. For this fraction of motionally perturbed water (H_2O_p), the transverse relaxation rate is increased. These two fractions of water are also present in the hydrogels of PC-C32-PC and 2-hydroxyethyl cellulose, but in the sample with 30 mg/ml Sephadex G75 they are spatially separated from each other. The existence of two separated water populations, H_2O_b and H_2O_p , with different transverse relaxation rates should result in two separated peaks in the T_2 -distributions. However, only one broad major T_2 -peak is observed at 30 °C for Sephadex G75. This might be explained as follows: As described above, it was found that polymer surfaces will dynamically perturb only the water in the one or two molecular layers adjacent to the surface.^[90] This dynamically perturbed water exchanges on a submillisecond level with the surrounding water.^[74] In small pores, the vast majority of the water molecules will be dynamically perturbed in that way on the relaxation timescale of a few seconds. Water is free to diffuse between the inside and the outside of the beads.^[95] As a result, this fraction of perturbed water will exchange by diffusion with the bulk water. Therefore, there are two parameters, which determine the occurrence of a bimodal or monomodal T_2 -distribution, namely the mean diffusion distance d_m between the particular populations and the mean diffusion coefficient D_m . For Sephadex G75 at 30 °C, both parameters allow the populations H_2O_b and H_2O_p to rapidly exchange with each other, which results in only one broad major T_2 -peak. This broad major T_2 -peak represents the weighted sum of all possible states from highly perturbed to completely unperturbed water molecules.

This can be visualized by a simple experiment, which was performed with the same sample of Sephadex G75: In the first step, most of the excess water was removed. The resulting major T_2 -peak was considerably narrower due to the decreased fraction of unperturbed water (Figure 3.2.12). The T_{2m} -value determined for this sample is 1.73 s. In the second step, most of the remaining excess water was carefully absorbed with a paper tissue. As a consequence, the obtained T_2 -distribution can be fully attributed to the protons of the perturbed water. The major T_2 -peak of this distribution was as narrow as that observed for pure deionized water

($T_{2m} = 3.07$ s), but significantly shifted to lower T_2 -values ($T_{2m} = 1.39$ s) due to the dynamical perturbation of the water molecules by the hydrogel matrix. Figure 3.2.12 clearly shows that the broad major T_2 -peak of 30 mg/ml Sephadex G75 ($T_{2m} = 1.94$ s) at 30 °C results from diffusional exchange between the fractions of perturbed and unperturbed water.

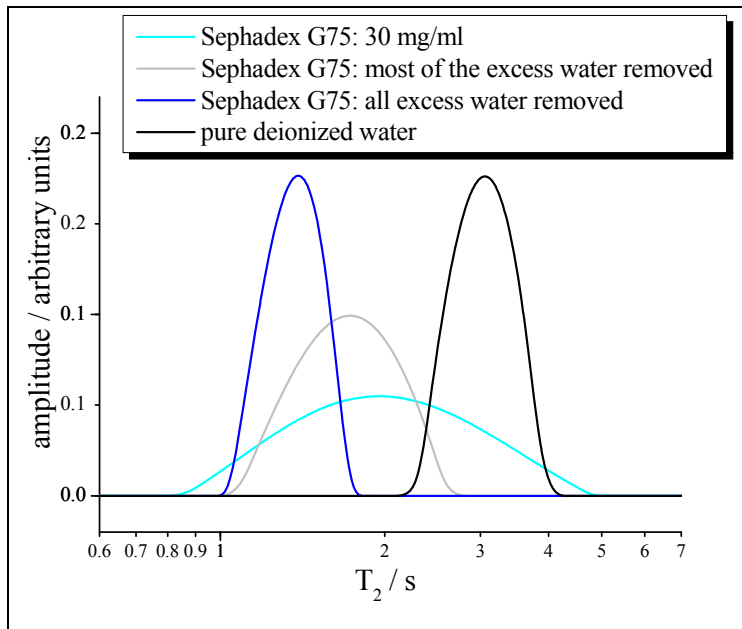


Figure 3.2.12

Major T_2 -peaks for water and fully swollen Sephadex G75 particles with varying content of excess water at 30 °C.

A second model experiment with 30 mg/ml Sephadex G10, G25, G50, G75 and G100 in deionized water was performed in order to demonstrate the correlation between the relaxation behavior and the sample morphology. From Sephadex G10 to G100, the degree of swelling in water is gradually increased. Therefore, the resulting pore sizes, represented by the fractionation size range (Figure 3.2.13), are also increased. All these samples consist of a fraction of fully swollen Sephadex particles and a considerable fraction of excess water, which is gradually decreasing from Sephadex G10 to Sephadex G100.

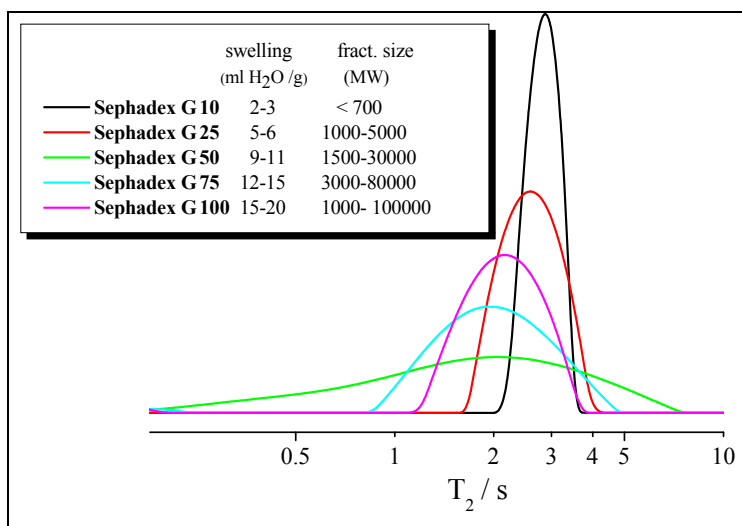


Figure 3.2.13

Major T_2 -peaks obtained at 30 °C for 30 mg/ml Sephadex G10, G25, G50, G75 and G100: Influence of the degree of swelling and the resulting pore size, characterized by the fractionation size, on the resulting major T_2 -peak.

Figure 3.2.13 shows that there is a significant correlation between the appearance of the major T_2 -peak and the different swelling behavior of the Sephadex particles. Compared to pure water (T_{2m} : 3.07 s), the major T_2 -peak obtained for Sephadex G10 is only slightly shifted (2.88 s) and broadened. This can be explained by the low degree of swelling, which results in small particles with small pores. Therefore, the fraction of H_2O_p is relatively low. For Sephadex G25, the degree of swelling increases and an increased fraction of perturbed water can be expected. Therefore, the peak is considerably broadened and shifted with respect to Sephadex G10. For Sephadex G50, the degree of swelling further increases as well as the fraction of perturbed water. The influence of the wide pore size distribution on the transverse relaxation has reached a maximum for Sephadex G50, which is reflected in an extremely broad major T_2 -peak due to the wide distribution of transverse relaxation times.

A further increase in the uptake of water in Sephadex G75 and Sephadex G100 is not resulting in a further increasing peak width of the major T_2 -peak, but in a substantial decrease. This might be explained as follows: For Sephadex G75 and G100, the mean diameter of the water filled pores is increased with respect to Sephadex G50. The resulting increase of the pore volume is considerably larger than the concomitant increase of the surface area of the pores. The dynamical perturbation experienced by the particular water molecules inside the larger pores will therefore be decreased with respect to Sephadex G50.

The relaxation data discussed for the Sephadex samples help, to some extent, to understand the observed relaxation behavior of the water protons in the hydrogel with 30 mg/ml Me_2PE -C32- Me_2PE . As described above, aqueous samples of Sephadex have to be regarded as heterogeneous systems on the micrometer distance scale, since they contain sedimented hydrogel beads with water filled pores and excess water. The resulting spatially separated water populations H_2O_b and H_2O_p are in fast diffusional exchange with each other. At 30 °C, the resulting major relaxation peak is the weighted sum of all possible states from highly perturbed to completely unperturbed water molecules.

For 30 mg/ml Me_2PE -C32- Me_2PE at pH 5, a broad monomodal major T_2 -peak is also observed. This indicates that a significant degree of heterogeneity on the micrometer distance scale is present inside the hydrogel formed by 30 mg/ml Me_2PE -C32- Me_2PE at pH 5. These heterogeneities are most probably due to a large number of lamellar aggregates, which coexist with the nanofibers. As described in Section 3.1, direct evidence for the existence of a considerable amount of lamellar aggregates in hydrogels with concentrations ≥ 2 mg/ml

Me₂PE-C32-Me₂PE at pH 5 still remains to be given. However, this assumption is clearly supported by a number of experimental facts. These are:

- 1) The observation of darker, almost rectangular areas in cryo-TEM images of 0.3 mg/ml Me₂PE-C32-Me₂PE in acetate buffer pH 5.^[15]
- 2) The turbid appearance of hydrogels with concentrations ≥ 2 mg/ml Me₂PE-C32-Me₂PE at pH 5 (Figures 3.1.3A and 3.2.10A).
- 3) The interpretation of the relaxation data of water protons in a hydrogel with 30 mg/ml Me₂PE-C32-Me₂PE at pH 5 in terms of the existence of a considerable degree of heterogeneity.
- 4) The observation of syneresis upon storage for the same hydrogel (Figure 3.2.10B).
- 5) The identification of lamellar aggregates as the dominating self-assemblies of MePE-C32-MePE due to a further decrease of the space requirement of the headgroups.^[19]
- 6) The direct evidence for a considerable number of rectangular lamellar aggregates for Me₂PE-C34-Me₂PE, dMe₂PE-C34-Me₂PE (a partially deuterated analogue) and Me₂PE-C36-Me₂PE at pH 5 by cryo-TEM (1 mg/ml) and TEM (0.3 mg/ml).^[23] Due to the longer alkyl chains compared to Me₂PE-C32-Me₂PE, these bolaamphiphiles show a higher tendency to form these lamellar aggregates.
- 7) The occurrence of turbidity and syneresis for aqueous samples with 1 mg/ml Me₂PE-C34-Me₂PE, dMe₂PE-C34-Me₂PE or Me₂PE-C36-Me₂PE at pH 5 (shown in Fig. 5 for dMe₂PE-C34-Me₂PE in ^[23]) in analogy to the observations for Me₂PE-C32-Me₂PE.

For the hydrogel with 30 mg/ml Me₂PE-C32-Me₂PE at pH 5, the presence of a considerable degree of heterogeneity on the micrometer distance scale indicates that the lamellar aggregates are not uniformly distributed throughout the sample volume, but are, at least in part, organized in lamellar domains. Analogous to the situation in Me₂PE-C34-Me₂PE, dMe₂PE-C34-Me₂PE and Me₂PE-C36-Me₂PE, these domains may consist of stacked single lamellae.^[23] The fact that at 5 °C the broad major T₂-peak, obtained at 25 °C, is found to be splitted into two separated peaks, gives evidence that these lamellar domains are in the micrometer range. Lillford et al.^[96] suggested that multiexponential relaxation will be observed, if there are heterogeneities within the sample over spatial regions larger than the region sampled by one water molecule during its intrinsic relaxation time. This was confirmed by Belton et al.,^[97] who provided the theoretical framework to explain the change from monoexponential to biexponential relaxation for agarose gels that were freeze-thawed. These authors were able to show that heterogeneities on a distance scale of about 110 to 140 μm are

necessary to obtain multiexponential relaxation behavior at room temperature. The authors demonstrated that the mean diffusion distance d_m of 110 μm , as the limit for diffusional averaging of the relaxation, can be easily derived from the mean diffusion coefficient D_m of the water molecules. It is calculated as the average distance that a freely diffusing water molecule travels during the time t equal to T_{2m} :

$$d_m^2 = 6 D_m t = 6 D_m T_{2m} \quad (3.2)$$

The broad major T_2 -peak at room temperature and its splitting into two peaks at 5 °C may therefore be explained as follows: The relaxation of water protons in a hydrogel with 30 mg/ml Me₂PE-C32-Me₂PE is strongly influenced by the presence of the lamellar domains. Besides a fraction of more or less unperturbed water, a considerable number of water molecules will be present inside the extended lamellar domains, most probably in the thin layers of water between two adjacent lamellae. The dwelling time of a particular water molecule in such a cluster of lamellae will be increased compared to the dwelling time at the fiber surface, since the diffusion distance to the fraction of unperturbed water is now longer. As a result, the motional perturbation exerted by the surface of the lamellae on the water molecules is considerably increased, which leads to a relaxation rate enhancement and therefore to lower T_{2m} -values. T_{2m} as well as D_m are temperature dependent, which results in significant differences in the T_2 -distributions obtained at different temperatures. For 30 mg/ml Me₂PE-C32-Me₂PE at 25 °C, for example, the mean diffusion coefficient of the water molecules is large enough to enable a sufficiently fast exchange between the fractions of perturbed and almost unperturbed water. This results in a broad, but monomodal major T_2 -peak, which is a weighted sum of all relaxation times of the particular water protons in the sample. Therefore, the obtained T_{2m} -value was found to be considerably decreased with respect to that of pure buffer. When the temperature is decreased to 5 °C, a bimodal major T_2 -peak is obtained instead of the broad monomodal peak at 25 °C. One can assume that the size of the lamellar domains remains almost unchanged during the time of this experiment of about 90 minutes. Therefore, the splitting of the major T_2 -peak can be attributed to the decrease of the mean diffusion coefficient, which is not sufficiently large enough at 5 °C to enable fast exchange between the perturbed and almost unperturbed water molecules. As described below, the size range of the lamellar domains present in a hydrogel with 30 mg/ml Me₂PE-C32-Me₂PE at pH 5 can be estimated by determination of the mean diffusion coefficients at different temperatures.

When the temperature is increased from 25 to 80 °C, the T_{2m} -values indicate considerable changes of the relaxation behavior at about 45 °C, which is the temperature of the first endothermic transition. For Me₂PE-C34-Me₂PE and dMe₂PE-C34-Me₂PE, no lamellar

aggregates, but only fibers were found by SANS and cryo-TEM above the temperature of the first transition.^[23] For 30 mg/ml Me₂PE-C32-Me₂PE at pH 5, it seems likely that the transition at 45 °C is also related to a complete disintegration of the lamellar aggregates, since this changes the degree of heterogeneity and is therefore detectable by determining the T_{2m}-values. This conclusion is also supported by the fact that turbidity is observed for the hydrogels with ≥ 2 mg/ml Me₂PE-C32-Me₂PE at pH 5 only below 45 °C, but not above this temperature.

The second endothermic transition at about 70 °C, which is related to a breakdown of the fiber network into micellar aggregates, is not reflected in the T_{2m}-values. This shows that the observed transverse relaxation behavior of the water protons is only sensitive to changes in the aggregate morphologies, when they are related to changes of the degree of heterogeneity.

Such changes of the degree of heterogeneities are also occurring when the upon storage of the hydrogel with 30 mg/ml Me₂PE-C32-Me₂PE at pH 5, since syneresis is caused by a considerable increase of the size of the lamellar domains. This could be shown previously for dMe₂PE-C34-Me₂PE.^[23] The gel cake of this bolalipid is apparently composed of large clusters of stacked lamellae. Whereas the water between the clusters is slowly released during syneresis, the hydration of the headgroups was found to remain unchanged and the amount of water trapped between adjacent single lamellae is only slightly reduced. This could be confirmed by X-ray diffraction experiments.^[23]

For the sample with 30 mg/ml Me₂PE-C32-Me₂PE after syneresis, the increase of the size of the lamellar domains is well reflected in the obtained T₂-distribution, since a bimodal major T₂-peak is obtained at 25 and 30 °C. This indicates that the sizes of a considerable number of these domains now exceed the mean diffusion distance of the water molecules, which can be assumed to be almost unchanged compared to the freshly prepared sample. However, the size of the lamellar domains can be expected to grow only moderately upon storage, because a broad monomodal major T₂-peak is obtained at 40 °C. This means that at this temperature, the mean diffusion coefficient is again large enough to enable efficient diffusive exchange between the different fractions of water.

In order to confirm the conclusions drawn from the NMR relaxation data obtained for 30 mg/ml Me₂PE-C32-Me₂PE at pH 5, a last relaxation experiment was carried out. The lamellar aggregates are exclusively found for aqueous samples of the longer chain (n = 32-36) derivatives of the Me₂PE-(CH₂)_n-Me₂PE family. Therefore, the relaxation behavior of 30 mg/ml Me₂PE-C32-Me₂PE at pH 5 was compared to that determined for aqueous samples of Me₂PE-C28-Me₂PE, Me₂PE-C34-Me₂PE and Me₂PE-C36-Me₂PE at the same concentration and pH. The results are shown in Figure 3.2.14.

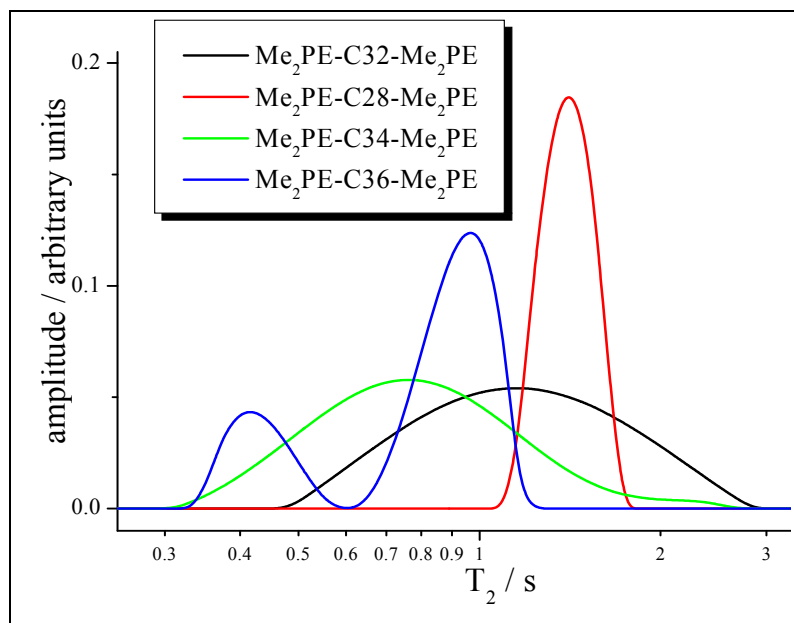


Figure 3.2.14

Major T_2 -peaks obtained at 25 °C for samples with 30 mg/ml of $\text{Me}_2\text{PE-C}_n\text{-Me}_2\text{PE}$ ($n = 28, 32, 34, 36$) in acetate buffer pH 5.

For the transparent hydrogel with 30 mg/ml $\text{Me}_2\text{PE-C28-Me}_2\text{PE}$, which can be expected to be free of lamellar aggregates, a narrow major T_2 -peak is observed. The width of this peak corresponds to that obtained for PC-C32-PC, which gives evidence for the exclusive presence of fibers in this sample. Compared to PC-C32-PC, the major T_2 -peak obtained for $\text{Me}_2\text{PE-C28-Me}_2\text{PE}$ is shifted to lower T_2 -values, which indicates a considerably higher mean relaxation rate as a result of a stronger perturbation of the water molecules. This may be explained by the effect of hydrogen bonding.

As described above, direct evidence for the presence of a large number of lamellar aggregates in aqueous samples of $\text{Me}_2\text{PE-C34-Me}_2\text{PE}$ could be given by SANS and electron microscopy. The aqueous sample with 30 mg/ml $\text{Me}_2\text{PE-C34-Me}_2\text{PE}$ at pH 5 was found to be highly turbid and the obtained major T_2 -peak resembles that of $\text{Me}_2\text{PE-C32-Me}_2\text{PE}$, but is further shifted and broadened. This similarity between the major T_2 -peaks of $\text{Me}_2\text{PE-C32-Me}_2\text{PE}$ and $\text{Me}_2\text{PE-C34-Me}_2\text{PE}$ can be seen as a sufficient evidence that it is reliable to interpret the relaxation behavior of $\text{Me}_2\text{PE-C32-Me}_2\text{PE}$ in terms of the presence of a large number of lamellar aggregates.

The sample of $\text{Me}_2\text{PE-C36-Me}_2\text{PE}$ was also turbid and even showed visible signs of syneresis within two hours after the preparation. Analogous to the sample of $\text{Me}_2\text{PE-C32-Me}_2\text{PE}$ after syneresis, the major T_2 -peak was not unimodal, but separated into two well defined peaks.

One can conclude that the relaxation behavior of water protons in a hydrogel of 30 mg/ml $\text{Me}_2\text{PE-C32-Me}_2\text{PE}$ at pH 5 can be interpreted in terms of a significant degree of heterogeneity in this sample. The origin of the heterogeneity can be found in the presence of extended stacks of lamellae. All obtained results from the relaxation measurements as well

as the occurrence of syneresis can be explained by the existence of these lamellar domains. Instability of a Me₂PE-C32-Me₂PE hydrogel upon storage due to syneresis can be seen as an obstacle for potential applications of this hydrogel in the biomedical field. Hydrogels of PC-C32-PC, on the other hand, were found to be stable over several months and may therefore be the more promising candidates for such applications.

3.2.2 Mean diffusion coefficients of the water molecules

As described above, diffusion of the water molecules has a high influence on the obtained T₂-distributions. Therefore, the mean diffusion coefficients of water were determined for 30 mg/ml PC-C32-PC in deionized water and 30 mg/ml Me₂PE-C32-Me₂PE at pH 5. This was done by means of the pulsed gradient stimulated echo (PGSTE) method^[46,47] according to the procedure described in Section 2.2.2.

Stimulated echos were recorded for different values of the duration (D3) of the gradient pulses. With increasing D3, the echo amplitudes (A_{2τ}) decrease substantially compared to the echo amplitude obtained without the application of the gradient pulses (A₀).

The obtained values of $\ln\left(\frac{A_{2\tau}}{A_0}\right)$ were plotted against the term $D3^2\left(D4 - \frac{1}{3}D3\right)$ as is shown in Figure 3.2.15 for both bolaamphiphiles at a temperature of 30 °C.

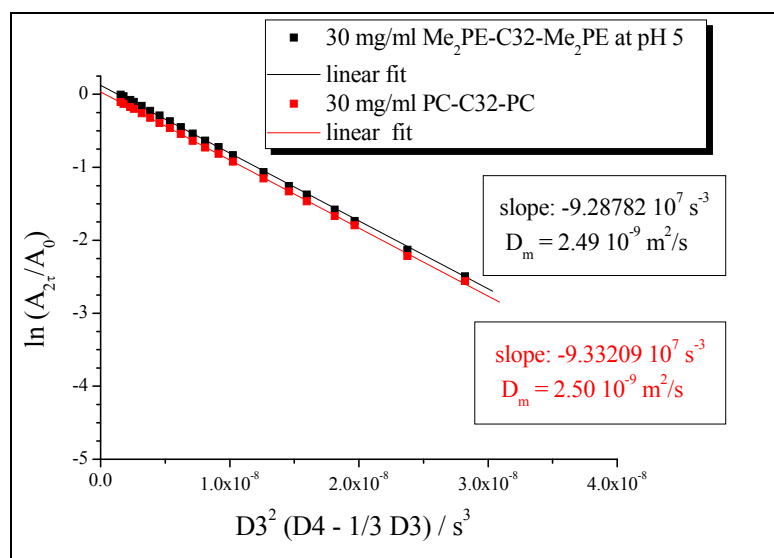


Figure 3.2.15

Hydrogels with 30 mg/ml PC-C32-PC or 30 mg/ml Me₂PE-C32-Me₂PE at 30 °C:

Plotting $\ln(A_{2\tau}/A_0)$ against $D3^2(D4 - 1/3 D3)$. From the obtained value of the slope, the mean diffusion coefficients D_m of water can be calculated.

By linear fitting, the values of the slope are determined for each sample. According to Equation 2.28, the values of the slope correspond to $-\gamma^2 g^2 D_m$ and can therefore be used to calculate the mean diffusion coefficient D_m for the water molecules in the particular sample. At 30 °C, the values of the mean diffusion coefficients $D_{m(30\text{ °C})}$ of the water molecules in

hydrogels with 30 mg/ml PC-C32-PC in deionized water and 30 mg/ml Me₂PE-C32-Me₂PE in acetate buffer pH 5 are calculated to be $2.50 \cdot 10^{-9} \text{ m}^2/\text{s}$ and $2.49 \cdot 10^{-9} \text{ m}^2/\text{s}$, respectively.

As shown in Figure 3.2.16, there are also no significant differences observable between the obtained D_m -values of both samples at temperatures ranging from 30 to 52 °C. Therefore, one can conclude that the translational mobility of the water molecules is essentially the same for both hydrogels, although there are distinct differences observable regarding the relaxation behavior of the water protons. This supports the interpretation of the relaxometry results in terms of an diffusional averaging of the relaxation times that is mainly depending on the distance scale of the heterogeneities present in the particular sample.

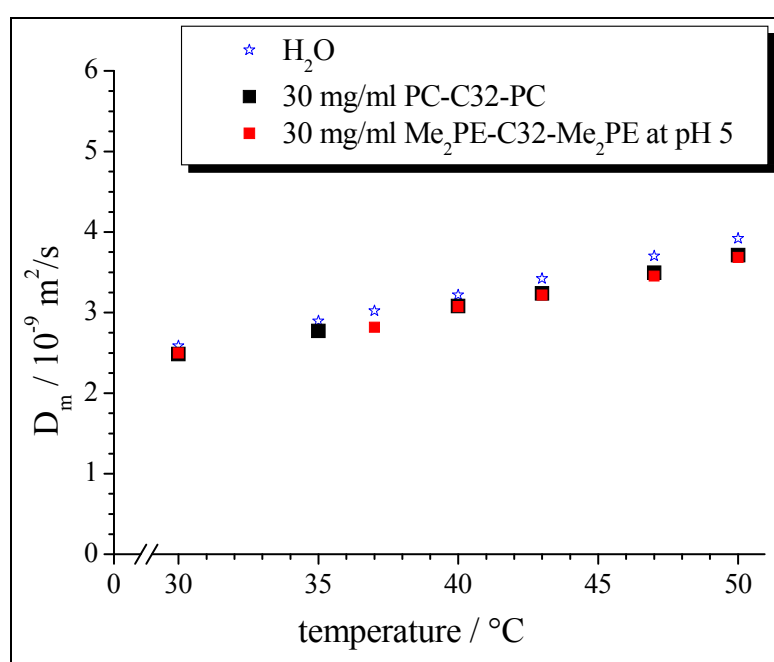


Figure 3.2.16

Temperature dependent mean diffusion coefficients determined for deionized water, 30 mg/ml PC-C32-PC in deionized water and 30 mg/ml Me₂PE-C32-Me₂PE in acetate buffer pH 5.

Figure 3.2.16 also shows that the mean diffusion coefficients of the water molecules in the hydrogels are only slightly decreased with respect to the values of pure water. This small decrease of the D_m -values by about 3 to 7% is in agreement with the results obtained for other hydrogels of comparable gelator concentrations.^[84,98] In these investigations, the obtained diffusion coefficients were found to be dependent only of the solid volume fraction, but not of the macroscopic state^[84] or of the cross-linker content.^[98] The observed small decrease in D_m with respect to pure water may therefore also be interpreted as a concentration effect.

The D_m -values obtained for water in 30 mg/ml Me₂PE-C32-Me₂PE at pH 5 can be used to estimate the distance scale that is characterizing the identified heterogeneities in this sample. As described above, Belton et al. suggested that heterogeneities on a distance scale of about 110-140 μm are necessary to obtain multiexponential relaxation at room temperature.^[97] The

authors showed that the mean diffusion distance is a good estimate for this limit of diffusional averaging of the transverse relaxation times. It is calculated by comparing the mean diffusion coefficient D_m and the mean transverse relaxation time T_{2m} : $d_m = \sqrt{6D_m T_{2m}}$ (Equation 3.2)

Applied to the aqueous sample with 30 mg/ml Me₂PE-C32-Me₂PE at pH 5, this provides a good estimate for the distance scale of the heterogeneities that are present due to the existence of the lamellar stacks:

Upon storage, syneresis is observed for the hydrogel with 30 mg/ml Me₂PE-C32-Me₂PE at pH 5 due to a distinct growth of the lamellar domains. As a result, a bimodal major T₂-peak is obtained for this sample at 25 and 30 °C, which indicates that the mean diffusion coefficient of the water molecules is not large enough to enable a sufficiently fast exchange between the populations of perturbed and unperturbed water. This means that the sizes of the lamellar domains now exceed the mean diffusion distance of the water molecules. At 30 °C, the values of the mean diffusion coefficient and the mean transverse relaxation time are about 2.5 10⁻⁹ m²/s and 1.3 s, respectively. Using equation 3.2, the mean diffusion distance d_m of the diffusing water molecules is calculated to be about 1.4 10⁻⁴ m or 140 μm, which is in agreement with the results of Belton and co-workers.^[97] Therefore, one can conclude that the lower range for the distance scale of the heterogeneities inside the hydrogel of 30 mg/ml Me₂PE-C32-Me₂PE at pH 5 after syneresis is 140 μm.

At 40 °C, however, a monomodal T₂-peak is obtained for the same sample, which indicates that at this temperature, the diffusion coefficient is large enough to enable efficient diffusive exchange between the different water populations. Therefore, the upper range for the distance scale of the heterogeneities is calculated to be 190 μm ($D_{m(40\text{ °C})}$ 3.1 10⁻⁹ m²/s, T_{2m} 1.95 s). Therefore, the observation of syneresis for the hydrogel with 30 mg/ml Me₂PE-C32-Me₂PE at pH 5 can be explained by a significant growth of the lamellar domains. These lamellar domains could be shown to reach average sizes in the range between 140 μm and 190 μm.

As shown in Figure 3.2.9, a bimodal major T₂-peak is also obtained for the freshly prepared NMR sample of Me₂PE-C32-Me₂PE, when the temperature is decreased from 25 to 5 °C. This is due to a substantially decreased mean diffusion coefficient of the water molecules at this temperature, which is obviously not large enough to enable diffusive averaging. The value of $D_{m(5\text{ °C})}$ was not determined, but can be estimated to be approximately 10⁻⁹ m²/s. If one uses the lower T_{2m}-value of 0.42 s from the bimodal major peak of the T₂-distribution obtained at 5 °C, the mean diffusion distance is only 5 10⁻⁵ m or 50 μm. One can therefore conclude that the distance scale of the heterogeneities present in the freshly prepared hydrogel of 30 mg/ml Me₂PE-C32-Me₂PE at pH 5 exceeds 50 μm. No relaxation measurement was performed at

temperatures between 5 and 25 °C. Therefore, the broad monomodal peak at 25 °C is used to define the upper range of the distance scale for this sample. If one uses an estimated diffusion coefficient of $2.1 \cdot 10^{-9} \text{ m}^2/\text{s}$ and the T_{2m} -value of 1.11 s, it is calculated to be 120 μm .

One can therefore conclude that the distance scale of the heterogeneities present in the freshly prepared hydrogel of 30 mg/ml Me₂PE-C32-Me₂PE at pH 5 lies in the range between about 50 and 120 μm . These heterogeneities are most probably due to extended stacks of lamellar aggregates. Upon storage at room temperature for 48 hours, these lamellar domains are growing to sizes between 140 and 190 μm .

3.2.3 Relaxation behavior of the bolaamphiphile protons

3.2.3.1 PC-C32-PC in D₂O

Compared to the T_2 -distribution of water, the hydrogel sample of 30 mg/ml PC-C32-PC showed a small additional peak at about 1 ms (Figure 3.2.5). This peak corresponds to the relaxation of the protons of the PC-C32-PC molecules. If the gel is prepared by dispersing PC-C32-PC in D₂O instead of H₂O, it is possible to obtain echo envelopes and T_2 -distributions, which are only representing the relaxation behavior of the PC-C32-PC protons (Figure 3.2.17). As described above, the rate of dipole-dipole relaxation depends on the frequency of the fluctuating local magnetic fields. In the densely packed nanofibers, the mobility of the particular protons is considerably restricted and the correlation time τ_R is very short. This enables very efficient transverse relaxation of these protons. Efficient relaxation corresponds to a high relaxation rate and a very fast decay of the echo intensity is observed (Figure 3.2.17A). The resulting T_2 -distribution shows two separated peaks (Figure 3.2.17B). As will be discussed below, these peaks may correspond to two different proton populations, which have different correlation times.

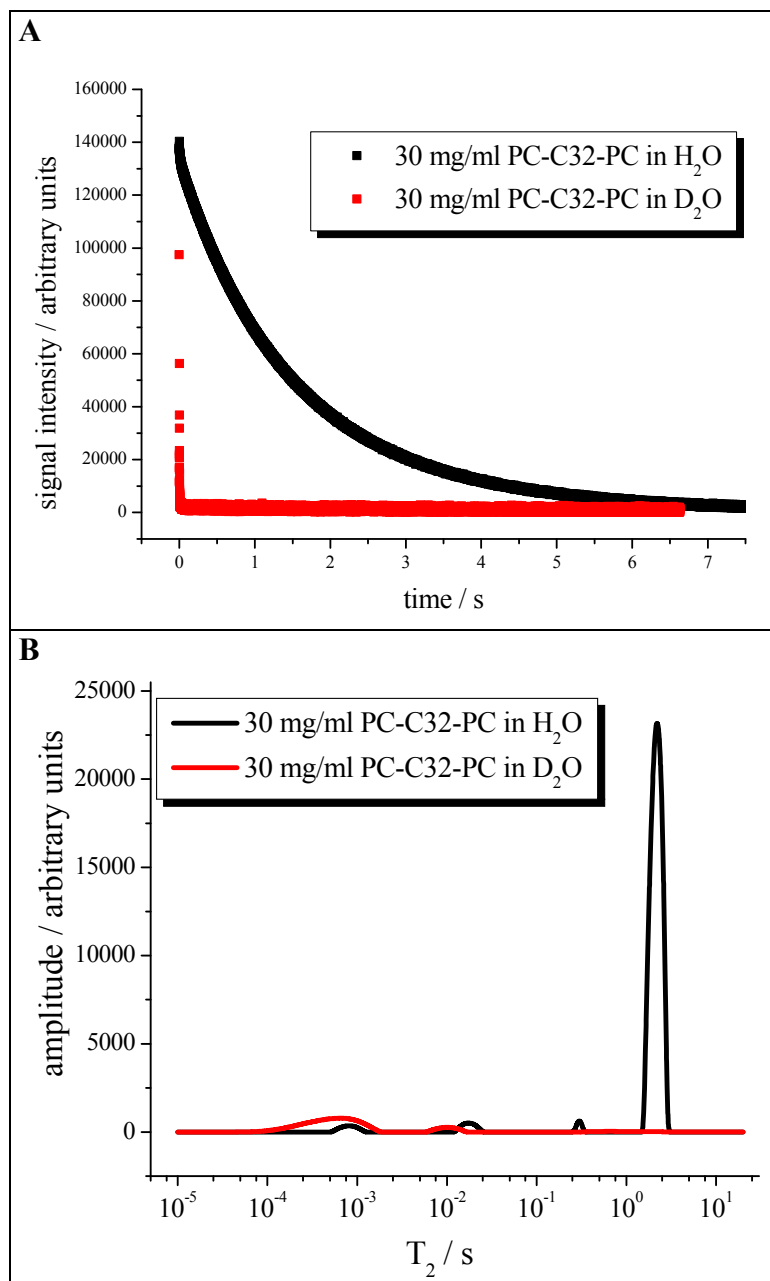


Figure 3.2.17

NMR relaxation experiment at 25 °C performed for the hydrogel with 30 mg/ml PC-C32-PC in D₂O compared to that with 30 mg/ml PC-C32-PC in H₂O:

(A) Obtained echo envelopes.

(B) Calculated T₂-distributions.

At 25 °C, the transverse relaxation of the bolaamphiphile protons is completed after about 20 ms. This means that the relaxation process leads to a complete loss of coherence within this time. Due to the fast relaxation, the number of detected echos per scan could be decreased from 36864 to 512. This means a considerably reduced measuring time compared to the H₂O samples.

It has to be noted that the T₂-distributions obtained by repeating the experiment with the same sample were found to vary to some extent. In general, two peaks are observable in the T₂-distributions generated by WinDXP, one centered at about 0.5 to 0.9 ms (denoted as peak 1) and the other at T₂-values in the range of 8 to 20 ms (peak 2). In many cases, these peaks are symmetrical and completely separated from each other. However, due to the rather small

number of about 40 spin echos that are detected during the relaxation time, WinDXP regularly produces T_2 -distributions with distorted or overlapping peaks. Therefore, the experiment was repeated ten times at every temperature and the T_2 -distribution that was best representing the general trend was selected. These representative T_2 -distributions for 30 mg/ml PC-C32-PC in D_2O at temperatures ranging from 26 to 55 °C are compiled in Figure 3.2.18.

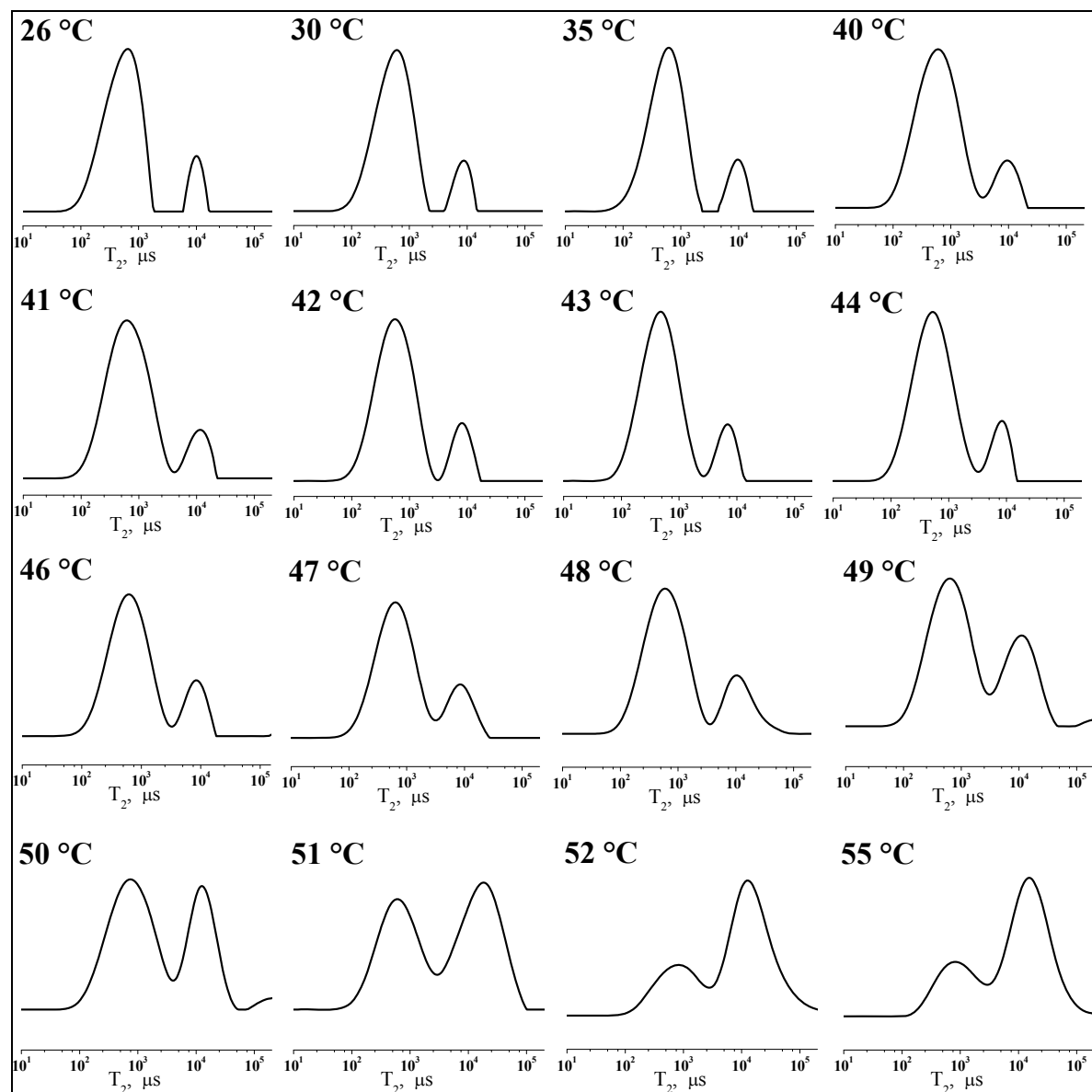


Figure 3.2.18 Representative T_2 -distributions obtained for 30 mg/ml PC-C32-PC in D_2O at temperatures ranging from 26 to 55 °C.

For the T_2 -distribution obtained at 26 °C, the proportionate peak areas of peak 1 and peak 2 were determined by WinDXP to be 89% and 11%, respectively. This corresponds roughly to the different fractions of protons of the PC-C32-PC molecule, in which the CH_2 protons make up about 80% and the protons of the CH_3 groups 20% of the total hydrogen content. The

motional freedom of the methyl groups, which are located in the bolaamphiphilic headgroups, can be expected to be considerably higher compared to that of the CH₂ groups, especially compared to that in the long alkyl chain. This seems to be a reasonable explanation for the observation of the two T₂-peaks, since increasing motional freedom is causing a decrease in the relaxation rate and therefore larger T₂-values.

However, the aim of these investigations was to demonstrate that low field NMR relaxometry can, in principle, be used to study the endothermic transitions occurring for PC-C32-PC. The important information is therefore lying in the relative changes that are observed when the temperature is gradually increased. These changes are mainly occurring between 48 and 52 °C as is clearly visible in Figure 3.2.18. In this temperature region, amplitude and proportional peak area of peak 2 are increasing considerably, whereas that of peak 1 are found to be decreased. In order to quantify these changes, the proportionate peak area of both peaks are plotted against temperature in Figure 3.2.19.

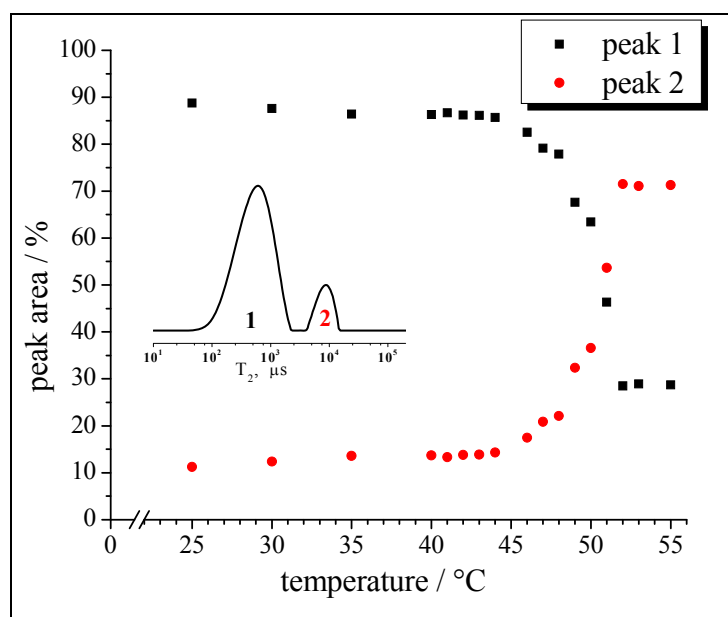


Figure 3.2.19
30 mg/ml PC-C32-PC in D₂O: Temperature dependence of the peak areas of peak 1 and peak 2, which were determined by WinDXP from the particular T₂-distribution.

With increasing temperature, the peak areas remain nearly unchanged up to 44 °C. At this temperature, peak 1 makes up about 86% of the total peak area. Therefore, the endothermic transition observed for PC-C32-PC at 43.8 °C is obviously not causing a detectable change in the relaxation behavior of the bolaamphiphile protons. The second transition at 48.7 °C, however, is clearly detected by a significant change in the peak areas. As described above, this transition is related to a complete breakdown of the fibers and only micellar aggregates are found well above the transition temperature. Due to increased trans-gauche isomerization and a significant loss of order in the micelles, the mobility of most protons is significantly

increased with respect to the bolaamphiphilic fibers. Therefore, peak 2, which is representing the more mobile fraction of the bolaamphiphile protons, increases in both amplitude and peak area and is now found to represent about 70% of the total peak area. Simultaneously, the average increase of the motional freedom is reflected by a shift of the peak center from about 9 ms to about 15 ms. On the other hand, the position of peak 1 is not shifted. This peak still represents 30% of the bolaamphiphile protons that appear to be motionally restricted even in the micelles that are present at 55 °C. The ESR data presented in Section 3.3, indicates that these immobilized protons may be located in the center of the bolaamphiphilic alkyl chains.

3.2.3.2 *Me₂PE-C32-Me₂PE in acetate buffer pD 5*

In order to assess the relaxation behavior of the protons of Me₂PE-C32-Me₂PE, a hydrogel with 30 mg/ml Me₂PE-C32-Me₂PE in acetate buffer pD 5 was prepared. For the pure D₂O buffer, no significant contribution to the obtained NMR signal was observed. The T₂-distributions that were obtained for Me₂PE-C32-Me₂PE at temperatures ranging from 26 to 90 °C are compiled in Figure 3.2.20.

At 26 °C, the T₂-distribution obtained for Me₂PE-C32-Me₂PE resembles that of PC-C32-PC, but a small additional peak (denoted as peak 3) is observed at about 18 ms. Furthermore, the positions of peak 1 (Me₂PE-C32-Me₂PE: T_{2m} = 0.48 ms vs. PC-C32-PC: T_{2m} = 0.64 ms) and peak 2 (3.71 ms vs. 9.77 ms) were found to be slightly shifted to lower T₂-values. At room temperature, the determined proportionate areas are approximately 86.5% for peak 1, 11.5% for peak 2 and 2% for peak 3. One could speculate that these peaks may correspond to the CH₂ groups (about 83.5% of the total hydrogen content of the Me₂PE-C32-Me₂PE molecule), the CH₃ groups (14%) and to the hydrogen atoms of the NH(CH₃)₂ groups (2.5%), respectively.

As noted above, the important information is the relative trend that can be observed in the T₂-distributions with increasing temperature. Therefore, Figure 3.2.21 shows the proportionate peak areas for peak 1, representing the immobile protons, and that for peak 2 and peak 3, which are corresponding to the more mobile protons. Since peak 1 and peak 2 overlap considerably at some temperatures, the determined values always correspond to the areas left and right of the local minimum, respectively.

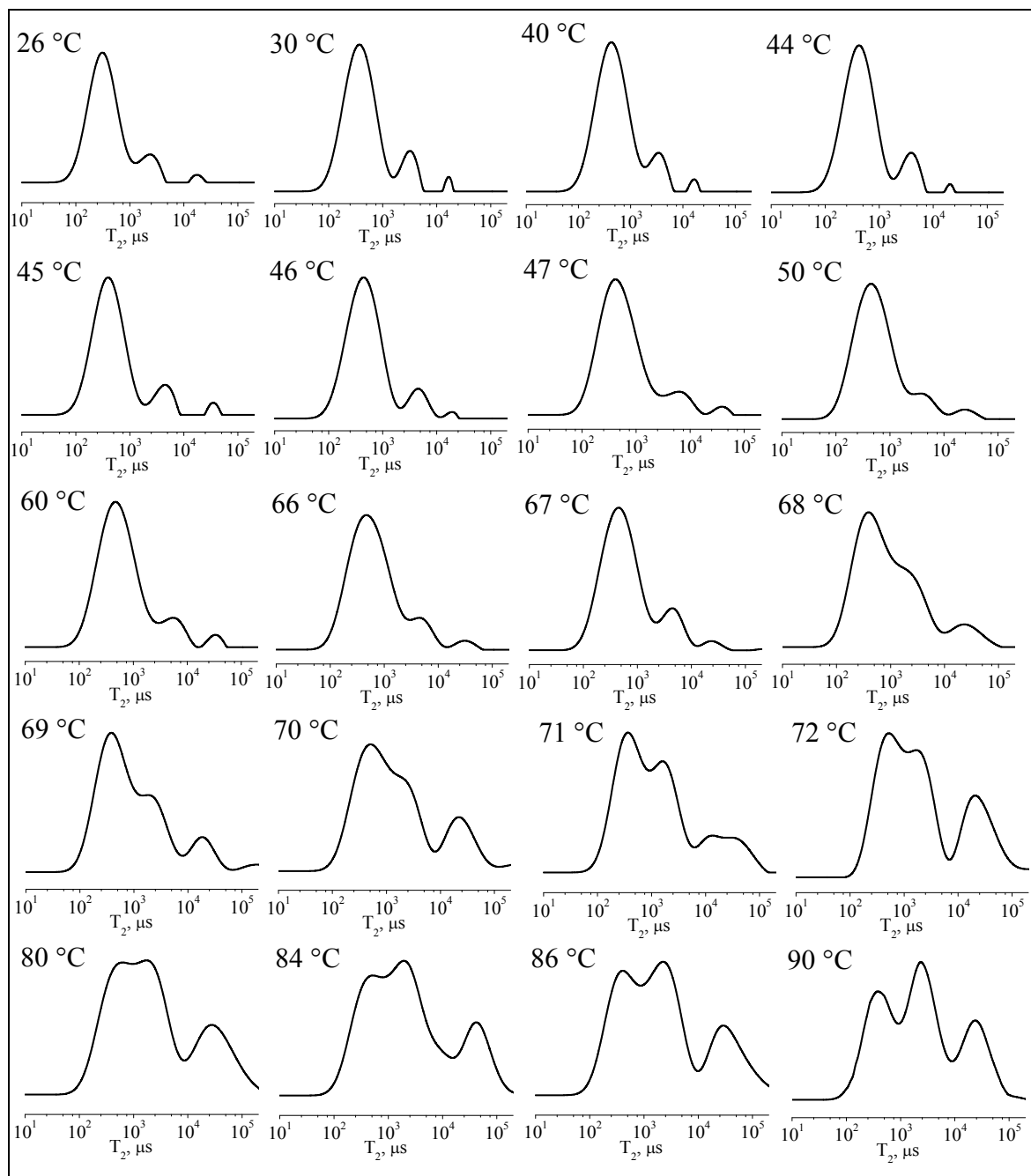


Figure 3.2.20 Representative T_2 -distributions obtained for 30 mg/ml Me₂PE-C32-Me₂PE in acetate buffer pH 5 at selected temperatures ranging from 26 to 90 °C.

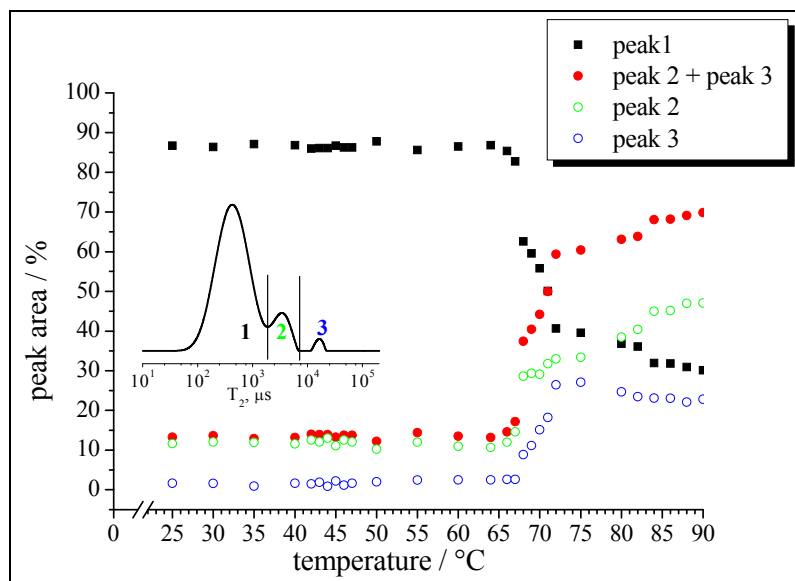


Figure 3.2.21
30 mg/ml Me₂PE-C32-Me₂PE at pD 5:
Temperature dependence of the peak areas, determined from the T₂-distributions by WinDXP for peak 1, peak 2 and peak 3. The sum of the peak areas of peak 2 and 3 is also shown, since it represents the whole fraction of the more mobile protons of Me₂PE-C32-Me₂PE.

In analogy to PC-C32-PC, the first transition of Me₂PE-C32-Me₂PE, which is observed at 45.5 °C in the DSC thermograms, is not causing a measurable change of the relaxation behavior of the bolaamphiphile protons. Therefore, the increase in the motional freedom of the particular protons, that is related to this transition, is not large enough to significantly increase the fraction of the more mobile protons (peak 2 and peak 3). The second transition at approximately 70 °C, however, is clearly reflected in the T₂-distributions. This transition is related to a breakdown of the fibers and the formation of micellar aggregates. Well above this transition temperature, the immobile proton fraction still makes up about 40% of the total hydrogen content, but is further reduced during the third transition, which is detected at about 85 °C. This transition represents a micelle-micelle transition and seems to be related to a further distinct increase in the motional freedom of the bolaamphiphile protons.

One can therefore conclude that the substitution of H₂O by D₂O as the dispersive phase allows to study the relaxation behavior of the bolaamphiphile protons. If a particular transition substantially increases the average motional freedom of the bolaamphiphile molecules inside the aggregates, this transition will be reflected in the T₂-distributions calculated by WinDXP. WinDXP can also be used to determine the relative area for each peak. This parameter was found to be suitable to visualize the relative changes in the relaxation behavior.

3.3 Electron spin resonance (ESR) spectroscopy

3.3.1 ESR measurements with tempolbenzoate

The first spin probe, that was introduced into the aqueous bolaamphiphile samples, was 4-hydroxy-2,2,6,6-tetramethylpiperidine-1-oxyl (tempolbenzoate, TB). The chemical structure is shown in Figure 3.3.1.

Tempolbenzoate has a n-octanol/water distribution coefficient of approximately 300.^[99] Therefore, TB was found to be very suitable to study multiphase systems with a high lipid content. In such systems like solid lipid nanoparticles,^[99] nanocapsules^[100] or self emulsifying pellet formulations,^[101] TB was found to preferentially accumulate in the lipophilic parts. Due to the sensitivity of its spectra to changes in the mobility and polarity of the surrounding environment, it provided unique information about these systems.

The hydrogels formed by Me₂PE-C32-Me₂PE and PC-C32-PC are biphasic systems with a relatively small lipid content. It was tested, whether tempolbenzoate could be used to gain insight into the lipophilic domains that are present due to the aggregation of the long chain bolaamphiphiles.

Figure 3.3.2 shows representative ESR spectra recorded for tempolbenzoate dissolved in acetate buffer at pH 5 and in a hydrogel formed by 10 mg/ml Me₂PE-C32-Me₂PE in acetate buffer at pH 5.

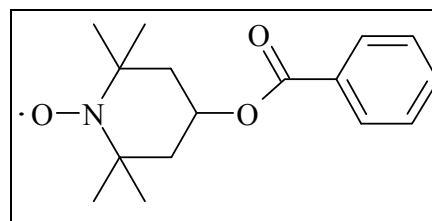


Figure 3.3.1 Chemical structure of tempolbenzoate (TB).

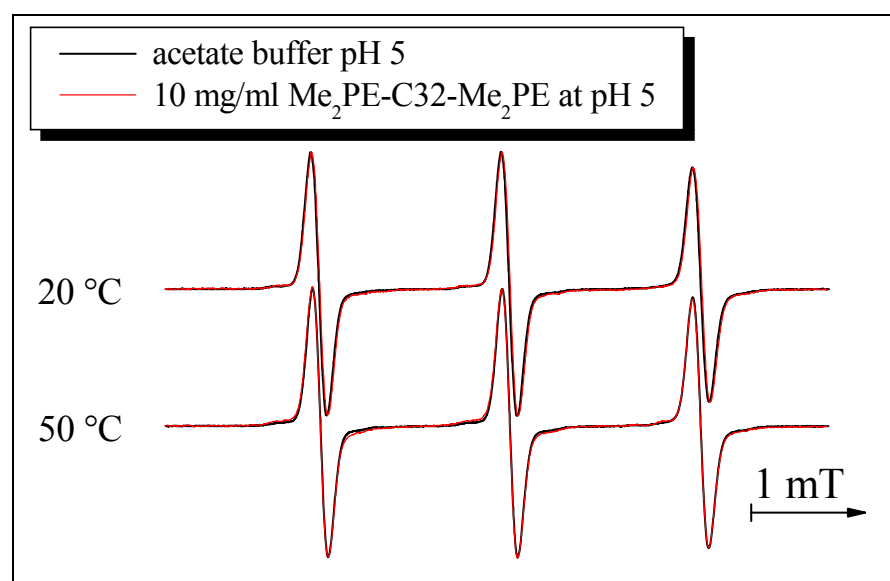


Figure 3.3.2 ESR spectra obtained at 20 and 50 °C for 0.025 mM tempolbenzoate (TB) dissolved in acetate buffer at pH 5 and in a hydrogel formed by 10 mg/ml Me₂PE-C32-Me₂PE in acetate buffer at pH 5.

As Figure 3.3.2 shows, no differences are observable between the spectra of TB obtained for the pure aqueous medium and for the hydrogel of Me₂PE-C32-Me₂PE at pH 5. The same result was obtained for the hydrogel with 10 mg/ml PC-C32-PC in deionized water. This indicates that the TB molecules experience essentially the same environment inside the dense bolaamphiphilic fiber network as in the pure aqueous medium. A considerable accumulation of the TB molecules in the more hydrophobic regions of the nanofibers can therefore be excluded. This would have resulted in a decrease of the hyperfine splitting constant A_N due to the decreased average polarity of the TB environment. No accumulation of TB is observed, which can be explained by the comparably low lipid concentration and by a relatively low affinity of the aromatic tempolbenzoate for the aliphatic lipid chains.

A considerable change in the rotational mobility of the TB molecules, on the other hand, would have resulted in a detectable broadening of the spectral lines, especially of the third line. The absence of such broadening shows that the dynamical properties of water, which is macroscopically immobilized, correspond to that observed in the pure medium on the molecular level. This finding confirms the results that were obtained in the NMR relaxation measurements for 30 mg/ml PC-C32-PC. The relaxation behavior of the water protons was found to be essentially the same for pure water and for the PC-C32-PC hydrogel (Section 3.2.1). For 30 mg/ml Me₂PE-C32-Me₂PE at pH 5, however, a considerable difference in the relaxation behavior was observed for the hydrogel compared to pure buffer due to the existence of thin layers of water between the lamellar aggregates. This difference in the relaxation behavior must be attributed to a significant motional restriction of this fraction of the water protons. As described above, TB is solely distributed throughout the aqueous phase inside the Me₂PE-C32-Me₂PE hydrogel and is therefore roughly representing the motional dynamics of the water molecules. The obvious motional restriction of the water molecules residing in the thin layers of water between the lamellar aggregates, however, is not detected in the ESR spectra of TB. One possible explanation for this finding is the lower concentration of Me₂PE-C32-Me₂PE in the ESR sample compared to that used for the NMR measurements. The number of lamellar aggregates will therefore be smaller and also the total number of water molecules that are residing between these aggregates. Furthermore, it is unlikely that a considerable amount of TB molecules, which is relatively large compared to the water molecules, can enter the thin layers of water between these lamellar aggregates. Therefore, the ESR spectra of TB in 10 mg/ml Me₂PE-C32-Me₂PE at pH 5 represent only the main fraction of the water molecules, but not the water in the lamellar domains. This main fraction, however, seems to be completely unaffected by the presence of 10 mg/ml Me₂PE-C32-Me₂PE regarding the rotational mobility of the particular water molecules.

3.3.2 ESR measurements with n-doxyl stearic acid

3.3.2.1 General remarks

Major processes during the endothermic transitions of PC-C32-PC and Me₂PE-C32-Me₂PE are occurring in the alkyl chain region of the bolaamphiphilic self-assemblies. In order to obtain insight into the microscopic order and the motional dynamics of this alkyl chain region at different temperatures, a systematic ESR spin probe study was carried out.

For this study, three derivatives of n-ketostearic acid with a doxyl (4,4-dimethyloxazolidine-N-oxy) group attached at positions 5, 12 and 16 of the alkyl chain were chosen. The chemical structures of these n-doxyl stearic acid (n-DSA) spin probes are shown in Figure 3.3.3 together with their molecular axes system, which is important to understand the molecular motions that are responsible for the different spectral line shapes. By convention, the principal axes of the hyperfine coupling tensor A and the g -tensor of nitroxides are taken such that the z_m axis is parallel to the $2p\pi$ -orbital of nitrogen and oxygen containing the unpaired electron (Section 2.2.3). For n-DSA, this z_m -axis corresponds to the long molecular axis.^[102,103] The x_m -axis is lying along the N-O bond and the y_m -axis perpendicular to the other two. In oriented samples, for example in glass-supported bilayers, the largest hyperfine splitting, A_{zz} , is obtained, when the external magnetic field is applied parallel to the fatty acid long axis z_m .

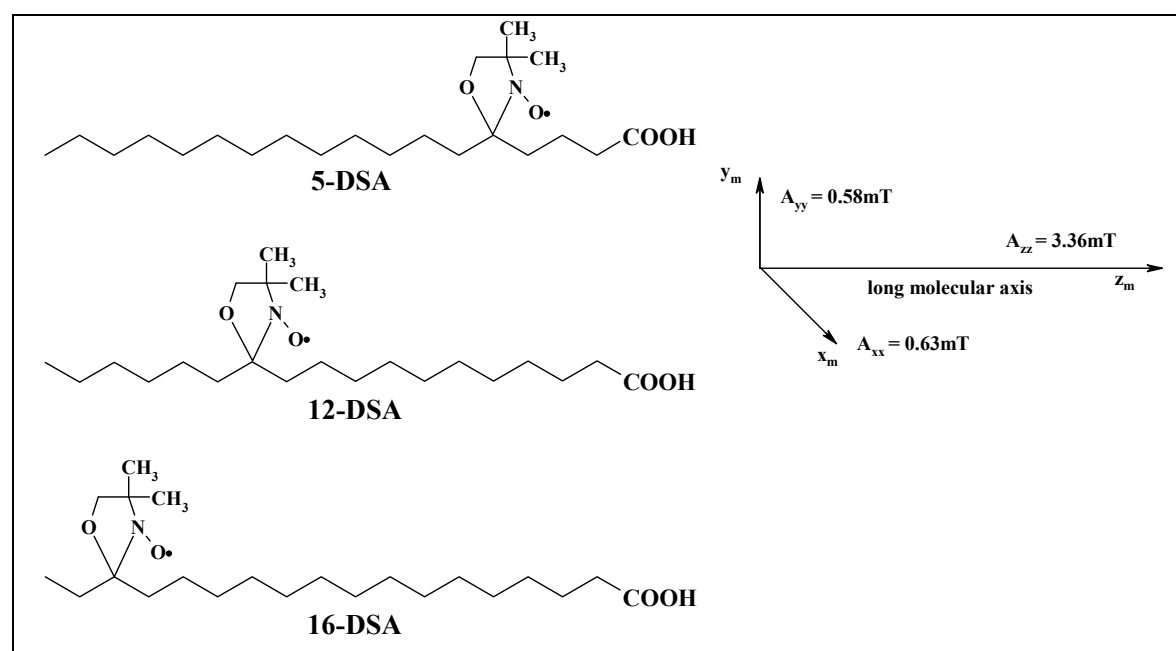


Figure 3.3.3 Chemical structures of the n-doxyl stearic acid spin probes 5-DSA, 12-DSA and 16-DSA together with their corresponding molecular axes system. The principle values for A_{xx} , A_{yy} and A_{zz} are also given, which were taken from single crystal measurements with 5-doxyl palmitic acid.^[104]

In many experiments, n-DSA spin probes were found to serve as good indicators of the phase state^[103,105] and were used to detect phase transitions.^[106,107] It should be noted here that spin probes only indirectly reflect the ordering of the host system and that they were found to be slightly less ordered than the host molecules.^[102]

ESR spectra of n-DSA incorporated into the bolaamphiphilic self-assemblies provide no direct information about the macroscopic hydrogel state, but only reflect the reorientational motion of the nitroxyl groups inside the aggregates. This reorientational motion of a particular nitroxyl group depends strongly on the motional freedom of the alkyl chain segment to which it is bound. This is the major difference between 5-DSA, 12-DSA and 16-DSA. In 12-DSA and 16-DSA, the doxyl group is located farther away from the carboxyl group than in 5-DSA.

As described above, PC-C32-PC and Me₂PE-C32-Me₂PE were shown by TEM and SANS to form nanofibers at low temperatures. This aggregation process is mainly driven by hydrophobic interactions between the long alkyl chains, which come in close contact to each other inside the formed self-assemblies. When a n-DSA molecule is incorporated into these aggregates, its polar carboxyl group is expected to be anchored in the polar headgroup region. Due to the high degree of order inside the nanofibers, the alkyl chain of the spin probe molecule, which is bearing the doxyl group, most probably adopts an extended conformation and is aligned parallel to the alkyl chains of the bolaphospholipids. As outlined in Figure 3.3.4, the doxyl group of the spin probes 12-DSA and 16-DSA should therefore be accommodated deeper inside the alkyl chain region compared to that of 5-DSA. If there are differences present in the microscopic order and motional freedom between the outer and the inner regions of the alkyl chain region, these differences will be reflected by differences in the ESR spectra of n-DSA.

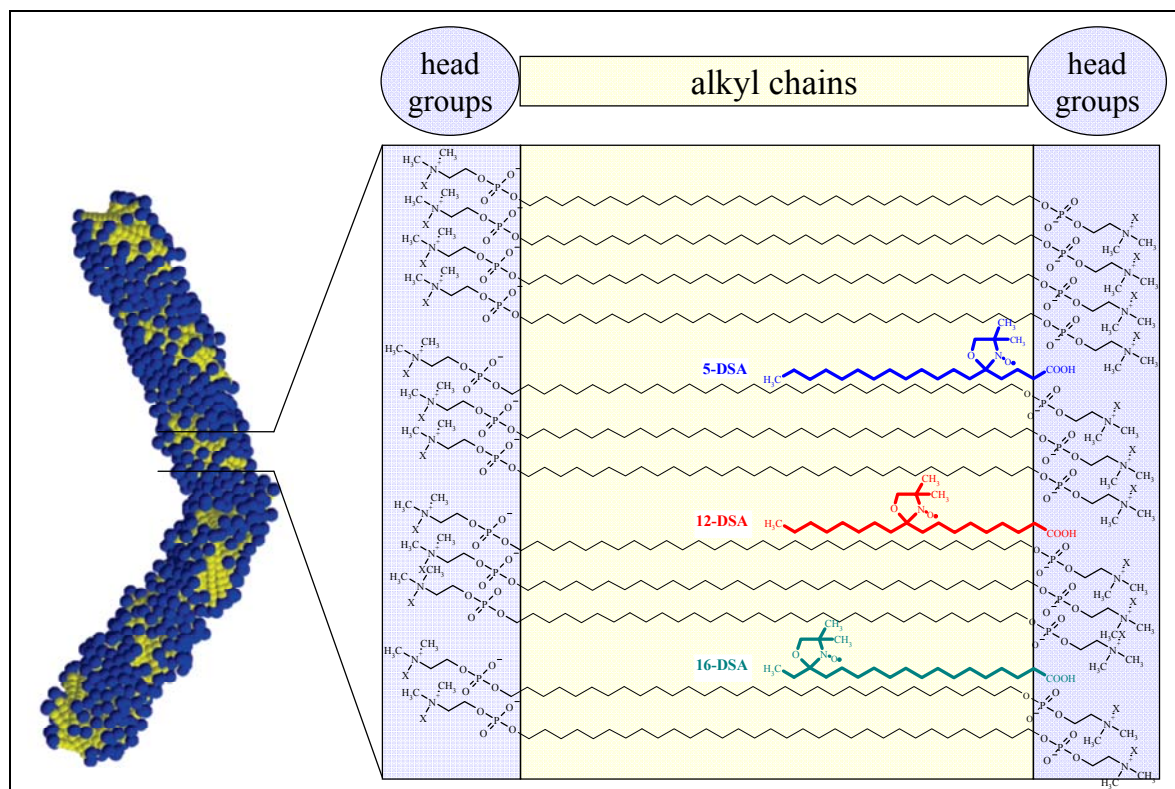


Figure 3.3.4 Schematic representation of the expected positions of the doxyl groups of 5-DSA, 12-DSA and 16-DSA inside the alkyl chain region of the bolaamphiphilic nanofibers. The picture of the fiber model was taken from.^[14]

3.3.2.2 *n*-DSA in PC-C32-PC

5-DSA in 10 mg/ml PC-C32-PC

When 0,05 mM of the spin probe 5-DSA are dissolved in pure deionized water, narrow ESR spectra are obtained as shown in Figure 3.3.5. In analogy to the results obtained with tempolbenzoate, these narrow spectra indicate a high degree of motional freedom of the spin probe molecules, which enables fast reorientation of the nitroxyl groups in the magnetic field.

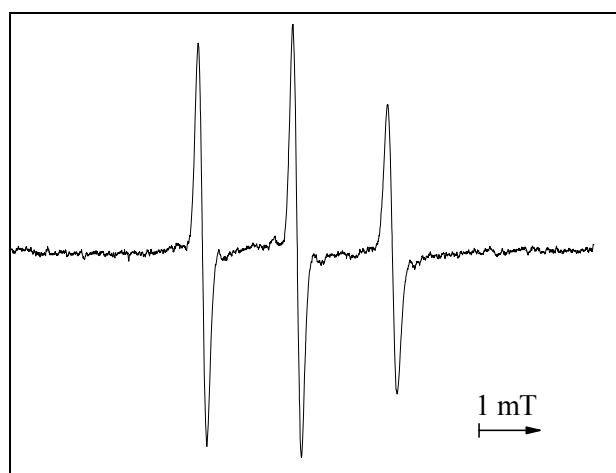


Figure 3.3.5 ESR spectrum of 5-DSA dissolved in deionized water at 20 °C.

5-DSA was incorporated into an aqueous sample with 10 mg/ml PC-C32-PC according to the procedure described in Section 2.2.3. The resulting molar ratio between n-DSA and PC-C32-PC was about 1:100. Representative spectra, that were obtained for this sample at different temperatures, are displayed in Figure 3.3.6.

These spectra of 5-DSA in 10 mg/ml PC-C32-PC differ substantially from that in pure water. The spectral line shapes at low temperatures are typical for nearly immobilized spin probes in macroscopically nonoriented systems.^[50] This indicates that nearly all 5-DSA molecules can be expected to be incorporated inside the highly ordered alkyl chain region of the bolaamphiphilic aggregates as is outlined in Figure 3.3.4. Macroscopically, no preferential order of the 5-DSA molecules with respect to the external magnetic field can be observed. Such preferential orientation could only be realized by a nearly perfect parallel ordering of the fibers relative to the capillary wall, which is not likely to occur because highly diluted samples were used for the measurements. Therefore, the z_m -axes of the 5-DSA molecules assume all possible angles relative to the external magnetic field, and the obtained spectra have to be regarded as a superposition of the ESR signals of the particular spin probe molecules.

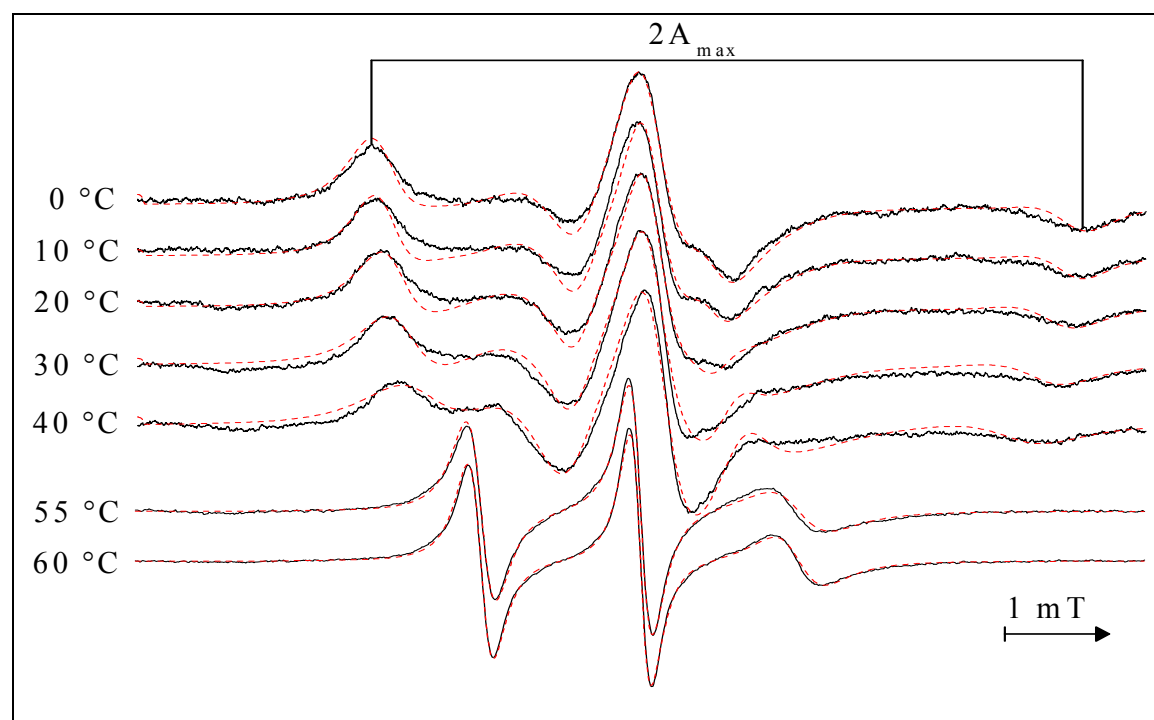


Figure 3.3.6 Experimental (—) and simulated (- - -) ESR spectra of 5-DSA in 10 mg/ml PC-C32-PC recorded at different temperatures. $2A_{\max}$ values were determined from the separation of the outermost extrema with an accuracy of about 0.1 mT. All ESR spectra were adjusted to approximately the same peak height of the central peak in order to compare the particular line shapes.

The ESR spectrum of 5-DSA in 10 mg/ml PC-C32-PC at 0 °C shows high anisotropy close to the rigid limit. Whereas the motion of the whole nanofibers can be neglected on the ESR timescale,^[108] slow rotational reorientation of the 5-DSA molecules affects the spectral line shape by averaging the anisotropic contributions to a small extent. This results in a decrease in separation between the outer extrema compared to a rigid limit spectrum ($2A_{\max} < 2A_{zz}$). When the temperature is increased from 0 to 40 °C, only small changes in the spectral line shape are found to occur and the outermost extrema gradually move toward the center. The major line shape changes take place between 40 and 55 °C as is shown in Figure 3.3.7. As described above, DSC thermograms show endothermic transitions at 43.8 and 48.7 °C.^[12] One additional transition is observed at 73 °C, outside the temperature range of the ESR spectrometer. The considerably less anisotropic ESR spectra recorded at 55 and 60 °C indicate that at these temperatures, rotational reorientation is fast on the ESR time scale.

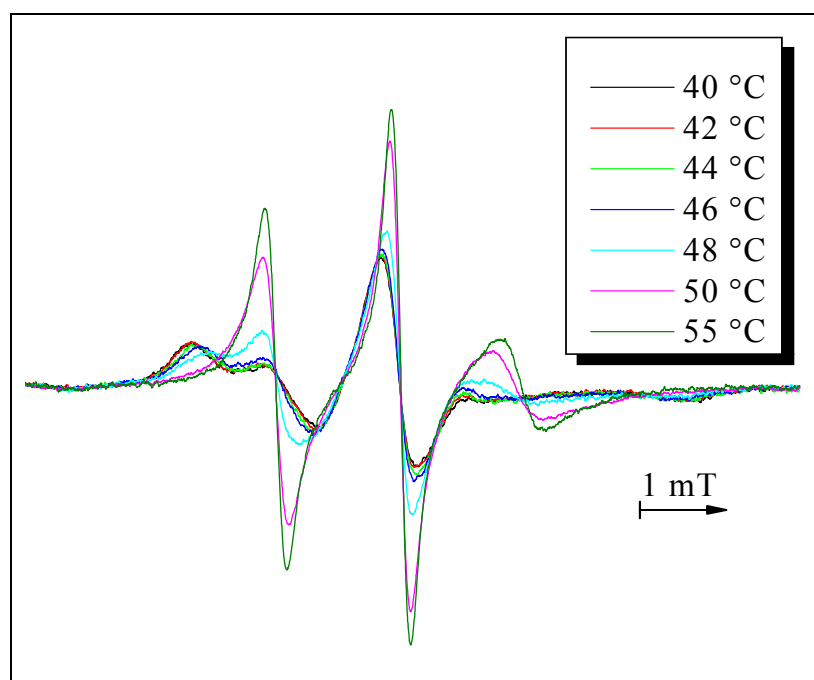


Figure 3.3.7

Experimental ESR spectra obtained for 5-DSA in 10 mg/ml PC-C32-PC at temperatures between 40 and 55 °C.

For the determination of transition temperatures with the ESR spin probe technique, different approaches were described in the literature. Spectral parameters, that were successfully used for this purpose, are hyperfine splitting values,^[103,106,109] order parameters^[106,109] and peak heights.^[110,111]

For all spectra recorded for n-DSA in the course of this ESR spin probe study, it turned out to be most practicable and reliable to simply plot the hyperfine splitting parameter $2A_{\max}$ against the temperature. $2A_{\max}$, the distance between the outermost extrema, can be measured directly from the spectra as is shown in Figure 3.3.6. This parameter is known to reflect well relative

changes of the local order and of the motional dynamics.^[50] Figure 3.3.8 shows the temperature dependence of the $2A_{\max}$ values that were obtained from the spectra of 5-DSA in the sample with 10 mg/ml PC-C32-PC in deionized water.

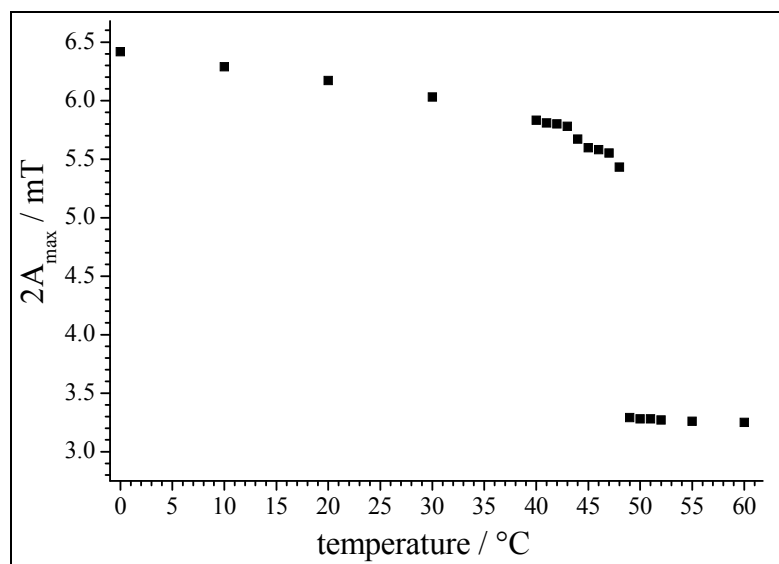


Figure 3.3.8
5-DSA in 10 mg/ml PC-C32-PC: $2A_{\max}$ versus temperature. Transition temperatures were determined from this plot as midpoint temperatures with an accuracy of about ± 0.5 °C.

In the temperature region from 0 °C to 40 °C, $2A_{\max}$ is linearly decreasing from 6.42 to 5.83 mT. This decrease of $2A_{\max}$ is due to increased thermal motions of the spin probe molecules inside the bolaamphiphilic aggregates. The high degree of order and the resulting restrictions for rotational reorientation of the 5-DSA molecules are maintained up to 40 °C. The severe changes of the spectral line shape are well reflected by the $2A_{\max}$ values. When the temperature is gradually increased from 40 to 55 °C, the $2A_{\max}$ values of the recorded spectra are not decreasing linearly, but show a small and a large discontinuity. This indicates distinct changes in the spin probe environment during the endothermic transitions. The transition temperatures of 43.5 and 48.5 °C, which were determined as midpoint temperatures from the particular discontinuities of $2A_{\max}$, are in good agreement with the DSC data (Table 3.3.1).

Table 3.3.1 Transition temperatures of PC-C32-PC determined by DSC and with the ESR spin probe technique.

DSC	ESR		
	5-DSA	12-DSA	16-DSA
43.8 °C	43.5 °C	43.5 °C	41.0 °C
48.7 °C	48.5 °C	51.0 °C	47.5 °C
73.0 °C	-	-	-

The second transition clearly marks the main transition and is related to a decrease in $2A_{\max}$ by about 2.2 mT. Above this transition temperature, the gel character of the PC-C32-PC samples is completely lost. This is due to a complete disintegration of the network of nanofibers into small fiber pieces and micellar aggregates as could be shown by TEM^[13] and SANS.^[18] A drastic change in the ESR line shape from a slow motion to a fast motion ESR spectrum is observed during this transition (Figure 3.3.7), which results in a distinct decrease in $2A_{\max}$. This indicates that rotational reorientation of the 5-DSA molecules is considerably faster in these smaller aggregates compared to the nanofibers. The increase in motional freedom of the spin probe molecule gives evidence that a distinct loss of order inside the alkyl chain region is related to the transitional breakdown of the fibers. This finding is in agreement with the FT-IR data, which revealed a distinct increase in the number of gauche conformers above the transition temperature.

The first discontinuity in $2A_{\max}$ corresponds to the pre-transition observed in the DSC thermograms. Above the transition temperature, rod-like aggregates are still present, as was shown by TEM^[13] and SANS.^[18] ³¹P-NMR revealed that the pre-transition is related to a significant increase in the headgroup mobility.^[18] As described above, the dynamic viscosity η was found to be dramatically decreased at the temperature of the pre-transition (Figure 1.6A), which was indicating that a significant number of fiber-fiber cross-links are breaking down above this temperature.^[13] The ESR data, however, indicate only small changes in the molecular arrangement inside the nanofibers, because 5-DSA molecules experience an only slightly less ordered environment above the transition temperature. It was concluded before that the small changes in the local order of the nanofibers lead to a substantial reduction in the accessibility of the hydrophobic parts of the fibers, which would lead to a significant loss of fiber-fiber cross-links.^[91] However, due to the temperature dependent rheological data that was obtained by oscillatory rheometry (Section 3.1), this conclusion must be corrected. As is shown in Figure 3.1.4, a series of rheograms obtained for hydrogels of PC-C32-PC did not show the expected decrease of the G' and G'' values at the temperature of the pre-transition, but rather a slight increase. This is in contradiction to the results obtained for the dynamic viscosity, since it indicates slightly more efficient hydrophobic interaction between the fibers. Due to the very small effect that was observed in the ESR spectra, it seems to be more likely that there are no major changes in the alkyl chain region that could lead to a drastic loss of fiber-fiber cross-links, which supports the data obtained by performing oscillatory rheometry.

Therefore, one can conclude that above the pre-transition temperature, small changes in the local order inside the alkyl chain region of the PC-C32-PC nanofibers are reflected in the spectra of 5-DSA. This is in agreement with the ^{31}P -NMR measurements, which revealed an increase in the mobility of the phosphocholine headgroups. These changes in the arrangement can be assumed to have an effect on the degree of fiber-fiber cross-linking.

In order to further analyze the spectra of 5-DSA in 10 mg/ml PC-C32-PC and also to theoretically confirm the interpretation of the observed spectral changes in terms of changes in the motional freedom of the nitroxyl group, full line shape simulations were performed for selected spectra.

Spectra of 5-DSA in 10 mg/ml PC-C32-PC at temperatures between 0 °C and 60 °C cover the slow motional and the fast motional regime. Therefore, they have to be calculated on the basis of the stochastic Liouville equation and the motional narrowing approximation, respectively.

As described in Section 2.2.3, rotational reorientation of the spin probe molecules is the most important dynamic process in spin probe ESR. Motional reorientation of a 5-DSA molecule, incorporated into an aggregate of PC-C32-PC, can be described by an axially symmetric rotation. This means that reorientation of the nitroxyl group in the external magnetic field is realized by rotation about the long molecular axis z_m (\parallel) and by rotation of the axis perpendicular to the long axis (\perp). These motions are characterized by the rotational correlation times τ_{\parallel} and τ_{\perp} , respectively, and by their anisotropy $N_R = \tau_{\perp} / \tau_{\parallel}$.

At low temperatures, τ_{\perp} lies well in the slow motional regime ($500 \text{ ns} > \tau_{\perp} > 5 - 10 \text{ ns}$). Thus, spectral line shape simulations have to be performed on the basis of the Stochastic Liouville equation. In the present work, the slow-motion simulation algorithm implemented in the function »chili« of EasySpin version 2.6.1 was used. EasySpin is a software package developed by Stoll and Schweiger.^[51,52] EasySpin is running on Matlab (The Mathworks, Natick, MA, USA). The slow motion simulation algorithm of the EasySpin function »chili« is based on the well known program developed by Freed and co-workers.^[112] The theoretical background for the simulation algorithm can be found in the cited literature.

Here, only a brief description of the established simulation procedure and the experimental, static and dynamic input parameters of the spin system is given. An example for the command structure, which was used to calculate the ESR spectra with EasySpin, is given in Figure S.2 in the Supplement.

The input structure "Exp" is used by »chili« to specify the experimental parameters. These are the spectrometer frequency in GHz ('mwFreq', 9.4) and the sweep range, which is defined by the center field and the full field sweep range, both in mT ('CenterSweep', [334.9 9.8]). By

using the function »pseudomod«, it is also possible to take the modulation amplitude of 0.125 mT into account.

"Sys" is the structure containing the static parameters of the paramagnetic molecules. In nitroxides, hyperfine splitting is realized by interaction of the free electron with the magnetic moment of ^{14}N ('Nucs', '14N'). The starting values for the principal g tensors (g_{xx} 2.0088, g_{yy} 2.0061, g_{zz} 2.0027) and hyperfine tensors (A_{xx} 0.63 mT, A_{yy} 0.58 mT, A_{zz} 3.36 mT) were taken from single crystal data of 5-doxylpalmitic acid in BSA.^[104] »Chili« requires the values of the hyperfine splitting to be given in MHz. In order to convert these values from G or mT into MHz, the EasySpin function »mt2mhz« can be used. The ordering effect of the bolaamphiphiles on the spin probe molecules are taken into account by the Euler angle β in $^\circ$ or rad. β is the average tilt angle of all z_m -axes with respect to the local director ('Apa', [α β γ]* $\pi/180$). For an axially symmetric spin probe, the orientational order parameter S is defined as^[113,114]

$$S = \left\langle \frac{1}{2}(3 \cos^2 \beta - 1) \right\rangle \quad (3.3)$$

The dynamics of the spin probe molecules are characterized by the input structure "Dyn". Brownian rotational diffusion is assumed in the EasySpin function »chili« and rotational diffusion tensors R_{\perp} and R_{\parallel} are used, which are related to the corresponding correlation times by

$$R_{\parallel, \perp} = \frac{1}{6\tau_{\parallel, \perp}} \quad (3.4)$$

The mean rotational correlation time τ_{Rm} can be calculated from τ_{\perp} and τ_{\parallel} according to^[115]

$$\tau_{Rm} \equiv \sqrt[3]{\tau_{\parallel} \tau_{\perp}^2} \quad (3.5)$$

An additional dynamical parameter to be defined is the residual line width lw , which is given in units of MHz.

If the EasySpin command structure is correctly constructed, the output arguments "B" and the corresponding ESR signal amplitude "spc0" are obtained, which are further processed in order to take the modulation amplitude into account.

After constructing a suitable EasySpin command structure, the optimization process was started in order to obtain the best parameters for the spectral simulation. This optimization was done manually for every single experimental spectrum that was selected before. Starting with the g and A tensors from the single crystal data, a first set of simulations was performed by independently varying the diffusion tensor elements R_{\perp} and R_{\parallel} , the tilt angle β and the residual line width lw . This optimization was focussed on fitting the shape of the

central peak and on adjusting amplitude and position of the outermost extrema. In the next step, the A and g tensors were varied in order to further improve the simulations. For this step, the simulation parameters given by Schorn et. al^[116] were of considerable help. Finally, the first optimization step was repeated until a suitable simulated spectrum could be obtained that was fitting the experimental spectrum to a good approximation. The effect of varying the particular parameters is documented in Figures S.3 to S.7 in the Supplement.

At low temperatures, experimental spectra of 5-DSA in 10 mg/ml PC-C32-PC can be simulated reasonably well with EasySpin (Figure 3.3.6). With increasing temperature, however, τ_{\perp} approaches the fast motional regime, and spectral simulation becomes more difficult. Therefore, only selected spectra up to 40 °C were simulated with EasySpin 2.6.1.

At 55 °C, well above the temperature of the main transition of PC-C32-PC, molecular reorientation is considerably faster compared to 40 °C. The resulting almost isotropic spectra could therefore be simulated on the basis of the motional narrowing approximation, which is implemented in the program EPRSIM.^[53] This program uses averaged magnetic tensors and can automatically fit isotropic and anisotropic spectra with mean correlation times ranging from 0.01 to 10 ns.

The final simulated spectra for 5-DSA in 10 mg/ml PC-C32-PC are plotted together with the experimental spectra in Figure 3.3.6. A compilation of the optimized parameters for simulating the particular spectra is given in Table S.3 in the Supplement.

The values established in the optimization process for τ_{\perp} , lie well inside the slow motion region for all temperatures from 0 to 40 °C. On the other hand, the values of τ_{\parallel} are intermediate between slow and fast motion region for 0 and 10 °C before entering the fast motion region at 20 °C. The ratio between τ_{\perp} and τ_{\parallel} , which characterizes the anisotropy of the rotational motion, is increasing from 7.5:1 at 0 °C to 15:1 at 20 °C. Only a single rotational correlation time is calculated with the program EPRSIM for the fast motion spectra. Therefore, the axial symmetric components τ_{\perp} and τ_{\parallel} , obtained from the slow motion simulations, had to be converted into the mean rotational correlation time τ_{Rm} (Equation 3.5) in order to compare the reorientational rates below and above the transitions. The τ_{Rm} values and order parameters, established for 5-DSA in 10 mg/ml PC-C32-PC at different temperatures, are displayed in Figure 3.3.9.

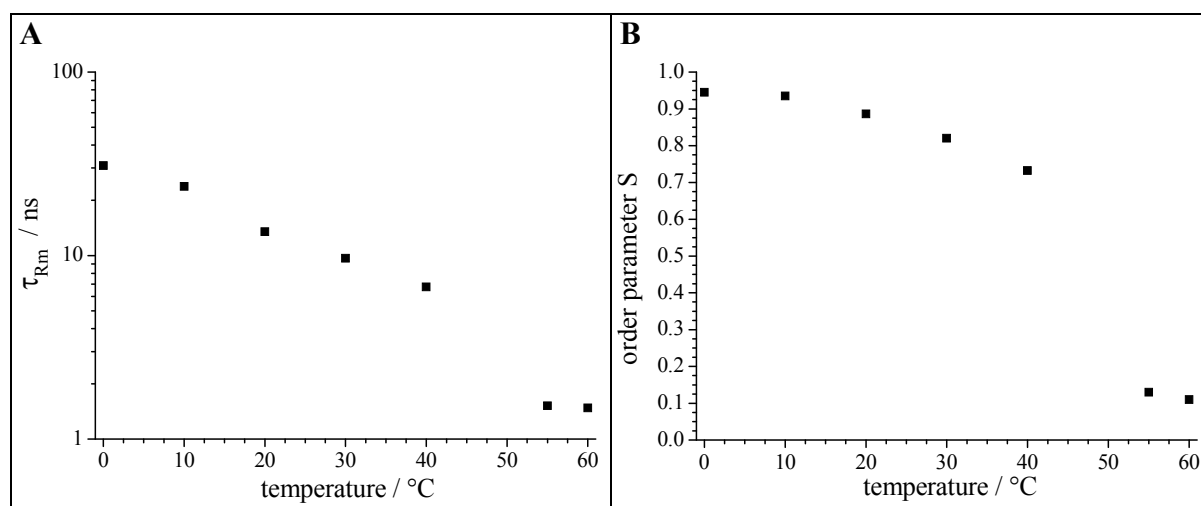


Figure 3.3.9 5-DSA in 10 mg/ml PC-C32-PC: (A) Mean rotational correlation time τ_{Rm} and (B) order parameter S versus temperature.

With increasing temperature, the mean correlation time τ_{Rm} and the order parameter S qualitatively show the same behavior as $2A_{max}$, which gives evidence for the reliability of the established simulation parameters. At 0 °C, 5-DSA molecules experience a highly ordered environment ($S = 0.95$), which allows for only slow reorientational motion with a calculated τ_{Rm} value of about 31 ns. When the temperature is increased from 0 to 40 °C, S and τ_{Rm} are found to be moderately decreased to 0.73 and 7 ns, respectively. At 60 °C, well above the second transition temperature, the order parameter and the mean rotational correlation time are decreased to 0.11 and 1.48 ns, respectively. This indicates a high degree of disorder and fast reorientational motion inside the micellar aggregates, which are present at this temperature. Motional averaging of the anisotropic interactions is much more efficient for 5-DSA inside these micelles than inside the densely packed nanofibers. Besides considerably faster rotational motion of the 5-DSA molecules, trans-gauche isomerization of the spin probe chain and overall motion of the whole micelles provide additional sources of motional averaging by changing the orientation of the nitroxyl group in the magnetic field.^[117]

12-DSA in 10 mg/ml PC-C32-PC

Additional to 5-DSA, the spin probes 12-DSA and 16-DSA were used in order to gain insight into different positions inside the alkyl chain region. As stated above, the doxyl groups of 12-DSA and 16-DSA are attached farther away from their carboxyl groups compared to 5-DSA. The doxyl groups of 12-DSA and 16-DSA could therefore be expected to be situated deeper inside the alkyl chain region of the bolaamphiphilic aggregates than that of 5-DSA (Figure 3.3.4). If there are differences present regarding the local order and the motional

freedom at these deeper positions of the alkyl chain region, these differences will be reflected in a changed spectral line shape.

Representative spectra, recorded for 12-DSA incorporated into aggregates of PC-C32-PC, are displayed in Figure 3.3.10 together with their best simulations. These spectra are, in general, very similar to that of 5-DSA. However, there are some small but decisive differences present in the spectral line shapes. At low temperatures, only minor differences in the central part of the spectra are observable. When the temperature is gradually increased to 40 °C, the position and shape of the outermost extrema in the spectra of 12-DSA are considerably less affected by the increasing thermal motions. The major line shape changes are again observed between 40 and 55 °C as is shown in Figure 3.3.11, but the high anisotropy of the spectra is maintained up to a higher temperature compared to 5-DSA.

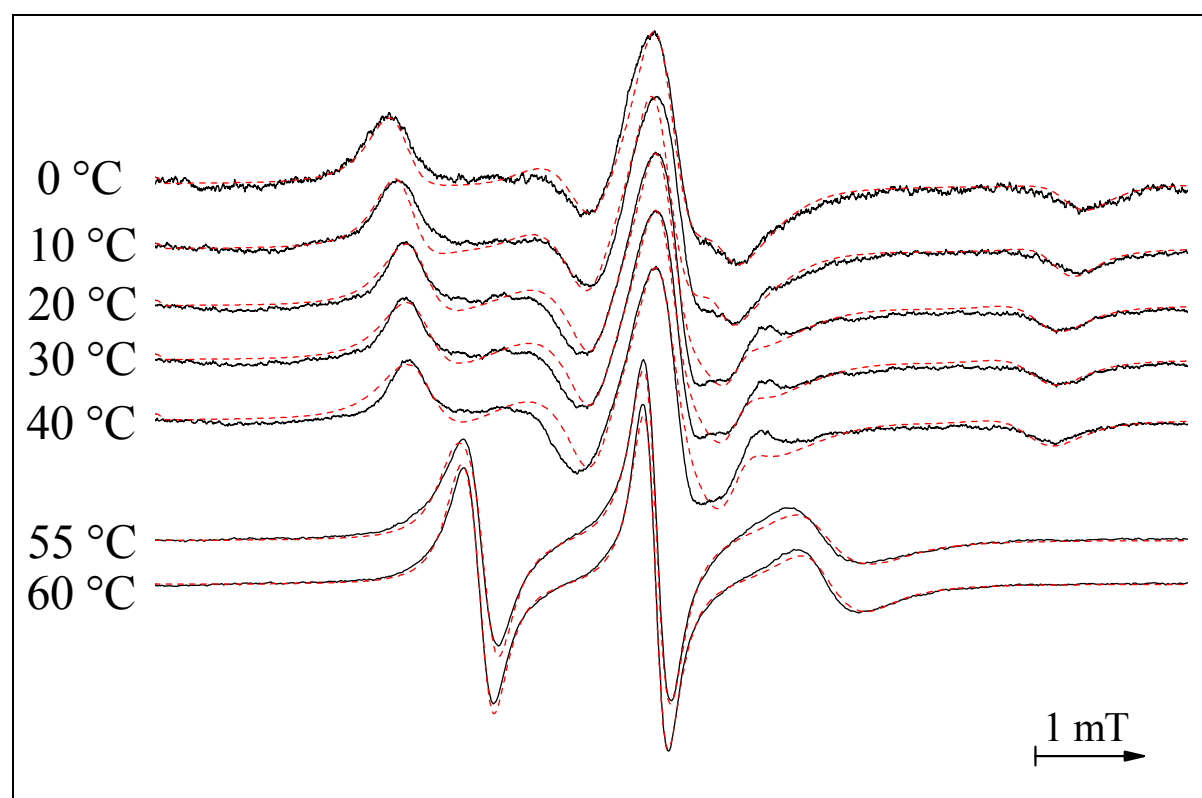


Figure 3.3.10 Experimental (—) and simulated (- - -) ESR spectra of 12-DSA in 10 mg/ml PC-C32-PC recorded at different temperatures. All ESR spectra were adjusted to approximately the same peak height of the central peak in order to compare the particular line shapes.

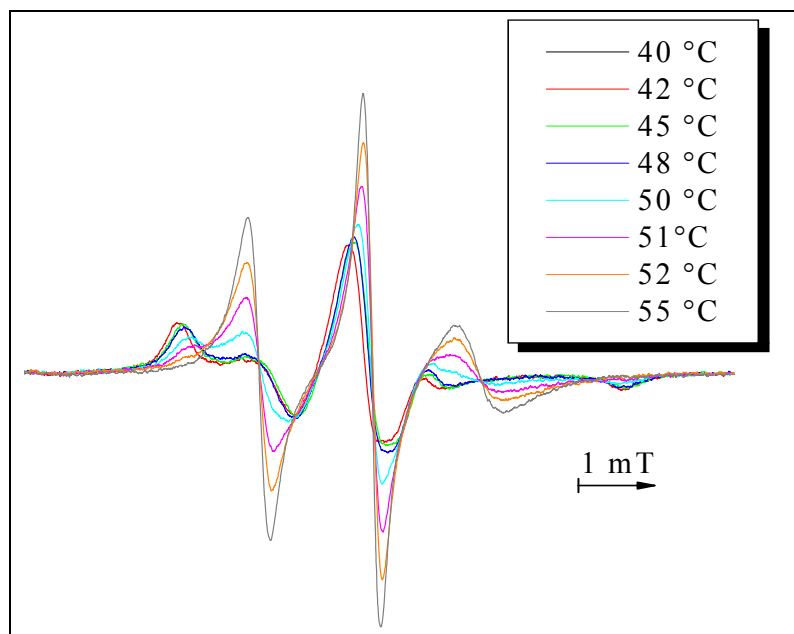


Figure 3.3.11
Experimental ESR spectra obtained for 12-DSA in 10 mg/ml PC-C32-PC at temperatures between 40 and 55 °C.

The differences between the spectra of 12-DSA and 5-DSA become also clearly apparent by determining the temperature dependent $2A_{\max}$ values for 12-DSA and plotting them together with that of 5-DSA (Figure 3.3.12).

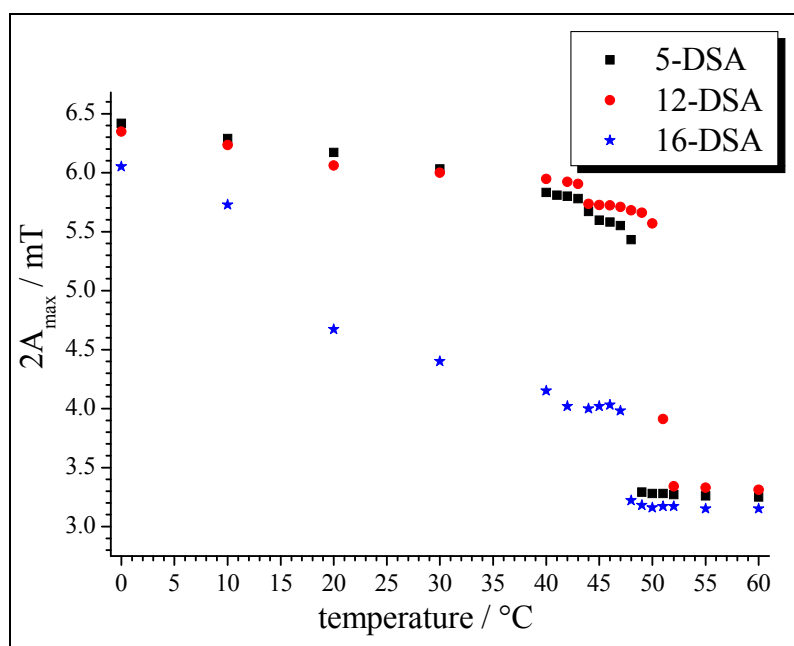


Figure 3.3.12
n-DSA in 10 mg/ml PC-C32-PC: $2A_{\max}$ versus temperature.

At temperatures up to 30 °C, slightly lower $2A_{\max}$ values are observed for 12-DSA compared to 5-DSA. When approaching the first transition temperature, accelerating thermal motions and increasing trans-gauche isomerization of the bolaamphiphilic alkyl chains reduce the order inside the aggregates. Decreasing local order leads to increasing motional freedom of

the alkyl chain segments that are bearing the nitroxyl groups and is therefore reflected in a more efficient motional averaging of the spectral anisotropies. As a consequence, the $2A_{\max}$ values are gradually decreased for both spin probes in the temperature range from 0 to 40 °C. The decrease of $2A_{\max}$ with increasing temperature is more obvious for 5-DSA compared to 12-DSA. As a result, the $2A_{\max}$ values of 12-DSA were found to be larger for all temperatures above 30 °C. This points to a more pronounced trans-gauche isomerization in the outer parts of the alkyl chain region, whereas in the region deeper inside the aggregates, which is probed by 12-DSA, the order remains significantly higher.

This conclusion is supported by the fact that the second transition temperature was determined to be 51 °C for 12-DSA, which represents an increase of 2.5 °C with respect to the results obtained for 5-DSA and by DSC (Table 3.3.1). As described above, the second transition is the main transition and results in a breakdown of the three-dimensional network of nanofibers, which is accompanied by a significant loss of order inside the alkyl chain region. Compared to 5-DSA, the loss of order in the environment of the nitroxyl group of 12-DSA appears to be considerably delayed. This can be only interpreted in terms of a delayed trans-gauche isomerization in the central part of the alkyl chains. One can therefore conclude that trans-gauche isomerization can be expected to begin in the outer parts of the aggregates and to proceed toward the central region with increasing temperature. As will be shown below, this interpretation is supported by the results obtained for 12-DSA in Me₂PE-C32-Me₂PE at pH 5.

Analogous to 5-DSA, spectral simulations were performed for selected spectra obtained of 12-DSA. As shown in Figure 3.3.10, the central region of the final simulated spectra differs to some extent from the experimental slow motion spectra especially between 20 and 40 °C. For these spectra, it was not possible to obtain better simulations of the central region. The same problem was also observed for 12-DSA in hydrogels formed by 10 mg/ml Me₂PE-C32-Me₂PE at pH 5.

In Figure 3.3.13A and 3.3.13B, the temperature dependent mean rotational correlation times τ_{Rm} and the order parameters S are plotted, respectively. For comparison, the corresponding values obtained for 5-DSA are again showed. These τ_{Rm} and S values qualitatively show the same behavior as the determined $2A_{\max}$ values. With increasing temperature from 0 to 40 °C, both parameters are found to be only moderately decreased, whereas a substantial decrease is again observed between 40 and 55 °C due to the transitional changes of the aggregation behavior.

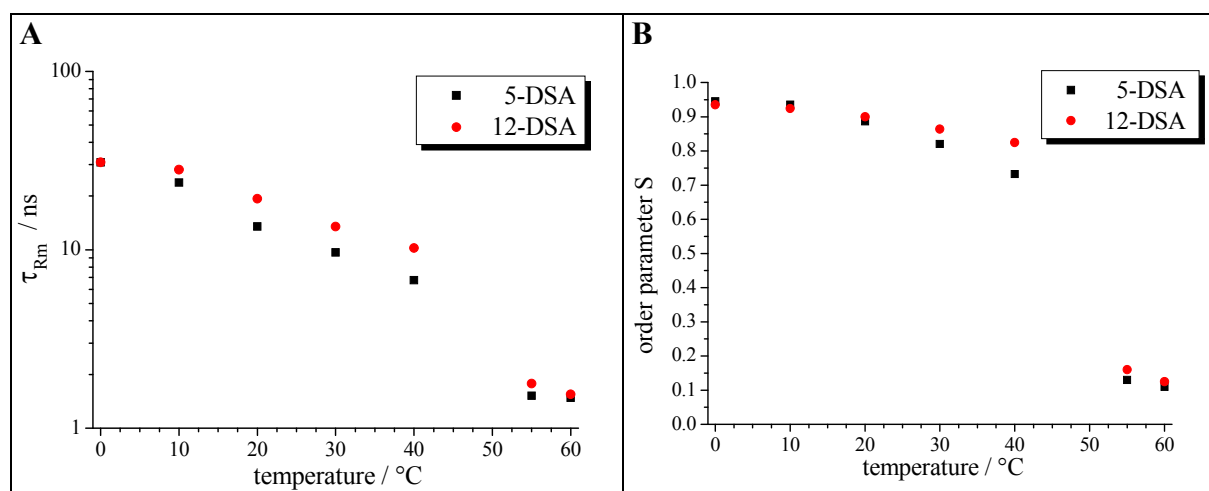


Figure 3.3.13 12-DSA in 10 mg/ml PC-C32-PC: (A) Mean correlation time τ_{Rm} and (B) order parameter S versus temperature. For comparison, the data of 5-DSA is also plotted.

16-DSA in 10 mg/ml PC-C32-PC

The spectra obtained for 16-DSA in 10 mg/ml PC-C32-PC are shown in Figure 3.3.14.

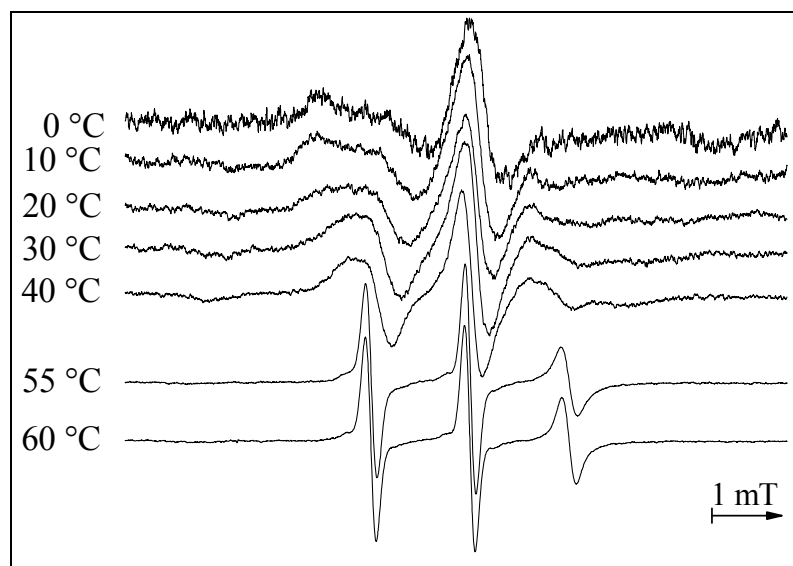


Figure 3.3.14

Experimental ESR spectra obtained for 16-DSA in 10 mg/ml PC-C32-PC recorded at different temperatures. All ESR spectra were adjusted to approximately the same peak height of the central peak. No spectral simulations were performed for 16-DSA.

The spectra of 16-DSA show significantly less anisotropic behavior compared to 5-DSA and 12-DSA, which indicates much faster reorientational motion of the nitroxyl group. In 16-DSA, the doxyl group is attached near the terminal methyl group. Therefore, rotation about a single bond can overlap the segmental motion of the alkyl chain. Such rotation allows for more efficient motional averaging of the spectral anisotropies. Furthermore, there is some uncertainty about the position of the doxyl group when the spin probe is incorporated into the nanofibers. Since it is attached farther away from the carboxyl group, it was assumed to be situated deeper inside the hydrophobic region compared to 5-DSA and 12-DSA (Figure 3.3.4).

However, in different amphiphilic systems, such as monolayers^[118] and bilayers,^[119] the doxyl group of 16-DSA was found to reside in the headgroup region. Analysis of the obtained spectra indicates that for 16-DSA in aggregates of PC-C32-PC, the doxyl groups can also be expected to preferentially reside in the outer part of the alkyl chain region near the headgroups. In contrast to 12-DSA, the high degree of order deep inside the alkyl chain region is not reflected in the spectra of 16-DSA. As a consequence, the $2A_{\max}$ values obtained for 16-DSA are significantly decreased compared to the other spin probes (Figure 3.3.12). The transitions are again reported by two discontinuities in $2A_{\max}$, but both transition temperatures were found to be shifted downward with respect to the other spin probes (Table 3.3.1).

For 12-DSA, the increased transition temperature with respect to 5-DSA was interpreted in terms of a deeper position of the doxyl group inside the alkyl chain region. Following this interpretation, the determination of lower transition temperatures for 16-DSA is a clear indication that the doxyl group of 16-DSA is not residing in the inner part (I in Figure 3.3.15), but in the outer part of the alkyl chain region. This preferential location of the doxyl group near the headgroup region could be realized by a bent conformation of the 16-DSA chain (II in Figure 3.3.15) as was suggested for other systems.^[118,119] However, because of the larger volume and the hydrophilicity of the doxyl group at the end of the chain, 16-DSA molecules may also be incorporated into the aggregates with the carboxyl group inside the hydrophobic part (III in Figure 3.3.15). This inversion of orientation would move their nitroxyl groups to the headgroup region without bending the fatty acid chain, which would be a conformation with higher energy. Therefore, this inverted conformation seems to be most likely for 16-DSA inside the self-assemblies of PC-C32-PC.

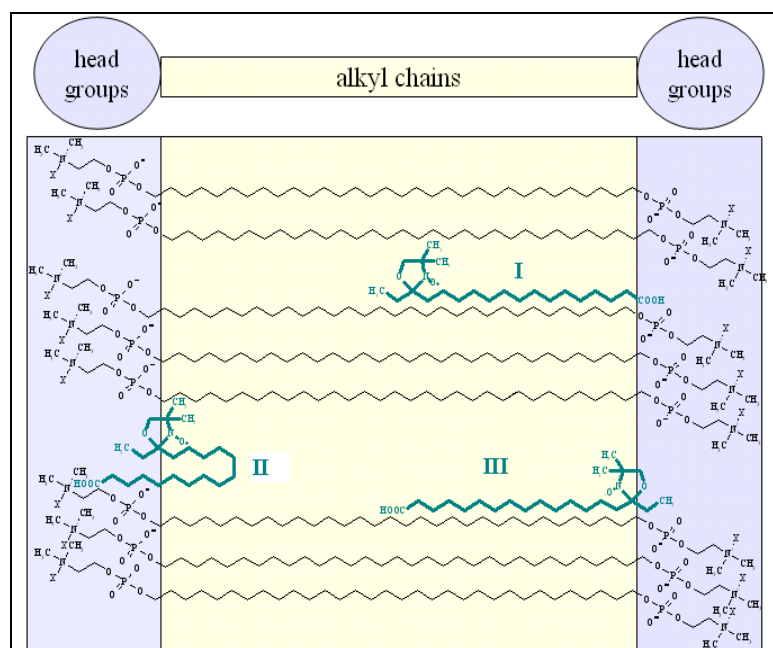


Figure 3.3.15

Schematic representation of the possible conformations of 16-DSA inside the alkyl chain region of the bolaamphiphilic self-assemblies:

(I) Extended conformation with the carboxyl group in the headgroup region.

(II) Bent conformation, which brings the doxyl group near the headgroups.

(III) Extended conformation with the doxyl group in the alkyl chain region.

Reduction assay

In order to confirm the conclusions regarding the positions of the particular doxyl groups inside the bolaamphiphilic alkyl chain region, a reduction assay with ascorbic acid^[100] was carried out. This kind of assay was also used in unilamellar liposomes to study the effect of the position of the doxyl group on the rate of reduction.^[120]

Aminoxyl radicals (R-NO \cdot) are efficiently reduced by ascorbic acid to the corresponding hydroxyl amines (R-NOH). These hydroxylamines are not contributing to the ESR signal, they are ESR silent. Therefore, the rate of reduction is directly reflected in a decrease of the signal intensity. Depending on the position of the particular doxyl group inside the bolaamphiphilic aggregates, the rate of reduction can be expected to vary, because the hydrophilic ascorbic acid cannot enter the hydrophobic parts very easily.

The reduction assay with ascorbic acid was carried out as described in Section 2.2.3. The first spectrum was obtained two minutes after addition of ascorbic acid. The height of the central line was determined from this spectrum (Figure 3.3.16A) as the starting value for the signal intensity (I_{2min}). In order to obtain time dependent signal intensities (I_t), ESR spectra were recorded during a period of 20 minutes. A representative set of time dependent spectra is shown in Figure 3.3.16B. During the time of the experiment, the ESR signal intensities are found to be substantially decreased.

The reduction of n-DSA molecules by ascorbic acid was found to be much more efficient, when the spin probes are dissolved in water without PC-C32-PC. In this case, no ESR signal could be detected already after 4 min. This means that incorporation of the n-DSA molecules inside the nanofibers leads to a significant protection of the spin probe molecules from ascorbic acid.

As described above, the signal intensity I_t of each spectrum was determined, which represents the remaining number of spin probe molecules at time t . These time dependent signal intensities were used to calculate the relative intensities I_t/I_{2min} (Figure 3.3.16C). The rate of reduction was then obtained from plotting $\ln(I_t/I_{2min})$ versus time (Figure 3.3.16D). The final reduction rate constants were calculated for every spin probe as the average of five determinations. These final reduction rates of n-DSA in PC-C32-PC by ascorbic acid were determined to be

$$\begin{aligned} &0.110 \pm 0.013 \text{ min}^{-1} \text{ for 5-DSA} \\ &0.102 \pm 0.010 \text{ min}^{-1} \text{ for 12-DSA and} \\ &0.166 \pm 0.015 \text{ min}^{-1} \text{ for 16-DSA.} \end{aligned}$$

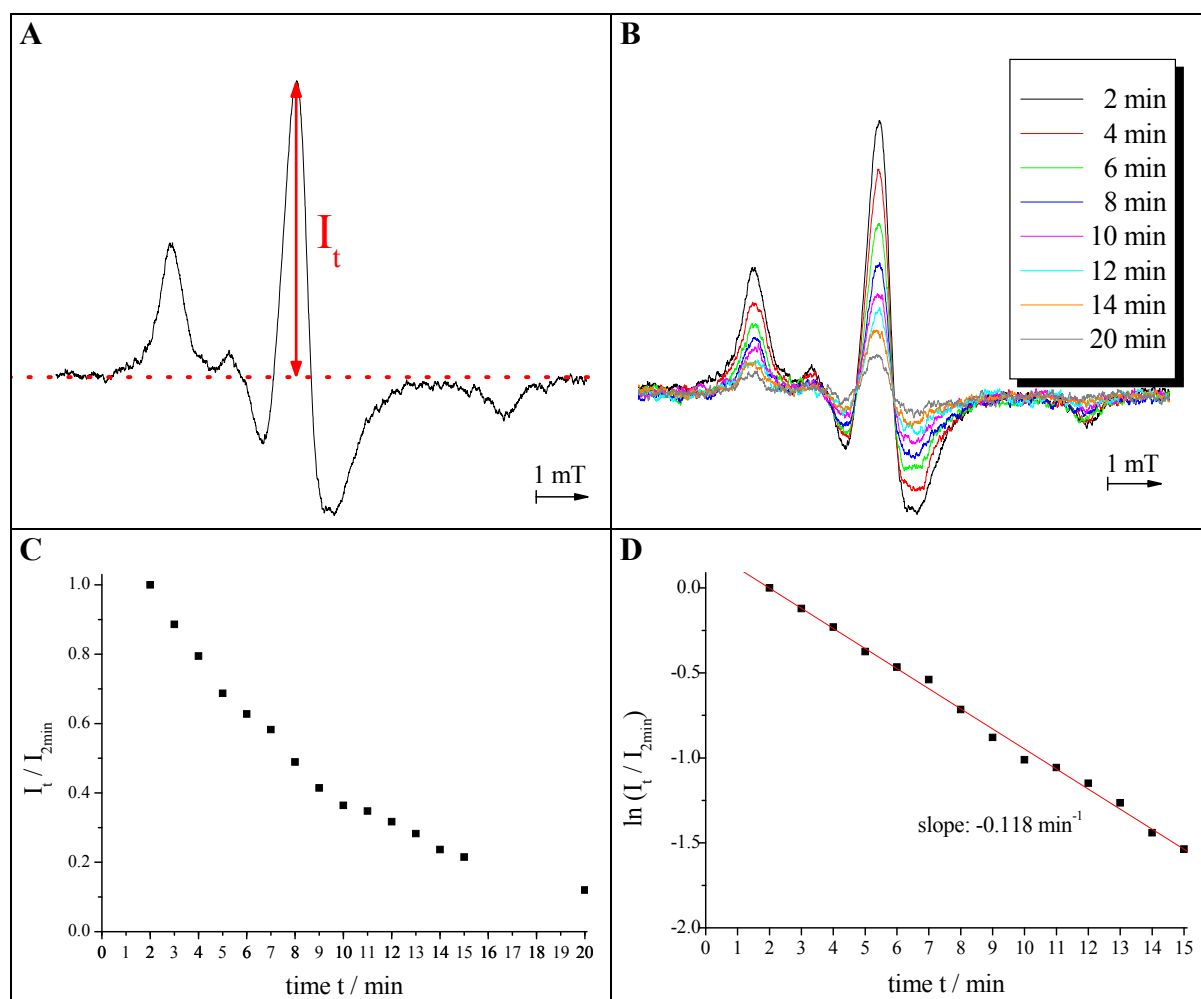


Figure 3.3.16 Ascorbic acid reduction assay:

- (A) Determination of the signal intensity I_t at time t from the obtained ESR spectrum.
- (B) Spectra of 5-DSA in 10 mg/ml PC-C32-PC recorded at different times after addition of ascorbic acid.
- (C) Resulting relative signal intensities I_t / I_{2min} for each spectrum.
- (D) Determination of the slope of $\ln(I_t / I_{2min})$ plotted against time.

The results of the reduction assay confirm the conclusions that were drawn from the experimental data for the predominant positions of the doxyl groups of 5-DSA, 12-DSA and 16-DSA. Due to a significant protection from reduction by the presence of PC-C32-PC compared to the pure aqueous medium, the vast majority of the spin probe molecules can be expected to be incorporated inside the alkyl chain region of the nanofibers. The differences between the reduction rates of the particular n -DSA molecules indicate differences regarding the position of their doxyl groups inside the alkyl chain region. The reduction rate determined for 12-DSA is slightly smaller than that of 5-DSA, which points to a position of the nitroxyl group deeper inside the hydrophobic region. It has to be noted, however, that these differences between 5-DSA and 12-DSA are within the observed error range and may therefore not be accounted to be significant. Interpretation of the small differences between 5-DSA and

12-DSA is also complicated by the fact that the hydrophobic region is not completely shielded by the hydrophilic headgroups, but can be expected to be partially exposed to the aqueous medium (see fiber model in Figure 3.3.4). Therefore, reduction of the nitroxyl groups of 5-DSA and 12-DSA is not only dependent on their predominant position inside the alkyl chain region relative to the headgroups.

The reduction rate of 16-DSA, on the other hand, is significantly larger compared to that of 5-DSA and 12-DSA. This indicates that ascorbic acid has considerably better access to the nitroxyl group of 16-DSA. This result confirms the conclusion that the majority of the doxyl groups of 16-DSA is not residing deep inside the alkyl chain region of the aggregates, but in the outer region near the headgroups of the bolaamphiphiles.

3.3.2.3 *n*-DSA in Me_2PE -C32- Me_2PE

5-DSA in 10 mg/ml Me_2PE -C32- Me_2PE at pH 5

Experimental spectra obtained for 5-DSA incorporated into aggregates formed by 10 mg/ml Me_2PE -C32- Me_2PE in acetate buffer at pH 5 are shown in Figure 3.3.17.

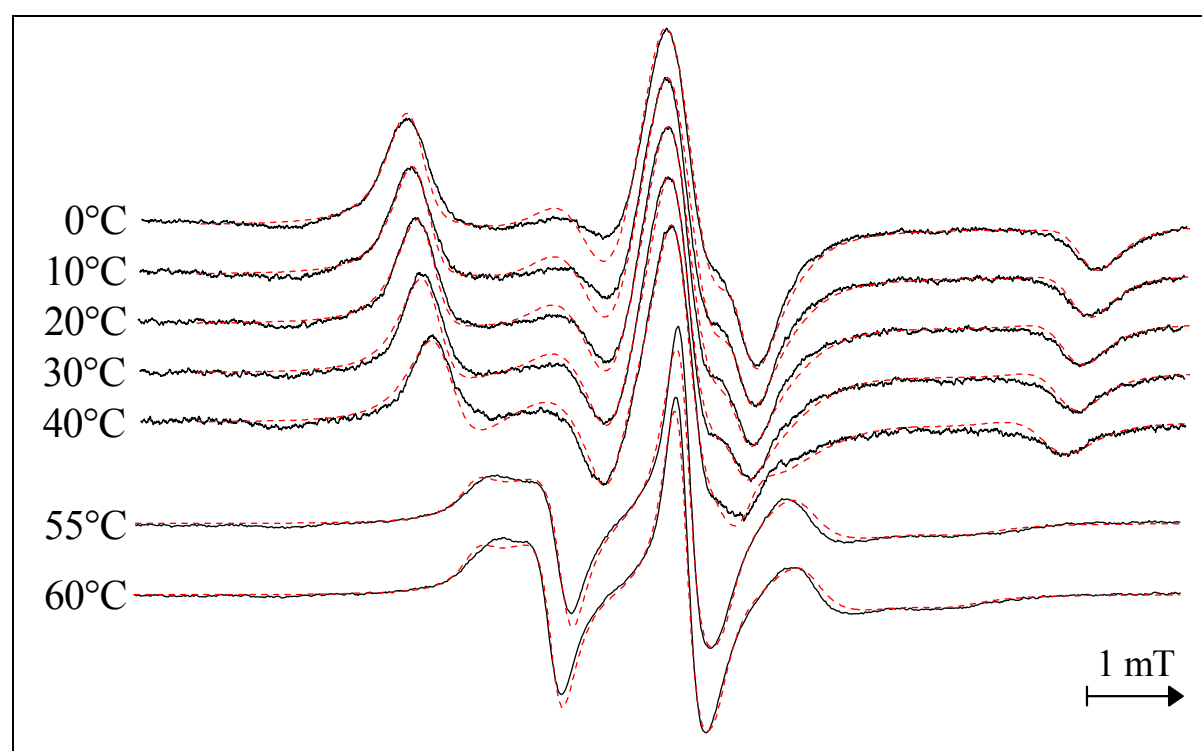


Figure 3.3.17 Experimental (—) and simulated (- - -) ESR spectra of 5-DSA in 10 mg/ml Me_2PE -C32- Me_2PE at pH 5 recorded at different temperatures. All ESR spectra were adjusted to approximately the same peak height of the central peak in order to compare the particular line shapes.

When 5-DSA is incorporated into aggregates formed by 10 mg/ml Me₂PE-C32-Me₂PE at pH 5, the resulting ESR spectra up to 40 °C resemble that obtained for 5-DSA in 10 mg/ml PC-C32-PC (Figure 3.3.6). This indicates that there are no major differences regarding the position of the doxyl group inside the bolaamphiphilic aggregates. However, some small differences can be found between the spectra of 5-DSA in Me₂PE-C32-Me₂PE and PC-C32-PC at temperatures ranging from 0 to 40 °C. For example, the shape of the outer extrema is noticeably less influenced by the averaging effect of the increasing thermal motions in the spectra of 5-DSA in 10 mg/ml Me₂PE-C32-Me₂PE at pH 5.

The major line shape changes are again observed between 40 and 55 °C (Figure 3.3.18). The spectra of 5-DSA in Me₂PE-C32-Me₂PE at 55 and 60 °C are considerably more anisotropic compared to that of 5-DSA in PC-C32-PC. This indicates a significantly higher order that is remaining in the environment of the 5-DSA molecules inside the aggregates of Me₂PE-C32-Me₂PE. As described above, only micellar aggregates are present for PC-C32-PC above 50 °C, whereas the nanofibers formed by Me₂PE-C32-Me₂PE at pH 5 remain intact up to 69 °C. This is due to the stabilizing effect of the hydrogen bonds that are formed between the headgroups of Me₂PE-C32-Me₂PE at pH 5.

The higher degree of the remaining order is also reflected in the significantly higher 2A_{max} values of 5-DSA in Me₂PE-C32-Me₂PE at 55 and 60 °C compared to PC-C32-PC (Figure 3.3.19).

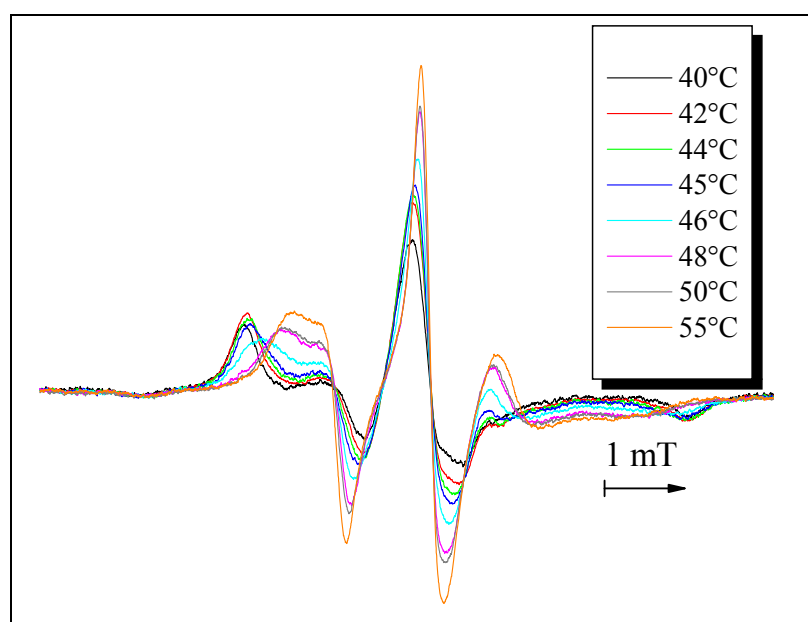


Figure 3.3.18

Experimental ESR spectra obtained for 5-DSA in 10 mg/ml Me₂PE-C32-Me₂PE at pH 5 and temperatures between 40 and 55 °C.

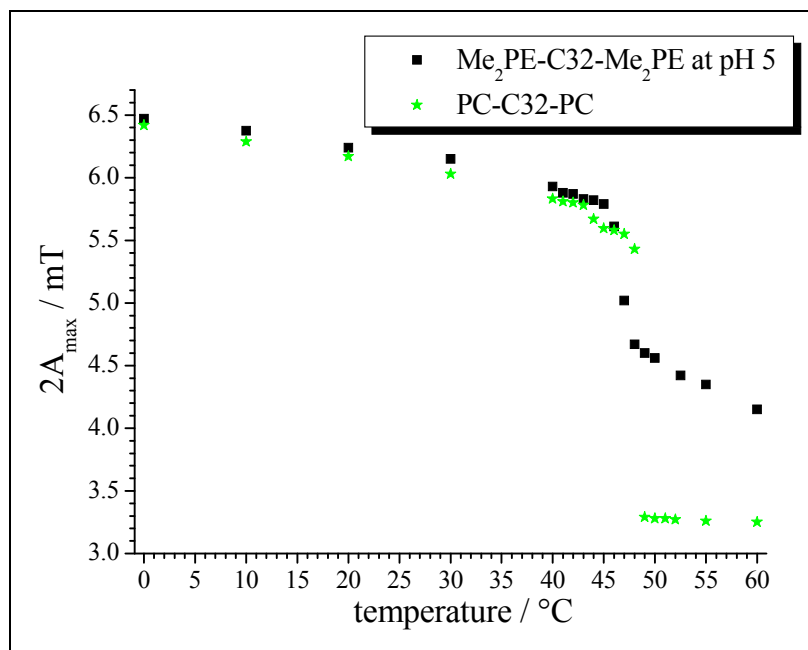


Figure 3.3.19

5-DSA in 10 mg/ml Me₂PE-C32-Me₂PE at pH 5 and in 10 mg/ml PC-C32-PC: 2A_{max} versus temperature.

At low temperatures, the 2A_{max} values obtained for 5-DSA in 10 mg/ml Me₂PE-C32-Me₂PE at pH 5 are slightly increased with respect to PC-C32-PC. This might be also attributed to the effect of hydrogen bonding.

In analogy to PC-C32-PC, the 2A_{max} values determined for 5-DSA in Me₂PE-C32-Me₂PE at pH 5 are found to be gradually decreased, when the temperature is increased from 0 to 40 °C due to increased thermal motions. The decrease in 2A_{max} inside this temperature range is slightly smaller for Me₂PE-C32-Me₂PE (0.54 mT) compared to PC-C32-PC (0.59 mT).

Above the first transition temperature, rod-like aggregates are still present for both bolaamphiphiles. This transition is characterized by only a small decrease in 2A_{max} of about 0.19 mT in the case of PC-C32-PC, whereas for 5-DSA in Me₂PE-C32-Me₂PE at pH 5, a more pronounced decrease of 1.12 mT is observed. This indicates a higher loss of order inside the fibers of Me₂PE-C32-Me₂PE above the temperature of the first transition. Differences between PC-C32-PC and Me₂PE-C32-Me₂PE regarding the first transition were observed before by various methods: Analogous to PC-C32-PC, the ³¹P-NMR data revealed that the headgroup mobility is significantly increased for Me₂PE-C32-Me₂PE at pH 5 above the first transition temperature.^[18] Almost isotropic mobility of the headgroups, however, is only reached inside the aggregates of PC-C32-PC, but not inside that of Me₂PE-C32-Me₂PE. A significant increase in the number of gauche conformers at the first transition was not detected by FT-IR for PC-C32-PC,^[13] but for Me₂PE-C32-Me₂PE at pH 5.^[15] In PC-C32-PC, this transition can therefore be expected to be mainly associated with changes in the mobility of the headgroups, whereas in aggregates of Me₂PE-C32-Me₂PE, distinct changes in the alkyl chain region are also involved. This conclusion seems to be supported by the data obtained by

performing oscillatory rheometry (Section 3.1). For PC-C32-PC, fiber-fiber cross-linking is solely due to hydrophobic interactions. Severe changes in the alkyl chain region can therefore be expected to have a strong influence on the determined storage and loss moduli. Such changes can be excluded, because only a very small effect was observed for the first transition. For Me₂PE-C32-Me₂PE at pH 5, on the other hand, a significant decrease in the storage and loss moduli was observed above the temperature of the first transition. This indicates a distinct decrease in the number of cross-links between the fibers of Me₂PE-C32-Me₂PE. The hydrogel state, however, was found to still persist for 10 mg/ml Me₂PE-C32-Me₂PE at pH 5 above the transition temperature, which indicates a considerable number of remaining cross-links.

As described in Section 3.2.1, none of the transitions of 30 mg/ml PC-C32-PC could be detected by means of ¹H-relaxometry, whereas for 30 mg/ml Me₂PE-C32-Me₂PE at pH 5 the first transition was found to be connected with a distinct increase in the determined T_{2m}-values. This increase in T_{2m} was attributed to a considerable degree of heterogeneity that is only present inside the network formed by Me₂PE-C32-Me₂PE below the first transition temperature. The experimental data indicate that these heterogeneities are due to a large number of lamellar aggregates, which may form extended stacks inside the network of nanofibers.^[23] No considerable degree of heterogeneity is present above the first transition temperature, which causes the T_{2m}-values to be significantly increased. Therefore, this transition is connected with a transformation of lamellar aggregates into other aggregates, most probably into nanofibers.

Besides the nanofibers, a considerable number of lamellar aggregates can also be expected to be present in the ESR sample containing 5-DSA in 10 mg/ml Me₂PE-C32-Me₂PE at pH 5. The proposed arrangement of the bolaamphiphiles inside these square lamellae can be expected to lead to a higher order inside the hydrophobic region due to better packing of the alkyl chains compared to the fibers. 5-DSA molecules, which can be assumed to reside inside the alkyl chain regions of both types of aggregates, will therefore experience a different average motional freedom compared to PC-C32-PC. This could be one reason for the slightly increased 2A_{max} values that were obtained for 5-DSA in Me₂PE-C32-Me₂PE compared to PC-C32-PC. The differences between both bolaamphiphiles regarding the loss of order above the temperature of the first transition might also be attributed, at least in part, to the presence of the lamellar aggregates at low temperatures and their transformation into fibers during this transition.

From the $2A_{\max}$ values obtained for 5-DSA in 10 mg/ml Me₂PE-C32-Me₂PE at pH 5, a transition temperature of 46.5 °C was determined for the first transition,. This value is about 1 °C higher than the one obtained by DSC (Table 3.3.2). For 5-DSA in PC-C32-PC, such a shift of the transition temperature was not observed. Following the interpretation developed above for 12-DSA in PC-C32-PC, this would mean that 5-DSA is expected to reside deeper inside the alkyl chain region of the aggregates of Me₂PE-C32-Me₂PE compared to 5-DSA in PC-C32-PC. Due to the decrease of the pH, the number of deprotonated carboxyl groups of the 5-DSA molecules can be expected to be considerably smaller for the sample of Me₂PE-C32-Me₂PE at pH 5 compared to PC-C32-PC in deionized water. Protonated fatty acid spin probes in lipid systems were found to be situated deeper inside the hydrocarbon region.^[121] Therefore, the shift in the transition temperature could probably be explained with the preferential location of the 5-DSA molecules deeper inside the alkyl chain region compared to PC-C32-PC. On the other hand, the hydrogel of Me₂PE-C32-Me₂PE represents a more complex system than that of PC-C32-PC. The observed temperature shift may, for example, also be due to a preferential location of the 5-DSA molecules either in the nanofibers or in the lamellar aggregates. Therefore, a definite interpretation of the observed small temperature shift is not possible without further experiments. Such experiments could involve the application of pulsed ESR techniques. For example, detailed information about the position of the doxyl groups of the n-DSA molecules in frozen vesicles could be achieved by studying the interaction of the nitroxide group with D₂O by means of the electron spin echo modulation (ESEM) method.^[119] However, such techniques were not applied in the course of this spin probe study.

Therefore, the interpretation of the experimental data was focussed on the relative differences that could be observed by varying the temperature of the particular sample and between the different spin probes.

Table 3.3.2 Transition temperatures of Me₂PE-C32-Me₂PE at pH 5 determined by DSC and with the ESR spin probe technique.

DSC	ESR		
	5-DSA	12-DSA	16-DSA
45.5 °C	46.5 °C	48.5 °C	45.5 °C
69.5 °C	-	-	-
85.0 °C	-	-	-

In analogy to PC-C32-PC, spectral simulations were also performed for 5-DSA in 10 mg/ml Me₂PE-C32-Me₂PE at pH 5. The final simulated spectra are shown in Figure 3.3.17 together with the experimental spectra. The obtained values of the mean rotational correlation time τ_{Rm} and the order parameter S are plotted in Figure 3.3.20.

As expected, the established values for τ_{Rm} and S reflect well the differences of 5-DSA in Me₂PE-C32-Me₂PE with respect to PC-C32-PC. At 0 °C, the mean rotational correlation time of the nitroxyl groups inside the alkyl chain region is increased for Me₂PE-C32-Me₂PE (64.98 ns) compared to PC-C32-PC (30.96 ns). The established order parameters at this temperature are 0.96 and 0.95 for Me₂PE-C32-Me₂PE and PC-C32-PC, respectively. When the sample temperature is increased to 30 °C, well below the first transition temperature, the motional freedom of the 5-DSA molecules is found to be significantly more affected in PC-C32-PC (τ_{Rm} : 9.66 ns, S: 0.86) than in Me₂PE-C32-Me₂PE (τ_{Rm} : 28.39 ns, S: 0.92).

Above the first transition temperature, rotational reorientation becomes significantly faster for 5-DSA in Me₂PE-C32-Me₂PE, but still not fast enough to completely average out the anisotropic contributions. Thus, up to 60 °C, the ESR spectra remain anisotropic in their character, which is not the case for PC-C32-PC. Almost isotropic molecular motion of the nitroxyl groups of 5-DSA inside the aggregates of Me₂PE-C32-Me₂PE will only occur above the second transition at about 69 °C, which is outside the temperature range of the ESR spectrometer. Due to the relatively high degree of anisotropy in the spectra of Me₂PE-C32-Me₂PE above the first transition temperature, spectral simulation in the fast motion region was complicated. Therefore, the simulations obtained for 5-DSA in Me₂PE-C32-Me₂PE at 55 and 60 °C are not as good as that obtained for PC-C32-PC, but, as shown in Figure 3.3.20, the established simulation parameters can nevertheless be used as an approximate measure for the relative changes in the environment of the 5-DSA molecules.

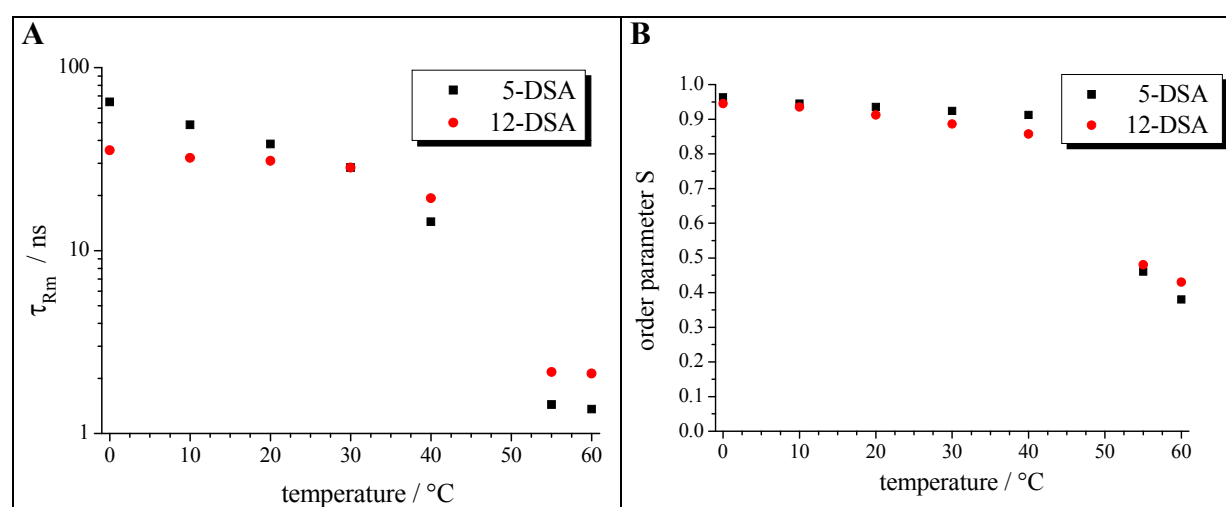


Figure 3.3.20 5-DSA and 12-DSA in 10 mg/ml Me₂PE-C32-Me₂PE at pH 5: (A) Mean rotational correlation time τ_{Rm} and (B) order parameter S versus temperature.

12-DSA in 10 mg/ml Me₂PE-C32-Me₂PE at pH 5

Experimental spectra, obtained for 12-DSA in a sample with 10 mg/ml Me₂PE-C32-Me₂PE in acetate buffer at pH 5, are shown in Figure 3.3.21. The corresponding $2A_{\max}$ values are displayed in Figure 3.3.22.

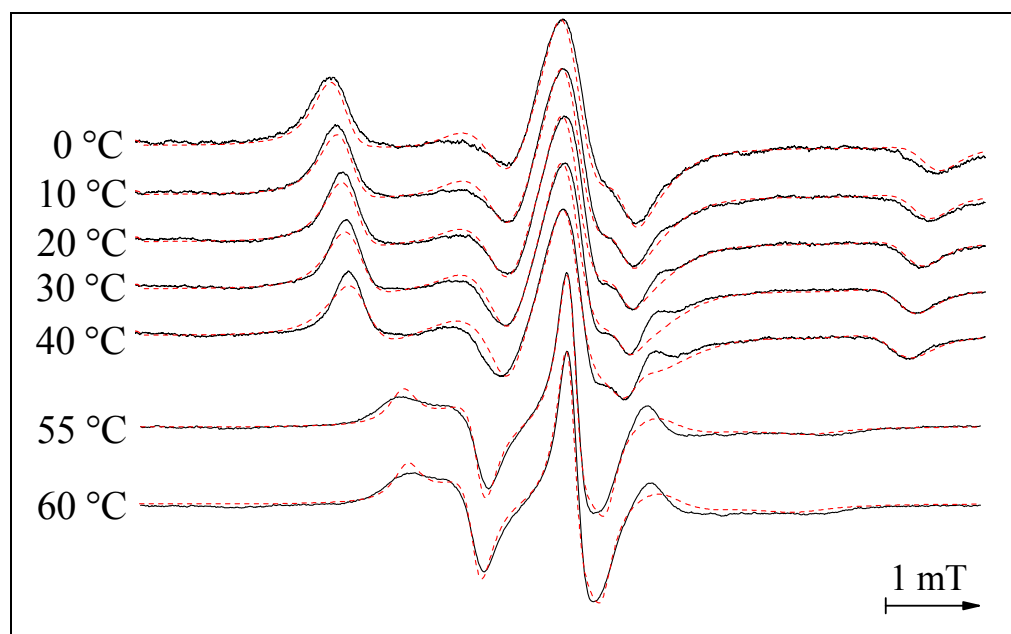


Figure 3.3.21 Experimental (—) and simulated (- - -) ESR spectra of 12-DSA in 10 mg/ml Me₂PE-C32-Me₂PE in acetate buffer pH 5 recorded at different temperatures. All ESR spectra were adjusted to approximately the same peak height of the central peak in order to compare the particular line shapes.

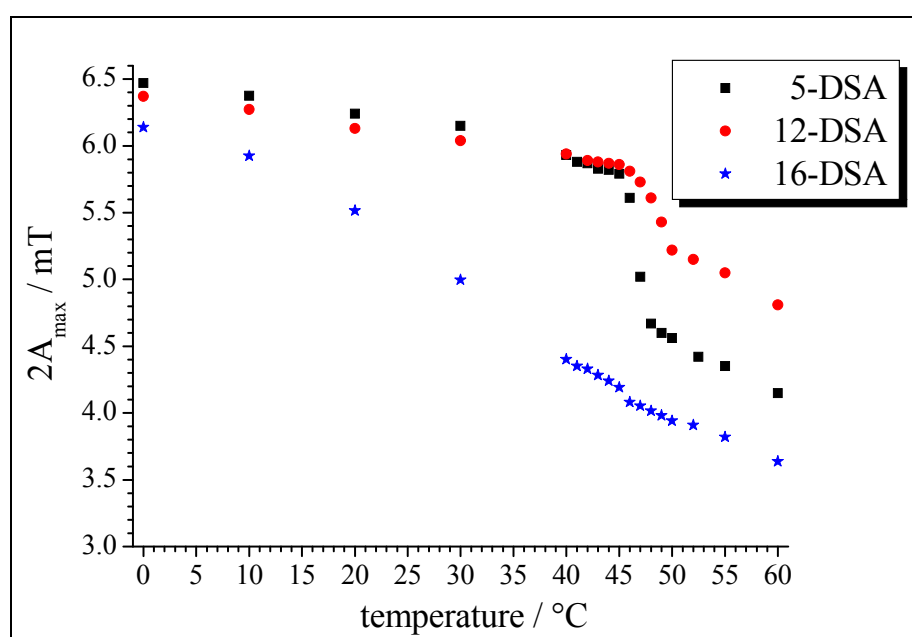


Figure 3.3.22 n-DSA in 10 mg/ml Me₂PE-C32-Me₂PE at pH 5: $2A_{\max}$ versus temperature.

For 10 mg/ml Me₂PE-C32-Me₂PE at pH 5, the doxyl group of 12-DSA can be expected to be situated deeper inside the alkyl chain region of the aggregates than that of 5-DSA, analogous to the situation in PC-C32-PC (Figure 3.3.4). The $2A_{\max}$ values obtained for 12-DSA in 10 mg/ml Me₂PE-C32-Me₂PE at pH 5 at increasing temperatures support this prediction. The most interesting feature of these $2A_{\max}$ values is that the decrease above the first transition temperature is clearly less pronounced and shifted upwards by 2 °C compared to 5-DSA (Table 3.3.2). A shift of the transition temperature with respect to 5-DSA was also observed for 12-DSA in PC-C32-PC (Table 3.3.1). This shift was interpreted in terms of a deeper position of the doxyl group inside the alkyl chain region in the case of 12-DSA. The origin of the delayed response to the changes occurring during the transition was attributed to a preferential trans-gauche isomerization in the outer parts of the aggregates, which extends towards the center of the alkyl chain region with increasing temperature. In addition to the temperature shift, there are clear differences observable in the $2A_{\max}$ values of 12-DSA and 5-DSA in Me₂PE-C32-Me₂PE at pH 5 above the transition temperature. The $2A_{\max}$ values of 12-DSA are clearly less reduced by the transitional changes, which indicates a substantially higher degree of order that is remaining in the environment of the doxyl groups of 12-DSA deep inside the alkyl chain region. This higher degree of order can only be due to more densely packed alkyl chains of the bolaamphiphile molecules. Such dense packing can only be realized, when the trans-gauche ratio remains comparably large. This is supporting the conclusion that trans-gauche isomerization is preferentially starting in the outer part of the alkyl chain region and is only extending towards the center, when the temperature is increased.

Spectral simulation was also performed for spectra of 12-DSA in 10 mg/ml Me₂PE-C32-Me₂PE at pH 5 (Figure 3.3.21, Table S.6 in the Supplement). In analogy to 12-DSA in 10 mg/ml PC-C32-PC, the shape of the central part became increasingly difficult to simulate for the slow motion spectra. Therefore, the simulations are not as good as that obtained for 5-DSA. One could only speculate about the qualitative reason. One possible explanation might be the following: Due to the deeper position of the doxyl group inside the alkyl chain region of the bolaamphiphilic aggregates, a number of these doxyl groups can be expected to reside inside regions of the nanofibers that are exposed to the aqueous medium (see fiber model in Figure 3.3.4). It seems reasonable to assume that some of these doxyl groups are not embedded between the alkyl chains of the bolaamphiphiles, but stick out of the densely packed arrangement. The reorientational motion of such doxyl groups will be much faster compared to the doxyl groups embedded between the bolaamphiphilic alkyl chains. If the number of these molecules is large enough, their contribution will have a visible influence on

the shape the recorded ESR spectra especially on the central region. This might also be an explanation for the fact that at low temperatures, all determined ESR parameters (Figures 3.3.20 and 3.3.22) were found to be slightly smaller for 12-DSA compared to 5-DSA.

16-DSA in 10 mg/ml Me₂PE-C32-Me₂PE at pH 5

Spectra of 16-DSA in 10 mg/ml Me₂PE-C32-Me₂PE at pH 5 are differing substantially from that of 5-DSA and 12-DSA (Figure 3.3.23). These spectra indicate that the reorientational motion of the nitroxyl group of the 16-DSA molecules is considerably faster than that of 5-DSA and 12-DSA. The determined $2A_{\max}$ values are decreasing rapidly with increasing temperature and the transition is detected by only a very small discontinuity (Figure 3.3.22). This allows to conclude that the doxyl group of 16-DSA is not residing deep inside the alkyl chain region, but near the headgroups analogous to the situation described for 16-DSA in 10 mg/ml PC-C32-PC.

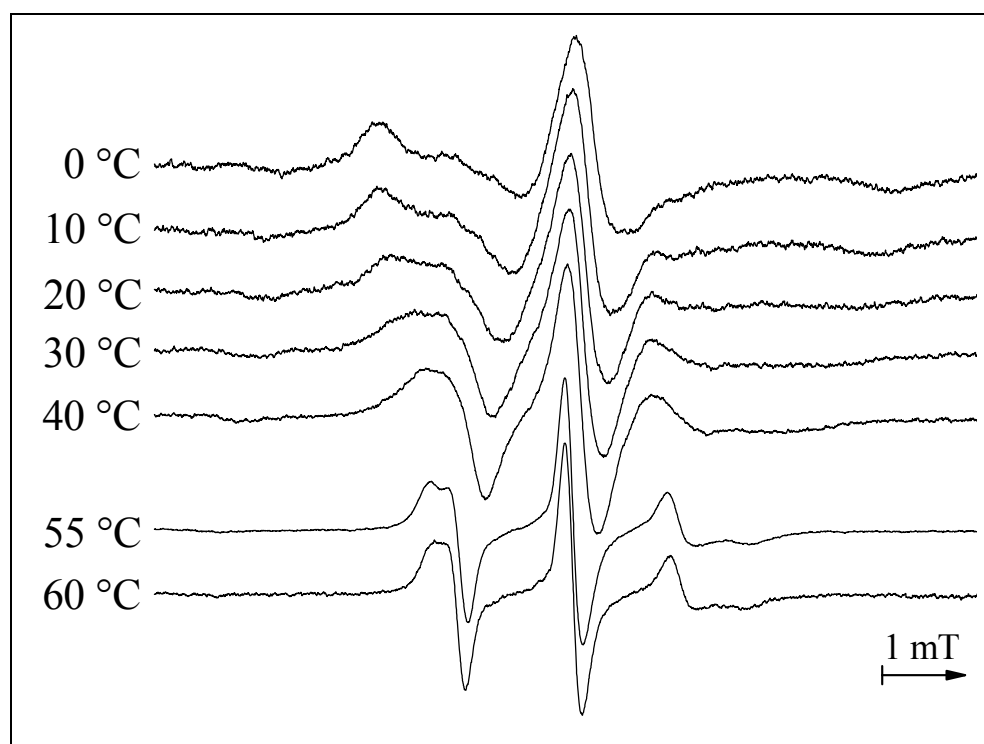


Figure 3.3.23 Experimental ESR spectra of 16-DSA in 10 mg/ml Me₂PE-C32-Me₂PE at pH 5 recorded at different temperatures. All ESR spectra were adjusted to approximately the same peak height of the central peak in order to compare the particular line shapes. No spectral simulations were performed for 16-DSA.

Reduction assay

For Me₂PE-C32-Me₂PE at pH 5, the proposition about the location of the spin probes inside the alkyl chain region is again supported by the data obtained by performing the ascorbic acid assay. The rate of reduction was determined for the particular spin probes to be

$$0.085 \pm 0.014 \text{ min}^{-1} \text{ for 5-DSA}$$

$$0.084 \pm 0.005 \text{ min}^{-1} \text{ for 12-DSA and}$$

$$0.151 \pm 0.009 \text{ min}^{-1} \text{ for 16-DSA.}$$

In analogy to PC-C32-PC, the reduction rate determined for 16-DSA is higher compared to the other spin probes. This gives evidence for the preferential location of the doxyl group of 16-DSA not deep inside the alkyl chain region, but in the outer part of the aggregates near the bolaamphiphilic headgroups.

n-DSA in 1 mg/ml and 10 mg/ml Me₂PE-C32-Me₂PE at pH 10

As described above, increasing the pH value from 5 to 10 leads to negatively charged headgroups and thus changes the aggregation behavior of Me₂PE-C32-Me₂PE due to electrostatic repulsion. Depending on the concentration, the Me₂PE-C32-Me₂PE molecules preferentially self-assemble into rod-like aggregates (10 mg/ml) or micelles (1 mg/ml) as could be shown by SANS measurements.^[18] At these concentrations, hydrogelation is not observed for Me₂PE-C32-Me₂PE at pH 10 and ³¹P-NMR measurements revealed that the headgroups can reorientate much faster compared to pH 5.^[18]

The ESR spectra of 5-DSA, 12-DSA and 16-DSA incorporated into the self-assemblies of Me₂PE-C32-Me₂PE in carbonate buffer at pH 10 give again some insight into the motional dynamics inside the alkyl chain region (Figure 3.3.24).

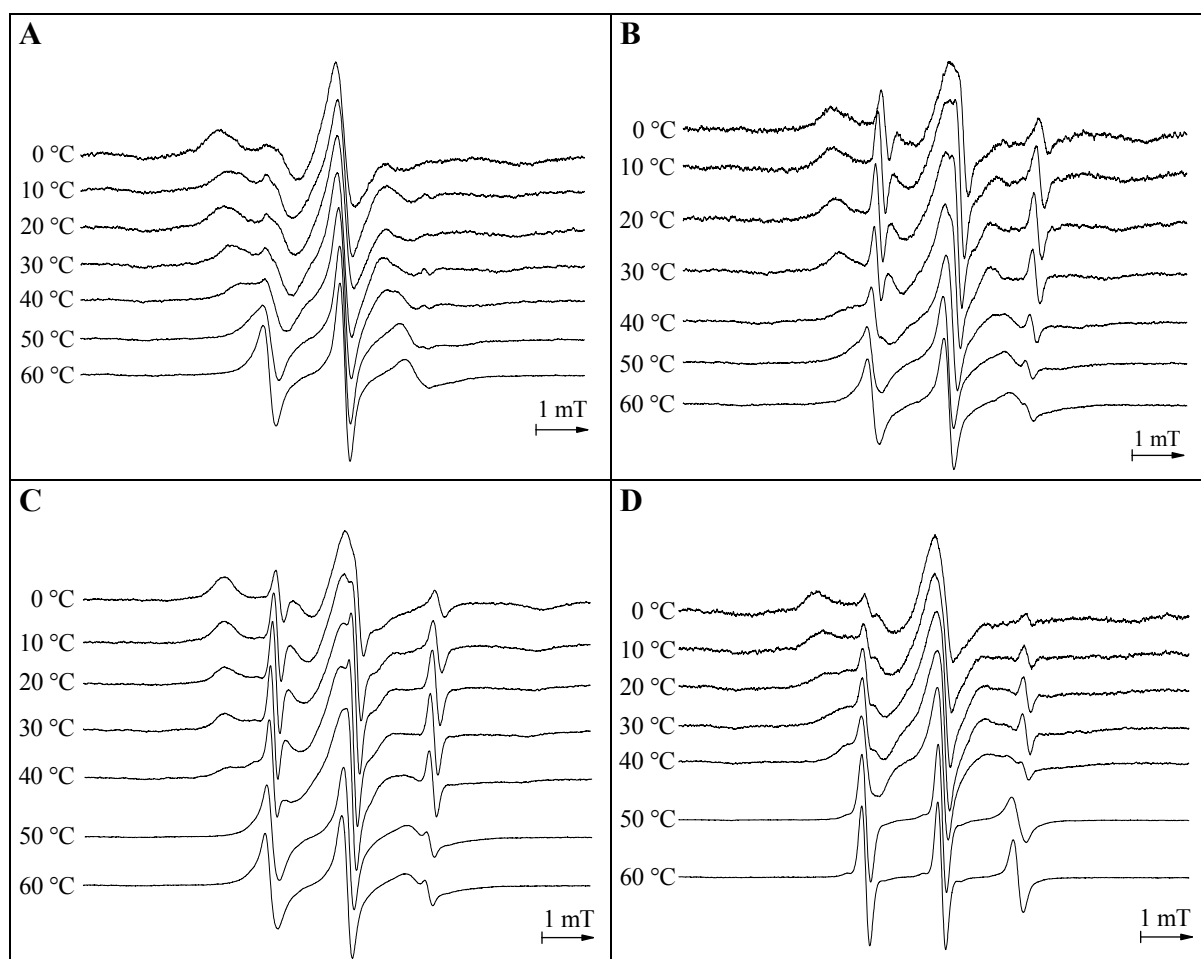


Figure 3.3.24 Experimental ESR spectra of n-DSA in Me₂PE-C32-Me₂PE at pH 10 and temperatures from 0 to 60 °C: (A) 5-DSA in 10 mg/ml Me₂PE-C32-Me₂PE (B) 5-DSA in 1 mg/ml Me₂PE-C32-Me₂PE (C) 12-DSA in 10 mg/ml Me₂PE-C32-Me₂PE (D) 16-DSA in 10 mg/ml Me₂PE-C32-Me₂PE

One interesting feature of all these spectra is the overlap of an anisotropic and an isotropic spectrum. This indicates the existence of two different fractions of spin probe molecules in these samples. One fraction is obviously incorporated into the bolaamphiphilic aggregates and experiences a relatively highly ordered environment, whereas the other fraction of spin probe molecules can rotate almost unrestricted. This mobile fraction can be identified as n-DSA molecules dissolved in the buffer. The existence of this fraction of dissolved n-DSA molecules can be explained by a lower partition coefficient of the negatively charged spin probes into the aggregates formed by Me₂PE-C32-Me₂PE. The alkaline pH value leads to deprotonation of the carboxyl groups of the n-DSA molecules and therefore to the formation of negatively charged spin probes. This negative charge causes electrostatic repulsion between the nitroxides and the headgroups of the bolaamphiphiles, which are also negatively charged at pH 10. Furthermore, the negative charge will increase the water solubility of the

n-DSA molecules in general due to ion-dipole interactions, which do not exist for uncharged n-DSA molecules.

As described above, the aggregation behavior of Me₂PE-C32-Me₂PE becomes concentration dependent at pH 10. Therefore, 5-DSA was not only incorporated into a sample containing 10 mg/ml Me₂PE-C32-Me₂PE, but also into a sample with 1 mg/ml Me₂PE-C32-Me₂PE (Figure 3.3.24B).

Despite the existence of two components in the spectra, the outer extrema of the anisotropic spectra, which correspond to the fraction of n-DSA molecules inside the alkyl chain region, are well-resolved. Therefore, the $2A_{\max}$ values of the anisotropic spectra could be determined for 5-DSA in the whole temperature range. The spectra of 12-DSA and 16-DSA in Me₂PE-C32-Me₂PE at pH 10 indicate that the fraction of the molecules dissolved in the buffer, is considerably larger for these spin probes compared to 5-DSA, which has a longer unperturbed alkyl chain. As a consequence, the $2A_{\max}$ values of 12-DSA and 16-DSA could be exactly determined only up to 30 °C for these two samples (Figure 3.3.25).

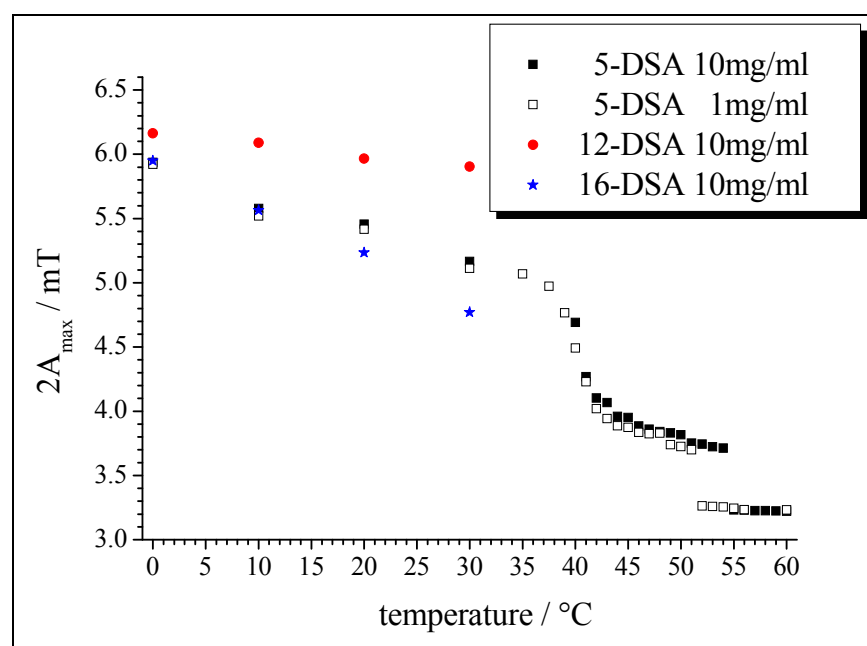


Figure 3.3.25
n-DSA in 10 mg/ml Me₂PE-C32-Me₂PE at pH 10: $2A_{\max}$ versus temperature.

For 5-DSA in 10 mg/ml Me₂PE-C32-Me₂PE at pH 10, significantly lower $2A_{\max}$ values are obtained at compared to pH 5. At 20 °C, for example, the $2A_{\max}$ value is found to be reduced from 6.24 mT to 5.46 mT when the pH is increased from 5 to 10. This decrease in $2A_{\max}$ indicates increased motional freedom of the 5-DSA molecules, which is due to a loss of order inside the alkyl chain region near the headgroups. This decrease of local order is caused by electrostatic repulsion between the negatively charged headgroups, which prevents a dense

packing of the alkyl chains in the region near the headgroups and therefore allows for faster reorientational motion of the nitroxyl groups of the 5-DSA molecules.

The results obtained with 12-DSA indicate that the order farther away from the headgroups is not as strongly affected by the electrostatic repulsion as the region near the headgroups. At 20 °C, the $2A_{\max}$ value obtained for 12-DSA in 10 mg/ml Me₂PE-C32-Me₂PE is only slightly decreased from 6.13 mT at pH 5 to 5.97 mT at pH 10. This small decrease of $2A_{\max}$ indicates that the aggregation behavior of Me₂PE-C32-Me₂PE is not generally changed when the pH value is increased to 10, but the self-assembly is only perturbed by the electrostatic repulsion between the headgroups. Due to the densely packed alkyl chains at pH 5, Me₂PE-C32-Me₂PE can self-assemble into nanofibers that become long enough to form a three-dimensional network with a large number of fiber-fiber cross-links analogous to that of PC-C32-PC. This network of nanofibers is additionally stabilized by the formation of hydrogen bonds between the zwitterionic headgroups. At pH 10, on the other hand, the headgroups of Me₂PE-C32-Me₂PE are not zwitterionic, but negatively charged. These negative charges destabilize the aggregates by introducing a significant perturbation on the organization of the alkyl chains. Due to this perturbation, the alkyl chains are prevented from becoming densely packed, especially in the region near the headgroups. The results obtained with 5-DSA and 12-DSA indicate that this perturbing effect is decreasing with increasing distance of the particular alkyl chain region from the headgroup region. This means that the central part of the alkyl chain region can be expected to remain almost unchanged, whereas its outer parts are strongly affected. The destabilizing effect of electrostatic repulsion obviously prevents the formation of long nanofibers and only shorter rod-like aggregates are obtained for a sample containing 10 mg/ml Me₂PE-C32-Me₂PE at pH 10.

As was shown by SANS,^[18] the size of the aggregates was found to be further decreased, when the concentration of Me₂PE-C32-Me₂PE was decreased from 10 mg/ml to 1 mg/ml Me₂PE-C32-Me₂PE at pH 10. In the temperature range from 0 to 50 °C, however, only very slight differences in the $2A_{\max}$ values are observable for 5-DSA in 1 mg/ml and 10 mg/ml Me₂PE-C32-Me₂PE at pH 10 (Figure 3.3.25). This indicates that the molecular arrangement is almost equal in the aggregates, which are present in these samples. Micelles of 1 mg/ml Me₂PE-C32-Me₂PE at pH 10 are therefore probably very short rods rather than being spherical in shape. One can conclude that increasing the concentration of Me₂PE-C32-Me₂PE from 1 mg/ml to 10 mg/ml at pH 10 is apparently not connected with a distinct change of the organization of the bolaamphiphiles, but mainly causes a one-dimensional growth of the micellar aggregates.

As the ESR data of 12-DSA and 5-DSA show, a similar conclusion may be drawn for the effect of a decrease of the pH value from 10 to 5, which is also accompanied by a significant growth and stabilization of the aggregates. This conclusion is supported by the obvious similarities regarding the temperature dependence of the aggregation behavior of Me₂PE-C32-Me₂PE at pH 5 and at pH 10, since the same transitions are detected at both pH values by DSC. The transition temperatures, however, are significantly decreased for pH 10 with respect to pH 5 due to the destabilizing effect of electrostatic repulsion (Table 1.1).

For 5-DSA in the samples containing 1 mg/ml and 10 mg/ml Me₂PE-C32-Me₂PE at pH 10, each of the two endothermic transitions, that are lying inside the temperature range of the ESR spectrometer, are detected by a discontinuity of the $2A_{\max}$ values. The decrease of $2A_{\max}$ during the first transition is approximately 1 mT for both concentrations, which was also the case for 5-DSA in 10 mg/ml Me₂PE-C32-Me₂PE at pH 5. In agreement with the DSC data, the second transition temperature was found to be concentration dependent and shifted upwards with increasing concentration (Table 3.3.3). Only at 60 °C, well above the second transition temperature, the ESR spectra of 5-DSA in Me₂PE-C32-Me₂PE at pH 10 become almost isotropic. For both concentrations, micellar aggregates are present at this temperature. In these micelles, the order inside the alkyl chain region is substantially decreased due to a fluidization of the bolaamphiphilic chains. This distinct decrease in order allows for almost unrestricted motion of the spin probe molecules, which enables efficient motional averaging. The conformation of the bolaamphiphiles inside such micellar aggregates with low order remains unknown up to now. Due to the hydrophilic headgroups on both ends of the long alkyl chain, bolaamphiphiles cannot easily self-assemble into conventional micelles. The separation of the hydrophilic headgroups and the hydrophobic chains inside an aggregate can be accomplished by either bending the bolaamphiphile molecules into a U-shaped conformation or by leaving the molecules in a more extended conformation with the headgroups located on opposite sides of the aggregates.

Analogous to Me₂PE-C32-Me₂PE at pH 5, the doxyl group of 16-DSA can again be expected to preferentially reside in the headgroup region of the bolaamphiphilic self-assemblies, since a considerably more pronounced decrease of the $2A_{\max}$ values is observed for this spin probe compared to 5-DSA and 12-DSA when the temperature is increased from 0 to 30 °C (Figure 3.3.25).

Table 3.3.3 Transition temperatures of Me₂PE-C32-Me₂PE at pH 10 determined by DSC and with the ESR spin probe technique.

concentration of Me ₂ PE-C32-Me ₂ PE	DSC	ESR 5-DSA
10 mg/ml	42.9 °C	41.5 °C
	55.5 °C	54.5 °C
	75.0 °C	-
1 mg/ml	43.5 °C	41.0 °C
	52.0 °C	51.5 °C
	70.0 °C	-

Reduction assay

When the aqueous medium is changed from acetate buffer at pH 5 to carbonate buffer at pH 10, the reduction rate of the dissolved 5-DSA molecules is found to be decreased from $>1 \text{ min}^{-1}$ to about 0.017 min^{-1} .

A significant decrease of the reduction rates was also observed for the samples containing 10 mg/ml Me₂PE-C32-Me₂PE at pH 10 compared to pH 5:

$$0.0063 \pm 0.001 \text{ min}^{-1} \text{ for 5-DSA}$$

$$0.0061 \pm 0.0012 \text{ min}^{-1} \text{ for 12-DSA}$$

$$0.0134 \pm 0.005 \text{ min}^{-1} \text{ for 16-DSA}$$

Since the deprotonated form of ascorbic acid is involved in the reduction process, this decrease may be ascribed to electrostatic repulsion between the ascorbate anion and the spin probes and bolaamphiphiles, which are also negatively charged. On the other hand, a considerable number of spin probe molecules are not incorporated inside the aggregates of Me₂PE-C32-Me₂PE, but are dissolved in the carbonate buffer, where they are not protected from ascorbic acid. Therefore, the decrease of the reduction rate is found to be less pronounced for the bolaamphiphile samples compared to the decrease observed between the reduction rates of 5-DSA in pure acetate buffer pH 5 and in pure carbonate buffer pH 10.

The reduction rate, determined for 16-DSA in 10 mg/ml Me₂PE-C32-Me₂PE at pH 10, is again significantly larger than that of 5-DSA and 12-DSA. Therefore, the doxyl groups of the 16-DSA molecules can be expected to reside near the bolaamphiphilic headgroups analogous to the situation described for PC-C32-PC and Me₂PE-C32-Me₂PE at pH 5.

3.4 Bolaamphiphiles with a diacetylene group

3.4.1 General remarks

As described above, hydrogelation is observed for PC-C32-PC and Me₂PE-C32-Me₂PE even at low concentrations due to their self-assembly into an extended network of well-defined nanofibers. For PC-C32-PC, this self-assembly into nanofibers and also the fiber-fiber cross-linking is solely due to hydrophobic interactions. For Me₂PE-C32-Me₂PE at pH 5, the formation of hydrogen bonds is also contributing to some extent. As a result, the thermal stability of the formed nanofibers is increased for Me₂PE-C32-Me₂PE compared to PC-C32-PC and the hydrogel state persists even above 60 °C.

Regarding their consistency, the hydrogels formed by PC-C32-PC or Me₂PE-C32-Me₂PE at concentrations between 1 and 30 mg/ml are rather "weak" gels, because they can be temporarily destroyed by vigorous shaking for only a short moment. This indicates that the nanofibers and the connections between them are relatively fragile. Therefore, an attempt to chemically cross-link the bolaamphiphiles was made so as to transform the physical network into a chemical one. The idea behind this approach was the combination of the advantages of the well-defined and controllable self-assembly with that of a stable polymeric network.

In principle, polymerizable groups could be introduced either into the headgroups or into the long alkyl chains of the bolaamphiphile molecules. In order to spare the headgroups for further functionalization, it was chosen to modify the alkyl chains by the introduction of two adjacent triple bonds at the center. The synthetic work was again done in the group of Prof. B. Dobner by Dipl. Pharm. K. Piksa and Dr. S. Drescher and lead to the diacetylene bolaamphiphiles PC-C32diAc-PC and Me₂PE-C32diAc-Me₂PE.^[22,33,34] The chemical structures are shown in Figure 3.4.1.

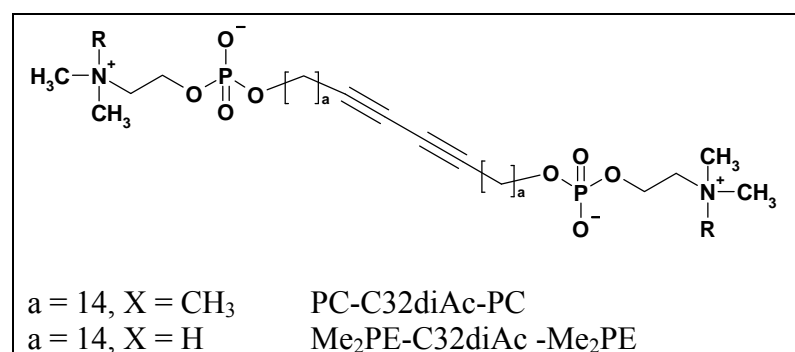


Figure 3.4.1

Chemical structure of the synthesized diacetylene bolaamphiphiles.

3.4.2 PC-C32diAc-PC

3.4.2.1 Properties

In contrast to PC-C32-PC, the synthesized PC-C32diAc-PC was of very low density and found to be hygroscopic. Differences between PC-C32-PC and PC-C32diAc-PC were also observed for their corresponding aqueous samples. For PC-C32diAc-PC, no elevated temperatures were needed to obtain a homogeneous dispersion immediately after addition of deionized water. All dispersions, that were prepared for concentrations of PC-C32diAc-PC ranging from 1 to 30 mg/ml according to the procedure described in Section 2.2.4, were found to be of low viscosity. Hydrogelation was not observed for any of these samples even after storage for 24 hours between 2 and 8 °C.

These findings point to a drastically changed aggregation behavior of PC-C32diAc-PC compared to PC-C32-PC. This is not completely unexpected, since the self-assembly of the PC-C32-PC molecules into nanofibers is mainly due to hydrophobic interactions between the long alkyl chains, which are predominantly in an all-trans conformation. These alkyl chains were modified in PC-C32diAc-PC by the replacement of four CH₂ groups by a diacetylene group. This introduces some degree of rigidity into the center of the alkyl chains and prevents a dense chain packing in this region. As a consequence, no long nanofibers are formed, but smaller micellar aggregates as could be shown by TEM (Figure 3.4.2A). This is also reflected in the DSC thermogram obtained for a sample with 10 mg/ml PC-C32diAc-PC in deionized water (Figure 3.4.2B), which shows only one endothermic transition at approximately 6 °C.

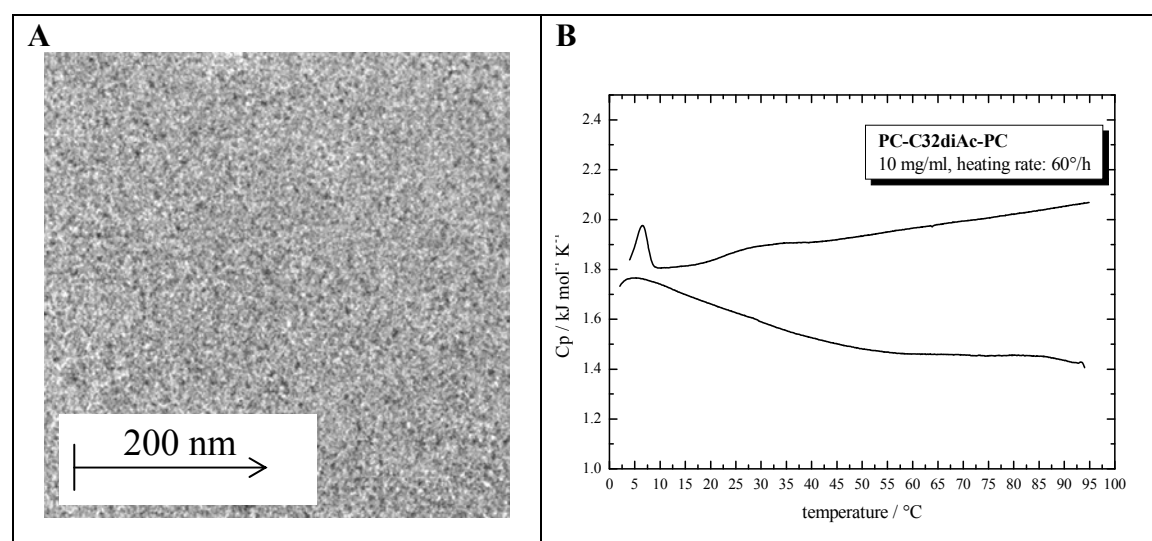


Figure 3.4.2 (A) TEM image of 0.3 mg/ml PC-C32diAc-PC in deionized water. (B) DSC thermogram of 10 mg/ml PC-C32diAc-PC in deionized water.

3.4.2.2 UV-polymerization

The polymerization experiments with aqueous dispersions of PC-C32diAc-PC were carried out inside a quartz cuvette (path length 10 mm) at about 0 °C well below the detected transition temperature of 6 °C.

The principle construction of the UV-polymerization chamber is outlined in Figure 3.4.3. It consists of a polystyrene box, which was filled with some dry ice for cooling. For the UV-polymerization, a low-pressure Hg-lamp (254 nm, 15 W) was placed at a distance of about 3 cm from the bolaamphiphile dispersion. During the UV-polymerization, this dispersion was cautiously stirred.

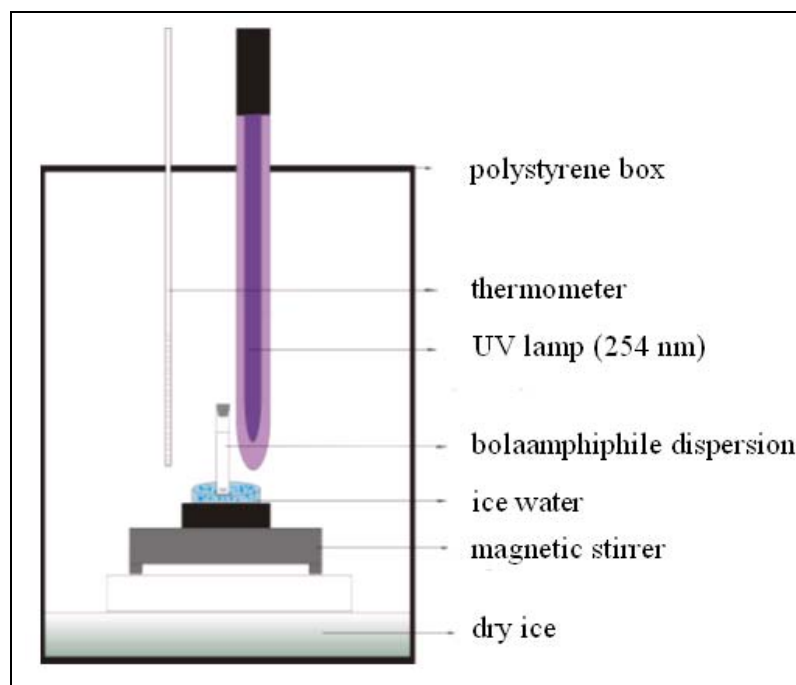


Figure 3.4.3
Schematic representation of the UV-polymerization chamber.

UV-polymerization of 5 mg/ml or 10 mg/ml PC-C32diAc-PC at 0 °C was found to lead to a blue coloration of the sample already after about 5 minutes. The polymerization process was interrupted after selected exposure times in order to record the UV-VIS spectra corresponding to the different UV-exposure times (Figure 3.4.4). These spectra reflect well the progress of the polymerization. The obtained absorption curves show a maximum at approximately 640 nm and an additional small peak at approximately 590 nm. Similar UV-VIS spectra were obtained before for various polymerized diacetylenes as the typical spectra of the blue phase of these PDAs.^[54,57,122]

UV-polymerization was stopped after an exposure time of 90 minutes, which yielded an intensive blue dispersion of polymerized PC-C32diAc-PC (pPC-C32diAc-PC, Figure 3.4.4).

Besides pPC-C32diAc-PC, this dispersion can be expected to contain a significant amount of unpolymerized PC-C32diAc-PC, since complete conversion of diacetylenes is usually not observed.^[54]

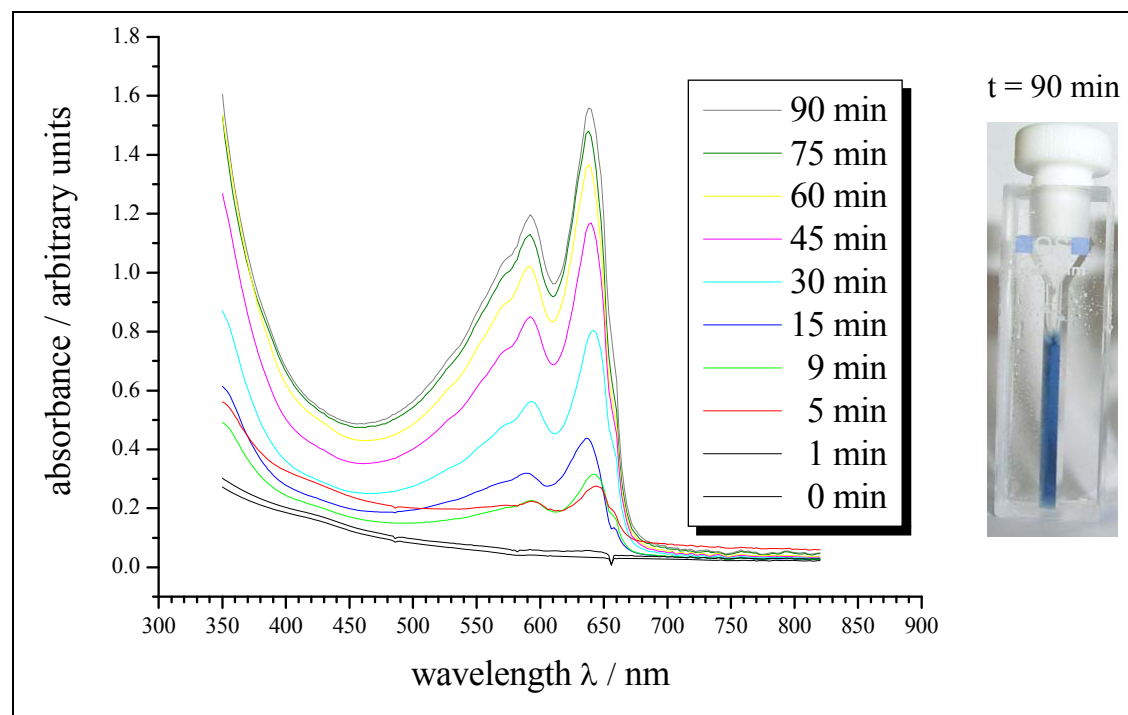


Figure 3.4.4 UV-polymerization of 10 mg/ml PC-C32diAc-PC in deionized water at 0 °C: **(left)** UV-VIS spectra at different exposure times. **(right)** Photograph of the blue dispersion after 90 min exposure to UV-irradiation.

From a diluted blue dispersion of polymerized PC-C32diAc-PC, cryo-TEM images were obtained, which show regions with a relatively high degree of order (Figure 3.4.5). In these regions, the linear π -conjugated polymer backbones of pPC-C32diAc-PC (Section 2.2.4) seem to be aligned parallel to each other. Such parallel ordering of the polymer chains is usually observed for PDA crystals.^[54]

The existence of these relatively long linear π -conjugated polymer backbones indicates that the formation of the enyne-conjugations is not only occurring inside the relatively small micelles observed by TEM, but also involves a one-dimensional growth of the resulting polymers.

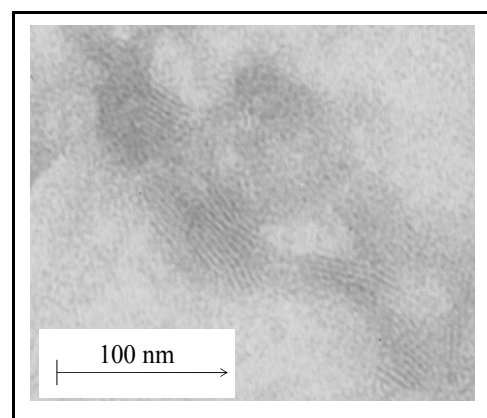


Figure 3.4.5 cryo-TEM image of a blue dispersion of pPC-C32diAc-PC.

The polymerization experiment described above, was also performed at room temperature well above the transition temperature of 6 °C. The UV-VIS spectra recorded at different UV-exposure times resemble that obtained for the UV-polymerization attempt at 0 °C. No clear differences could be observed between the obtained dispersions of polymerized PC-C32diAc-PC for both polymerization temperatures after 90 minutes of irradiation.

A third UV-polymerization attempt was made with PC-C32diAc-PC in the solid state. For this purpose, 5 mg of solid PC-C32diAc-PC were spread on a glass plate and polymerized in the reaction chamber for 90 minutes without any cooling. The originally white color of the solid PC-C32diAc-PC started to change after about 10 minutes exposure time to the UV-radiation and was found to be grayish blue after 90 minutes. When 1 ml of deionized water were added, elevated temperatures of about 60 °C were needed to achieve a homogeneous dispersion of 5 mg/ml pPC-C32diAc-PC. Due to the temperature treatment, the resulting color of the aqueous sample was not blue, but red. As will be shown below, this is due to an irreversible transition of the polymerized PC-C32diAc-PC from its blue phase to its red phase. As a consequence, the position of the corresponding absorption maximum in the UV-VIS spectrum (Figure 3.4.6) differs from that obtained for the polymerized aqueous dispersion. In addition, the absorbance is found to be significantly decreased, which points to a lower polymerization degree that is obtained for the UV-polymerization of PC-C32diAc-PC in the solid form. This might be explained by the relatively low penetration depth of the UV-radiation. In order to achieve quantitative polymerization for solid PC-C32diAc-PC, it would be necessary to use penetrating ionizing radiation like ^{60}Co - γ -ray.^[59]

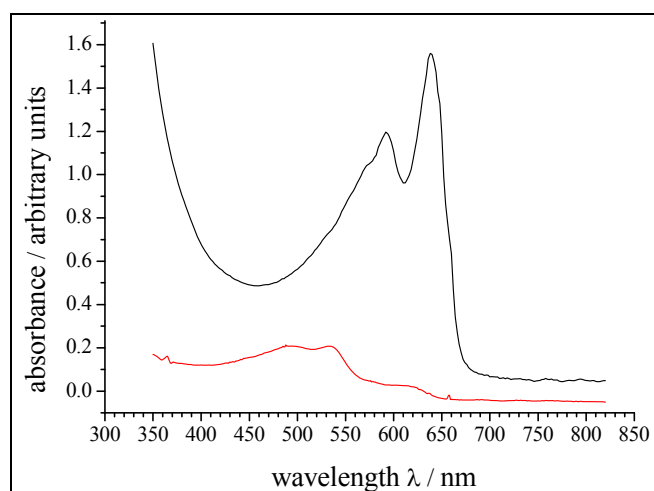


Figure 3.4.6
UV-VIS spectra of 5 mg/ml polymerized PC-C32diAc-PC in deionized water obtained after 90 minutes exposure time to UV-irradiation of the aqueous dispersion of PC-C32diAc-PC (—) and of the solid PC-C32diAc-PC (—).

3.4.2.3 Characterization of the polymerized PC-C32diAc-PC

Temperature dependence

The samples used for investigating the temperature dependence of pPC-C32diAc-PC were obtained by UV-polymerization of aqueous dispersions of 5 mg/ml PC-C32diAc-PC at room temperature.

When dispersions of pPC-C32diAc-PC were heated and cooled in preliminary tests, the sample color was always found to be changed. These thermochromic transitions of pPC-C32diAc-PC were studied in more detail. For this purpose, the temperature of the samples was increased from 0 to 90 °C at increments of 10 °C by the heating unit of the UV-spectrometer. The resulting UV-VIS spectra are shown in Figure 3.4.7 together with the corresponding photographs of the samples, which were taken at each temperature directly after recording the spectrum and prior to the cooling to 0 °C.

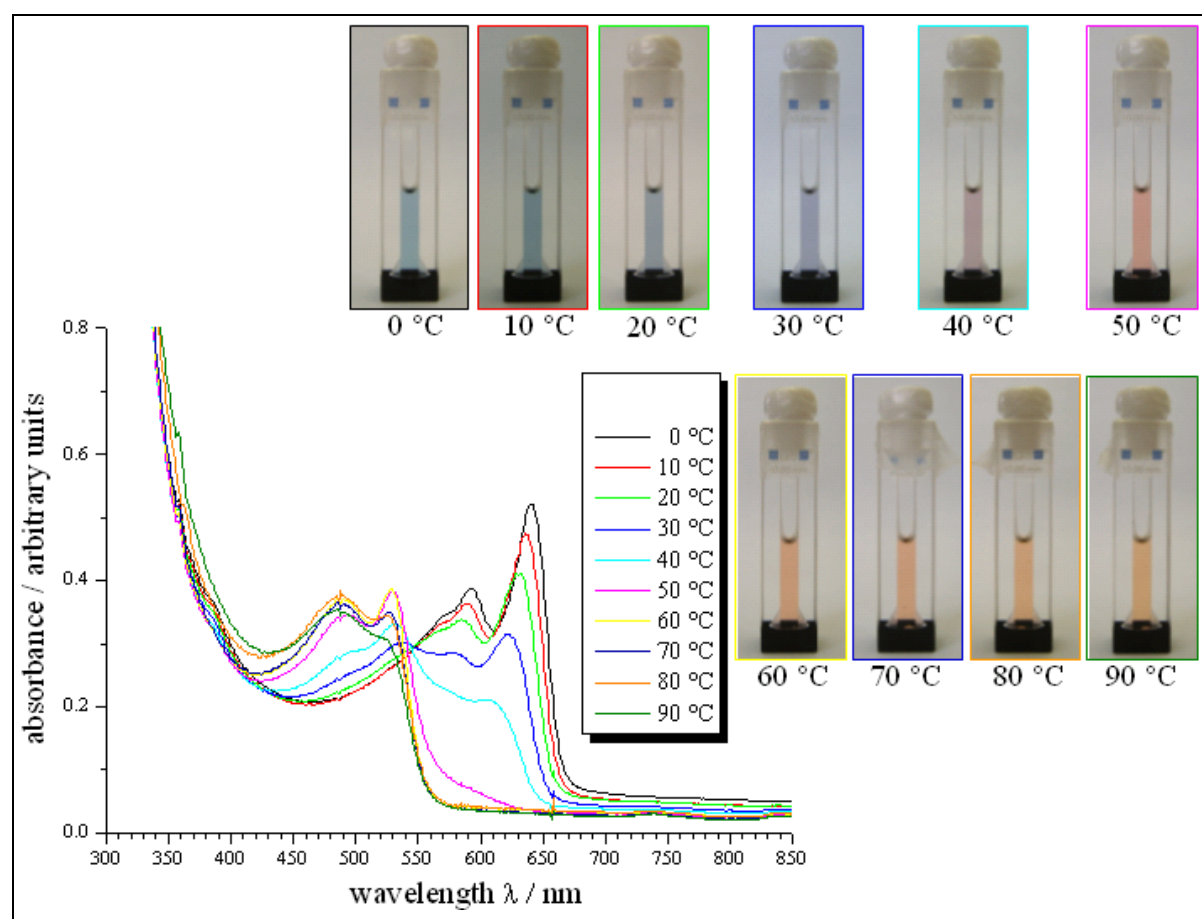


Figure 3.4.7 Temperature dependent UV-VIS spectra obtained for 5 mg/ml pPC-C32diAc-PC in deionized water together with the corresponding photographs of the samples.

At **0 °C**, the UV-VIS spectrum obtained for a dispersion of 5 mg/ml pPC-C32diAc-PC shows a main absorption peak at 641 nm and an additional smaller peak at 592 nm. This corresponds to an absorption of the red and orange components of the electromagnetic spectrum and the sample appears to be of blue color. pPC-C32diAc-PC is denoted to be in the blue phase at this temperature. When the temperature is increased to **10 °C**, the blue color of the sample seems to be unchanged. Compared to 0 °C, the peak absorptions are decreased to some extent and the peak positions are slightly shifted to lower wavelengths (636 nm, 588 nm).

At **20 °C**, the peak positions are further shifted (632 nm, 585 nm) and the peak absorptions are again decreased. This decrease is more pronounced for the main peak. As a consequence, the color of the dispersion still appears to be blue, but contains a small proportion of purple.

At **30 °C**, the absorption spectrum is considerably changed and includes an additional peak at 538 nm, which corresponds to absorption of the green component of the electromagnetic spectrum. As a result, the sample color is purple. The obtained photograph, which is shown in Figure 3.4.7, is not completely reflecting this purple color. This is due to the fact that the cuvette had to be removed from the spectrometer and the photograph was taken only after about 60 seconds at room temperature. Within this time span, the color was visibly changing due to the decreased temperature and the originally purple color became more blueish again. This indicates that the thermochromic transition is reversible to some extent. The experiment performed for testing the reversibility of the thermochromic transitions is described below.

The purple color of the sample was turning to red with a proportion of blue, when the temperature was increased from 30 to **40 °C**. At this temperature, the absorption peak at 532 nm is clearly the main peak, whereas only a small peak shoulder is left from the peaks at higher wavelengths. Besides the main peak at 530 nm, a second peak at about 493 nm is found to appear at this temperature. This second peak corresponds to absorption of the blue component of the electromagnetic spectrum. At 40 °C, the color of the sample was found to be intensively red. In the temperature range from **60 to 90 °C**, the absorption peak at about 490 nm becomes the main peak, whereas the absorption at 530 nm is considerably decreased. As a result, the sample color is found to be changed to orange-red with a decreasing proportion of red when the temperature was increased.

One can conclude that the transition from the blue to the red phase could be shown for pPC-C32diAc-PC to occur between 20 and 50 °C. As described in Section 2.2.4, this blue-to-red transition is one of the most striking features observed for polydiacetylenes. Besides heat, various other stimuli were found to induce this transition for certain PDAs. Therefore, PDAs have attracted attention for application in sensor devices.^[69,70]

The underlying mechanism behind the observed chromatic transitions of the PDAs is not fully understood yet. The experimental and theoretical data regarding the transitions of various polydiacetyenes were reviewed and discussed by Carpick et al.^[66] and by Schott.^[60] The decisive factor for all the observed chromatic transitions can be seen in the influence of the side groups on the conformation of the polymer backbone. PDA solutions in good solvents are yellow (λ_{max} near 470 nm).^[60] Relevant aggregation of the side groups can be excluded in these solutions. Only when the solvent quality is decreased, for example by decreasing the temperature or by adding a non-solvent, the color of the samples turns from yellow to red or blue. This is due to dispersed red or blue PDA aggregates with optical properties quite similar to those of solid phases of the same color.^[60] The side-groups are determining this aggregation behavior and therefore also the resulting color of the aggregates.

In unpolymerized PC-C32diAc-PC, hydrophobic interaction between the long alkyl chains dominates the self-assembly. Since polymerization of diacetylenes proceeds in a lattice controlled reaction, the extended backbones will form in a strained configuration due to geometrical constraints resulting from the side-chain packing. The application of heat leads to side-chain fluctuations and reconfigurations, which allow the backbone to adopt a more relaxed conformation. This relaxation process involves rotation about the C-C backbone bonds, and thus leads to changes in the optical absorption spectrum.^[66] The release of mechanical strain in the backbone due to the transition from the blue to the red phase could be shown experimentally by Lee et al.^[64] for PDAs with urethane substituted side-groups.

PDA chains in the blue phase are known to be planar with an enyne-type of alternation of C-C bond lengths.^[60] The red chain is known to have the same enyne type bond lengths and the same repeat unit length.^[123] The red phase may therefore consist of a non-planar backbone configuration in conjunction with rotated and/or distorted alkyl side-chains.^[66] This could be realized by rotation about one of the C-C bonds of the polymer backbone, which would dramatically change the π -overlap^[66,124] and therefore results in a significant blue-shift of the absorption maximum.

Due to the participation of the side-chains, the blue-to-red transition is a not only a conformation change of the pPC-C32diAc-PC backbone, but a phase change of the system as a whole.

Besides the absorption maxima that correspond to the blue and the red phase, two additional absorption peaks are observed in Figure 3.4.7, namely at wavelengths of approximately 590 nm (0 to 30 °C) and 485 nm (50 to 90 °C). Polymer chains that show absorption at about 590 nm may be denoted as the purple phase of pPC-C32diAc-PC. This absorption feature was

observed before for other PDA samples. Carpick et al. proposed that the purple form is a thermally distorted configuration of the blue form and that the purple form may represent a transition state in the conversion to the red form.^[66]

The appearance of the absorption peak at 485 nm indicates that increasing the temperature weakens the interaction between the alkyl chains. As described above, solutions of PDAs in good solvents are yellow and show an absorption maximum at about 470 nm. The increasing absorption at about 485 nm in the obtained UV-VIS spectra at temperatures above 40 °C may therefore be attributed to partially dissolved pPC-C32diAc-PC chains.

Reversibility of the chromatic transitions

As described above, the chromatic transitions were found to be reversible to some extent. In order to study the reversibility of the absorption behavior, a sample containing 5 mg/ml pPC-C32diAc-PC in deionized water was examined in the temperature range from 10 to 70 °C (Figure 3.4.8).

Initially, a spectrum was recorded at 10 °C and used as the reference spectrum for the blue phase. At increments of 10 °C, the temperature was then increased and two UV-VIS spectra were obtained for each temperature, the first one after heating from 10 °C to the particular temperature and the second one after subsequent quenching back to 10 °C. Prior to each measurement, the sample temperature was allowed to equilibrate for at least 10 minutes.

The UV-VIS spectra, obtained from these heating-quenching cycles (10 °C → T → 10 °C), reveal that the reversibility is significantly reduced with increasing temperature. After quenching from 20 °C, the absorption spectrum is found to be almost quantitatively recovered, whereas quenching from 30 °C already leads to distinct changes of the absorption spectrum compared to the reference spectrum. The sample color, however, appeared to be almost recovered from purple to blue for this heating-quenching cycle. A distinct decrease of the reversibility is obtained for the heating-quenching cycle 10 °C → 40 °C → 10 °C. A color transition from blue to red was observed upon heating, whereas the dispersion exhibited a purple color after quenching from 40 to 10 °C.

At 50 °C, reversibility of the peaks at longer wavelenghts is further decreased before they completely disappear in the spectra obtained after quenching from 60 and 70 °C. For these heating-quenching cycles, the changes in the absorption spectra were found to be almost irreversible.

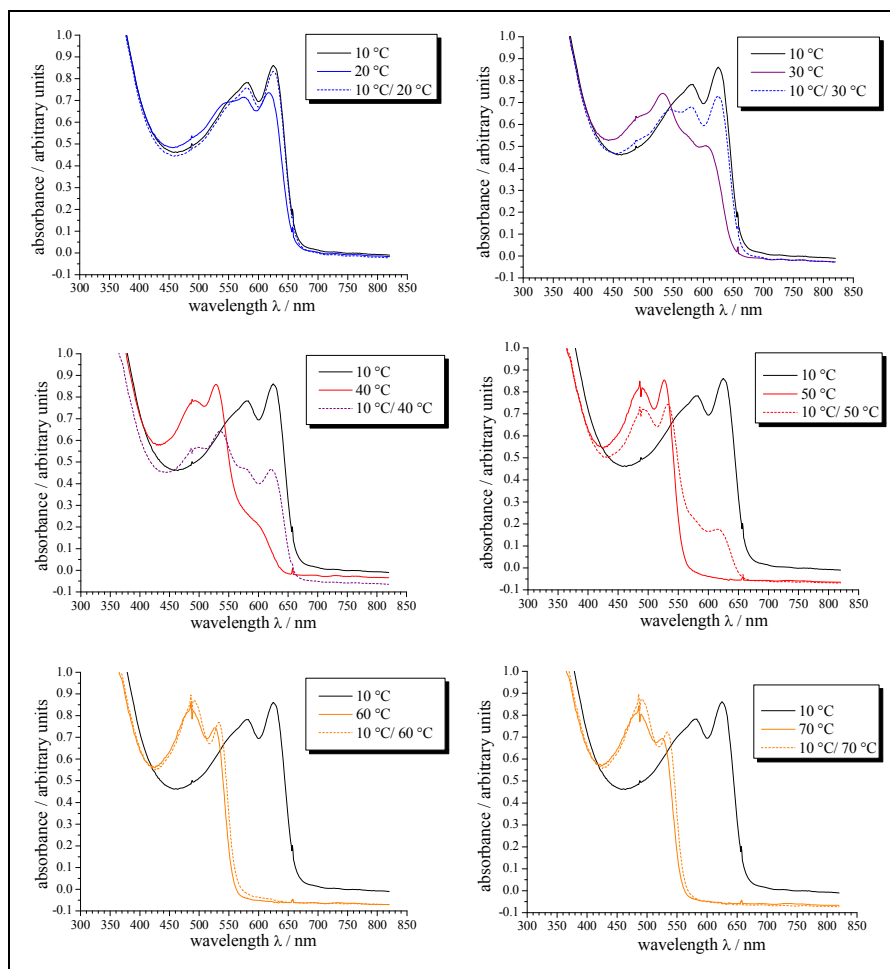


Figure 3.4.8 Reversibility test of the chromatic transitions: UV-VIS spectra of 5 mg/ml pPC-C32diAc-PC in deionized water at temperatures ranging from 10 to 70 °C (—) and quenched from each temperature to 10 °C (-----).

One can conclude that for pPC-C32diAc-PC, the transition from the blue to the purple phase was found to be partially reversible, whereas the transition to the red phase seems to be an irreversible process. The observed irreversibility of the transitions is due to the involvement of the alkyl chains, which have to undergo severe reorganizations in order to allow the backbone to adopt another conformation. Reversibility of the transition from the blue to the purple phase and irreversibility of the transition to the red phase was also reported for PDAs in Langmuir films.^[66]

3.4.3 Me₂PE-C32diAc-Me₂PE

3.4.3.1 Properties

Besides PC-C32diAc-PC, its dimethyl derivative Me₂PE-C32diAc-Me₂PE (Figure 3.4.1) was also synthesized.

In analogy to PC-C32diAc-PC, substitution of four CH₂ groups by a diacetylene group results in distinct changes of the aggregation behavior of Me₂PE-C32diAc-Me₂PE compared to Me₂PE-C32-Me₂PE. No hydrogelation is observed at concentrations up to 10 mg/ml Me₂PE-C32diAc-Me₂PE in acetate buffer pH 5, even when the samples were stored for 24 hours between 2 and 8 °C. In analogy to PC-C32diAc-PC, the TEM image of a sample with 0.3 mg/ml Me₂PE-C32diAc-Me₂PE at pH 5 only shows micelles (Figure 3.4.9A). An endothermic transition is also found in the DSC thermogram obtained for a sample with 5 mg/ml Me₂PE-C32diAc-Me₂PE at pH 5 (Figure 3.4.9B). The observed increase of the transition temperature compared to PC-C32diAc-PC can be attributed to the stabilizing effect of hydrogen bonds, which are formed between the headgroups of Me₂PE-C32diAc-Me₂PE at pH 5. In addition to the main peak, a pre-transition at 12.5 °C is observed.

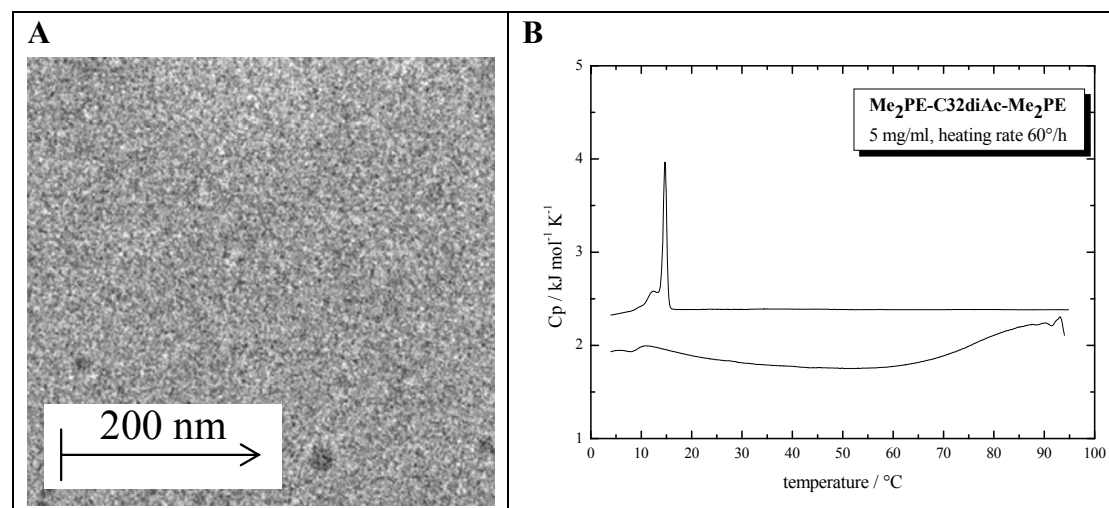


Figure 3.4.9 (A) TEM image of 0.3 mg/ml Me₂PE-C32diAc-Me₂PE in acetate buffer pH 5. (B) DSC thermogram of a sample with 5 mg/ml Me₂PE-C32diAc-Me₂PE in acetate buffer pH 5.

3.4.3.2 UV-polymerization

The UV-polymerization attempts for Me₂PE-C32diAc-Me₂PE were made according to the procedures described for PC-C32diAc-PC. However, blue or red coloration was observed neither for the aqueous dispersions nor in the solid state. Instead, all these samples turned yellow upon UV-radiation. By UV-irradiation of a cooled dispersion of 5 mg/ml Me₂PE-C32diAc-Me₂PE at pH 5 and a temperature of approximately 0 °C, an intensively yellow sample is obtained, which is shown in Figure 3.4.10A together with the corresponding UV-VIS spectrum. For the UV-polymerization at room temperature, well above the transition temperature, only a slightly yellowish dispersion is obtained (Figure 3.4.10B).

As described above, PDAs dissolved in good solvents are known to also exhibit a yellow color. However, unlike PC-C32diAc-PC, the polymerization attempt with solid Me₂PE-C32diAc-Me₂PE at pH 5 also leads only to a faintly yellow coloration of the crystals. The absence of blue or red coloration may therefore be attributed rather to incomplete polymerization of Me₂PE-C32diAc-Me₂PE. As described above, the crucial factor for the photoreactivity of diacetylenes is the mean distance between adjacent diacetylene groups, which should be about 4.9 Å. In contrast to PC-C32diAc-PC, it seems likely to assume that this mean distance inside the formed crystals or self-assemblies is unfavorable for the polymerization process in the case of Me₂PE-C32diAc-Me₂PE. The formation of hydrogen bonds between the headgroups of Me₂PE-C32diAc-Me₂PE can be expected to be the decisive factor for the exact arrangement of the bolaamphiphiles and therefore for the deviation of the mean distance between the diacetylene groups from the optimal value of 4.9 Å. As a consequence, the initialized polymerization process cannot proceed and is ceased at considerably shorter conjugation lengths compared to PC-C32diAc-PC. This means that, unlike PC-C32diAc-PC, UV-polymerization of Me₂PE-C32diAc-Me₂PE molecules does not lead to polydiacetylenes with conjugated polymer backbones that are long enough to exhibit blue or red color.

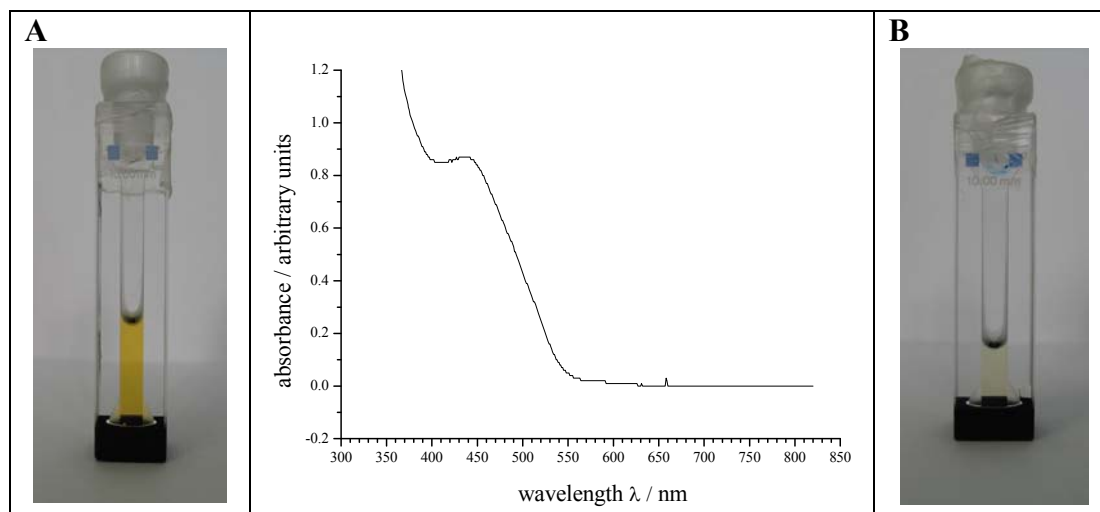


Figure 3.4.10 Results of the polymerization attempts with 5 mg/ml Me₂PE-C32diAc-Me₂PE at pH 5: (A) Photograph and absorption spectrum after polymerization at 0 °C. (B) Photograph after polymerization at room temperature.

The bolaamphiphiles PC-C32diAc-PC and Me₂PE-C32diAc-Me₂PE were synthesized by introducing a diacetylene group into the center of the alkyl chain of PC-C32-PC and Me₂PE-C32-Me₂PE, respectively. One can conclude that the aggregation behavior of these diacetylene bolaamphiphiles was found to be completely changed compared to PC-C32-PC and Me₂PE-C32-Me₂PE, since their self-assembly does not lead to nanofibers, but only to micellar aggregates. As a consequence, hydrogelation is observed for PC-C32diAc-PC or Me₂PE-C32diAc-Me₂PE neither in their aqueous dispersions nor after the UV-polymerization experiments. Therefore, the approach to transform the self-assembled bolaamphiphilic network into a three-dimensional chemical network of polydiacetylenes was not successful. Nevertheless, the UV-polymerization attempts performed with PC-C32diAc-PC and Me₂PE-C32diAc-Me₂PE revealed interesting findings. Whereas the samples of Me₂PE-C32diAc-Me₂PE appeared to be yellow after exposure to UV-radiation for 90 minutes, the samples with PC-C32diAc-PC exhibited an intensive blue coloration. By increasing the temperature, a partially reversible chromatic transition from the blue to the purple phase and an irreversible transition to the red phase of pPC-C32diAc-PC could be induced.

3.5 Biological tests

Additional to the physico-chemical characterization of the bolaamphiphiles, two pilot studies were performed in order to obtain preliminary data about the biological activity of this class of bolaphospholipids. One of these studies was concerned with the potential cytotoxic effects of PC-C32-PC and Me₂PE-C32-Me₂PE, whereas the antifungal activity was tested for 12 single-chain bolaamphiphiles in the second pilot study.

3.5.1 MTT-assay

3.5.1.1 General remarks

The alkylphosphocholine miltefosine (hexadecylphosphocholine, Figure 3.5.1) is a drug, which is applied against leishmania infections (Impavido[®]) and against skin metastases in breast cancer patients (Miltex[®]). The mechanisms that are responsible for the observed cytotoxic effect of miltefosine are not fully understood, but it is known that miltefosine has a high affinity to the cell membranes and interferes in the synthesis of membrane phospholipids. Other alkylphosphocholines like edelfosine, perifosine and erufosine were also found to show cytotoxic effects.^[125]

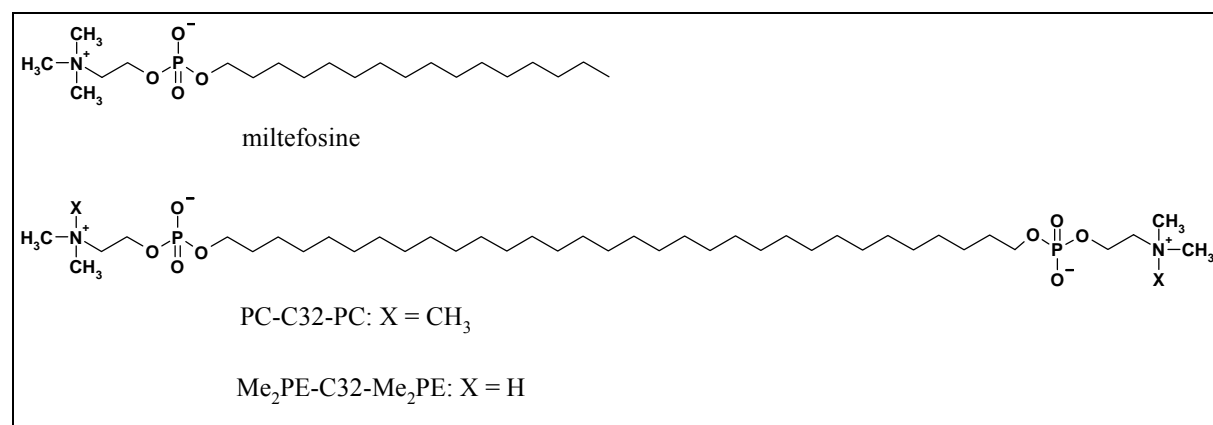


Figure 3.5.1 Chemical structure of miltefosine. For comparison, the chemical structures of PC-C32-PC and Me₂PE-C32-Me₂PE are also shown.

Due to the structural relationship between miltefosine and the investigated bolaamphiphiles (Figure 3.5.1), cytotoxic effects on certain cells may also be present for PC-C32-PC or Me₂PE-C32-Me₂PE. Since potential biomedical applications of the hydrogels of PC-C32-PC or Me₂PE-C32-Me₂PE presuppose their biological compatibility, such effects would rule out

the use of the bolaamphiphiles in these fields. On the other hand, one of the bolaamphiphiles of the PC-Cn-PC or of the Me₂PE-Cn-Me₂PE family might also be a potential drug candidate.

3.5.1.2 Obtained results

In order to attain first data about the cytotoxicity of PC-C32-PC and Me₂PE-C32-Me₂PE, the MTT-assay was carried out on human lung carcinoma cells (A549 cells) according to the procedures described in Section 2.2.5. This was done in coThe obtained results of these preliminary experiments are shown in Figure 3.5.2.

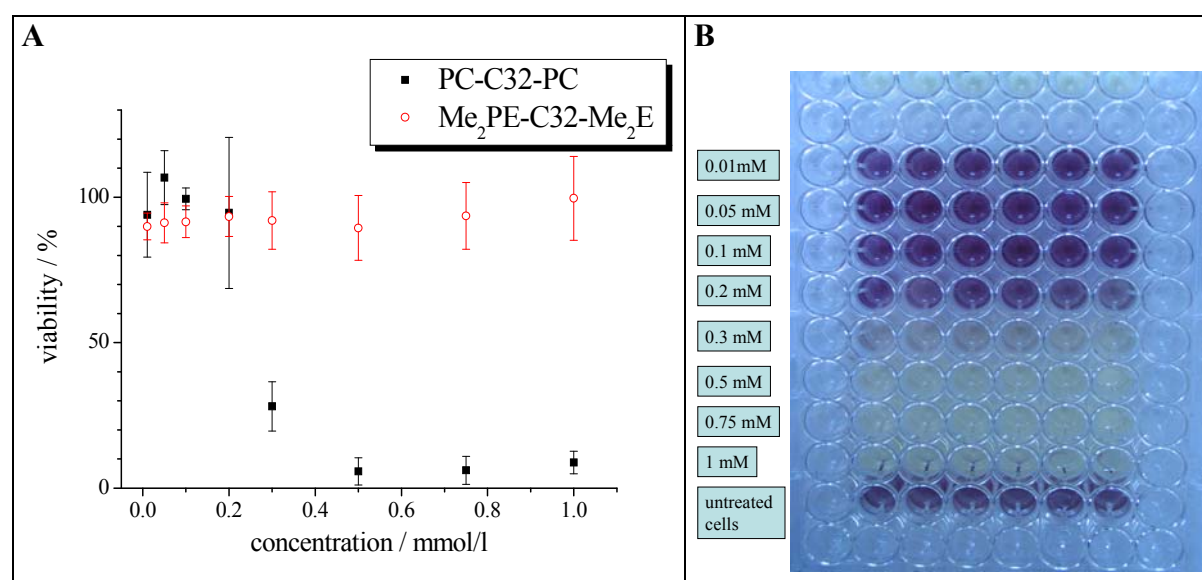


Figure 3.5.2 Results of the MTT-assay: (A) Determined cell viabilities after incubation of A549 cells for 24 hours with different concentrations of PC-C32-PC and Me₂PE-C32-Me₂PE. (B) Photograph of a microtiter plate after performing the MTT-assay with PC-C32-PC.

As Figure 3.5.2 shows, incubation of A549 cells with PC-C32-PC at higher concentrations substantially reduces the viability of these cells to less than 10%. For Me₂PE-C32-Me₂PE, on the other hand, no significant influence on the viability of the A549 cells was found up to concentrations of 1 mmol/l. Only for PC-C32-PC, a value for the half-maximal inhibitory concentration (IC₅₀) could therefore be estimated. This IC₅₀ value was found to lie between 200 and 300 μmol/l of PC-C32-PC in the tested A549 cells. In viability tests with erufosine (eruoylphosphomocholine) in 14 different human tumor cell lines, A549 cells were found to show rather low sensitivity to the cytotoxic agent.^[125] The IC₅₀ value determined for erufosine for these A549 cells was 27.6 μmol/l, which is lower by a factor of about 10 compared to the IC₅₀ value determined for PC-C32-PC. However, the incubation time in

these experiments was 5 days compared to 1 day in the MTT-assay performed for PC-C32-PC and Me₂PE-C32-Me₂PE. The number of treated cells and other factors can be expected to also have an influence on the determined IC₅₀ values. It is therefore not appropriate to compare the IC₅₀ value of PC-C32-PC with that of erufosine in order to estimate the degree of cytotoxicity of PC-C32-PC. The preliminary data obtained for PC-C32-PC indicate that significant cytotoxic effects on certain cells cannot be excluded for this bolaamphiphile. This shows that prior to potential applications in the biomedical field, the biocompatibility of this bolaamphiphile and its hydrogels must be carefully investigated. Such investigation should include extensive experiments with different cell lines and the use of one or more standard cytotoxic agents like miltefosine as reference substances.

The obtained results for Me₂PE-C32-Me₂PE seem to indicate a very low cytotoxicity and therefore good biocompatibility of this bolaamphiphile. An explanation for the apparently low cytotoxicity of Me₂PE-C32-Me₂PE might be a result of the difference between its headgroups and that of PC-C32-PC and miltefosine. However, it is not appropriate to conclude from this single experiment that Me₂PE-C32-Me₂PE shows no cytotoxic effects. In order to confirm this preliminary result, a series of experiments with different cell lines similar to that suggested for PC-C32-PC have to be carried out. Moreover, the influence of the self-assembly of the bolaamphiphiles in the aqueous cell media can be expected to have an influence on the observed effects and should be also addressed in these experiments.

3.5.2 Testing the antifungal activity

3.5.2.1 General remarks

As described above, Bierer et al. isolated the bolaamphiphile irlbacholine (PC-C22-PC) from the plants *Irlbachia alata* and *Anthocleista djalonenensis*.^[4] In an antifungal susceptibility test using a 96-well plate broth assay, irlbacholine revealed potent in-vitro activity against *Candida albicans*, *Cryptococcus neoformans*, *Aspergillus fumigatus* and *Trichophyton rubrum*.^[4] The minimal inhibitory concentrations were determined to be 1.25, 0.04, 0.08 and 0.04 µg/ml, respectively.

Potent antifungal activity in combination with the hydrogelation properties of the bolaamphiphiles would open a very interesting prospective for a practical application of these systems. Therefore, 12 different bolaamphiphiles including irlbacholine were tested for a potential antifungal activity against the pathogenic fungus *Candida albicans* and the dermatophyte *Trichophyton rubrum*.

3.5.2.2 Obtained results

The pilot study for testing the antifungal activity of a series of synthesized single chain bolaamphiphiles was carried out as described in Section 2.2.5. Besides PC-C32-PC and Me₂PE-C32-Me₂PE, all of their available derivatives with chain lengths ranging from 22 to 30 CH₂ groups were tested (Figure 2.2.17). In addition, a bolaamphiphile with a modified long chain was also included in this experiment, namely PC-C11-S-C8-S-C11-PC, in which two CH₂ groups are substituted by sulfur.^[24]

Photographs of the agar plates I-V, that were used for testing the effect of the bolaamphiphiles against *Candida albicans*, and VI-IX (*Trichophyton rubrum*) are shown in Figure 3.5.3 and Figure 3.5.4, respectively. As these photographs clearly show, no inhibitory effect on the growth of *Candida albicans* or *Trichophyton rubrum* was observed after 7 days for any of the tested bolaamphiphiles. Since activity against *Candida albicans* and *Trichophyton rubrum* was discovered before for irlbacholine (PC-C22-PC) in a susceptibility test,^[4] the absence of any growth inhibition for this substance was rather unexpected. An explanation might be found in the fact that the in-vitro experiment carried out with the agar plates considerably differs from the described susceptibility test, which was performed as a 96-well microplate broth assay. Because of the clear absence of any inhibitory effect for all tested bolaamphiphiles, the study for testing the antifungal activity was not continued and no further experiments were performed.

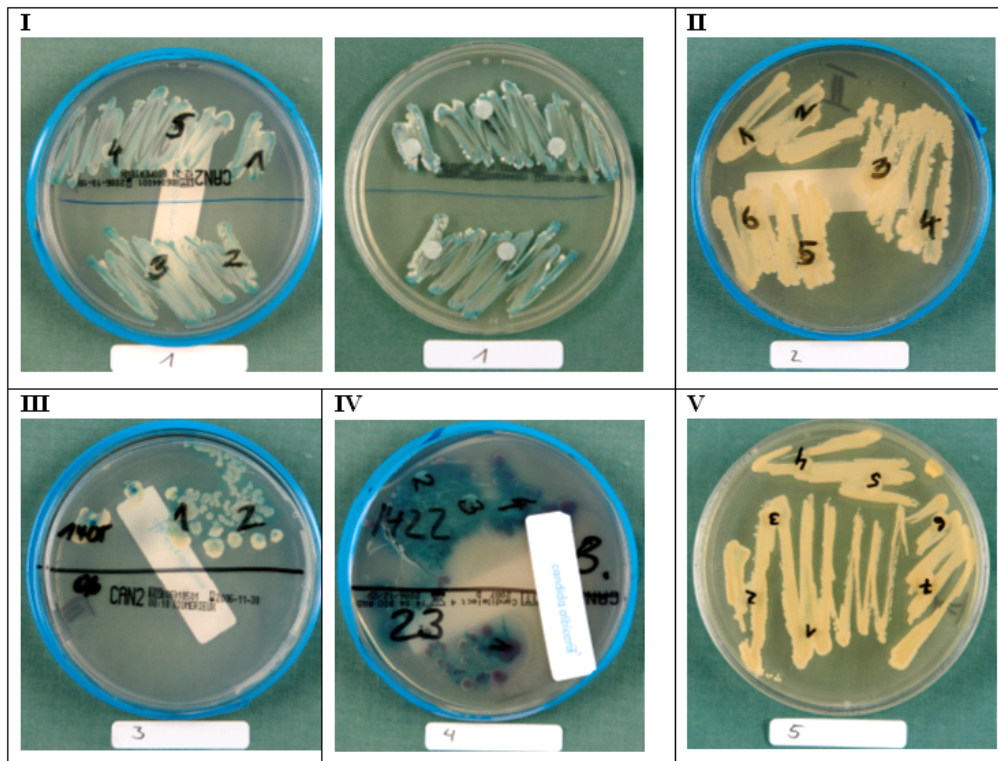


Figure 3.5.3 Testing the activity against *Candida albicans* according to the sampling scheme given in Table 2.2.1: Photographs of the plates after incubation for 7 days. Plate I is shown in the bottom and in the top view, whereas only the bottom view is shown for plates II – V.

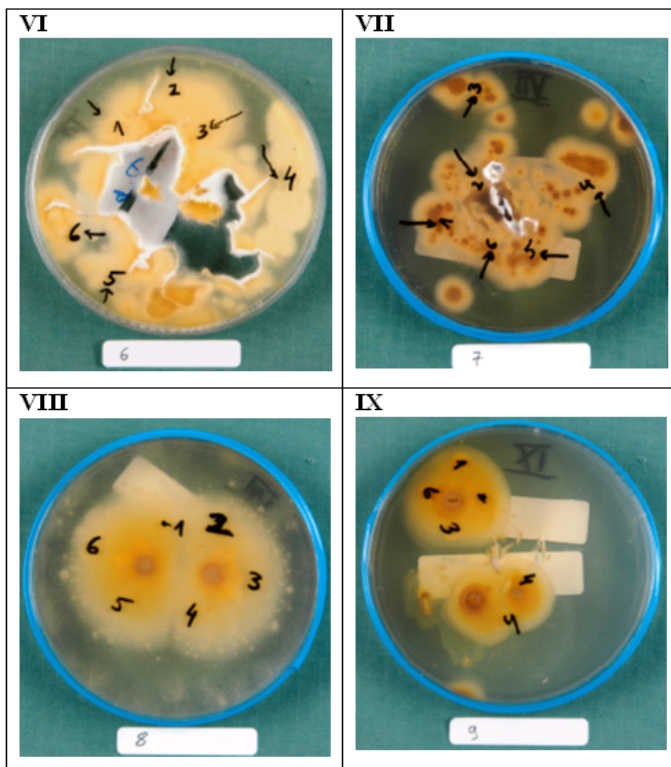


Figure 3.5.4 Testing the activity against *Trychophyton rubrum* according to the sampling scheme given in Table 2.2.1: Photographs of the plates VI–IX after incubation for 7 days are shown in the bottom view.

4 Summary and perspectives

The symmetrical single-chain bolaamphiphiles PC-C32-PC and Me₂PE-C32-Me₂PE were found to exhibit unique aggregation behavior in aqueous media. They turned out to form hydrogels at concentrations of only 1 g/l, which corresponds to a macroscopic “immobilization” of approximately 45000 water molecules per bolaamphiphile molecule. This is quite impressive and shows that PC-C32-PC and Me₂PE-C32-Me₂PE are highly efficient low molecular weight hydrogelators. Hydrogelation is realized by a self-assembly of the bolaamphiphiles into a dense network of well-defined nanofibers.

The aggregation behavior of PC-C32-PC and Me₂PE-C32-Me₂PE was intensively studied before, which enabled a good understanding of the basic principles of their aggregation behavior. However, there are still interesting features of these unique systems that remain to be investigated and open questions that remain to be answered.

Therefore, the aim of this thesis was the further physico-chemical characterization of the aggregation behavior of PC-C32-PC and Me₂PE-C32-Me₂PE. These investigations were focussed on the rheological characterization of the hydrogels and on studying the dynamics that are present inside these systems. Furthermore, the aggregation behavior and the UV-polymerization properties of the diacetylene bolaamphiphiles PC-C32diAc-PC and Me₂PE-C32diAc-Me₂PE were studied and two pilot studies were performed to investigate a potential biological activity of selected single-chain bolaphospholipids.

Oscillatory rheometry

The rheological data presented in this thesis, for the first time enable direct comparison of the mechanical properties of the hydrogels formed by PC-C32-PC and Me₂PE-C32-Me₂PE. The previous rheological data for PC-C32-PC and Me₂PE-C32-Me₂PE were obtained by different methods and included only a single concentration and a few temperatures.^[12,13,18]

Systematic measurements were performed by means of oscillatory rheometry in order to study the concentration dependence as well as the temperature dependence of the rheological parameters. By covering the air-water surface with low-viscous silicone oil, evaporation of water during the measurements could be circumvented. Therefore, it was possible to gradually increase the sample temperature up to 75 °C with sufficiently long waiting times at each temperature for equilibration.

Comparison of the G' and G'' values of PC-C32-PC and Me₂PE-C32-Me₂PE, obtained at concentrations ranging from 1 to 8 mg/ml, revealed interesting differences between the

hydrogels. These differences were interpreted in terms of the existence of an increasing fraction of lamellar aggregates inside the hydrogel formed by Me₂PE-C32-Me₂PE in acetate buffer pH 5.

By increasing the temperature from 25 to 75 °C, each of the transitions, that are detected in the DSC thermograms, was reflected in a clear discontinuity of the storage and loss moduli. For PC-C32-PC, the main transition at approximately 49 °C is related to the breakdown of the hydrogel state and therefore resulted in a drastic decrease of both G' and G'' to values that correspond to that of pure water. The pre-transition, on the other hand, was reflected not by a decrease, but in a small increase of the G' values for all tested concentrations. Therefore, the processes occurring at the pre-transition temperature may not leading to a partial loss of fiber-fiber cross-links, but rather to an increase in their number or stability.

For Me₂PE-C32-Me₂PE at pH 5, a distinct decrease of the G' and G'' values was observed for each of the two transitions. The first transition at approximately 45 °C was characterized by a decrease of G' and G'' by about one order of magnitude, which indicates the breaking-up of part of the cross-links inside the fiber network. Due to the persisting hydrogel state, the G' and G'' values remain relatively large above the temperature of the first transition. The breakdown of the hydrogel was only observed above the second transition temperature.

Besides the mechanical properties of the hydrogels, the kinetics of network formation were studied over a period of 60 minutes at 25 °C after cooling from 75 °C. The obtained time dependent G' values reveal interesting information about the hydrogelation process, which was found to proceed considerably faster for Me₂PE-C32-Me₂PE at pH 5 compared to PC-C32-PC, especially at low concentrations. Furthermore, the recovery of the G' values was studied over a time period of 60 minutes following to the application of extreme mechanical stress. The fast recovery of the G' values indicates that both hydrogels exhibit good self-healing properties.

NMR relaxometry and diffusometry

NMR relaxometry and diffusometry was used to investigate the dynamical properties of the water molecules inside the bolaamphiphilic hydrogels. Considerable differences could be observed between the hydrogels containing 30 mg/ml PC-C32-PC in deionized water and 30 mg/ml Me₂PE-C32-Me₂PE in acetate buffer pH 5. The rotational and translational mobility of the water molecules inside the PC-C32-PC hydrogel was found to be only slightly influenced by the presence of the bolaamphiphiles independently of the formed self-assemblies. For Me₂PE-C32-Me₂PE at pH 5, the translational mobility, characterized by the mean diffusion coefficient, was again only slightly influenced. The relaxation behavior of the water

protons however, was found to be considerably changed inside the hydrogel of Me₂PE-C32-Me₂PE compared to PC-C32-PC. The major T₂-peak was considerably broadened and shifted to lower T₂-values. By comparison of the T₂-distribution obtained for 30 mg/ml Me₂PE-C32-Me₂PE with that obtained for a series of different hydrogel systems, this remarkable relaxation behavior could be attributed to the existence of a considerable degree of heterogeneity in this hydrogel. For Me₂PE-C32-Me₂PE at pH 5, it is the first time that evidence is provided for the existence of such heterogeneities in the micrometer range. The origin of these heterogeneities can be found in the presence of domains that are most probably consisting of stacked lamellar aggregates. Such lamellar aggregates were found before in the cryo-TEM images obtained for highly diluted dispersions of Me₂PE-C32-Me₂PE,^[15] but their existence could not fully explained at that time. Upon storage of the NMR sample for 48 hours, the phenomenon of syneresis was observed. This was also attributed to the presence of the lamellar regions, which could be shown to grow in size upon storage. Instability of Me₂PE-C32-Me₂PE hydrogels upon storage due to syneresis can be seen as an obstacle for potential applications. Hydrogels of PC-C32-PC, on the other hand, were found to be stable over several months.

The obtained mean diffusion coefficients of the water molecules, which determine the mean diffusion distance during the time of the relaxation processes, were used to estimate the distance scale of the heterogeneities. It was found that the distance scale of the heterogeneities, that are present inside the freshly prepared hydrogel of 30 mg/ml Me₂PE-C32-Me₂PE at pH 5, lies in the range between about 50 and 120 μm. In the sample after syneresis, these lamellar domains seem to reach sizes between 140 to 190 μm.

Additionally to the characterization of the relaxation behavior of the water protons, the relaxation of the bolaamphiphile protons was accessible by substituting H₂O by D₂O. For both bolaamphiphiles, the relaxation behavior was found to be considerably changed during the transitions, which are related to the breakdown of the fibers into micellar aggregates.

ESR

The spin probe tempolbenzoate (TB) was found to be solely distributed throughout the aqueous phase of the bolaamphiphilic hydrogels. The results obtained with TB indicate that the dynamical properties of water, which is macroscopically immobilized, correspond to that observed in pure medium on a microscopic level.

A systematic spin probe study was performed using three n-doxyl stearic acid spin probes, which were found to be incorporated inside the alkyl chain region of the particular self-assemblies of PC-C32-PC and Me₂PE-C32-Me₂PE. The recorded ESR spectra provided

information about the molecular order and the motional dynamics at different positions inside this alkyl chain region. At temperatures ranging from 0 to 40 °C, highly anisotropic spectra were obtained for 5-DSA and 12-DSA in the samples containing PC-C32-PC or Me₂PE-C32-Me₂PE at pH 5. This indicates a low degree of motional freedom of the spin probes that were residing between the densely packed bolaamphiphilic alkyl chains. Between 40 and 55 °C, the high degree of order was lost due to the transitional changes, which were found to be characterized by a fluidization of the alkyl chains. These transitions were sensitively reflected in the spectral lineshape. The hyperfine splitting parameter $2A_{\text{max}}$ was found to be a reliable measure for the degree of order and the motional freedom at the particular sample temperature. The $2A_{\text{max}}$ values could also be used to determine the transition temperatures, which were found to be in good agreement with the DSC data for 5-DSA. For 12-DSA, on the other hand, a significant shift to higher temperatures was observed for particular transitions. Since 12-DSA is residing deeper inside the alkyl chain region, these temperature shifts were interpreted in terms of a delayed chain fluidization in this region. As a consequence, it was concluded that trans-gauche isomerization of the bolaamphiphilic alkyl chains is preferentially starting in the outer parts of the aggregates and is only extending toward the central part, when the temperature is further increased. By simulation of selected spectra, it was possible to theoretically confirm the proposed relationship between the observed spectral lineshapes and the rotational reorientation of the nitroxyl group inside the external magnetic field.

Compared to 5-DSA and 12-DSA, 16-DSA was found to represent an exceptional case for all bolaamphiphile samples. Its doxyl groups are apparently residing near the bolaamphiphilic headgroups and not deep inside the alkyl chain region as could be expected. By carrying out a reduction assay with ascorbic acid, this proposed location of the doxyl group near the headgroup region could be confirmed for all investigated bolaamphiphile samples.

For Me₂PE-C32-Me₂PE at pH 10, the ESR data indicates that the general aggregation behavior is not changed compared to pH 5. The electrostatic repulsion between the negatively charged headgroups only introduces a considerable perturbation on the packing of the alkyl chains, especially in the region near the headgroups. Due to this destabilization, no long nanofibers are formed by the Me₂PE-C32-Me₂PE molecules, but only rod-like aggregates with varying lengths, which depend on the bolaamphiphile concentration.

Bolaamphiphiles with a diacetylene group

The approach to chemically cross-link the diacetylene-modified bolaamphiphiles by UV-polymerization resulted in very interesting findings. However, it was not fully successful yet, since fiber network and hydrogel formation could be achieved neither before nor after the

UV-polymerization. This is due to the substitution of four CH₂ groups by a diacetylene group in the center of the alkyl chain, which causes severe changes of the aggregation behavior and prevents the formation of well defined nanofibers.

The results obtained by UV-polymerization of PC-C32diAc-PC point to the general suitability of this approach. The obtained polymerized PC-C32diAc-PC was found to exhibit the typical properties that were described for other polydiacetylenes. These properties are intensive coloration due to characteristic absorption maxima and temperature dependent color transitions, which were found to be partially reversible.

The results obtained for Me₂PE-C32diAc-Me₂PE, on the other hand, indicate that the ability of the bolaamphiphilic diacetylenes to polymerize upon UV-irradiation strongly depends on the exact geometric arrangement inside the formed aggregates. The crucial factor for the UV-polymerization is the mean distance between adjacent diacetylene groups, which is mainly determined by the arrangement of alkyl chains and also by the ordering effect of the headgroups of the bolaamphiphiles. Inside the aggregates of Me₂PE-C32diAc-Me₂PE, the mean distance between the diacetylene groups seems to deviate considerably from the optimal value of 4.9 Å, since only yellow coloration was observed for all samples upon UV-irradiation.

Biological tests

Due to the structural similarity of PC-C32-PC and Me₂PE-C32-Me₂PE to the cytotoxic drug miltefosine, the biocompatibility of these bolaamphiphiles must be carefully evaluated prior to a potential application of their hydrogels in the biomedical field. In order to obtain preliminary data about the cytotoxicity of PC-C32-PC and Me₂PE-C32-Me₂PE, a MTT-assay was performed with A549 cells. From this assay, the IC₅₀ value was determined to be lie between 200 and 300 µmol/l for PC-C32-PC, whereas for Me₂PE-C32-Me₂PE, no change in the viability of the cells was observed up to a concentration of 1 mmol/l. However, further extensive experiments with different cell lines and one or more standard cytotoxic agents like miltefosine are required to provide evidence for the biocompatibility of PC-C32-PC and Me₂PE-C32-Me₂PE.

Since activity against *Candida albicans* or *Trichophyton rubrum* was reported before for PC-C22-PC, an in-vitro experiment was performed. 12 bolaamphiphiles were tested for a potential effect on the growth of these fungi. No growth inhibition and therefore no antifungal activity could be observed in this experiment for any of these bolaamphiphiles.

Future perspectives

Since this work was focussed on the bolaamphiphiles PC-C32-PC and Me₂PE-C32-Me₂PE, all described experiments could theoretically be extended to the other members of this family of single-chain bolaamphiphiles.

For example, it seems desirable to systematically study the rheological behavior of the hydrogels formed by the bolaamphiphiles with shorter or longer chain lengths than PC-C32-PC and Me₂PE-C32-Me₂PE. A significant influence of the chain length on the obtained G' and G'' values can be expected. The effect of hydrogen bonding on the “strength” of the formed hydrogels could not be quantified for the pair PC-C32-PC/Me₂PE-C32-Me₂PE due to the unpredictable influence of the lamellar aggregates, which are present inside the hydrogels of Me₂PE-C32-Me₂PE. Here, the comparison of the bolaamphiphile pair PC-C26-PC/Me₂PE-C26-Me₂PE should yield valid information. Another detail that needs to be clarified by oscillatory rheometry, is the confirmation of the results that were obtained for the pre-transition of PC-C32-PC. Here, experiments with PC-C30-PC, PC-C34-PC and PC-C36-PC will probably provide useful information. The preliminary results that are described in this thesis for the time dependent rheometry, should also be confirmed.

Until now, the dynamics, that are present in the aqueous bolaamphiphile systems, were investigated by various methods including FT-IR, rheometry, NMR (³¹P, ¹H, ²D) and ESR. Fluorescence correlation spectroscopy (FCS) is a promising method to further study these dynamics. FCS represents a very sensitive method to study intermolecular interactions and diffusion. Therefore, it may provide unique information about the translational diffusion of the particular bolaamphiphiles inside the nanofibers and also about the flexibility of these nanofibers, which can be expected to be dependent on the stability and density of fiber-fiber cross-links.

Promising future work can also be seen in the synthesis and characterization of polymerizable bolaamphiphiles. The synthesis of diacetylene bolaamphiphiles with considerably longer alkyl chains than in PC-C32diAc-PC and Me₂PE-C32diAc-Me₂PE is already on the way.

To find practical applications for this promising class of materials is the main future goal to be set. Due to their tunable hydrogelation properties, they may be used, for example, as drug carriers. However, this would require extensive experiments to provide evidence for the biocompatibility of these systems. Because of their well defined self-assembly on a nanoscopic level, they may also find application in nanodevices. A successful development of stimuli-responsive polydiacetylenes, for example, would provide a promising class of materials for nanosensors.

5 References

1. Fuoss, R. M.; Edelson, D.: Bolaform electrolytes. I. Di-(beta -trimethylammonium ethyl) succinate dibromide and related compounds. *J. Am. Chem. Soc.* **1951**, *73*, 269-273.
2. Fuhrhop, J. H.; Mathieu, J.: Pathways to functionalized vesicle membranes without proteins. *Angew. Chem.* **1984**, *96* (2), 124-137.
3. Kates, M.: Membrane lipids of archaea. In *The biochemistry of Archaea (Archaeobacteria)*, Kates, M., Kushner, D. J., Matheson, A. T., Eds.; Elsevier: Amsterdam, **1993**; pp 261-295.
4. Bierer, D. E.; Gerber, R. E.; Jolad, S. D.; Ubillas, R. P.; Randle, J.; Nauka, E.; Latour, J.; Dener, J. M.; Fort, D. M.: Isolation, Structure Elucidation, and Synthesis of Irlbacholine, 1,22-Bis[[[2-(trimethylammonium)ethoxy]phosphinyl]oxy]docosane: A Novel Antifungal Plant Metabolite from *Irlbachia alata* and *Anthocleista djalonensis*. *J. Org. Chem.* **1995**, *60* (21), 7022-7026.
5. Fuhrhop, J. H.; Wang, T.: Bolaamphiphiles. *Chem. Rev.* **2004**, *104* (6), 2901-2937.
6. Meister, A.; Blume, A.: Self-assembly of bipolar amphiphiles. *Curr. Opin. Colloid Interface Sci.* **2007**, *12* (3), 138-147.
7. Benvegna, T.; Brard, M.; Plusquellec, D.: Archaeobacteria bipolar lipid analogues: structure, synthesis and lyotropic properties. *Curr. Opin. Colloid Interface Sci.* **2004**, *8* (6), 469-479.
8. Estroff, L. A.; Hamilton, A. D.: Water Gelation by Small Organic Molecules. *Chem. Rev.* **2004**, *104* (3), 1201-1217.
9. Heiser, U. F.; Dobner, B.: Copper-catalyzed coupling of undec-10-enylmagnesium bromide with w-functionalised halogenoalkanes as a key reaction for the preparation of novel bipolar phospholipids with different head groups and chain length. *J. Chem. Soc., Perkin Trans. 1* **1997**, (6), 809-815.
10. Heiser, U. F.: Synthese langkettiger bolaamphiphiler Phospholipide. *PhD thesis (MLU Halle-Wittenberg)* **1998**.
11. Heiser, U. F.; Wolf, R.; Dobner, B. Simple and high yield synthesis of (+-)-10,10'-dimethyl-dotriacontan-1,1'-diol as a building block for branched bola compounds. Preparation of (+-)-10,10'dimethyl-dotriacontan-1,1'-diyl-bis[2-(trimethylammonio)ethyl phosphate] and the corresponding unbranched equivalent. *Chem. Phys. Lipids* **1997**, *90* (1,2), 25-30.
12. Koehler, K.; Foerster, G.; Hauser, A.; Dobner, B.; Heiser, U. F.; Ziethe, F.; Richter, W.; Steiniger, F.; Drechsler, M.; Stettin, H.; Blume, A.: Self-Assembly in a Bipolar Phosphocholine-Water System: The Formation of Nanofibers and Hydrogels. *Angewandte Chem. Int. Ed. Engl.* **2004**, *43*, 245-247.

13. Koehler, K.; Foerster, G.; Hauser, A.; Dobner, B.; Heiser, U. F.; Ziethe, F.; Richter, W.; Steiniger, F.; Drechsler, M.; Stettin, H.; Blume, A.: Temperature-Dependent Behavior of a Symmetric Long-Chain Bolaamphiphile with Phosphocholine Headgroups in Water: From Hydrogel to Nanoparticles. *J. Am. Chem. Soc.* **2004**, *126* (51), 16804-16813.
14. Meister, A.; Drescher, S.; Mey, I.; Wahab, M.; Graf, G.; Garamus, V. M.; Hause, G.; Mogel, H. J.; Janshoff, A.; Dobner, B.; Blume, A.: Helical Nanofibers of Self-Assembled Bipolar Phospholipids as Template for Gold Nanoparticles. *J. Phys. Chem. B* **2008**, *112* (15), 4506-4511.
15. Koehler, K.; Meister, A.; Foerster, G.; Dobner, B.; Drescher, S.; Ziethe, F.; Richter, W.; Steiniger, F.; Drechsler, M.; Hause, G.; Blume, A.: Conformational and thermal behavior of a pH-sensitive bolaform hydrogelator. *Soft Matter* **2006**, *2* (1), 77-86.
16. Ziethe, F.: Synthese und physikochemische Charakterisierung von Modellsubstanzen der Archaeobakterienlipide. *PhD thesis (MLU Halle-Wittenberg)* **2003**.
17. Cevc, G.: *Phospholipids Handbook*; Marcel Dekker Ltd: New York, **1993**.
18. Meister, A.; Bastrop, M.; Koschoreck, S.; Garamus, V. M.; Sinemus, T.; Hempel, G.; Drescher, S.; Dobner, B.; Richtering, W.; Huber, K.; Blume, A.: Structure-Property Relationship in Stimulus-Responsive Bolaamphiphile Hydrogels. *Langmuir* **2007**, *23* (14), 7715-7723.
19. Meister, A.; Drescher, S.; Garamus, V. M.; Karlsson, G.; Graf, G.; Dobner, B.; Blume, A.: Temperature-Dependent Self-Assembly and Mixing Behavior of Symmetrical Single-Chain Bolaamphiphiles. *Langmuir* **2008**, *24* (12), 6238-6246.
20. Meister, A.; Koehler, K.; Drescher, S.; Dobner, B.; Karlsson, G.; Edwards, K.; Hause, G.; Blume, A. Mixing behaviour of a symmetrical single-chain bolaamphiphile with phospholipids. *Soft Matter* **2007**, *3* (8), 1025-1031.
21. Drescher, S.; Meister, A.; Blume, A.; Karlsson, G.; Almgren, M.; Dobner, B. General synthesis and aggregation behaviour of a series of single-chain 1,w-bis(phosphocholines). *Chem. --Eur. J.* **2007**, *13* (18), 5300-5307.
22. Drescher, S.: Synthese und physiko-chemische Charakterisierung einkettiger symmetrischer Bolaamphiphile. *PhD thesis (MLU Halle-Wittenberg)* **2008**.
23. Meister, A.; Drescher, S.; Karlsson, G.; Hause, G.; Baumeister, U.; Hempel, G.; Garamus, V. M.; Dobner, B.; Blume, A.: Formation of square lamellae by self-assembly of long chain bolaphospholipids in water. *Soft Matter* **2010**, *6*, 1317-1324.
24. Drescher, S.; Meister, A.; Graf, G.; Hause, G.; Blume, A.; Dobner, B.: General synthesis and aggregation behaviour of new single-chain bolaphospholipids: variations in chain and headgroup structures. *Chem. --Eur. J.* **2008**, *14* (22), 6796-6804.

25. Weiss, R. G.; Terech, P.; Editors *Molecular Gels: Materials with Self-Assembled Fibrillar Networks*; Springer: Dordrecht, The Netherlands, **2006**.
26. Peppas, N. A.; Bures, P.; Leobandung, W.; Ichikawa, H.: Hydrogels in pharmaceutical formulations. *Eur. J. Pharm. Biopharm.* **2000**, *50* (1), 27-46.
27. McConville, P.; Whittaker, M. K.; Pope, J. M.: Water and Polymer Mobility in Hydrogel Biomaterials Quantified by ¹H NMR: A Simple Model Describing Both T1 and T2 Relaxation. *Macromolecules* **2002**, *35* (18), 6961-6969.
28. Jeong, B.; Kim, S. W.; Bae, Y. H.: Thermosensitive sol-gel reversible hydrogels. *Adv. Drug Delivery Rev.* **2002**, *54* (1), 37-51.
29. Baroli, B.: Hydrogels for tissue engineering and delivery of tissue-inducing substances. *J. Pharm. Sci.* **2007**, *96* (9), 2197-2223.
30. Nayak, S.; Lyon, L. A.: Soft nanotechnology with soft nanoparticles. *Angewandte Chem. Int. Ed. Engl.* **2005**, *44* (47), 7686-7708.
31. de Loos, M.; Feringa, B. L.; van Esch, J. H.: Design and application of self-assembled low molecular weight hydrogels. *Eur. J. Org. Chem.* **2005**, (17), 3615-3631.
32. Blume, A.: Dynamics. In *Phospholipids Handbook*, Cevc, G., Ed.; Marcel Dekker Ltd: New York, **1993**.
33. Piksa, K.: Einführung von mittelständigen polymerisierbaren Dreifachbindungen in bolaamphiphile Verbindungen. *Diploma thesis (MLU Halle-Wittenberg)* **2007**.
34. Drescher, S.; Helmig, K.; Langner, A.; Dobner, B.: Synthesis of novel symmetrical, single-chain, diacetylene-modified bolaamphiphiles with different alkyl chain lengths. *Monatsh. Chem.* **2010**, *141*, 339-349.
35. Mezger, T.: *Das Rheologie-Handbuch*; Curt R. Vincentz Verlag: Hannover, **2000**.
36. Levitt, M.: H. *Spin Dynamics*; 1st ed.; John Wiley&Sons, Ltd.: Chichester, **2001**.
37. Winter, R.; Noll, F.: *Methoden der biophysikalischen Chemie*; B. G. Teubner: Stuttgart, **1998**.
38. Kimmich, R.; Editor. *NMR-Tomography, Diffusometry, Relaxometry*; **1997**.
39. Abragam, A.: *The Principles of Nuclear Magnetism*; Clarendon Press, Oxford: **1961**.
40. Bloembergen, N.; Purcell, E. M.; Pound, R. V.: Relaxation effects in nuclear magnetic resonance absorption. *Phys. Rev.* **1948**, *73*, 679-712.
41. Mathur, A. M.; Scranton, A. B.: Characterization of hydrogels using nuclear magnetic resonance spectroscopy. *Biomaterials* **1996**, *17* (6), 547-557.
42. Hahn, E. L.: Spin Echos. *Phys. Rev.* **1950**, *80* (4), 580-601.
43. Carr, H. Y.; Purcell, E. M.: Effects of Diffusion on Free Precession in Nuclear Magnetic Resonance Experiments. *Phys. Rev.* **1954**, *94* (3), 630-638.

44. Meiboom, S.; Gill, D.: Modified spin-echo method for measuring nuclear relaxation times. *Rev. Sci. Instrum.* **1958**, *29*, 688-691.
45. *RI WinDXP User Manual v. 2.9 (RI WinDXP software release version 1.9)*, Oxford Instruments (Abingdon, UK): **2004**
46. Stejskal, E. O.; Tanner, J. E.: Spin diffusion measurements: spin echoes in the presence of a time-dependent field gradient. *J. Chem. Phys.* **1965**, *42* (1), 288-292.
47. Tanner, J. E.: Use of stimulated echos in NMR diffusion studies. *J. Chem. Phys.* **1970**, *62*, 2523.
48. *MARAN Ultra Non-Expert User Manual v1.6.3*, version v1.6.3 December 2004; Oxford Instruments (Abingdon, UK): **2004**
49. Berliner, L. J.: *Spin Labeling: Theory and Applications*; Academic Press: New York, **1976**.
50. Griffith, O. H.; Jost, P. C.: Lipid spin labels in biological membranes. In *Spin Labelling: Theory and Applications*, Berliner, L. J., Ed.; Academic Press: New York, **1976**; pp 453-523.
51. Stoll, S.; Schweiger, A.: EasySpin: Simulating cw ESR Spectra, Appendix 6. In *ESR Spectroscopy in Membrane Biophysics*, Hemminga, M., Berliner, L. J., Eds.; Springer: New York, **2007**; pp 299-321.
52. Stoll, S.; Schweiger, A.: EasySpin, a comprehensive software package for spectral simulation and analysis in EPR. *J. Magn. Reson.* **2006**, *178* (1), 42-55.
53. Strancar, J.; Sentjurc, M.; Schara, M.: Fast and accurate characterization of biological membranes by EPR spectral simulations of nitroxides. *J. Magn. Reson.* **2000**, *142* (2), 254-265.
54. Tieke, B.: Polymerization of butadiene and butadiyne(Diacetylene) derivatives in layer structures. *Adv. Polym. Sci.* **1985**, *71*, 74-151.
55. Bader, H.; Ringsdorf, H.: Liposomes from alpha ,w-dipolar amphiphiles with a polymerizable diyne moiety in the hydrophobic chain. *J. Polym. Sci. , Polym. Chem. Ed.* **1982**, *20* (6), 1623-1628.
56. Saremi, F.; Maassen, E.; Tieke, B.; Jordan, G.; Rammensee, W.: Self-assembled alternating multilayers built-up from diacetylene bolaamphiphiles and poly(allylaminehydrochloride): Polymerization properties, structure, and morphology. *Langmuir* **1995**, *11*, 1068-1071.
57. Song, J.; Cheng, Q.; Kopta, S.; Stevens, R. C.: Modulating artificial membrane morphology: pH-induced chromatic transition and nanostructural transformation of a bolaamphiphilic conjugated polymer from blue helical ribbons to red nanofibers. *J. Am. Chem. Soc.* **2001**, *123*, 3205-3213.

58. Kew, S. J.; Hall, E. A. H.: Structural effect of polymerisation and dehydration on bolaamphiphilic polydiacetylene assemblies. *J. Mater. Chem.* **2006**, *16*, 2039-2047.
59. Tieke, B.; Bloor, D.; Young, R. J.: Solid-state polymerization of tricoso-10,12-diyonic acid. *J. Mater. Sci.* **1982**, *17*, 1156-1166.
60. Schott, M.: The colors of polydiacetylenes: a commentary. *J. Phys. Chem. B* **2006**, *110* (32), 15864-16868.
61. Olmstedt, J.; Strand, M. Fluorescence of polymerized diacetylene bilayer films. *J. Phys. Chem.* **1983**, *87* (24), 4790-4792.
62. Tieke, B.; Lieser, G.; Wegner, G.: Polymerization of diacetylenes in multilayers. *J. Polym. Sci., Polym. Chem. Ed.* **1979**, *17*, 1631-1644.
63. Wenzel, M.; Atkinson, G. H.: Chromatic properties of polydiacetylene films. *J. Am. Chem. Soc.* **1989**, *111*, 6123-6127.
64. Lee, D.-C.; Sahoo, S. K.; Cholli, A. L.; Sandman, D. J.: Structural aspects of the thermochromic transition in urethane-substituted polydiacetylenes. *Macromolecules* **2002**, *35*, 4347-4355.
65. Nallicheri, R. A.; Rubner, M. F.: Investigations of the mechanochromic behavior of poly(urethane-diacetylene) segmented copolymers. *Macromolecules* **1991**, *24*, 517-525.
66. Carpick, R. W.; Sasaki, D. Y.; Marcus, M. S.; Eriksson, M. A.; Burns, A. R.: Polydiacetylene films: A review of recent investigations into chromogenic transitions and nanomechanical properties. *J. Phys. : Condens. Matter* **2004**, *16*, 679-697.
67. Cheng, Q.; Stevens, R. C.: Charge-induced chromatic transition of amino acid-derivatized polydiacetylene liposomes. *Langmuir* **1998**, *14*, 1974-1976.
68. Jonas, U.; Shah, K.; Norvez, S.; Charych, D. H.: Reversible color switching and unusual solution polymerization of hydrazide-modified diacetylene lipids. *J. Am. Chem. Soc.* **1999**, *121*, 4580-4588.
69. Song, J.; Cisar, J. S.; Bertozzi, C. R.: Functional self-assembling bolaamphiphilic polydiacetylenes as colorimetric sensor scaffolds. *J. Am. Chem. Soc.* **2004**, *126*, 8459-8465.
70. Chen, X.; Kang, S.; Kim, M. J.; Kim, J.; Kim, Y. S.; Kim, H.; Chi, B.; Kim, S.-J.; Lee, J. L.; Yoon, J.: Thin-film formation of imidazolium-based conjugated polydiacetylenes and their application for sensing anionic surfactants. *Angewandte Chem. Int. Ed. Engl.* **2010**, *49*, 1422-1425.
71. Mosmann, T.: Rapid colorimetric assay for cellular growth and survival: application to proliferation and cytotoxicity assays. *J. Immunol. Methods* **1983**, *65* (1-2), 55-63.

72. Mohammed, Z. H.; Hember, M. W. M.; Richardson, R. K.; Morris, E. R.: Kinetic and equilibrium processes in the formation and melting of agarose gels. *Carbohydr. Polym.* **1998**, *36*, 15-26.
73. Hoffman, A. S.: Hydrogels for biomedical applications. *Adv. Drug Delivery Rev.* **2002**, *43*, 3-12.
74. Roorda, W. E.; de Bleyser, J.; Junginger, H. E.; Leyte, J. C.: Nuclear magnetic relaxation of water in hydrogels. *Biomaterials* **1990**, *11* (1), 17-23.
75. Provencher, S. W.: CONTIN: A general purpose constrained regularization program for inverting noisy linear algebraic and integral equations. *Comput. Phys. Commun.* **1982**, *27* (229).
76. Hills, B. P.; Snaar, J. E. M.: Water proton relaxation studies of pore microstructure in monodisperse glass bead beds. *Mol. Phys.* **1995**, *84* (1), 141-157.
77. Hills, B. P.; Manning, C. E.: NMR oxygen-17 studies of water dynamics in heterogeneous gel and particulate systems. *J. Mol. Liq.* **1998**, *75* (1), 61-76.
78. Britton, M. M.; Graham, R. G.; Packer, K. J.: NMR relaxation and pulsed field gradient study of alginate bead porous media. *J. Magn. Reson.* **2004**, *169* (2), 203-214.
79. Chiotelli, E.; Pilosio, G.; Le Meste, M.: Effect of Sodium Chloride on the Gelatinization of Starch: A Multimeasurement Study. *Biopolymers* **2002**, *63*, 41-58.
80. Tang, H. R.; Brun, A.; Hills, B.: A proton NMR relaxation study of the gelatinization and acid hydrolysis of native potato starch. *Carbohydr. Polym.* **2001**, *46* (1), 7-18.
81. Mitchell, J.; Stark, S. C.; Strange, J. H.: Probing surface interactions by combining NMR cryoporometry and NMR relaxometry. *J. Phys. D: Appl. Phys.* **2005**, *38*, 1950-1958.
82. Schaumann, G. E.; Hobley, E.; Hurraß, J.; Rotard, W.: H-NMR relaxometry to monitor wetting and swelling kinetics in high-organic matter soils. *Plant Soil* **2005**, *275*, 1-20.
83. Li, R.; Kerr, W. L.; Toledo, R. T.; Carpentier, J. A.: ¹H NMR Studies of Water in Chicken Breast Marinated with Different Phosphates. *J. Food Sci.* **2000**, *65* (4), 575-580.
84. Duval, F. P.; Porion, P.; Faugère, A.-M.; Van Damme, H.: An NMR Investigation of Water Self-Diffusion and Relaxation Rates in Controlled Ionic Strength Laponite Sols and Gels. *J. Colloid Interface Sci.* **2001**, *242*, 819-826.
85. Roorda, W. E.; Bouwstra, J. A.; de Vries, M. A.; Junginger, H. E.: Thermal analysis of water in p(HEMA) hydrogels. *Biomaterials* **1988**, *9* (6), 494-499.

86. Roorda, W. E.; Bouwstra, J. A.; De Vries, M. A.; Junginger, H. E.: Thermal behavior of poly(hydroxyethyl methacrylate) (pHEMA) hydrogels. *Pharm. Res.* **1988**, *5* (11), 722-725.
87. Jhon, M. S.; Andrade, J. D.: Water and hydrogels. *J. Biomed. Mater. Res.* **1973**, *7* (6), 509-522.
88. Lee, H. B.; Jhon, M. S.; Andrade, J. D.: Nature of water in synthetic hydrogels. I. Dilatometry, specific conductivity, and differential scanning calorimetry of poly(hydroxyethyl methacrylate). *J. Colloid Interface Sci.* **1975**, *51* (2), 225-231.
89. Sung, Y. K.; Gregonis, D. E.; Jhon, M. S.; Andrade, J. D.: Thermal and pulse NMR analysis of water in poly(2-hydroxyethyl methacrylate). *J. Appl. Polym. Sci.* **1981**, *26* (11), 3719-3728.
90. Denisov, V. P.; Halle, B.: Protein hydration dynamics in aqueous solution: A comparison of bovine pancreatic trypsin inhibitor and ubiquitin by oxygen-17 spin relaxation dispersion. *J. Mol. Biol.* **1995**, *245* (6), 682-697.
91. Bastrop, M.; Meister, A.; Metz, H.; Drescher, S.; Dobner, B.; Maeder, K.; Blume, A.: The Motional Dynamics in Bolaamphiphilic Nanofibers and Micellar Aggregates: An ESR Spin Probe Study. *J. Phys. Chem. B* **2009**, *113* (2), 574-582.
92. Lewis, G. P.; Derbyshire, W.; Ablett, S.; Lillford, P. J.; Norton, I. T.: Investigations of the NMR relaxation of aqueous gels of the carrageenan family and of the effect of ionic content and character. *Carbohydr. Res.* **1987**, *160*, 397-410.
93. Tanaka, H.; Fukumori, K.; Nishi, T.: Study of chemical gelation dynamics of acrylamide in water by real-time pulsed nuclear magnetic resonance measurement. *J. Chem. Phys.* **1988**, *89* (5), 3363-3372.
94. Tanaka, N.; Matsukawa, S.; Kurosu, H.; Ando, I.: A study on dynamics of water in crosslinked poly(N-isopropylacrylamide) gel by n.m.r. spectroscopy. *Polymer* **1998**, *39* (20), 4703-4706.
95. Hills, B. P.; Wright, K. M.; Belton, P. S.: NMR studies of water proton relaxation in Sephadex bead suspensions. *Mol. Phys.* **1989**, *67* (1), 193-208.
96. Lillford, P. J.; Clark, A. H.; Jones, D. V.: Distribution of water in heterogeneous food and model systems. *ACS Symp. Ser.* **1980**, *127* (Water Polym.), 177-195.
97. Belton, P. S.; Hills, B. P.; Raimbaud, E. R.: The effects of morphology and exchange on proton NMR relaxation in agarose gels. *Mol. Phys.* **1988**, *63* (5), 825-842.
98. Penke, B.; Kinsey, S.; Gibbs, S. J.; Moerland, T. S.; Locke, B. R.: Proton Diffusion and T1 Relaxation in Polyacrylamide Gels: A Unified Approach Using Volume Averaging. *J. Magn. Reson.* **1998**, *132*, 240-254.
99. Jores, K.; Mehnert, W.; Maeder, K.: Physicochemical investigations on solid lipid nanoparticles and on oil-loaded solid lipid nanoparticles: a nuclear magnetic

- resonance and electron spin resonance study. *Pharm. Res.* **2003**, *20* (8), 1274-1283.
100. Ruebe, A.; Maeder, K.: Electron spin resonance study on the dynamics of polymeric nanocapsules. *J. Biomed. Nanotechnol.* **2005**, *1* (2), 208-213.
 101. Abdalla, A.; Maeder, K.: Preparation and characterization of a self-emulsifying pellet formulation. *Eur. J. Pharm. Biopharm.* **2007**, *66* (2), 220-226.
 102. Seelig, J.: Anisotropic motion in liquid crystalline structures. In *Spin Labelling: Theory and Applications*, Berliner, L. J., Ed.; Academic Press: New York, **1976**; pp 373-409.
 103. Alaouie, A. M.; Smirnov, A. I.: Ultra-stable temperature control in EPR experiments: Thermodynamics of gel-to-liquid phase transition in spin-labeled phospholipid bilayers and bilayer perturbations by spin labels. *J. Magn. Reson.* **2006**, *182* (2), 229-238.
 104. Gaffney, B. J.: The chemistry of spin labels, Appendix IV. In *Spin Labeling: Theory and Applications*. ed.; Berliner, L. J., Ed.; Academic Press: New York, **1976**; pp 183-238.
 105. Shimshick, E. J.; McConnell, H. M.: Lateral phase separations in binary mixtures of cholesterol and phospholipids. *Biochem. Biophys. Res. Commun.* **1973**, *53* (2), 446-451.
 106. Bruno, S.; Cannistraro, S.; Gliozzi, A.; De Rosa, M.; Gambacorta, A.: A spin label ESR and saturation transfer-ESR study of archaebacteria bipolar lipids. *Eur. Biophys. J.* **1985**, *13* (2), 67-76.
 107. Yamagata, Y.; Senna, M.: An Electron Spin Resonance Study on the Phase Transition of the Molecular Assembly Comprising Cetyltrimethylammonium Chloride/Cetyl Alcohol/Water. *Langmuir* **2000**, *16* (15), 6136-6140.
 108. Wikander, G.; Eriksson, P. O.; Burnell, E. E.; Lindblom, G.: ESR line shapes in lyotropic systems: the micellar and liquid-crystalline phases of the dodecyltrimethylammonium chloride/water system. *J. Phys. Chem.* **1990**, *94* (15), 5964-5972.
 109. Horasan, N.; Suennetcioglu, M. M.; Sungur, R.: EPR spin label study of walnut oil effects on phosphatidylcholine membranes. *Chem. Phys. Lipids* **2006**, *140* (1-2), 1-10.
 110. Besheer, A.; Wood, K. M.; Peppas, N. A.; Maeder, K.: Loading and mobility of spin-labeled insulin in physiologically responsive complexation hydrogels intended for oral administration. *J. Controlled Release* **2006**, *111* (1-2), 73-80.
 111. Riske, K. A.; Fernandez, R. M.; Nascimento, O. R.; Bales, B. L.; Lamy-Freund, M. T.: DMPG gel-fluid thermal transition monitored by a phospholipid spin labeled at the acyl chain end. *Chem. Phys. Lipids* **2003**, *124* (1), 69-80.

112. Schneider, D. J.; Freed, J. H.: Calculating slow motional magnetic resonance spectra: a user's guide. In *Biological Magnetic Resonance* 8, Berliner, L. J., B, Eds.; Plenum Press: New York, **1989**; pp 1-76.
113. Mason, R. P.; Polnaszek, C. F.; Freed, J. H.: Interpretation of electron spin resonance spectra of spin labels undergoing very anisotropic rotational reorientation. *Comments. J. Phys. Chem.* **1974**, 78 (13), 1324-1329.
114. Meirovitch, E.; Freed, J. H.: Analysis of slow-motional electron spin resonance spectra in smectic phases in terms of molecular configuration, intermolecular interactions, and dynamics. *J. Phys. Chem.* **1984**, 88 (21), 4995-5004.
115. Patyal, B. R.; Crepeau, R. H.; Freed, J. H.: Lipid-gramicidin interactions using two-dimensional Fourier-transform electron spin resonance. *Biophys. J.* **1997**, 73 (4), 2201-2220.
116. Schorn, K.; Marsh, D.: Lipid chain dynamics in diacylglycerol-phosphatidylcholine mixtures studied by slow-motional simulations of spin label ESR spectra. *Chem. Phys. Lipids* **1996**, 82 (1), 7-14.
117. Lange, A.; Marsh, D.; Wassmer, K. H.; Meier, P.; Kothe, G.: Electron spin resonance study of phospholipid membranes employing a comprehensive line-shape model. *Biochemistry* **1985**, 24 (16), 4383-4392.
118. Dzikovski, B. G.; Livshits, V. A.: EPR spin probe study of molecular ordering and dynamics in monolayers at oil/water interfaces. *Phys. Chem. Chem. Phys.* **2003**, 5 (23), 5271-5278.
119. Hiff, T.; Kevan, L.: Electron spin echo modulation studies of doxylstearic acid spin probes in frozen vesicles: interaction of the spin probe with water-d₂ and effects of cholesterol addition. *J. Phys. Chem.* **1989**, 93 (4), 1572-1575.
120. Sentjurc, M.; Bacic, G.; Swartz, H. M.: Reduction of doxyl stearates by ascorbate in unilamellar liposomes. *Arch. Biochem. Biophys.* **1990**, 282 (2), 207-213.
121. Rama, K. Y., V; Marsh, D.: Spin label ESR and ³¹P-NMR studies of the cubic and inverted hexagonal phases of dimyristoylphosphatidylcholine/myristic acid (1:2, mol/mol) mixtures. *Biochim. Biophys. Acta* **1990**, 1024 (1), 89-94.
122. Hupfer, B.; Ringsdorf, H.; Schupp, H.: Liposomes from polymerizable phospholipids. *Chem. Phys. Lipids* **1983**, 33, 355-374.
123. Tanaka, H.; Gomez, M. A.; Tonelli, A. E.; Thakur, M.: Thermochromic phase transition of a polydiacetylene, poly(ETCD), studied by high-resolution solid-state ¹³C NMR. *Macromolecules* **1989**, 22, 1208-1215.
124. Orchard, B. J.; Tripathy, S. K.: Molecular Structure and electronic property modification of Poly(diacetylenes). *Macromolecules* **1986**, 19, 1844-1850.
125. Steiger, M.: In-vitro-Untersuchungen zur Kombinatwirkung von Erucylphosphomocholin (ErPC3) und Strahlentherapie. *PhD thesis (LMU München)* **2008**.

Supplement

Oscillatory rheometry

Table S.1 Concentration dependence of the G' and G'' values obtained for PC-C32-PC and Me₂PE-C32-Me₂PE (pH 5) at 25 °C for 1% deformation and 1 rad/s.

concentration/ mg/ml	PC-C32-PC G' / Pa	PC-C32-PC G'' / Pa	Me ₂ PE-C32-Me ₂ PE G' / Pa	Me ₂ PE-C32-Me ₂ PE G'' / Pa
1	1.38	0.17	1.55	0.12
2	7.16	0.86	9.24	0.58
4	25.00	2.14	25.77	1.54
8	118.00	12.13	89.63	6.26

Nuclear magnetic resonance (NMR) spectroscopy

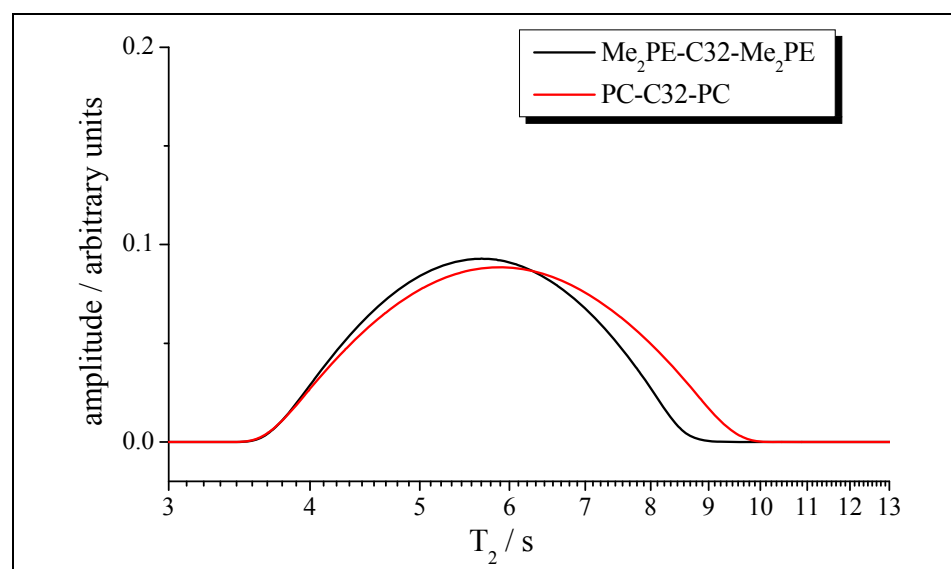


Figure S.1 Major T₂-peaks obtained at 80 °C for aqueous sample with 30 mg/ml PC-C32-PC in deionized water and 30 mg/ml Me₂PE-C32-Me₂PE in acetate buffer pH 5.

Table S.2 Compilation of the T_{2m} -values obtained in the course of the NMR relaxation measurements for the samples with 30 mg/ml PC-C32-PC and Me₂PE-C32-Me₂PE.

temperature in °C	mean transversal relaxation time T_{2m} in s			
	deionized water	30 mg/ml PC-C32- PC in deionized water	acetate buffer pH 5	30 mg/ml Me ₂ PE-C32- Me ₂ PE in acetate buffer pH 5
5	-	1.36	-	0.43 / 1.72
25	2.83	2.53	2.83	1.11
30	3.07	2.78	3.13	1.31
35	3.44	3.05	3.42	1.69
37.5	-	3.16	-	1.86
39	-	3.28	-	-
40	3.89	3.31	3.73	2.07
41	-	3.37	-	-
42	-	3.45	-	2.37
43	-	3.49	-	2.44
44	-	3.57	-	2.63
45	4.09	3.58	4.05	2.81
46	-	3.67	-	2.97
47	-	3.73	-	3.06
48	-	3.79	-	3.11
49	-	3.80	-	3.18
50	4.50	3.91	4.47	3.25
51	-	3.98	-	-
52	-	3.99	-	-
52.5	-	-	-	3.44
53	-	4.08	-	-
54	-	4.13	-	-
55	4.84	4.17	4.83	3.59
57.5	-	-	-	3.77
60	5.24	4.53	5.32	3.91
64	-	-	-	4.19
66	-	-	-	4.31
68	-	-	-	4.56
70	5.84	5.21	5.80	4.70
72	-	-	-	4.93
75	-	-	-	5.13
80	6.74	5.84	6.92	5.63

Electron spin resonance (ESR) spectroscopy

```
% Calculating the spectrum of 5-DSA in 10 m/ml PC-C32-PC in deionized
water at 20 °C

%=====

clear all, close all

% Parameters
%-----

g = [2.0088, 2.0066, 2.0026];
A = mt2mhz([6.4,5.7,32.9]/10); % G -> MHz
lw = mt2mhz(2.25/10); % G -> MHz
Sys = struct('g', g, 'Nucs', '14N', 'A',A, 'Apa', [0 14 0]*pi/180);
Exp = struct('mwFreq',9.4, 'CenterSweep',[334.9 9.8], 'Harmonic',0);
Dyn= struct('lw',lw, 'Diff',[5 75]*1e6);
Opt = struct('Verbosity',1, 'LLKM',[24 14 6 6]);
[B,spc0] = chili(Sys,Dyn,Exp,Opt);

plot(B,spc0);

ModulationAmplitude = 0.125; % mT
spc1 = pseumod(B,spc0,ModulationAmplitude);
subplot(2,1,1);
plot(B,spc0); axis tight
subplot(2,1,2);
plot(B,spc1); axis tight
xlabel('magnetic field [mT]');

output = [B,spc1];
output = [B',spc1'];
save '5-DSA PC-C32-PC 20 °C.dat' output -ascii;
```

Figure S.2 Command structure for calculating the spectrum of 5-DSA in 10 mg/ml PC-C32-PC at 20 °C by the EasySpin function »chili«.

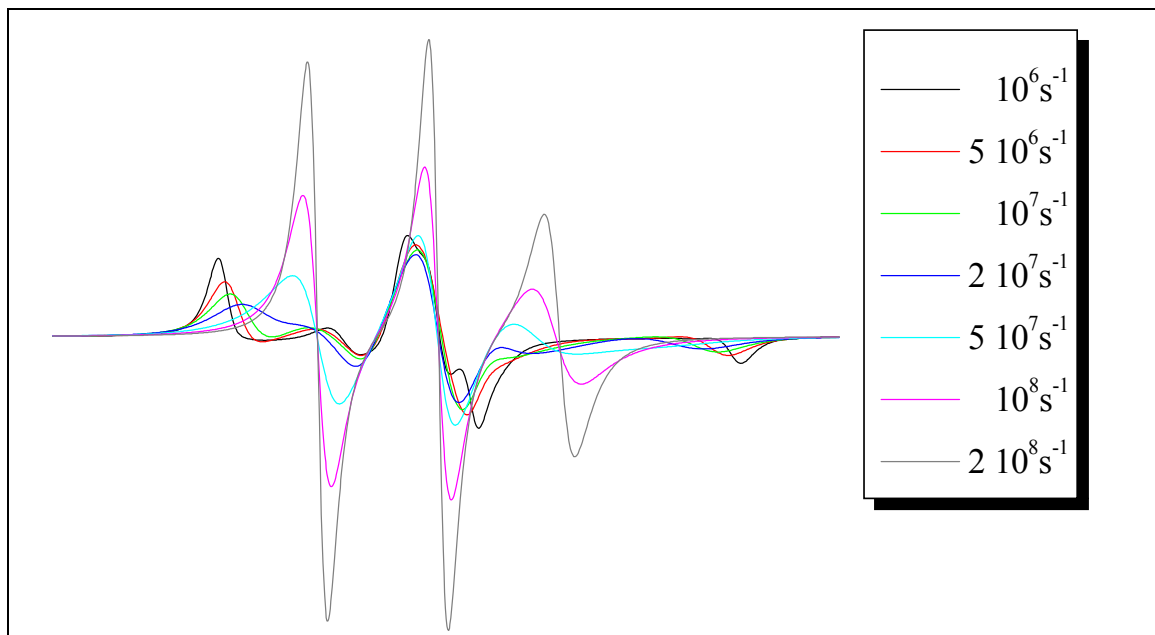


Figure S.3 Spectral simulation with the EasySpin function »chili«: Variation of a single rotational diffusion tensor R.

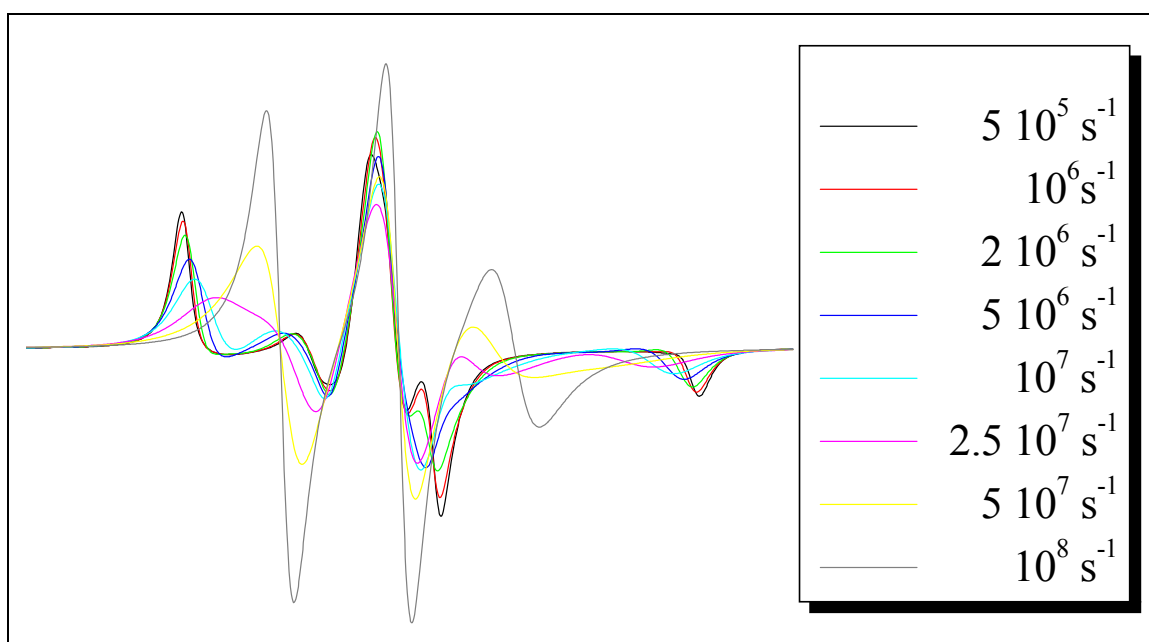


Figure S.4 Spectral simulation with the EasySpin function »chili«: Variation of two rotational diffusion tensors R_{\perp} and R_{\parallel} with a static ratio of 1:10. The given value is always that of R_{\perp} .

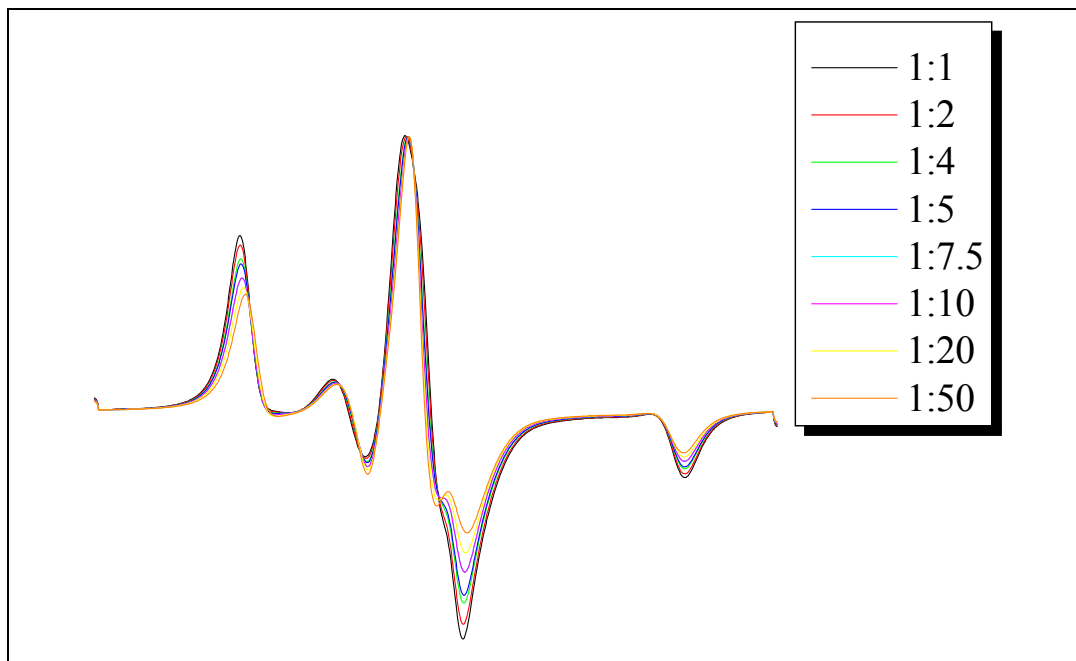


Figure S.5 Spectral simulation with the EasySpin function »chili«:

Static parameter: $R_{\perp} = 2.25 \cdot 10^6 \text{ s}^{-1}$

Varied parameter: $R_{\parallel} \rightarrow$ gradually increased starting from $2.25 \cdot 10^6 \text{ s}^{-1}$ (1:1)

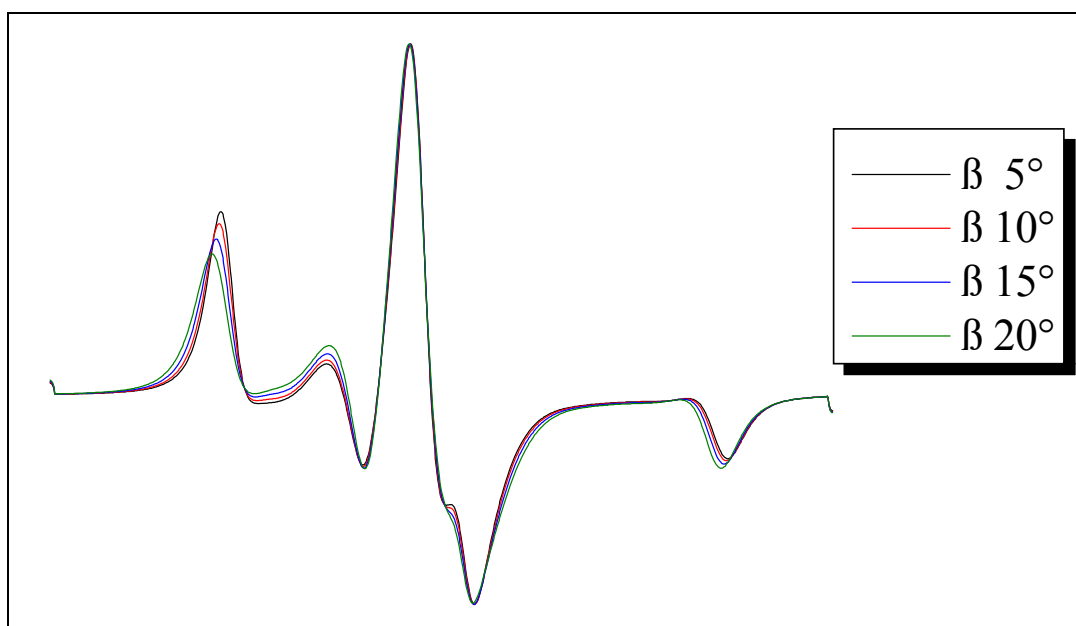


Figure S.6 Spectral simulation with the EasySpin function »chili«:

Static parameters: $R_{\perp} = 2.25 \cdot 10^6 \text{ s}^{-1}$, $R_{\parallel} = 12.25 \cdot 10^6 \text{ s}^{-1}$ (1:5)

Varied parameter: Euler angle β ('Apa', $[0 \beta 0] \cdot \pi/180$) \rightarrow gradually increased

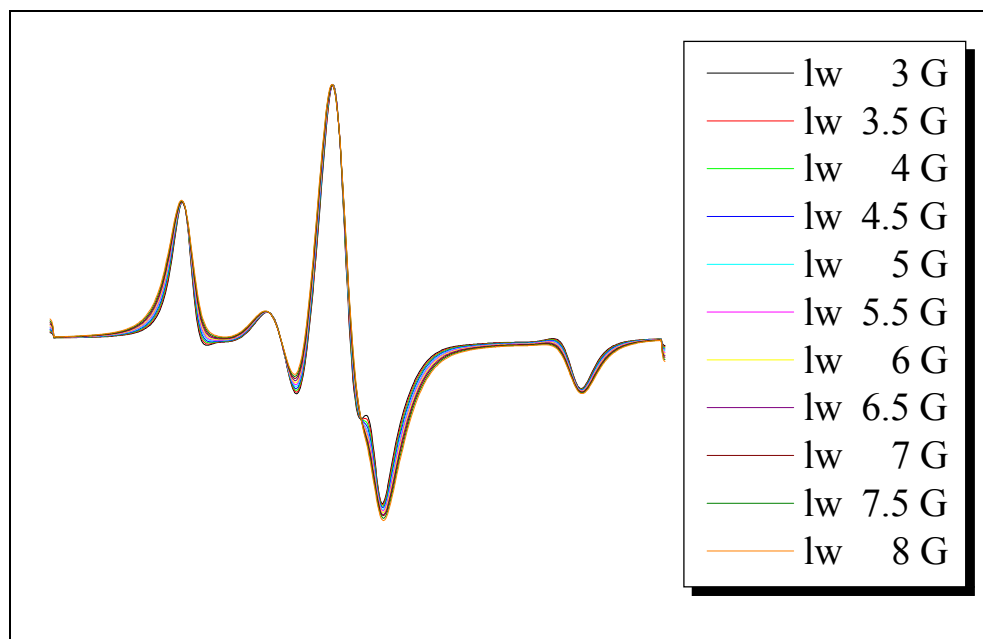


Figure S.7 Spectral simulation with the EasySpin function »chili«:

Static parameters: $R_{\perp} = 2.25 \cdot 10^6 \text{ s}^{-1}$, $R_{\parallel} = 12.25 \cdot 10^6 \text{ s}^{-1}$ (1:5), $\beta = 5^\circ$

Varied parameter: $lw \rightarrow$ gradually increased

Table S.3 Spectral parameters established for the simulation of the spectra obtained for 5-DSA in 10 mg/ml PC-C32-PC in deionized water (displayed in Figure 3.3.6) by the programs EasySpin (0-40 °C) and EPRSIM (55 and 60 °C). The following parameters were optimized initially and used for all simulated slow motion spectra: g_{xx} 2.0088, g_{yy} 2.0066, g_{zz} 2.0026, A_{xx} 6.4 G, A_{yy} 5.7 G

temperature / °C	A_{zz} / G	β / °	S	Lw / G	R_{\perp} / $10^6 s^{-1}$	R_{\parallel} / $10^6 s^{-1}$	τ_{\perp} / ns	τ_{\parallel} / ns	$N_R = \tau_{\perp} : \tau_{\parallel}$	τ_{Rm} / ns
0	32.9	11.0	0.95	3.5	2.75	20.6	60.61	8.08	7.5:1	30.96
10	32.9	12.0	0.94	2.5	3.25	32.5	51.28	5.13	10:1	23.81
20	32.9	14.0	0.91	2.25	5.00	75.0	33.33	2.22	15:1	13.51
30	32.9	18.0	0.86	2	7.00	10.5	23.81	1.59	15:1	9.66
40	32.9	25.0	0.73	2	10.00	150.0	16.67	1.11	15:1	6.76
55	-	-	0.13	-	-	-	-	-	-	1.52
60	-	-	0.11	-	-	-	-	-	-	1.48

Table S.4 Spectral parameters established for the simulation of the spectra obtained for 12-DSA in 10 mg/ml PC-C32-PC in deionized water (displayed in Figure 3.3.10) by the programs EasySpin (0-40 °C) and EPRSIM (55 and 60 °C). The following parameters were optimized initially and used for all simulated slow motion spectra: g_{xx} 2.0088, g_{yy} 2.0066, g_{zz} 2.0026, A_{xx} 6.4 G, A_{yy} 5.7 G

temperature / °C	A_{zz} / G	β / °	S	Lw / G	R_{\perp} / $10^6 s^{-1}$	R_{\parallel} / $10^6 s^{-1}$	τ_{\perp} / ns	τ_{\parallel} / ns	$N_R = \tau_{\perp} : \tau_{\parallel}$	τ_{Rm} / ns
0	33.0	12.0	0.94	2.50	2.50	25.0	66.67	6.67	10:1	30.95
10	32.2	13.0	0.92	2.25	2.75	27.5	60.61	6.06	10:1	28.13
20	31.5	15.0	0.90	2.25	4.00	40.0	41.67	4.17	10:1	19.35
30	31.5	17.5	0.87	2.00	5.00	75.0	33.33	2.22	15:1	13.51
40	31.5	20.0	0.82	1.80	6.00	120.0	27.78	1.39	20:1	10.24
55	-	-	0.16	-	-	-	-	-	-	1.78
60	-	-	0.13	-	-	-	-	-	-	1.55

Table S.5 Spectral parameters established for the simulation of the spectra obtained for 5-DSA in 10 mg/ml Me₂PE-C32-Me₂PE at pH 5 (displayed in Figure 3.3.17) by the programs EasySpin (0-40 °C) and EPRSIM (55 and 60 °C). The following parameters were optimized initially and used for all simulated slow motion spectra: g_{xx} 2.0088, g_{yy} 2.0066, g_{zz} 2.0026, A_{xx} 6.4 G, A_{yy} 5.7 G

temperature / °C	A_{zz} / G	β / °	S	Lw / G	R_{\perp} / $10^6 s^{-1}$	R_{\parallel} / $10^6 s^{-1}$	τ_{\perp} / ns	τ_{\parallel} / ns	$N_R = \tau_{\perp} : \tau_{\parallel}$	τ_{Rm} / ns
0	33.3	9.0	0.96	3.50	1.50	7.50	111.11	22.22	5:1	64.98
10	32.7	11.0	0.95	2.75	2.00	10.00	83.33	16.67	5:1	48.74
20	32.3	12.0	0.94	2.75	2.55	12.75	65.36	13.07	5:1	38.22
30	32.1	13.0	0.92	2.50	3.00	22.50	55.56	7.41	7.5:1	28.39
40	31.9	14.0	0.91	2.00	5.00	62.50	33.33	2.67	12.5:1	14.37
55	-	-	0.44	-	-	-	-	-	-	1.44
60	-	-	0.38	-	-	-	-	-	-	1.36

Table S.6 Spectral parameters established for the simulation of the spectra obtained for 12-DSA in 10 mg/ml Me₂PE-C32-Me₂PE at pH 5 by the programs EasySpin (0-40 °C) and EPRSIM (55 and 60 °C): Simulation parameters used to calculate the simulated spectra shown in Figure 3.3.20. The following parameters were optimized initially and used for all simulated slow motion spectra: g_{xx} 2.0088, g_{yy} 2.0066, g_{zz} 2.0026, A_{xx} 6.4 G, A_{yy} 5.7 G

temperature / °C	A_{zz} / G	β / °	S	Lw / G	R_{\perp} / $10^6 s^{-1}$	R_{\parallel} / $10^6 s^{-1}$	τ_{\perp} / ns	τ_{\parallel} / ns	$N_R = \tau_{\perp} : \tau_{\parallel}$	τ_{Rm} / ns
0	33.1	11	0.95	3.00	2.50	16.875	66.67	9.88	6.75:1	35.28
10	32.7	12	0.94	2.25	2.65	19.875	62.89	8.39	7.5:1	32.13
20	32.0	14	0.91	2.25	2.75	20.625	60.61	8.08	7.5:1	30.96
30	31.5	16	0.89	2.25	3.00	22.500	55.56	7.41	7.5:1	28.39
40	31.5	18	0.86	2.00	4.00	40.00	41.67	4.17	10:1	19.35
55	-	-	0.48	-	-	-	-	-	-	2.17
60	-	-	0.42	-	-	-	-	-	-	2.13

Table S.7 Compilation of all determined $2A_{\max}$ values.

T / °C	PC-C32-PC			Me ₂ PE-C32-Me ₂ PE pH 5			Me ₂ PE-C32-Me ₂ PE pH 10			
	5-DSA	12-DSA	16-DSA	5-DSA	12-DSA	16-DSA	5-DSA		12-DSA	16-DSA
							10 mg/ml	1 mg/ml		
0	6.42	6.35	6.05	6.47	6.37	6.14	5.94	5.92	6.16	5.95
10	6.29	6.23	5.73	6.37	6.272	5.92	5.58	5.52	6.09	5.56
20	6.17	6.06	4.67	6.24	6.13	5.51	5.46	5.42	5.97	5.23
30	6.03	6.00	4.40	6.15	6.04	5.00	5.17	5.11	5.90	4.77
35	-	-	-	-	-	-	-	5.07	-	-
37.5	-	-	-	-	-	-	-	4.97	-	-
39	-	-	-	-	-	-	-	4.77	-	-
40	5.83	5.95	4.15	5.93	5.94	4.40	4.69	4.49	-	-
41	5.81	-	-	5.88	-	4.35	4.27	4.23	-	-
42	5.80	5.92	4.02	5.87	5.89	4.33	4.10	4.019	-	-
43	5.78	5.90	-	5.83	5.88	4.28	4.07	3.94	-	-
44	5.67	5.73	4.00	5.82	5.87	4.24	3.96	3.89	-	-
45	5.60	5.73	4.02	5.79	5.86	4.19	3.95	3.87	-	-
46	5.58	5.73	4.03	5.61	5.81	4.08	3.88	3.84	-	-
47	5.55	5.71	3.98	5.02	5.73	4.05	3.86	3.82	-	-
48	5.43	5.68	3.22	4.67	5.61	4.02	3.84	3.83	-	-
49	3.29	5.66	3.18	4.60	5.43	3.98	3.83	3.74	-	-
50	3.28	5.57	3.16	4.56	5.22	3.94	3.82	3.73	-	-
51	3.28	3.91	3.17	-	-	-	3.75	3.70	-	-
52	3.27	3.34	3.17	-	-	3.91	3.74	3.26	-	-
52.5	-	-	-	4.42	5.15	-	-	-	-	-
53	-	-	-	-	-	-	3.72	3.26	-	-
54	-	-	-	-	-	-	3.71	3.25	-	-
55	3.26	3.33	3.15	4.35	5.05	3.82	3.23	3.24	-	-
56	-	-	-	-	-	-	3.23	3.23	-	-
57	-	-	-	-	-	-	3.23	-	-	-
58	-	-	-	-	-	-	3.23	-	-	-
59	-	-	-	-	-	-	3.22	-	-	-
60	3.25	3.31	3.15	4.15	4.81	3.64	3.22	3.23	-	-

List of publications

Meister, A.; Bastrop, M.; Koschoreck, S.; Garamus, V. M.; Sinemus, T.; Hempel, G.; Drescher, S.; Dobner, B.; Richtering, W.; Huber, K.; Blume, A.:
Structure-Property Relationship in Stimulus-Responsive Bolaamphiphile Hydrogels.
Langmuir, 23 (14), 7715-7723 (2007)

Kempe, S.; Metz, H.; Bastrop, M.; Hvilsom, A.; Vidor Contri, R.; Mäder, K.:
Characterization of thermosensitive chitosan-based hydrogels by Rheology and Electron Paramagnetic Resonance Spectroscopy. European Journal of Pharmaceutics and Biopharmaceutics, 68 (1), 26-33 (2008)

Bastrop, M.; Meister, A.; Metz, H.; Drescher, S.; Dobner, B.; Maeder, K.; Blume, A.:
The Motional Dynamics in Bolaamphiphilic Nanofibers and Micellar Aggregates: An ESR Spin Probe Study. J. Phys. Chem. B, 113 (2), 574-582. (2009)

Bastrop, M.; Meister, A.; Metz, H.; Drescher, S.; Dobner, B.; Maeder, K.; Blume, A.:
Water dynamics in bolaamphiphile hydrogels investigated by ¹H-NMR relaxometry and diffusometry. Submitted (2010)

Acknowledgements

The writing of this dissertation was one of the biggest challenges I ever had to face. Without the support, the patience and guidance of the following people, this would have not been realizable. It is to them that I owe my deepest gratitude.

First of all, I am grateful to my supervisors Prof. Karsten Mäder and Prof. Alfred Blume for the opportunity to work on this interesting topic, for the fruitful discussions and for the provided freedom for my work. I really appreciated to know that their doors have been always open for us.

My thanks and appreciation also go to PD Dr. Anette Meister for her kind advise, encouragement and help with everything concerning bolaamphiphiles.

Without Prof. Bodo Dobner, Dr. Simon Drescher and Dipl. Pharm. Katrin Helms, my work would have been limited to theoretical considerations, since they frequently provided me with the freshly synthesized bolaamphiphiles. I always enjoyed to enter their lab full of chemical equipment.

I would also like to thank Dr. Hendrik Metz for his help with the ESR and NMR measurements and with extracting the valuable information from the complex data.

There was a wide circle of people, who also contributed to this work as cooperators, advisors or suppliers. Since there were so many, I cannot name them all here, but I appreciate the help I received from each of them.

For the financial support, I want to thank the Cluster of Excellence “Nanostructured Materials” of the state of Saxony-Anhalt and the Institut für Angewandte Dermatopharmazie an der Martin-Luther-Universität e.V..

I will never forget the wonderful moments with Ahmed Abdalla, Ahmed Besheer, Anteneh Belete Shibeshi, Sabine Kempe and others, when we were forgetting about science and talking about all the world and his brother.

I would like to thank all colleagues from the groups of Prof. Mäder and Prof. Blume for the friendly atmosphere and the nice time that we had together.

This work is dedicated to Anke, Mira and all my family.

Curriculum vitae

Personal information

Name	Martin Bastrop
Born	02.02.1980 in Parchim, Germany
Nationality	Germany
Marital status	married with Anke Bastrop
Children	Mira Elisabeth Bastrop

Work experience

since 09/2010	Apotheke im PEP, Grimma <i>Pharmacist</i>
since 02/2010	DRK Bildungswerk Sachsen <i>Lecturer for pharmacology training</i>
01/2009-08/2010	LGHO GmbH, Leipzig <i>Head of manufacturing</i>
11/2006 – 12/2008	Waldbaur-Apotheke, Leipzig <i>Pharmacist</i>
01/2005– 06/2005	Zomba Central Hospital, Malawi, Cenral Africa <i>Pharmacist</i>

Education

08/2005 – 12/2008	Institute of Pharmacy, Martin-Luther-Universität Halle-Wittenberg <i>PhD student in the group of Prof. Karsten Mäder (Pharmaceutical Technology) in cooperation with Prof. Blume (Physical Chemistry)</i>
01/2005	<i>Approbation as a pharmacist</i>
12/2004	<i>Diploma degree in Pharmacy, Martin-Luther-Universität Halle-Wittenberg</i>
05/2004 – 10/2004	Bären-Apotheke, Leipzig <i>Practical training</i>
10/2003 – 04/2004	Institute of Pharmacy, Martin-Luther-Universität Halle-Wittenberg <i>Diploma student in the group of Prof. Karsten Mäder (Pharmaceutical Technology)</i>
10/1999 – 10/2003	Ernst-Moritz-Arndt-Universität, Greifswald <i>Pharmacy studies</i>
02/2001 – 03/2001	Universitätsklinikum, Rostock <i>Famulatur</i>
02/2000 – 03/2000	Rats-Apotheke, Parchim <i>Famulatur</i>
09/1998 – 06/1999	Neumünster/ Boostedt <i>Grundwehrdienst</i>
07/1998	Friedrich-Franz-Gymnasium, Parchim <i>Abitur</i>

Selbständigkeitserklärung

Hiermit erkläre ich, dass ich die Arbeit selbständig und ohne fremde Hilfe angefertigt, andere als die von mir angegebenen Quellen und Hilfsmittel nicht benutzt und die den Werken wörtlich oder inhaltlich entnommenen Stellen als solche kenntlich gemacht habe.

Die Dissertation wurde bisher keiner anderen Universität oder Hochschule im In- und Ausland vorgelegt.

Halle (Saale), September 2010

Martin Bastrop